Universidad Autónoma de Barcelona

Departamento de Microbiología y Genética

Facultad de Biociencias.

Bioluminescence Imaging for the Evaluation and Development of New Biomaterials for Tissue Engineering

Memoria Presentada por Olaia Fernández Vila para optar al grado de Doctora en Biotecnología por la Universidad Autónoma de Barcelona. Este trabajo ha sido realizado en el Instituto de Química Avanzada de Cataluña bajo la dirección del doctor Jerónimo Blanco Fernández y la tutoría del Doctor Antoni Villaverde Corrales.

El Director

Jerónimo Blanco Fernández

La Doctoranda

Olaia Fernández Vila

Barcelona, Octubre 2013.

I. **INDEX**

II. ABREVIATIONS

ATP	Adenosine triphosphate
BLI	Bioluminescence Imaging
BMP-2	Bone Morphogenetic Protein-2
BMSC	Bone Marrow Stem Cells
CaP	Calcium Phosphate
CCD	Charge Coupled Device
CD	Cluster of Differentiation
CFU-F	Fibroblast Colony-forming Units
CMV	Cytomegalovirus
CMV:PLuc	Plox-G·PLuc construct
CMV:RLuc	CMV:hRLuc:mRFP:ttk construct
CT	Computed Tomography
DMEM	Dulbecco's Modified Eagle`s Medium
DMEM-hg	Dulbecco's Modified Eagle`s Medium high glucose
DNA	Desoxiribonucleic Acid
ECM	Extracellular Matrix
eGFP	Enhanced Green Fluorescent Protein
ESCs	Embrionic Stem Cells
FACS	Fluorescence-Activated Cell Sorter

FBS	Fetal Bovine Serum
FGF-2	Fibroblast Growth Factor-2
GFP	Green Fluorescent Protein
GLuc	*Gaussia princeps* luciferase
GSL-IB_4	Griffonia simplicifolia Isolectin B4
hAMSCs	Human Adipose-derived Mesenchymal Stem Cells
HCl	Hydrochloric Acid
HE	Hematoxylin-eosin
hOCp	Human osteocalcin promoter
HRE:PLuc	Plox-HRE-12p:PLuc:eGFP
ip	Intra peritoneal
iPSC	Induced Pluripotential Stem Cells
iv	Intravenous
LD_{50}	Median Lethal Dose
Micro-CT/ μCT	Micro-Computed Tomography
MOI	Multiplicity of Infection
mRFP	Monomeric Red Fluorescent Protein
MRI	Magnetic Resonance Imaging
MSCs	Mesenchymal Stem Cells

NaCl	Sodium Chloride
NIR	Near Infrared
OC:PLuc	Plox-hOCp:PLuc:eGFP construct
PBS	Phosphate Buffered Saline
PDGF	Platelet-derived Growth Factor
PEG	Polyethylene Glycol
PEI	Polyethylenimine
PECAM	Platelet/endothelial cell adhesion molecule
PECAM:PLuc	Plox-hPECAM-1p:PLuc:eGFP construct
PET	Positron Emission Tomography
PFA	Paraformaldehyde
PGA	Poly(glycolic acid)
pH	Potential of Hydrogen
PHCs	Photon Counts
PLA	Poly(lactic acid)
PLGA	Poly(lactic-co-glycolic)Acid
PLuc	*Photinus pyralis* luciferase
PPLuc	*Pyrophorus plagiophalamus* luciferase
P/S	Penicillin/Streptomycin

RFP	Red Fluorescent Protein
RLuc	*Renilla reniformis* luciferase
RPM	Revolutions per minute
RT	Room temperature
sc	Subcutaneous
SCID	Severe Combined Immunodeficiency
SPECT	Single Photon Emission Computed Tomography
TBS	Tris-buffered saline
TE	Tissue Engineering
TGF-β	Transforming Growth Factor-beta
UV	Ultraviolet
VEGF	Vascular Endothelial Growth Factor
VSV-G	Vesicular stomatitis virus G
2D	Two-dimensional
3D	Three-dimensional

III. **INTRODUCTION**

The loss or failure of an organ or tissue is one of the most frequent, devastating, and costly problem of human health care (Langer & Vacanti 1993). In 2012 more than 4,000 transplants were performed in Spain (

Table 1) (Organizacion Nacional de Transplantes 2013), with an associated cost of 130.9 million euros per year (Organizacion Nacional de Transplantes 2007).

	2009	**2010**	**2011**	**2012**
Heart	275	221	241	248
Liver	1099	971	1137	1084
Pancreas	97	94	111	83
Lung	220	239	234	229
Kidney	2328	2098	2498	2551
Bowl	11	0	9	8
TOTAL	**4030**	**3623**	**4230**	**4203**

Table 1. Number of transplants performed in Spain in the last 3 years. Font: Spanish National Transplant Organization (ONT).

Loss of failure of organs or tissues may be due to accidents or to pathologies of different nature, like infectious (hepatitis C), congenital (lung atelectasis), hereditary (cystic fibrosis), autoimmune (diabetes mellitus) or degenerative diseases (osteoporosis). Incidence and gravity of these problems is really high and, with the progressive aging of the population, age-related degeneration of organs will increase in the future. Just diabetes affects about 371 million people in the world and causes death of more than 3 million each year, and the World Health Organization predicts that this figure will double in the next 15 years (World Health Organization 2013).

Current options for treatment of organ failure or tissue loss are explained below.

- Allotransplantation: it consists in the substitution of the diseased organ for a healthy one from a donor. Due to improvement of the techniques, nowadays it is possible to transplant most organs and tissues, what translates in an improvement in life quality and an increase in the life expectancy of the patient. However, allotransplants present two major problems. The first one is related to immune rejection; a compatible donor must be found and even then the patient would need to be treated with immunosuppressive drugs for life. The second one has to do with donor shortage; waiting lists are very long and unfortunately, a lot of patients die before they get a compatible organ. Data from the World Transplant Registry show that in 2008 organ donation only covered 46% of the organs needed for transplantation.

- Autotransplantation: it consists on the extraction of healthy tissue from the patient for being transplanted into the damaged tissue in the same patient. This approach avoids the need to wait for an organ to be available and the problems of immune rejection, so it is promising alternative for patients that still have enough healthy tissue to be transplanted into the injured site. Unfortunately, that is only the case of a few patients, since usually a large amount of healthy tissue or even a whole organ is needed.

- Xenotransplantation: it is the transplantation of a tissue or an organ from one species into an individual from a different species. While this approach solves the issue of donor shortage, it presents even worse immunorejection problems than allotransplantation. Humanized transgenic animals are being developed to avoid this problem, but there are still other matters to consider, like the possibility of transmitting pathogens form other species to humans that could give rise to diseases, even novel ones (Ogle & Platt 2002).

- Implantation of biomimetic devices: mechanical devices may be used to supply the functions of lost or injured organs. Artificial hearts, artificial heart valves or hip prosthesis, have been satisfactorily implanted in human patients during the last decades. However, these mechanical devices are subject to erosion and fracture, and frequently need to be replaced several times during the life of the patient, thus they don't represent a definitive solution.

As it has been shown, there are still important limitations to effective organ substitution, not being anyone of the current alternatives completely satisfactory. Thus, there is a need to develop new strategies that overcome the deficiencies of current replacement therapies.

1. TISSUE ENGINEERING

Tissue engineering (TE) was defined by Langer and Vacanti in 1993 as "an interdisciplinary field that applies the principles of engineering and the life sciences toward the development of biological substitutes that restore, maintain, or improve tissue function" (Langer & Vacanti 1993).

TE arises from the need of solving the deficiencies of classic therapies for tissue and organ substitution. It brings together the knowledge gained in fields like cell biology, biochemistry, molecular biology and biochemical and biomechanical engineering with the objective of developing new substitutes for human tissues.

Three general strategies have been adopted for the generation of new tissue, involving one or more of the three TE basic resources: cell transplants, biomaterials and regeneration-inducing molecules (*Fig. 1*).

1. **Implantation of isolated cells**. This approach consists on implanting certain a cell type that supplies the needed function. Cells may be injected alone or in combination with a biomaterial that behaves as a tridimensional biological support (scaffold). This approach avoids the complications of surgery and permits manipulation of the cells before infusion. Its potential limitations include failure of the infused cells to maintain their function in the recipient, and the immunological rejection of the transplanted cells.
2. **In situ tissue regeneration**. Based on using tissue repair inducing substances to stimulate the regeneration of the affected tissue. These substances may be single molecules (growth factors, hormones, etc.) or biomaterial scaffolds that, due their structure or composition, stimulate host cells to regenerate the tissue. The success of this approach depends on the purification and large-scale production of appropriate

signal molecules and, in many cases, the development of methods to deliver these molecules to their targets

3. **Growth and implantation of three-dimensional tissues**. These structures are created by assembling biomaterials and cells to obtain a certain three-dimensional structure. The matrices are fashioned from natural materials such as collagen or from synthetic polymers as polyethylene glycol. Immunological rejection may be prevented by immunosuppressive drugs or by using autologous cells.

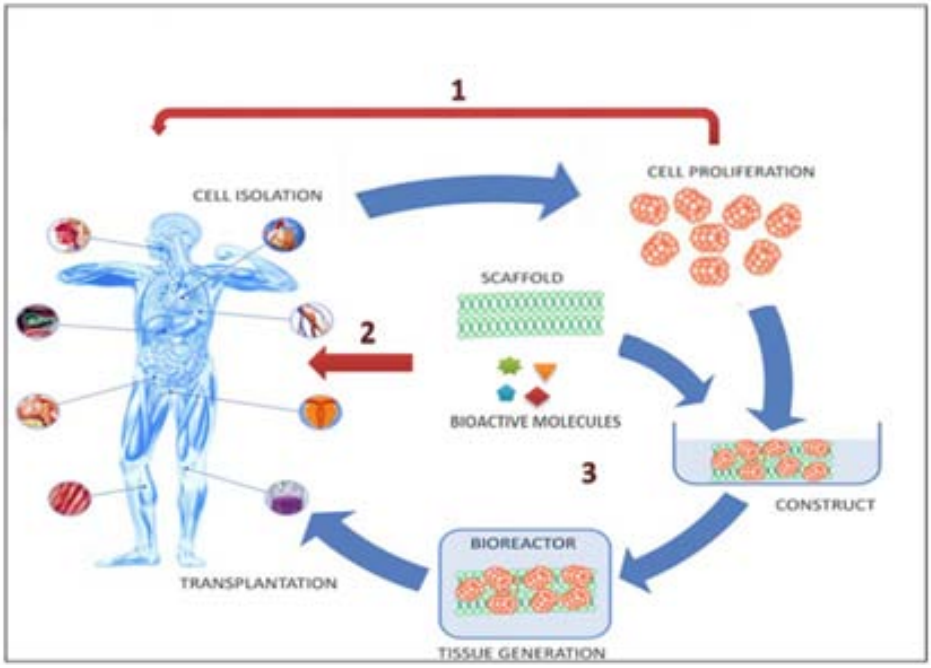

Fig. 1. Schematic representation of the different therapeutic approaches in Tissue Engineering. Adapted from www.springerimages.com.

1.1. Cell types in Tissue Engineering

A variety of cells has been used for TE. Initial work used fully mature cells taken from adult tissue but, although these have certain advantages including the possibility of using autologous cells to avoid immunological problems, they have low growth potential and a relatively high degree of senescence. Fully committed cells form foetal tissue have also been used and shown to be a good

source for TE. These cells have much greater proliferative capacity and show less senescence than adult cells (Polak & Hench 2005).

Stem cells provide many advantages over mature cells for TE. They are defined by three basic properties: the ability of self-renew indefinitely, the ability to differentiate into one or more specialized cell types and the capability for *in vivo* reconstitution of some tissues (Zuk et al. 2002).

The most primitive stem cell is the fertilized oocyte (the zygote). Once the fertilized egg starts dividing, the descendants of the first two divisions are the totipotent cells, able to form the embryo and trophoblast. After about 4 days, these totipotent cells forma hollow ball of cells, the blastocyst, containing a cluster of cells called the inner cell mass from which the embryo develops and embryonic stem cells (ESCs) are derived (*Fig. 2*).

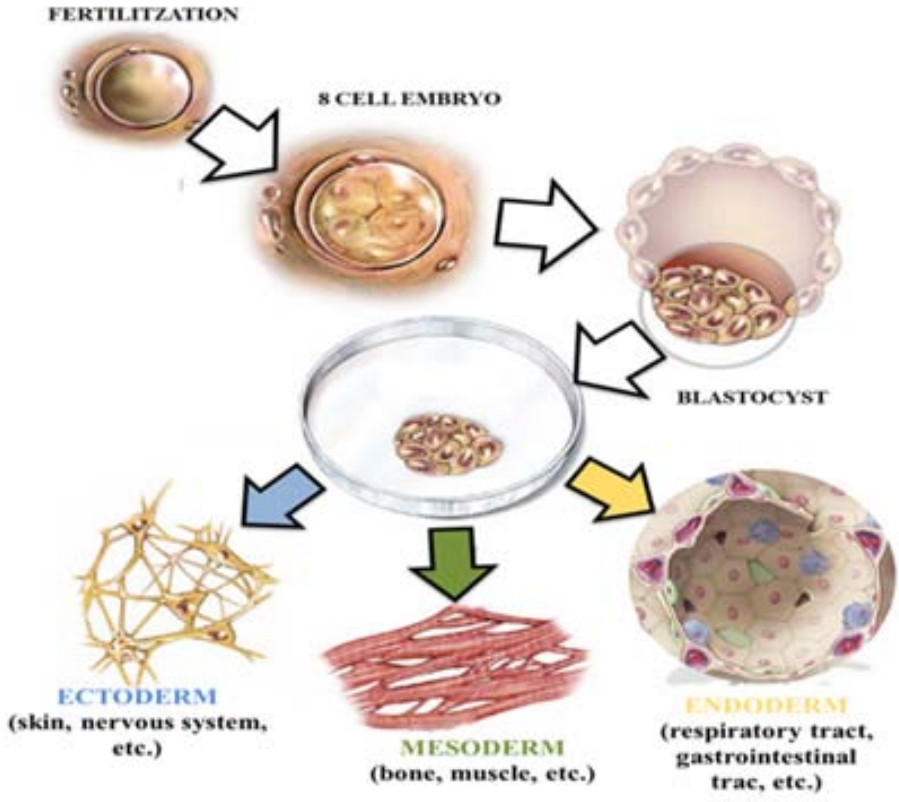

Fig. 2. Pluripotenciality of Embryonic Stem Cells (ESCs). ©Benjamin Cummings 2010.

Lower down in the hierarchical tree are the multipotent cells. Most adult tissues have multipotent stem cells that can produce a limited range of differentiated cell lineages appropriate to their location. At the bottom of the hierarchical tree are the unipotent stem cells, or committed progenitors, that generate one specific cell type.

1.1.1. Pluripotent Stem Cells

Among the different types of stem cells, pluripotent stem cells have the greatest differentiation potential as they can give rise to committed cell lineages comprising all three germ layers. Furthermore, pluripotent stem cells have infinite self-renewal capacity. To date, there are only two types of known pluripotent stem cells, namely embryonic stem cells (ESCs) and induced pluripotent stem cells (iPSCs).

Embryonic Stem Cells

Human ESCs (hESCs) could potentially be directed to differentiate into adult stem cells or tissues and be used clinically to reconstitute the depleted adult stem cell pool or degenerating organs. The following cells types have already been derived from hESCs: neural tissue, insulin secreting cells, cardiomyocytes, hematopoietic cells, endothelial cells, osteoblasts and hepatocytes (Lerou & Daley 2005).

There are some important limitations to the clinical application of hESCs to TE:

- Following extensive cultivation of ESCs, genetic and epigenetic changes can occur, frequently forming teratomas when implanted *in vivo* (Draper, Smith, et al. 2004; Draper, Moore, et al. 2004; Prokhorova et al. 2009).

- HESC populations are not homogeneous and selection strategies are required to obtain populations with a specific differentiation potential.
- HESCs are allogenic cells, with the associated immunological rejection problems.
- Ethical considerations and legal restrictions.

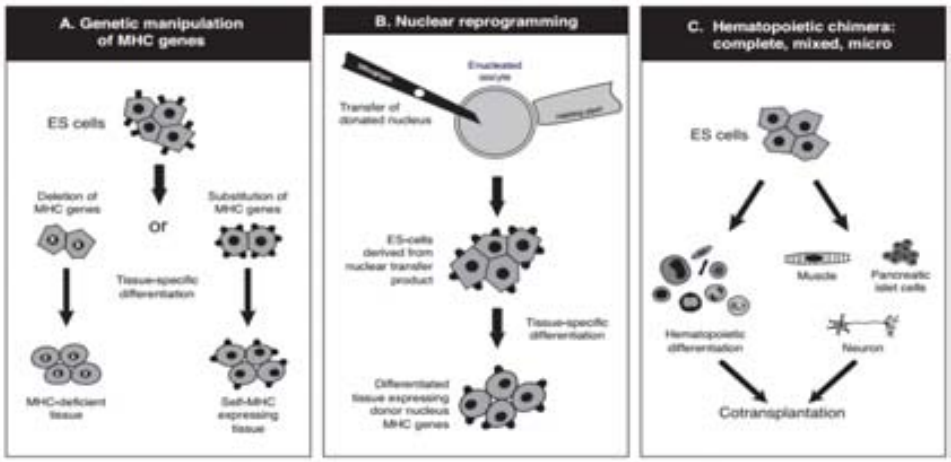

Fig. 3. Possible ways to avoid immune-mediated rejection of tissue transplants derived from human ESCs. From Odorico et al., 2001.

Solutions for some of these objections have been proposed by several investigators. Murry and Laflamme (Laflamme & Murry 2011) suggest genetic selection of the desired progenitor fraction among hESCs population to avoid heterogeneity and teratoma formation. Odorico et al (13) propose genetic manipulation for the generation of immunocompatible hESCs, suggesting three different approaches (*Fig. 3*). One potential method is to eliminate MHC genes or replace MHC genes with ones specifically matched to a particular transplant recipient. The second proposal is nuclear reprogramming by transferring a nucleus for a somatic cell of an individual to an enucleated oocyte; ESC derived from this oocyte would express all histocompatibility antigens identical to those of the person from whom the somatic cell was obtained (Hwang et al. 2005;

Hwang et al. 2004). The last approach is the transplantation at the same time of hematopoietic stem cells and the tissue of interest generated from the same parental ESC line, so a hematopoietic chimera is created, establishing immunologic tolerance to the second tissue.

Induced Pluripotent Stem Cells (iPSCs)

In 2006 Takahashi and Yamanaka reported the production of pluripotent stem cells by genetic modification of adult fibroblasts (Takahashi & Yamanaka 2006). They demonstrated that differentiated cells can be reprogrammed to and embryonic-like state by the ectopic co-expression of only four genes, under ESC culture conditions. These cells, designated induced Pluripotent Stem Cells (iPSCs), exhibit the morphology and growth properties of ESCs and express ESC marker genes.

The great advantage of these iPSCs compared to ESCs is that they can be obtained from adult cells from the patient, so they are fully immunocompatible and they avoid the controversial ethical issues surrounding ESCs. Reprogramming technology and iPSCs have potential to model and treat human disease by two different strategies (Fig. 4): in cases in which a disease-causing mutation is known, gene targeting could be used to repair de DNA sequence (right), the gene-corrected patient-specific iPSCs would then undergo directed differentiation into the affected cell type and transplanted into the patient; alternatively, directed differentiation of the patient-specific iPSCs into the affected cell type (left) will allow the patient's disease to be modeled *in vitro* and used to screen potential drugs, aiding in the discovery of novel therapeutic compounds.

Recent research showed the existence of numerous subtle but substantial molecular differences between ESCs and iPSCs, probably owing to technical limitations inherent to reprogramming procedure (Robinton & Daley 2012). It is

also unclear whether iPS would completely evade an immune response when returned to the patient, because a recent study has shown the immune rejection of teratomas formed form iPSCs (Zhao et al. 2011), even in syngeneic mice. These concerns have been addressed, in part, by more recent studies indicating that these genetic and epigenetic abnormalities may be obviated with careful generation, culture and selection of iPSCs(Hussein et al. 2011). Although pluripotent stem cells themselves are capable of forming teratomas *in vivo*, once they are differentiated into lineage committed cell fates, it is likely that the differentiated progeny will maintain their phenotype *in vivo* (Huang et al. 2012).

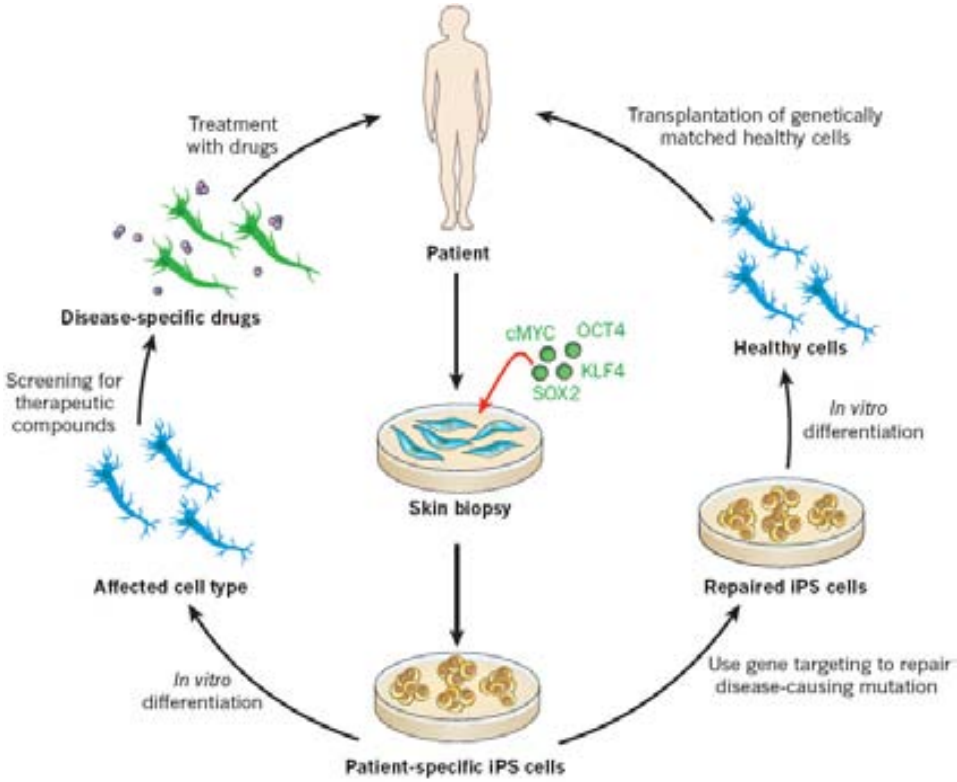

Fig. 4. Medical applications of induced Pluripotential Stem Cells (iPSCs). From Robinton and Daley, 2001.

1.1.2. Multipotent Stem Cells

Multipotent stem and progenitor cells can be derived from a variety of adult and fetal sources, including bone marrow, adipose tissue, muscle, lung and pancreas (da Silva Meirelles et al. 2006; Pittenger et al. 1999). Multipotent stem cells are identified based on their expression of multiple cells surface glycoproteins, as no one antigen is sufficient.

Unlike pluripotent stem cells, multipotent stem cells have limited self-renewal capacity and can only give rise to limited types of committed progeny. Since multipotent stem cells can be harvested autologously and because their application has lower regulatory hurdles, clinical trials of multipotent stem cells are furthest advanced in comparison to iPSC or ESC based therapies.

Traditionally, adult stem cells have been viewed as cells committed to producing mature cells from the tissue of origin but not cells of unrelated tissues. The first evidence of plasticity or transdifferentiation stemmed from the observation that, following gender mismatched bone marrow transplants, some donor cells could be found in multiple organs of the recipient, having adopted the characteristics of cells of the organ in which they had lodged. Various reports over the last years challenged this dogma by demonstrating that adult stem cells, under certain microenvironmental conditions, give rise to other cells types besides the original cell type, indicating that they can switch cell fate. This phenomenon has been termed “stem cell plasticity”.

Mesenchymal Stem Cells (MSC)

The most studied adult stem cell, the hematopoietic stem cell (HSC), resides in the bone marrow. They are responsible of production and maintenance of all the mature blood cells. Within bone marrow, hematopoiesis occurs in association with an heterogeneous population of non-hematopoietic cells, including mesenchymal cells, connective tissue-type cells, and their associated

extracellular matrix (ECM) components and growth factors, which as a collective, constitute the stroma of the bone marrow (Bonnet 2003).

Friedestein et al (Friedenstein et al. 1970) were the first to demonstrate the existence *in vitro* of stroma cell precursors using the CFU-F assay (colony forming unit resembling fibroblasts). The considerable heterogeneity of the CFU-F derived colonies in terms of morphology, size, proliferation, and developmental potential led to the hypothesis for the existence of a hierarchical organization of the stroma cell compartment with a pluripotent, self-renewing stroma stem cell (also known as bone marrow stromal stem cell, or bone marrow mesenchymal stem cell, BMSC) at the top of this hierarchy (Owen & Friedenstein 1988).

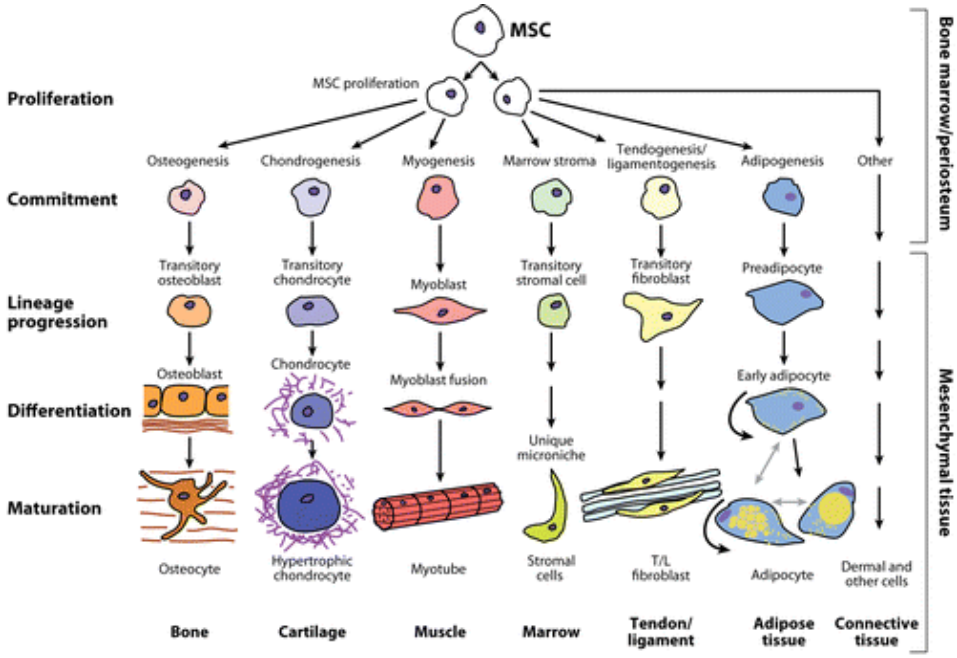

Fig. 5. Mesenchymal Stem Cell (MSC) potential. From Singer and Caplan, 2011.

BMSC can differentiate into mesoderm tissues, including bone, cartilage, fat, tendon, ligament and muscle (Chamberlain et al. 2007; Pittenger et al. 1999;

Colter et al. 2001; Schäffler & Büchler 2007) (*Fig. 5*). Although not immortal, they have the ability to expand manyfold in culture while retaining their growth and multilineage potential. Furthermore, they are easy to isolate, to maintain and expand *in vitro* with minimal requirements. All these properties make BMSCs promising candidates for TE. However, the clinical use of BMSCs has presented problems, including pain, morbidity and low cell number upon harvest (Zuk et al. 2002; Pittenger et al. 1999).

Adipose tissue, like bone marrow, is derived from the mesenchyme and contains a supportive stroma that is easily isolated. It has been demonstrated that human adipose-derived mesenchymal stem cells (hAMSCs) have a similar *in vitro* differentiation potential that BMSCs (De Ugarte et al. 2003). Furthermore, AMSCs have shown a superior proliferative capacity (De Ugarte et al. 2003; Nakagami et al. 2006). Based on this, adipose tissue may represent a source of stem cells that could have far-reaching effects on several fields. The advantage of adipose tissue as a source of multi-lineage cells is its relative abundance and ease of procurement by local excision or suction-assisted liposuction.

Factors such as donor age, type (white or brown adipose tissue), and localization (subcutaneous or visceral) of the adipose tissue, type of surgical procedure, culturing conditions, exposure to plastics, plating density, and media formulations might influence both proliferation rate and differentiation capacity of AMSCs (Schäffler & Büchler 2007).

1.2. Biomaterials

The role of biomaterials in TE has evolve from their first applications in orthopedics, where biomaterials were just synthetic substitutes for bone giving structural support, to the latest smart materials, that are able to interact with host cells to induce regeneration and fully integrate into the new formed tissue.

According to Polak and Lench (Polak & Hench 2005), an ideal scaffold for TE and regeneration:

- is made from a material that is biocompatible, that is, not cytotoxic;
- acts as a template for tissue growth in three dimensions;
- has an interconnected macroporous network with pore diameters in excess of 100 um for cell penetration, tissue ingrowth, vascularization and nutrient delivery throughout the regenerating tissue;
- bonds to host tissue without formation of intervening scar tissue;
- exhibit a surface texture and chemistry that promotes cell adhesion, adsorption of biological metabolites, including growth factors;
- influences the genes in stem cells to enhance differentiation and proliferation of all the phenotypes required for tissue regeneration while not altering clonogenic or proliferative potential of the cells.
- resorbs as the same rate as the tissue is repaired, with degradation products that are nontoxic and can be easily excreted;
- can be produced in irregular shapes to match the tissue defect;
- has mechanical properties sufficient to withstand applied stresses in clinical applications;
- has the potential to be commercially produced to the required ISO (International Standards Organization) and FDA (Food and Drug Administration) regulatory standards at a cost suitable for routine clinical use;
- does not alter clonogenic and proliferative potential of stem cells.

1.2.1. Ceramic Biomaterials

Ceramic materials were the first materials developed for use inside the human body. They were chosen for their mechanical properties and their “inertness”. Later, bioactive synthetic ceramics were developed, such as hydroxyapatite (HA), tricalcium phosphate or calcium phosphate. Ceramics have been used for clinical bone engineering for more than two decades, as they have proved osteoinductive and osteoconductive capability, but they present some important limitations, as a very slow resorption rate and the lack of interconnected pores, that difficult the ingrowth of new bone (Zippel et al. 2010).

1.2.2. Natural Biomaterials

Tissue-derived materials such as decellularized ECM, collagen, fibronectin, chitosan, gelatin, hyaluronate and alginate are widely used for tissue regeneration approaches. These naturally derived materials have the potential advantage of biological recognition that may positively support cell adhesion and function. However, they may exhibit immunogenicity and contain pathogenic impurities. There is also less control over their mechanical properties, biodegradability, and batch-to-batch consistency. Many of them are also limited in supply and can therefore be costly.

There are several concerns over the use of natural polymers as scaffolds for TE, including the risks of pathogen transmission and immunorejection associated with natural materials from animal and cadaver sources.

Decellularized matrices

Tissues and organs can be completely decellularized preserving their three-dimensional architecture with the abundant capillary network. Acellular xenogeneic scaffolds have the unique potential for host cell recolonization

without inducing an immunogenic response, since the amino acid sequence and quaternary structure of many ECM proteins are highly conserved among various species (Fitzpatrick et al. 2010).

Scaffolds derived from xenogeneic ECM have been used in numerous TE applications for several decades. The safety and efficacy of such scaffolds has been shown in both preclinical animal studies and in human clinical studies. They have been used for the repair and reconstruction of numerous body tissues including musculoskeletal, cardiovascular, urogenital and integumentary structures (Badylak et al. 1995; Cobb et al. 1996; Kochupura et al. 2005).

These scaffolds are typically prepared from porcine organs such as small intestine, urinary bladder or heart, which are subjected to decellularization and sterilization without significant loss of the biologic effects and the mechanical integrity of the ECM. The composition of these scaffolds includes the structural and functional proteins that are part of native mammalian ECM, presenting a three-dimensional organization that distinguishes these decellularized matrices from synthetic scaffold materials and is associated with constructive tissue remodeling instead of scar tissue (Badylak 2004).

Collagen

Of the naturally-derived materials, collagen is the most often used. It is the principal structural protein in mammals, being a main component of ECM of mammalian tissues including bone, cartilage, tendon, ligament, skin, etc. About of 25 types of collagen differing in their chemical composition and molecular structure have been identified so far while type I collagen is known to be the most abundant one of all (Liu & Ma 2004). Collagen is composed of three polypeptide chains that form a triple helix (Fig 6).

Collagen has been used commercially in various medical applications and wound dressings since the 1970s. Particularly, collagen is clinically well established and FDA approved matrices for wound healing to treat burns and chronic wounds (Still et al. 2003; Harding et al. 2002; Nambu et al. 2011). It is also widely used in regenerative applications of different organs and tissue as the urethra (Micol et al. 2012), the cornea (Krishnan et al. 2012; Mi et al. 2011), skin (Gaspar et al. 2011) and skeletal muscle (Yun et al. 2012), usually in combination with other biomaterials or growth factors.

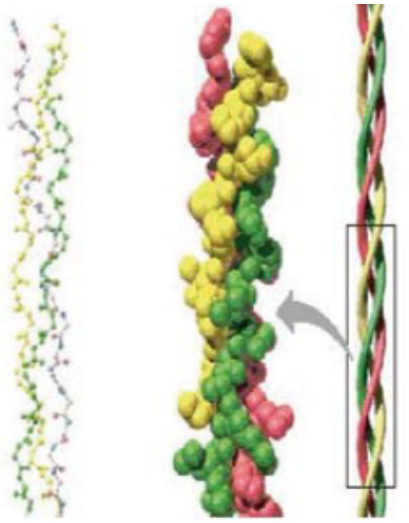

Fig. 6. Structure of collagen. ©Addison Wesley Longman, Inc.

Fibrin

Fibrin is a fibrous protein involved in the clotting of blood. It is formed from fibrinogen by the protease thrombin (*Fig. 7*). Fibrin-based materials are biocompatible and biodegradable and support angiogenesis and tissue repair. In addition, fibrin naturally contains sites for cellular binding and has been shown to have excellent cell seeding effects and good tissue development (Ye et al. 2000).

Fibrin can be produced as autologous scaffold material from as few as 50 mL of the patient's own blood. Completely autologous production lowers the possibilities of an inflammatory reaction due to a foreign body reaction or foreign antigenic epitopes, as well as the possibility of disease transmission (Cornelissen et al. 2012). Fibrin has the approval of Food and Drug Administration (FDA) for biomedical applications.

Furthermore, an interesting characteristic of fibrin gels is that they are obtained by the mixture of two liquid solutions, which allows the creation of complex geometries by using molds or the possibility of directly injecting both components as liquid solutions in the injure site to form the gel *in situ*.

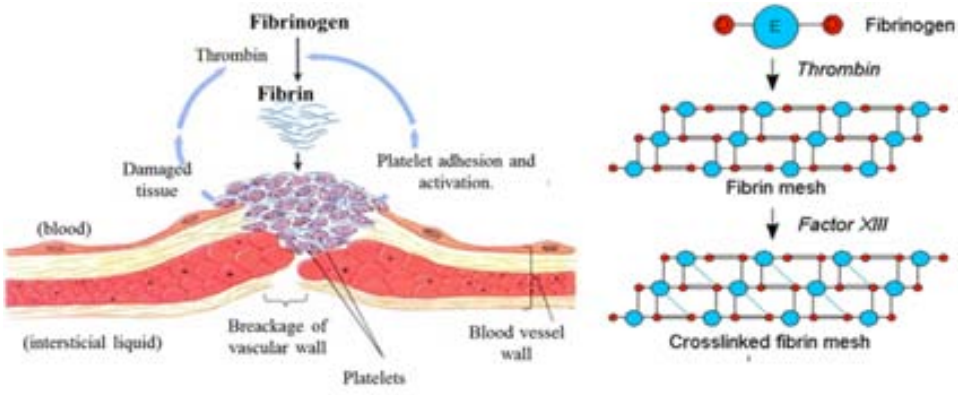

Fig. 7. Left: Biological process of fibrin mesh formation. Right: Changes on fibrinogen structure due to thrombin and Factor XIII. Adapted from Audesirk et al., 2003.

Fibrin gel use is limited by its mechanical weakness that requires *in vitro* culture of tissue-engineered constructs to provide a mechanically stable engineered tissue backbone. Nevertheless, fibrin has been studied as a biological scaffold in various TE applications, such as cardiac (Ye et al. 2000; Yuan Ye et al. 2011), muscle (Liu et al. 2012), spinal cord (Johnson et al. 2010), vascular(Shaikh et al. 2008) and respiratory (Cornelissen et al. 2012) regeneration.

Hyaluronic Acid (HA)

Hyaluronic acid (HA, hyaluronan) is a polysaccharide found in the connective tissue of virtually all animals and has been assigned important functions in a number of cellular processes, such as stabilizing and organizing the ECM, regulating cell adhesion and motility, and mediating cell proliferation and differentiation (Fraser et al. 1997; Cheung et al. 1999; Entwistle et al. 1996).

HA is a lineal polysaccharide composed of β–D-glucoronic acid and N-acetyl-β-D-glucosamine (Fig. 8).

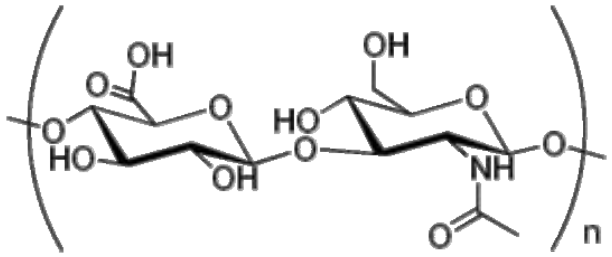

Fig. 8.Molecular structure of hyaluronic acid.

HA is easy to produce and modify, hydrophilic and naturally biodegradable, thus a suitable material for TE. Furthermore, HA is non-immunogenic and has unique viscoelastic and physiochemical properties with potential use in TE applications, as for example, in wound healing (Kirker et al. 2002), cartilage regeneration (Yamane et al. 2005) or development of vascular grafts (Turner et al. 2004).

1.2.3. Synthetic Biomaterials

The advantage of using synthetic polymers over natural ones is that they are more readily available, can be produced in large scale with low cost, have no risk of immunogenicity, and are easier to process and reproduce. Their main disadvantage is that their degradation products may not be among the metabolites naturally found in the body and might lead to problems if accumulated in tissues (Demirbag et al. 2011).

Poly(α-hydroxy acids)

Poly(α-hydroxy acids), including poly(glycolic acid) (PGA), poly(lactic acid) (PLA) (*Fig. 9*) and their copolymer PLGA, are the most popular and widely used synthetic polymeric materials in bone TE. These polymers, having a long history of use as degradable surgical sutures, have gained FDA approval for certain

clinical uses as sutures, bone plates pins and screws (Böstman 1991; Middleton & Tipton 2000) and are reasonably biocompatible.

The ester bonds in these polymers are hydrolytically labile and they degrade non-enzymatically (Therin et al. 1992). The degradation products of PGA, PA and PLGA are nontoxic natural metabolites and are eventually eliminated from the body in the form of carbon dioxide and water (Liu & Ma 2004). The degradation rates of these polymers can be tailored to satisfy the requirements from several weeks to several years by altering the chemical composition, crystallinity, molecular-weight, and molecular weight distribution. These polyesters are thermoplastics and can be formed into desired shapes by molding, extrusion, and solvent processing (Hubbell 1995).

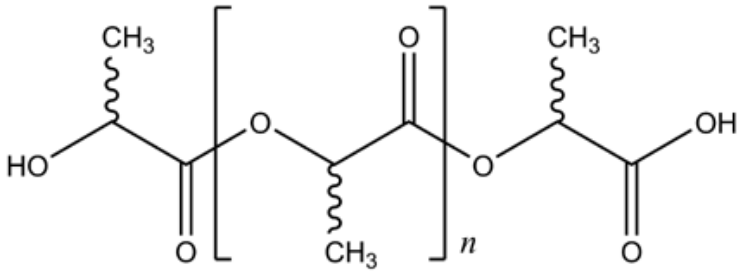

Fig. 9. Molecular structure of poly(lactic) acid (PLA).

These polymers have already been widely used in bone TE research (Kellomäki et al. 2000; Bolland et al. 2008; van der Elst et al. 1999) and there are ongoing research efforts in improving the functionality of these polymers to further expand their applications to areas like cartilage (Puelacher et al. 1994; Sherwood et al. 2002), central (Hurtado et al. 2011) and peripheral (Hsu et al. 2011; Evans et al. 2002) nervous system regeneration.

Other polymers have also been investigated for TE such as polyanhydrides, polycarbonates, polyphosphazene, polyfumarates, and poly(butylene terephthalate)/poly(ethylene oxide).

Polyethylene glycol (PEG)

Hydrogels made of PEG are highly biocompatible and exhibit versatile physical characteristics based on their weight percent, molecular chain length, and crosslinking density (Temenoff et al. 2002).

PEG hydrogels are attractive scaffolds to provide 3D templates in aqueous environments for tissue regeneration; however, PEG hydrogels typically exhibit minimal or no intrinsic biological activity due to the nonadhesive nature of PEG chains (Zhu 2010).

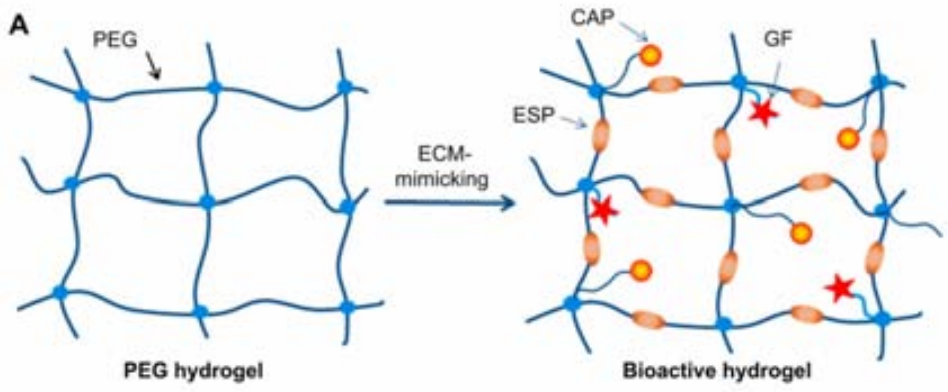

Fig. 10. Schematic Polyethylene glycol (PEG) modification to obtain bioactive gels. From J. Zhu, 2010.

Inspired by nature, researchers have developed a variety of bioactively modified PEG hydrogels (*Fig. 10*) to mimic the natural ECM (Tibbitt & Anseth 2009; Cushing & Anseth 2007). These modified hydrogels have been used in different TE applications, like cardiac (Shapira et al. 2008), brain (Marcano et al. 2012) or nerve regeneration (Scott et al. 2010).

1.2.4. Composite biomaterials

Most of the scaffolds used in TE are made of more than one material, trying to take advantage of the properties of each of the components. That's the case of

composites of a phosphate ceramic with a degradable polymer, that are widely used in bone TE since they combine appropriate mechanical and osteoconductive properties of the scaffold (Charles-Harris et al. 2008). Composites of collagen with ceramics or demineralized bone particles are also usual.

1.3. Bioactive Molecules

Recent research has demonstrated the relevance of some molecules, as growth factors, cytokines, vitamins or hormones, in guiding and modulating the differentiation of stem cells during tissue regeneration. These molecules interact with membrane receptors initiating a variety of signal cascades that result in the activation of proliferation, differentiation or migration processes (Fig. 11).

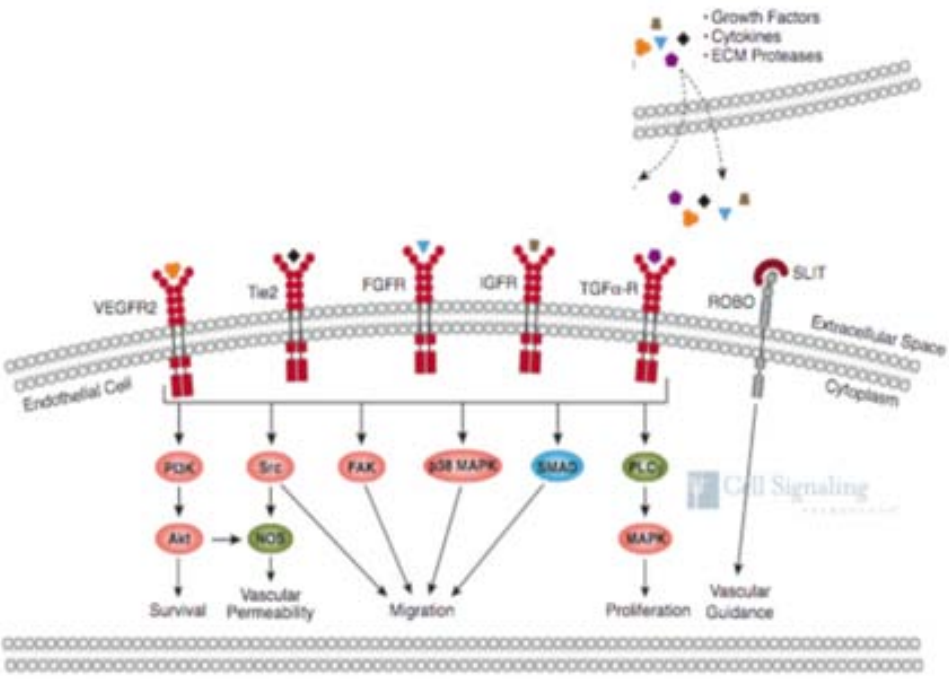

Fig. 11. Schematic representation of the interaction between soluble factors with membrane receptors and the posterior signal cascades. ©Cell Signaling Technology, Inc., 2008.

Within the bioactive molecules most frequently used in TE are growth factors and cytokines. These are proteins that by locally interacting with cell receptors usually at the membrane level, initiate reaction cascades that transfer information to the nucleus and stimulate cell specific proliferation and differentiation events. By stimulating angiogenic and regenerative processes resulting in better mechanical stability of the differentiated tissue, these factors have an important guiding role in the engineering of tissue repair to mimics the natural development process.

The most used growth factors for TE are:

- **Transforming Growth Factor-β (TGF-β).** TGF-β is a superfamily of mitogenic polypeptides that display reversible growth inhibitor activity and stimulate cell replication and ECM formation (Massagué 1990). They play a crucial role in cell proliferation, apoptosis and differentiation. Moreover, they are involved in the regulation of the cell cycle and immune system. TGF-β has been widely used in cartilage repair (Johnstone et al. 1998; Dickhut et al. 2010; Park et al. 2010).
- **Bone Morphogenetic Protein (BMP).** This protein, a member of the TGF-β1 superfamily, was first described by Urist about 40 years ago (Urist et al. 1973) and more than 14 types of human BMP have been described since. BMPs mostly influence bone, but also hematopoietic cell differentiation (Chadwick et al. 2003). BMPs induce MSC migration and their differentiation to the osteogenic phenotype (Lind et al. 1996; Reddi & Cunningham 1993), properties that have been exploited for therapeutic bone repair and regeneration (Kanakaris et al. 2009; Calori et al. 2008; Ronga et al. 2006; Grgurevic et al. 2011; Hollinger et al. 1998). Despite the significant evidence from animal models in support of the bone healing stimulatory effect of BMPs, future clinical investigations is required to better elucidate some still open questions, i.e. what is the ideal delivery

system for human BMPs, the suitable dosage, the actual concentration of BMPs at the graft sites (Calori et al. 2009), in addition to a better understanding of oncogenic safety issues surrounding the use of this factor.

- **Vascular Endothelial Growth Factor (VEGF).** VEGF is an endothelial-specific growth and chemotactic factor. VEGF was initially defined, characterized and purified for its capacity to induce vascular leak and permeability, as well as for its ability to promote vascular endothelial cell proliferation (Senger et al. 1983). Other members of the VEGF family were identified based on their homology to VEGF, including placenta growth factor (PICF) (Maglione et al. 1991), VEGF-B (Olofsson et al. 1996), VEGF-C (Joukov et al. 1996) and VEGF-D (Achen et al. 1998).
- **Fibroblast Growth Factor (FGF).** FGF was first described in 1975 (Gospodarowicz 1975). Today, FGF family comprises more of 20 related proteins involved in bone development. FGF-2, also known as basic Fibroblast Growth Factor (bFGF) increases cell proliferation and proteoglycans production. It is also commonly used as an exogenous culture medium supplement, adopted for the expansion stem cells in culture (Tasso et al. 2012). bFGF signaling is associated with the maintenance of a higher degree of "stemness" in a variety of stem cells, including MSC (Auletta et al. 2011).
- **Insulin-like Growth Factor (IGF).** IGF is a single polypeptide with protein sequence similar to that of insulin. It plays a key role in cartilage homeostasis, balancing proteoglycan synthesis and breakdown by the chondrocytes (Schmidt et al. 2006).
- **Platelet Derived Growth Factor (PDGF)**. PDGF is a polypeptide growth factor secreted from cytokine-laden granules of aggregated platelets early after tissue injury (Heldin & Westermark 1999). PDGFs comprise a family of mitogens for connective tissue cells such as smooth muscle cells, fibroblasts, and glial cells. Besides growth, the cellular effects of PDGFs

include chemotaxis, differentiation, and modulation of other cell functions such as the production of ECM components and contraction. Following its identification as a secretory product of platelets, PDGFs have been shown to be also synthesized by numerous normal cell types, including endothelial cells, monocytes/macrophages, smooth muscle cells, fibroblasts, placenta cytotrophoblasts, neurons, and certain glial cells. The PDGF family includes three dimeric ligands, PDGF AA, AB and BB, constituted by two polypeptide chains, PDGF A and B (Hart et al. 1990). In the adult, most of the proposed functions of PDGF relate to different responses to injury, for example, inflammation and wound healing (Levéen et al. 1994). This factor promotes the maturation of blood vessels by the recruitment of smooth muscle cells to the endothelial lining of nascent vasculature (Richardson et al. 2001). PDGF has also been shown to induce a potent chemotactic activity towards cells of mesenchymal origin, including fibroblasts, osteoblasts, chondrocytes and MSCs, and is thus believed to be capable of enhancing tissue regeneration and repair. (Phipps et al. 2012; Schmidt et al. 2006).

1.4. Mechanotransduction

Mechanotransduction, defined as the conversion of physical force into biochemical information, is relevant part of the physiology of many cell types and a fundamental agent guiding development. It provides the means by which cells respond to the environment, ensure structural stability, regulate morphogenetic movements to generate precise three-dimensional structures (Orr et al. 2006). Mechanical forces, such as applied forces or the rigidity of the ECM, are ever present in the cellular environment (*Table 2*) and crucially influence the form and function of cells and organisms. In the vascular system, pressure and shear stress from pumping blood influence the morphology and pathology of the heart and vasculature. Bone is shaped by forces from gravity

and muscle contraction. Hearing and touch are based on neural responses to pressure. Inflation and deflation of the lungs regulate their physiology.

Although is clear that common physiological processes expose cells to a variety of mechanical stimuli, how cells sense and integrate these forces at the molecular level to produce coordinated behaviors is an open question (C. S. Chen et al. 2004). The cellular components mainly involved in the signaling pathways include the membrane structures, such as caveolae, focal adhesions, stretch-activated ion channels, and integrins; intracellular signaling molecules, including G-proteins and mitogen-activated protein kinases (MAPK); and the cytoskeleton (Lionetti et al. 2011) (*Fig. 1*2). However, there still remains the question of how these cellular structures communicate with each other.

Physical Profile	Mechanical Stimulus	Typical Values	References
Arterial blood flow	Fluid shear stress	1–3 N/m^2	Davies, 1995
Cell migration	Traction stress	3.0–5.5 kN/m^2 (normal); 1 kN/m^2 (cancer)	Balaban et al., 2001; Munevar et al., 2001
Proximal tubule flow	Fluid shear stress Fluid drag force Bending torque	0.3 N/m^2 0.0074 pN/microvillus 0.016 pN-μm/microvillus	Guo et al., 2000
Stretch-activated channels	Membrane tension	0.012 N/m	Evans et al., 1976; Martinac and Hamill, 2002; Sukharev et al., 1999
Outer hair cell stereocilia	Compression stiffness Force/Δ membrane potential	0.001 N/m 0.1–20 pN/mV	Hallworth, 1995; Spector et al., 1999
Osteocyte processes (bone canaliculi)	Fluid shear stress Fluid drag force Tissue strain	0.8–3.0 N/m^2 20 × shear force 0.03%–0.1%	Weinbaum et al., 1994; You et al., 2001

Table 2. Estimated in vivo magnitudes of mechanical stimuli on cells. From Orr et al., 2006.

The role played by mechanical loading in the differentiation, maturation, and migration of stem cells during tissue repair/regeneration has begun to attract increased attention from several researchers. Recent studies showed that specific *in vitro* mechanical signals, in specially designed bioreactors, provide important adjuncts to biochemical signaling pathways for promoting engineered tissue growth (Doyle et al. 2009). Thus, the biomechanical aspects in TE become as important as biomaterial considerations.

Much of the work in this context has focused on musculoskeletal differentiation by MSCs, e.g., chondrogenesis has been demonstrated to be enhanced by dynamic compression in studies conducted by a number of groups using scaffolds including agarose, alginate and fibrin-polyurethane composites (Angele et al. 2004; Li et al. 2010; Mouw et al. 2007).

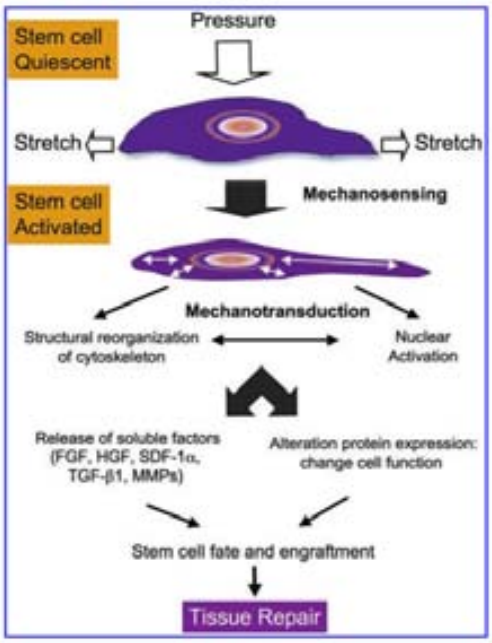

Fig. 12. Proposed mechanisms for stem cell activation by mechanical forces in tissue repair. From Lionetti* et al., *2011.

For example, high levels of shear stress (0.5-1 N/m^2) stimulate MSCs to release angiogenic growth factors and form microvessels (Lee & Niklason 2010), while moderate levels (<0.01 N/m^2) promote differentiation towards the osteoblastic lineage (McCoy et al. 2012; Sikavitsas et al. 2005; Zhao et al. 2007).

Future studies focused on a better understanding of the biomechanical pathways involved in mechanical signal transduction in stem cells will hopefully provide new insight to improve stem cell-based therapies.

2. CELL AND TISSUE CULTURE

2.1. 3D culture

When cells with therapeutic potential were first discovered, they were initially cultured and expanded in two-dimensional culture vessels such as plates or T-flasks. Nevertheless, in the body, nearly all tissue cells reside in an ECM consisting of a complex 3D fibrous meshwork with a wide distribution of fiber and gaps that convey complex biochemical and physical information. Additionally, the 3D microenvironment in which the different cell types are embedded are considerably different. Two dimensional culture substrates not only fall short of reproducing the complex and dynamic environments of the organism, but also are likely to misrepresent experimental findings by forcing cells to adjust to artificial flat and rigid surfaces (Lee et al. 2008). Thus, culture of cells in three dimensional structures would provide a more realistic model of a physiological environment (*Fig. 13*).

In addition to the biomaterial matrices mentioned in the previous section, a broad range of commercial matrices is also available, usually combining structural proteins and/or polysaccharides with an assortment of bioactive molecules. One of the most widely used is BD Matrigel™, a basement membrane matrix produced by a mouse sarcoma cell line. This matrix has been used to cultivate a large variety of cell types, like for example, ESCs (Ludwig et al. 2006) and iPSCs (Takahashi & Yamanaka 2006), and to perform angiogenesis assays both *in vivo* (Kisucka et al. 2006) and *in vitro* (Maeshima et al. 2001).

The use of these matrices facilitates the systematic analysis of cell behavior and the molecular events guiding it, significantly helping to improve our understanding of tissue physiology and pathophysiology.

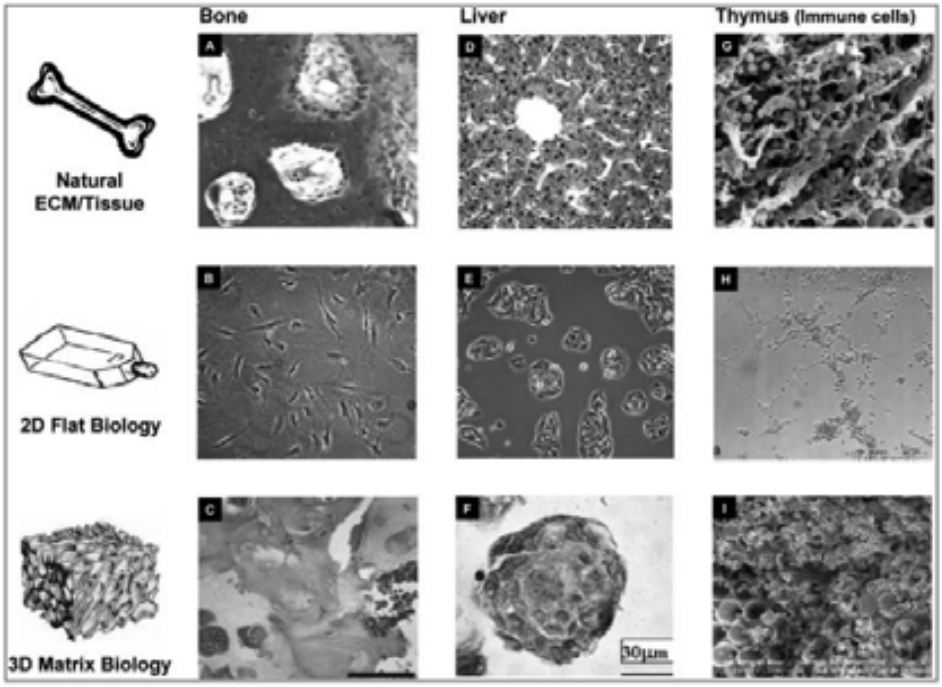

Fig. 13. Comparison of natural cell and tissue morphology cultured on 2D and 3D substrates. Histological images of (A) bone and (D) liver, and (G) scanning electron microscope image of the thymus. Optical microscope images of (B) osteoblasts, (E) hepatocytes, and (H) co-culture of lymphocytes and stromal cells. Cellular morphology becomes closer to that of natural tissue when cultured on 3D matrices; different appearance of (C) osteoblasts, F) hepatocytes, and (I) mononuclear cells. From Lee et al., 2008.

2.2. Bioreactors

Bioreactors are generally defined as devices in which biological and/or biochemical processes develop under closely monitored and tightly controlled environmental and operating conditions (e.g. pH, temperature, pressure, nutrient supply and water removal)(Martin et al. 2004).

Bioreactor systems play an important role in TE, as they allow safe and reproducible production of tissue constructs. For clinical applications, the use of bioreactors should be an advantageous method to produce materials with low contamination risk, ease of handling and scalability (Pörtner et al. 2005).

Bioreactors may also provide reliable model systems to investigate tissue growth under reasonably realistic conditions, (e.g. fluid flow, shear stress, etc.) providing technical means to perform controlled studies aimed at understanding specific biological, chemical or physical aspects of tissue regeneration.

2.2.1. Stirred-tank bioreactors

The supply of oxygen and soluble nutrients becomes critically limiting for the *in vitro* culture of 3D tissues. Because engineered constructs should be at least a few millimeters in size to serve as grafts for tissue replacement, mass-transfer limitations represent one of the greatest challenges to be addressed.

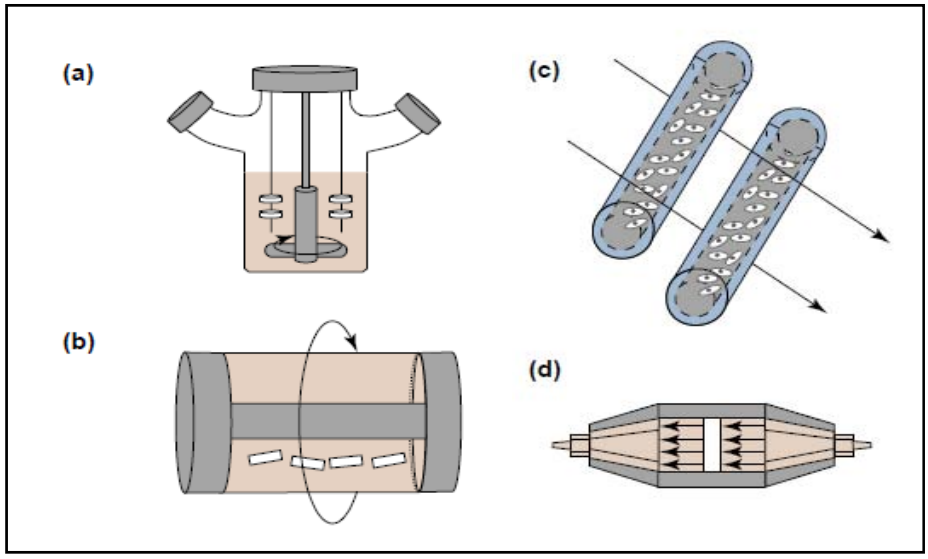

Fig. 14. Representative bioreactors for tissue engineering (TE) application: (a) Spinner-flask, (b) rotation-wall vessels), (c) hollow-fiber bioreactors, (d) direct perfusion bioreactors. Adapted from Martin et al.,2004.

External mass-transfer limitations can be reduced by cultivating constructs in a stirred flask (*Fig. 14*a). As one of the most basic bioreactors, the stirred flask induces mixing of oxygen and nutrients throughout the medium and reduces the concentration boundary layer at the construct surface, but also generates

turbulent eddies, which could be detrimental for the development of the tissue.
Depending on the type of cells cultured, it may be necessary to use microcarriers to allow attachment of adherent cells.

This type of bioreactors has been used for multiple TE applications like the expansion of hESCs (Krawetz et al. 2010), Neural Stem Cells (NSCs)(Ng & Chase 2008) and MSCs (Frith et al. 2010), the production of ESCs-derived osteoblasts and chondrocytes (Alfred et al. 2011) or tumor growth (Kang & Bae 2009).

2.2.2. Rotating-wall vessels

A dynamic laminar flow generated by a rotating fluid environment is an alternative and efficient way to reduce diffusional limitations of nutrients and waste while producing low levels of shear. Rotating bioreactors provide a dynamic culture environment to the constructs, with low shear stresses and high mass-transfer rates (*Fig. 14b*).
This type of bioreactor has mostly been used for bone (Nishi et al. 2012; Song et al. 2008) and cartilage (Buckley et al. 2009; Ohyabu et al. 2006) TE.

2.2.3. Hollow-fiber bioreactors

Hollow-fiber bioreactors can be used to enhance mass transfer during the culture of highly metabolic and sensitive cell types. In one configuration, cells are embedded within a gel inside the lumen of permeable hollow fibers and medium is perfused over the exterior surface of the fibers (*Fig. 14c*). This type of reactors has been used successfully to maintain the function of highly metabolic cells, e.g., hepatocytes (Mueller et al. 2011; De Bartolo et al. 2009), by increasing the mass transport of nutrients and oxygen.

2.2.4. Direct Perfusion Bioreactors

Direct perfusion bioreactors in which medium flows directly through the pores of the scaffold can be used for seeding and/or culturing 3D constructs (*Fig. 14d*). During seeding, cells are transported directly through the scaffold pores, yielding a highly uniform cell distribution. During culture, medium flowing through the construct enhances mass transfer, not only at the periphery, but also within its internal pores.

Perfusion bioreactors are widely used, because they allow to increase the mass transport of nutrients and oxygen and waste removal from the tissue culture environment. A particular type or perfusion, called interstitial or direct perfusion, is considered to be an important stimulus in the mechanobiology of several three-dimensional tissues, because hydrodynamic shear stresses may positively affect the cells viability, differentiation and protein production.

Perfusion bioreactors have been used for uniform and high-density cell seeding into scaffolds (Zhao & Ma 2005; Wendt et al. 2003), culture of cardiomyocytes (Carrier et al. 2002) and chondrocytes (Pazzano et al. 2000; Davisson et al. 2002), as well as for the study of osteogenic differentiation (Gomes et al. 2003).

2.2.5. Other bioreactors

Bioreactors that apply controlled mechanical forces, such as dynamic compression, to engineered constructs can be used as model systems of tissue development under physiological loading conditions, and to generate functional tissue grafts. Compressive deformation can be applied by a computer-controlled micro-stepper motor, and the stress on the constructs can be measured using a load cell. These bioreactors are mostly used for developing cartilage (Mouw et al. 2007; Puetzer et al. 2012) and bone grafts (McCoy et al. 2012; David et al. 2008).

2.3. Animal models

In vivo models are required when *in vitro* systems cannot provide a reproducible approximation of the real-life *in vivo* or clinical setting. Some obvious and common examples include the kinetics of delivery and distribution of drugs or bioactive factors; the biocompatibility and degradation properties of implant materials; the effect of intervention on the local secretion or release of cytokines and the flux and stability of *in vivo* cytokine gradients; the patterns and distribution of gradients associated with the mass transport of oxygen and other nutrients; the survival of cells and tissue after transplantation; the migration of cells through vascular systems (both immune/inflammatory response and stem cell or progenitor cell homing); the multicellular processes associated with budding angiogenesis and revascularization to reestablish the flow of blood in a tissue; the heterogeneous environment of mechanical stimuli associated with muscle contraction and mechanical deformation through extrinsic forces or intrinsic movement and vascular pulsation, etc. Although selected aspects of these processes can be studied *in vitro*, none of these environments or processes can be created reliably *in vitro* outside of very narrow and uniform conditions (Muschler et al. 2010).

Feasibility and bioactivity testing of implants for TE includes assessment of biocompatibility, toxicity, screening for adverse reactions and effectiveness, and is almost always done in small mammals, specifically in mice and rats. Genetic homogeneity (inbreed strains), availability of a great number of different transgenics, rapid occurrence of biological events, ease of handling and relatively low cost are some of the principal advantages of these models when compared with bigger animals.

In some settings, feasibility studies must be advanced into a larger animal, such as a rabbit, dog, sheep or goat. However, these settings are generally limited to just a few situations: (1) when the surgical procedure required cannot be

performed reproducibly in a smaller animal, (2) when the size of the implant or device under study exceeds the volume capacity of a smaller animal, and, similarly, (3) when there is the need to model effects of large diffusion distances or void volumes, as in the case of mass transport limitations in the survival of transplanted cells, or (4) when the effect of load must be taken into consideration.

Preclinical studies, where animal models are designed to create an environment that is as close as possible to the clinical setting in which a therapy will be applied, are also performed in larger animal species, biologically closer to human.

3. NONINVASIVE IMAGING

Despite their success, conventional microscopy methods (histopathological and cytological) suffer significant limitations when used for biological research. They usually require chemical fixation of tissues, involve the observation of biological samples under nonphysiological conditions, generally do not allow to investigate the dynamics of cellular processes, and most importantly, it has been very difficult to generate quantitative data using conventional microscopy (Phair & Misteli 2001).

Noninvasive imaging comprises a group of techniques that allow the monitoring of both the temporal and the spatial distribution of biological systems or specific probe molecules inside a living animal.

Noninvasive techniques are non-destructive, allowing the repetitive study of the same animal and the use of the same or alternative biological imaging procedures at different time points. Noninvasive procedures reveal dynamic and meaningful pictures of the progressive changes in biological parameters under analysis, while at the same time requiring fewer experimental animals, thus lowering research costs and animal suffering, an also appealing feature on ethical grounds.

Another benefit of noninvasive imaging assays is their quantitative nature. The images obtained are usually not just subjective or qualitative, as is the case with standard use of several conventional medical imaging modalities, but instead, usually provide meaningful numerical measures of biological phenomena. Such quantitative data could even be considered more useful that similar data obtainable *in vitro* or *ex vivo*, on account of preserving the intactness and the physiology of the experimental subject.

There has been considerable progress in the development of non-invasive small animal *in vivo* imaging technology. Magnetic Resonance Imaging (MRI),

Computed Tomography (CT), Positron Emission Tomography (PET) and optical imaging (bioluminescence (BLI) and fluorescence (FLI)) are the most popular techniques utilized by researchers in recent years (*Table 3*).

Imaging Technique	Portion of EM radiation spectrum used	Spatial resolution	Depth	Temporal resolution
PET	High-energy ɣ rays	1-2 mm	No limit	10 s to mins
SPECT	Lower-energy ɣ rays	1-2 mm	No limit	mins
BLI	Visible light	3-5 mm	1-2 cm	secs to mins
FLI	Visible or near-infrared light	2-3 mm	< 1 cm	secs to mins
MRI	Radiowaves	25-100 µm	No limit	mins to hours
CT/µCT	X-rays	5-200 µm	No limit	mins
Ultrasound	High-frequency sound	50-500 µm	mm to cm	Secs to mins

Table 3. Summary of the principal noninvasive imaging techniques used in biomedical research. Adapted from Massoud and Gambhir, 2003.

3.1. Magnetic Resonance Imaging

The fundamental principle underlying MRI is that magnetic dipoles, such as those of the proton, align themselves with the field lines when placed into a magnetic field. In a MRI scanner, a strong magnet produces a magnetic field surrounding the subject under investigation. The instrument contains also a radiofrequency coil that can produce a temporary radiofrequency pulse (with the corresponding magnetic component) to change the alignment of the nuclear spins. Following the pulse, the magnetic dipoles return or "relax" to their baseline orientation, producing an electromagnetic photon which is detected as a change in electromagnetic flux (Massoud & Gambhir 2003a) by the instruments antenna. An important function of the scanner is to determine the rate at which these dipoles relax to their baseline orientation following excitation; this measurement is translated into an MR signal. Dipoles, e.g.,

those of protons, in different physicochemical environments will have different MR frequencies (Jacobs & Cherry 2001). Thus, one of the main ways by which image contrast is achieved in MRI consists in using a central computer to scan the timing parameters of pulse excitation and recording, to probe the magnetic resonance of the target substance (usually water protons) and generate images representing levels of magnetic susceptibility. The two most frequently used timing parameters are known as T1 and T2 weighting. MRI is very sensitive to soft-tissue differences and abnormalities.

MRI has advantages over other imaging modalities. It produces higher resolution images, which falls within a micrometer range, compared to those generated by radionuclides and optical probes in the millimeters range. MRI is also attractive because of its low toxicity and low energy generating no ionizing radiation. In certain applications, MRI can simultaneously extract physiological, molecular and anatomical information. However, a disadvantage of MRI is that it is less sensitive than radionuclide or optical imaging technique and considerably more expensive.

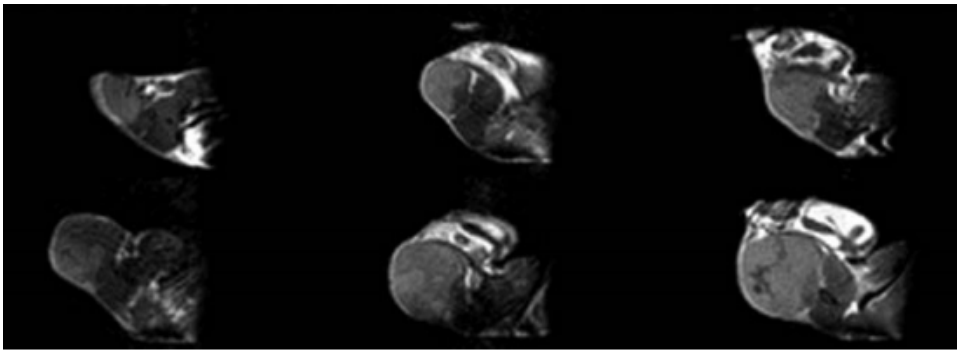

Fig. 15: Magnetic resonance images showing the growth of a subcutaneous (sc) tumor in mice. From top to bottom and from left to right: 9, 11, 13, 16, 18, and 20 days post inoculation. Adapted from Kersemans et al., 2012.

Recently, developments in animal MRI have focused on the development of new contrast agents that increase sensitivity and specificity.

MRI has been used to track MSCs (Bos et al. 2004), to measure tumor volume (Kersemans et al. 2012) and to monitor T-cell recruitment in tumors (Kircher et al. 2003).

3.2. Computed Tomography Imaging.

CT imaging is based, as is X-ray imaging, in the differential absorption of various-rays by tissues. A relatively low-energy X-ray source and a detector rotate around the subject, acquiring volumetric X-ray density data that a computer uses to generate 3D images. Most mouse CT images are collected with high-resolution phosphor screen/Charge Coupled Device (CCD) detectors to optimize image quality. The system spatial resolution is primarily limited by the pixel sampling rate, the X-ray source size and blurring in the phosphor screen. Resolution ranges from a few millimeters (clinical CT) to a few tens of micrometers (μCT), and even down to 100 nm (synchrotron radiation nano-CT) (van Lenthe et al. 2007).

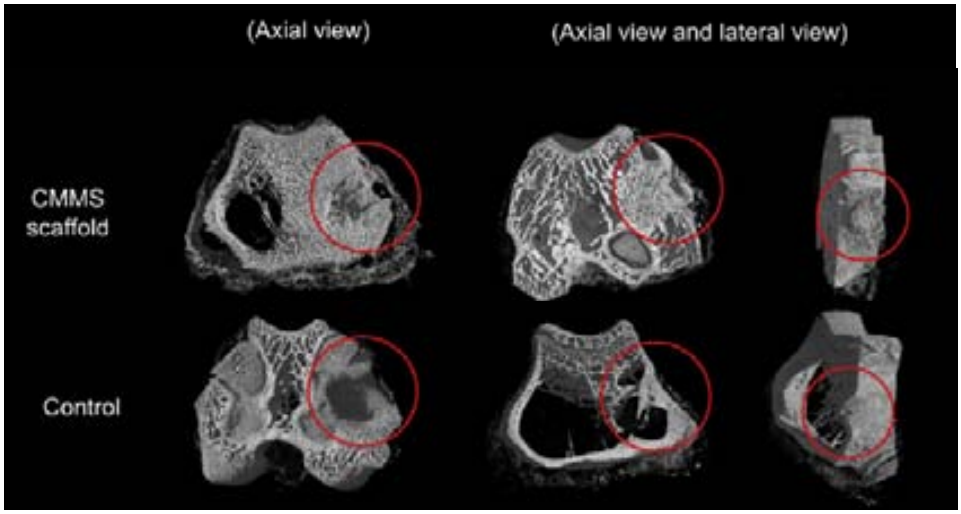

Fig. 16. Tridimensional reconstruction of cross-section images by Computed Tomography at 4 and 12 weeks after production of a cavitary defect in the rabbit femur. Adapted from Dai et al.,2011.

CT allows the generation of high-spatial resolution images in short periods of time. A typical scan of an entire mouse at a resolution of 100 µm would take about 15 minutes (Koo et al. 2006).

Unlike MRI, CT generates images with relatively poor soft-tissue contrast, often making it necessary to administer iodinated contrast media to delineate organs or tumors. Unfortunately, the use of contrast agent produces an ionization effect that results in radiation damage via superoxides and free radicals. Furthermore, the radiation dose of each scan is not negligible (0.6 Gy per scan; 5% of the LD_{50} for mice), thus this factors limit the possibility of repeated imaging of the same animal.

CT has been employed in non-invasive *in vivo* imaging to monitor colonic tumor growth (Pickhardt et al. 2005), to monitor bone regeneration (Gauthier et al. 2005; Dai et al. 2011) (*Fig. 16*), to detect tumors (Weber et al. 2004) and to analyze porous scaffolds (van Lenthe et al. 2007; Bohner et al. 2005).

3.3. Positron Emission Tomography and Single Photon Emission Computed Tomography.

PET records high-energy ɣ-rays emitted from within the subject. The underlying principle is that PET isotopes decay emitting β+ radiation (positrons) over time. Each positron undergoes an annihilation reaction with an electron, which results in the generation of two high energy ɣ-ray photons in opposite directions. The high energy ɣ-rays are detected by scintillating crystals and converted into visible light, which is detected by light sensors and imaging processing units.

Positron-emitting isotopes frequently used include ^{15}O, ^{64}Cu, ^{62}Cu, ^{124}I, ^{76}Br, ^{82}Rb and ^{68}Ga. Most of these isotopes are produced in a cyclotron and then chemically incorporated into a molecular probe. Labeled molecular probes or tracers can be introduced into the subject and imaged by PET to monitor their distribution and concentration. Many of the positron-emitting isotopes used

have relatively short half-lives of less than hours to days, so that the chemical reactions leading to incorporation of the isotope into the parent molecule and subsequent introduction into subject must take place relatively quickly. PET radiopharmacies exist throughout the world and are capable of providing commonly used PET tracers on a daily basis.

SPECT is a distinct form of radionuclide imaging that differs from PET in that isotopes emit only one gamma ray at a time that is detected using different instrumentation not allowing 3D imaging.

In recent years, small animal micro-PET scanners have been developed. Development of molecular imaging assays with PET is particularly advantageous because of the ability to validate probes in cell culture and small animal models prior to their use in established clinical PET centers. The ability to perform translational research from a cell culture setting to preclinical animal models to clinical applications is one of the unique and powerful features of PET technology.

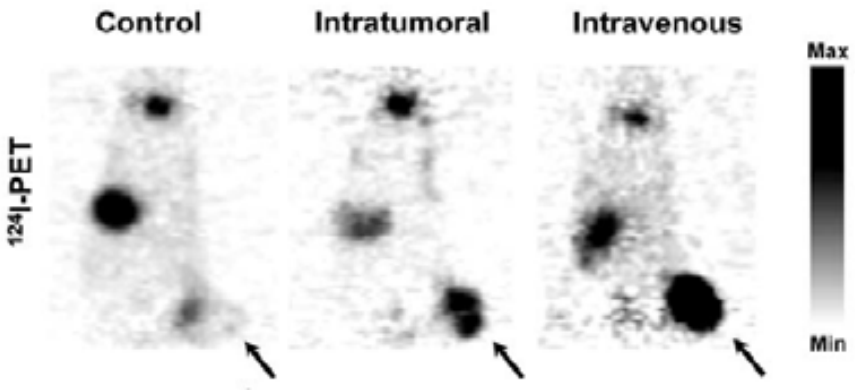

Fig. 17. Positron Emission Tomography (PET) imaging of a modified vaccinia virus replication in pancreatic carcinoma xenografts. Adapted from Haddad et al.,2012.

The major limitations of PET are its spatial resolution and image noise. Spatial resolution of PET scans is typically about 2^3 mm^3. Newer generation scanners

can achieve a resolution of about 1^3 mm^3 and have a relatively high sensitivity of approximately 10^{-11} to 10^{-12} mole/l.

PET has been used to localize MSCs implanted on mice and pig models (Miletic et al. 2007), to target tumor cells (X. Chen et al. 2004; Janssen et al. 2002) and to determine biodistribution of oncolytic virus (Haddad et al. 2012).

3.4. Ultrasound Imaging

Ultrasound imaging uses high-frequency sound waves to view soft tissues such as muscles and internal organs. High-frequency sound waves are emitted from a transductor, reflected in the tissue and then detected by a microphone. Each tissue reflects the sound with a different frequency based on their density and therefore, creates contrast images at 50-100 µm resolution (Ray 2011). Ultrasound is a real-time imaging modality, capturing data at up to 1000 frames per second. This means that not only is it capable of visualizing blood flow *in vivo*, it can even be used to study high speed events such as blood flow and cardiac function in mice. In addition, contrast agents in the form of microbubbles, which have different acoustic properties than those of tissues, can be introduced to highlight vasculature or to target specific receptors (Deshpande et al. 2010).

Micro-ultrasound systems have been specifically developed for small animal research, with frequencies ranging from 15 MHz to 80 MHz compared with clinical ultrasound systems which range from 3-15 MHz (Foster et al. 2009, p.15). Higher frequencies increase image resolution, however at the expense of penetration depth. Axial resolutions of 20-80 µm are achieved, allowing the visualization of tiny vascular structures. To image capillaries, this resolution can be further increased to 3-5 µm by injecting microbubble contrast agents. Furthermore, microbubbles can be conjugated to markers such as αvβ3 integrin and vascular endothelial growth factor receptors (VEGFR), in order to provide molecular visualization (Deshpande et al. 2010) (*Fig. 18*).

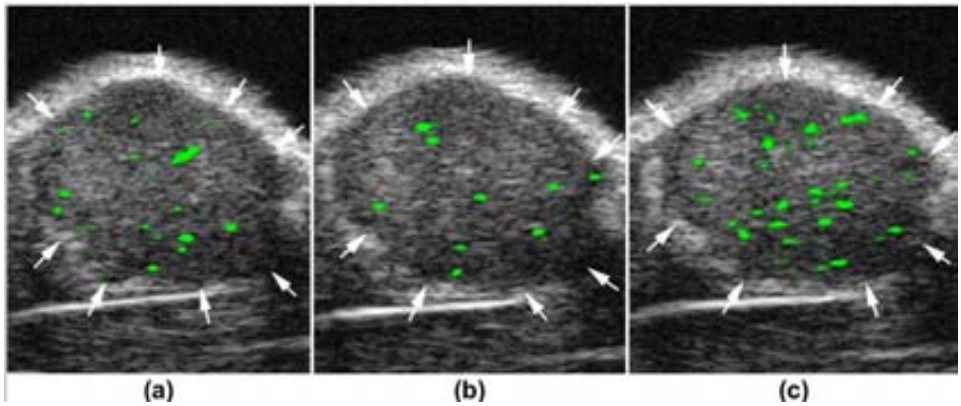

Fig. 18. Molecular ultrasound images of a sc human ovarian adenocarcinoma xenograft tumor (arrows) in a nude mouse after intravenous administration of singly-targeted microbubbles, targeted at vascular endothelial growth factor receptor type 2 (a) or αvβ3 integrin (b), and dual-targeted microbubbles (c). From Deshpande el al., 2010.

Non-targeted ultrasound contrast agents have been in clinical use for many years, however, the use of targeted microbubbles is currently still restricted to preclinical research.

Ultrasound systems present high spatial and temporal resolution, real-time imaging, non-invasiveness, relatively low costs, lack of ionizing irradiation and wide availability among the imaging community throughout the world. These are important advantages that will definitely lead to further development of this technique, both in preclinical research as well as in clinical applications.

3.5. Optical imaging

Molecular and cellular imaging has provided various techniques for identifying and tracking transplanted cells. MRI, CT, PET and SPECT offer deep tissue penetration and high spatial resolution. However, in small animal studies, these techniques are more costly and time consuming to implement compared with optical imaging.

Optical imaging techniques have already been developed for *in vitro* and *ex vivo* applications in molecular and cellular biology. An extension of this concept toward noninvasive *in vivo* imaging with light photons has led to the

development of fluorescence and bioluminescence imaging. Progress in optical molecular imaging strategies has come from the development of targeted bioluminescence probes, near-infrared fluorochromes, and red-shifted fluorescent proteins (Massoud & Gambhir 2003b).

A fundamental issue in optical imaging of living subjects is how to detect light emitted from within the subject's body, this being relevant to both bioluminescence and fluorescence imaging. In this regard, several technical advances for imaging of very low levels of visible light have emerged, based on the use of highly sensitive detectors. CCD detectors are made of silicon crystals sliced into thin sheets for fabrication into integrated circuits, using similar technologies to those used in making computer silicon chips. One of the properties of silicon-based detectors is their high sensitivity to light, allowing them to detect photons in the visible to near-infrared range. CCD cameras operate by converting the light photons that strike a CCD pixel with energy of just 2-3 eV into electrons. CCDs consist of a two dimensional array of photosensitive elements that convert incident photons in electrons that accumulate in potential wells having predetermined capacities. Reading of the accumulated charge after predetermined times reduces readout noise with an increase of signal to noise ratio. Moreover, in some devices, during the movement of electrons to the readout circuitry, an accelerating voltage can be applied that generates a signal amplifying cascade. In the newer-generation CCD cameras sensitivity is increased by reducing thermal noise, or dark current generated in the silicon lattice by thermal release of electrons by cooling to very low temperatures (-80^{o}C) Dark current falls by a factor of 10 for every 20^{o}C decrease in temperature (Spibey et al. 2001; Massoud & Gambhir 2003a). BLI CCD cameras are usually attached to a cryogenic refrigeration unit and mounted in a light-tight specimen chamber.

3.5.1. Fluorescence Imaging

Green Fluorescent Protein (GFP), a protein form the jellyfish *Aequorea Victoria*, has become very popular over the last decade as a reporter in fixed and live cells. Wild-type GFP emits green (509-nm) light when excited by violet (395-nm) light. The enhanced variant eGFP has a shifted excitation spectrum to longer wavelengths and has increased (35-fold) brightness (Massoud & Gambhir 2003a).

In fluorescence imaging (FLI), an excitation light of wavelength in the visible light range (396-600 nm) illuminates the living subject, stimulating electrons in fluorophors to a higher energy state. Return of excited electrons to the ground state, an event that happens within milliseconds of the absorption, results in emission of photons of lower energy (longer wavelength) that can be recorded by a CCD camera to generate images of the emitting source. This allows to image cells tagged with fluorescently labeled antibodies or that express fluorescent proteins.

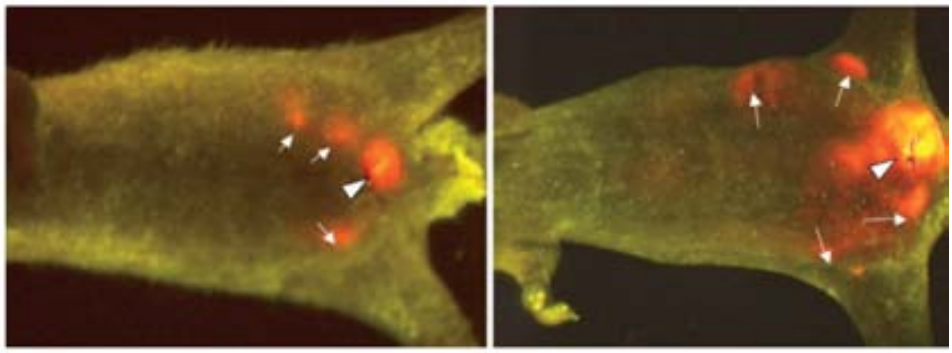

Fig. 19. Whole-body real-time fluorescent imaging of orthotopically-growing and metastasizing PC-3-RFP human prostate cancer in nude mice 2 and 4 weeks after implantation. Adapted from Yang et al., 2005.

The two main advantages of FLI are that it can be used as a reporter in both live and fixed cells/tissues and no substrate is required. However, these systems are not quantitative and the image information is surface-weighted (anything

closer to the surface will appear brighter compared with deeper structures). Moreover, many molecules in living organisms are fluorescent and compete with the signal from the fluorescent reporter.

FLI has been used to monitor bacterial infection (White et al. 2010; Hope-Roberts et al. 2011) and tumor growth and metastasis in mice (Yang et al. 2005; Suetsugu et al. 2012) (*Fig. 19*) among others.

In contrast to FLI in the visible light range, the use of the near infrared (NIR) spectrum in the 700-900 nm range maximizes tissue penetration and minimizes autofluorescence from non-target tissue (Rome et al. 2007). This is because hemoglobin and water, the major absorbers of visible and infrared light, respectively, have their lowest absorption coefficients in the NIR region (*Fig. 20*). Several NIR fluorochromes have recently become available that can be coupled to affinity molecules (peptides, antibodies) or that are activatable to bind proteins. This type of NIR fluorescence reflectance imaging is still limited to targets that are fairly near the illuminated surface.

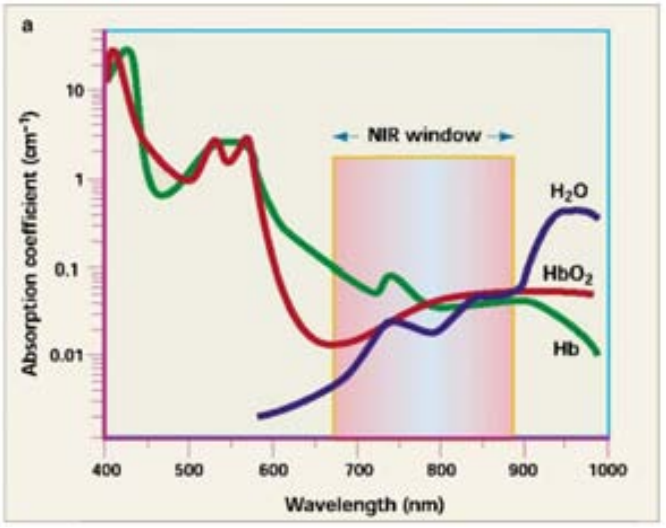

Fig. 20. Absorption coefficient of light in tissues. The absorption coefficient of light in tissue depends on wavelength and results from absorbers such as hemoglobins and water. Adapted from Rome et al., 2007.

A further development to FLI is Fluorescence Molecular Tomography (FMT). FMT employs a continuous pulse light from different sources to excite the fluorochrome label while multiple detectors in spatial arrangements similar to those of CT or MR scanners detect light to generate images with a 1-2mm resolution and nanomolar sensitivity (Ntziachristos et al. 2002; Ntziachristos & Weissleder 2002).

3.5.2. Bioluminescence Imaging

Luminescence consists on the emission of light photons as the product of a chemical reaction. All bioluminescent reactions are luciferase-catalyzed reactions of molecular oxygen with a luciferin (Wilson & Hastings 1998).

In nature, numerous luminous species exist in more than 700 genera, of which 80% are marine species (Widder 2010). Luciferase enzymes have been cloned from both marine and terrestrial eukaryotes and are commonly used as molecular reporters for *in vitro* and *in vivo* studies. Luciferases emit visible light ranging from the blue (>400 nm) to the red (>600 nm) and near-infrared regions of the spectrum, the latter been efficiently transmitted through mammalian tissues (Contag et al. 1998). These wavelengths can avoid the absorbing and scattering environment of mammalian tissues (Rice et al. 2001), thus, can be efficiently detected outside a small animal body using Bioluminescence Imaging (BLI).

In a bioluminescent reaction, the generation of light depends on several factors. Firefly *Photinus pyralis* luciferase (PLuc) requires ATP, Mg^{+2} and oxygen to catalyze the oxidation of its substrate D-luciferin to generate CO_2, AMP, inorganic pyrophosphate, oxyluciferin and a yellow-green light at wave-lengths that peaks at 562 nm (*Fig. 21*). By comparison, sea pansy *Renilla reniformis* luciferase (RLuc) catalyzes the oxidative decarboxylation of coelenterazine in the presence of dissolved oxygen to yield oxyluciferin, CO_2 and blue light that peaks at 480 nm (Lorenz et al. 1991).

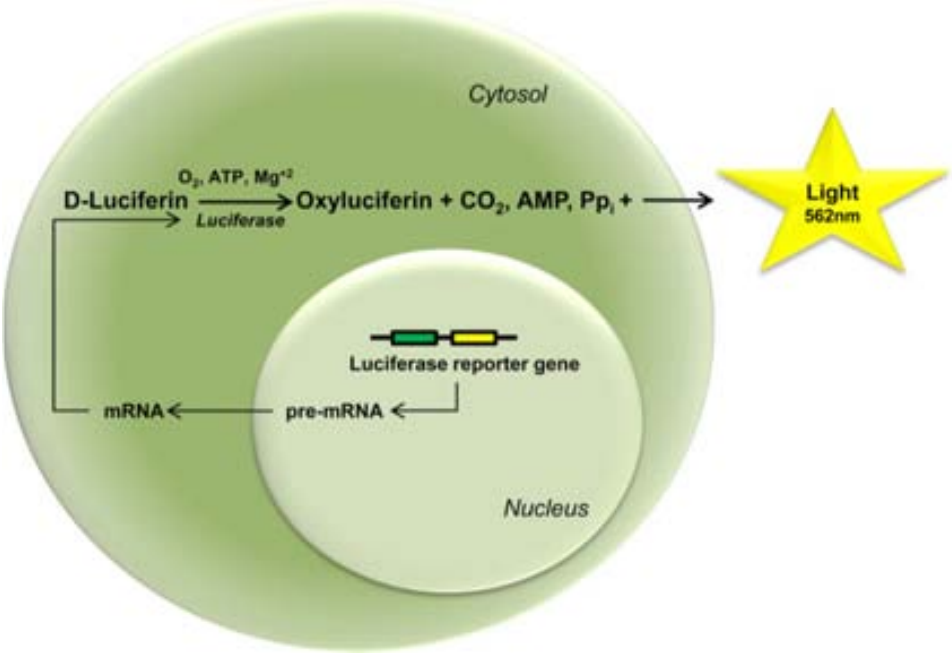

Fig. 21. Representation of the bioluminescence reaction of firefly luciferase. A cell expressing the firefly luciferase reporter gene produces the luciferase enzyme that in the presence of oxygen, ATP, and Mg2 catalyzes D-luciferin into oxyluciferin, CO_2, inorganic pyrophosphate (PPi), and light. From Almeida et al., 2001.

Noninvasive BLI is based on the use of high sensitivity CCD cameras to detect photons emitted by luciferase expressing cells implanted in live mice. Luminescent cells can be obtained directly by genetic modification (transduction) with luciferase reporter constructs or from transgenic luciferase-expressing mice. Once implanted in an animal, these cells can be tracked; following intraperitoneal (ip) or intravenous (iv) injection of a luciferase substrate in the anesthetized animal. To acquire images, the animal is placed in the light-tight chamber of the imaging system (*Fig. 22*) and bioluminescent photons generated by the luciferase reporter reaction are captured by a cooled CCD camera (Contag et al. 2000). Recorded BLI data can then be superimposed on b&w images of the mouse to register luciferase activity on the animal body (Wu et al. 2001). The sensitivity of detection depends on the wavelength of the light emission, expression, levels of the enzyme in the target cells, the location

of the source of bioluminescence in the animal, the efficiency of the collection optics, and the sensitivity of the detector (Wu et al. 2001).

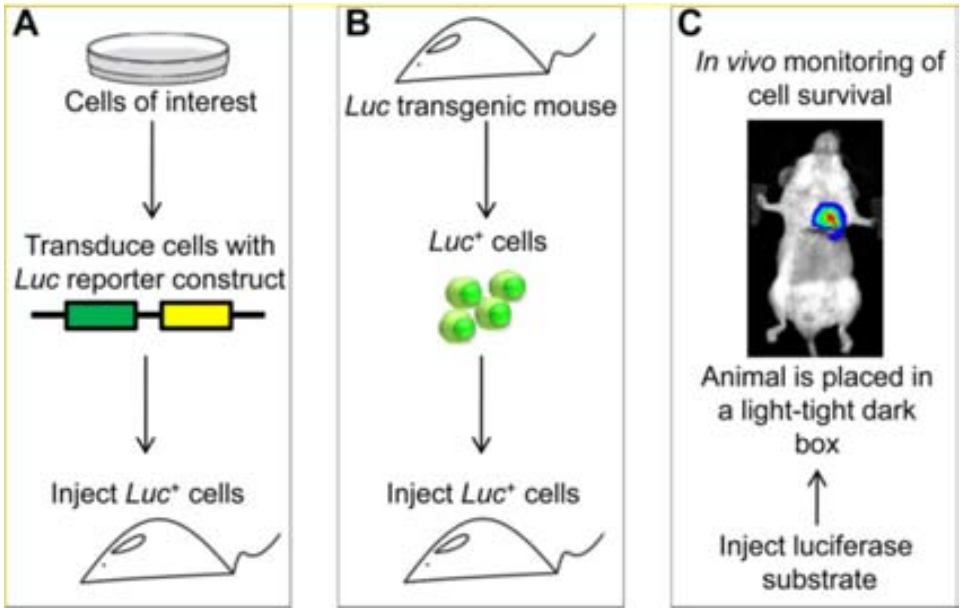

Fig. 22. Diagram illustrating steps required for bioluminescence imaging (BLI). A: therapeutic cells are transduced with a luciferase reporter construct and injected into an animal. B: alternatively, luciferase-expressing cells can be isolated from a luciferase transgenic animal and injected to the experimental subject. C: after substrate injection, a Coupled Charge Device camera can be used to localize the luciferase photon signals in vivo. Pseudo-colored images that represent signal intensity are overlaid with grayscale reference images of the animal to facilitate localization of the signal. From Almeida et al, 2001.

Reporter genes used for BLI.

Of the many naturally occurring luciferase enzymes, only a subset have been developed and used as reporter genes. Luciferase from the North American firefly PLuc is the most common choice, but other luciferases such as the sea pansy RLuc, the click beetle *Pyrophorus plagiophalamus* (PPLuc), and the copepod *Gaussia princeps* (GLuc) have also been investigated (31,32). GLuc and RLuc enzymes emit in the blue/green region of the UV visible spectrum, where light is strongly absorbed and scattered by tissues. Consequently, the imaging performance suffers from poor sensitivity and spatial resolution. On the

contrary, PLuc and PPLuc emit approximately 60% of their light at >600 nm, which enables great tissue penetration. PLuc has emission at 620 nm at 37°C, making it among the longest emitting luciferases at mammalian body temperatures and the most sensitive for *in vivo* applications (Zhao et al. 2005).

Mutations in luciferases can change the wavelength of the luminescence emitted. A mutation of a single amino acid has been shown to cause red-shifted luminescence and improve *in vivo* performance. Recently, a red-shifted mutant of PLuc was created and described to have an emission maximum of 612 nm at pH 7.0, a narrow emission bandwidth, and to be thermostable (with a half-life 8.8 h at 37°C vs. 0.26 h for the wild-type luciferase). This PLuc mutant, called Ppy RE-TS reporter, has been successfully used in small animals to visualize cancer progression and shown to have superior *in vivo* imaging performance compared with the wild-type PLuc (Branchini et al. 2010; Branchini et al. 2007).

The choice of reporter gene to be used should ultimately be based on the specific biological process to be monitored, the duration and intensity of the signal needed, and the tissue to be imaged (Cui et al. 2008; Zhao et al. 2005) (*Fig. 23*). As longer wavelengths of light penetrate mammalian tissues with less absorbance, PLuc (>600 nm) is more readily detected (Contag 2007). Moreover, its substrate D-luciferin remains in circulation longer than other substrates because it is poorly metabolized by mammalian tissues (Zhao et al. 2004). However, PLuc has the disadvantage of having a longer coding sequence compared with marine luciferases such as RLuc and GLuc. Another advantage of RLuc and GLuc over PLuc is the fact that they do not require ATP as a cofactor during bioluminescent reaction and thus can be used for imaging cells independent of their metabolic state (Bhaumik & Gambhir 2002). One particular characteristic of GLuc is that it is naturally secreted and therefore can be used as a reporter for quantitative assessment of cells *in vivo* by measuring its concentration in blood (Wurdinger et al. 2008). However, RLuc and GLuc produce shorter wavelengths of light (peaking at 480 nm), which are not

transmitted through tissues as effectively as PLuc (Zhao et al. 2005). Overall, the utility of RLuc and GLuc for *in vivo* BLI can benefit from improvements in sensitivity (Loening et al. 2007). Pharmacokinetics of its substrate coelenterazine are somewhat limiting *in vivo*. Coelenterazine is prone to quick inactivation, including degradation through autoxidation. This substrate is also costly, with low solubility. Furthermore, coelenterazine binds to serum proteins, is cleared rapidly from the bloodstream (Zhao et al. 2004) and decays rapidly with time (Bhaumik & Gambhir 2002). Therefore, when imaging *in vivo* with coelenterazine, the signal needs to be acquired immediately after substrate administration. On the other hand, this short half-life can be advantageous in cases in which sequential imaging of two luciferases is required to monitor two biological processes in tandem in the same animal (Bhaumik & Gambhir 2002).

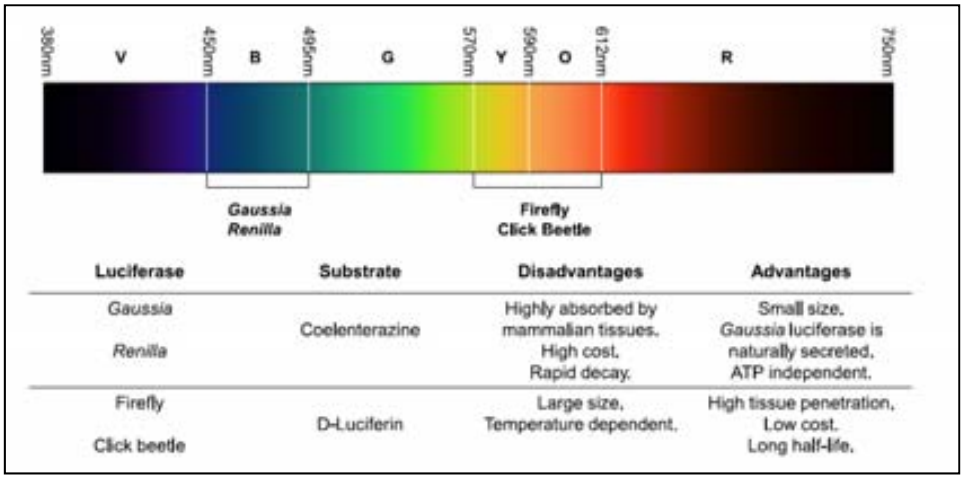

Fig. 23. Emission wavelengths for the most commonly used reporter luciferase enzymes in BLI and their advantages and disadvantages. V, violet; B, blue; Y, yellow; O, orange; R, red. From Almeida et al, 2001.

In summary, the development of reporter gene variants with better emission spectra, brightness, and stability can ultimately improve sensitivity and the overall performance of luciferases in BLI imaging studies. Moreover, cloning

new luciferases from different organisms, such as those from *Luciola italic* and *Cratomorphus distinctus*, can certainly improve current applications and make novel ones possible (Branchini et al. 2006; Viviani et al. 2004).

Vector mediated expression of reporter genes.

A fundamental requirement for BLI is the expression of a bioluminescent reporter gene by the cells to be imaged. This is generally accomplished by genetic manipulations to introduce an imaging reporter vector, comprising a luciferase gene driven by an eukaryotic promoter into cells *in vitro*, or alternatively, into embryonic cells to generate luciferase transgenic animals from which cells can also be (*Fig. 22*) (de Almeida et al. 2011).

Delivery of bioluminescent reporter genes to cells has been achieved through several means, but lentiviral-based gene transfer has been the method of choice because of its wide range of infectivity, effective gene delivery and high expression levels of transgenes in mammalian cells in culture as well as *in vivo* (De et al. 2008). Lentiviruses have the capability to deliver target genes to both dividing and nondividing cells and are capable of inserting genetic information into the host genome, ensuring prolonged gene expression with a more limited host immune response. The safety of the lentiviral vectors has been further improved with the generation of self-inactivating vectors and the use of minimal packaging systems. The efficiency of gene expression has been improved by the introduction of a relatively strong internal promoter such as cytomegalovirus (CMV). This promoter drives the expression of the reporter gene and guarantees that the reporter expression is always “on” under all conditions, in most tissue types. Moreover, lentiviral vectors can be used to simultaneously induce the expression of multiple genes in a cell. Coupling the expression of a gene with a luciferase reporter gene provides a simple yet effective mechanism for studying the regulation of gene expression and

monitoring it by BLI. This provides exciting opportunities for transcriptional targeting, double reporter labeling for BLI monitoring, as well as gene therapy. BLI has been used for monitoring different cell populations in the same animal for tumor cell therapy (M Vilalta et al. 2009; Alieva et al. 2012), or for analyzing survival and gene expression of MSCs during tissue regeneration (Bagó et al. 2012; Vila et al. 2012).

Limitations of BLI

BLI has been successfully used to obtain semiquantitative measurements of biological processes, because of a strong correlation between the number of cells and the bioluminescence signal detected both *in vitro* and *in vivo*. However, a simple quantification of light emission may not provide a true representation of biological processes. This is because the firefly luciferase reaction results from a complex interaction of a variety of molecules (e.g., ATP, Mg^{+2}, oxygen and luciferin) and because the intensity of the bioluminescence signal depends on multiple factors. In particular, the number of metabolically active luciferase-transfected cells, the concentration of luciferin, ATP and oxygen levels, the spectral emission of bioluminescence probes, and the depth and optical properties of tissues are known to alter the intensity of bioluminescence signal (Rice et al. 2001). Another issue that should be considered during quantitative BLI is the limited and wavelength-dependent transmission of light through animal tissues. Light sources closer to the surface of the animal appear brighter compared with deeper sources because of tissue attenuation properties (Weissleder 2001). It is estimated that for every centimeter of depth, there is a 10-fold decrease in bioluminescence signal intensity. Mathematical models can be used to predict *in vivo* imaging signal levels and spatial resolution as a function of depth and to help define the requirements for imaging instrumentation. However, the overall low spatial

resolution (3–5 mm range) and limited tissue penetrance restrict the use of BLI to small animal studies (Rice et al. 2001).

Changes in tissue oxygenation can also alter bioluminescence signal. Thus, for reliable BLI measurements, it is important to understand the effects of local niche in which the luciferase expressing cells of interest reside. Similarly, BLI quantification has to be carefully interpreted in studies that involve surgical procedures. Changes in tissue thickness because of the presence of inflammation, edema, sutures, and animal growth can alter light absorption and scattering as well as the bioluminescence signal (de Almeida et al. 2011).

IV. **OBJETIVES**

The general objective of this work was the development of analytical tools to aid in the generation of novel biomaterials for TE. More particularly, the objective was the development of a noninvasive imaging procedure for the analysis of cell behavior (proliferation and differentiation) in biomaterials implanted in live animals.

PART 1: Demonstrate the use of a BLI platform for *in vivo* analysis of cell behavior

1.1. Analyze the angiogenic capacity of a new composite biomaterial comprising poly(lactic acid) and calcium phosphate glass (PLA/CaP)

- Establish the *in vitro* and *in vivo* biocompatibility between the biomaterial and human adipose-tissue-derived mesenchymal stem cells (hAMSC).
- Monitor the differentiation state of hAMSC in the material.

1.2. Analyze the bone regeneration capacity of a new biomaterial comprising engineered fibrin binding growth factors.

- Study the effect of growth factors in the differentiation state of hAMSCs.
- Analyze the effect of growth factors in the formation of new bone.
- Analyze the effect of growth factors in the formation of new vasculature.
- Determine the role of hAMSCs in the formation of new bone and vasculature.

PART 2: Develop a miniaturized bioreactor system for systematic analysis of cells in scaffolds.

- Construction of a bioluminescence monitored bioreactor prototype
- Real-time imaging of cell seeding in a biomaterial.

- Long-time monitoring of cell number
- Real-time differentiation of hAMSCs in response to different stimuli.

V. MATERIALS AND METHODS

1. CELL TYPES

1.1. 293-T

Human cell line 293-T derives from embryonic kidney and constitutively expresses the SV40 large T antigen. It was obtained from the American Type Culture Collection (ATCC, Rochville, USA). This cell line is highly transfectable and it was used though this Doctoral Thesis for virus packaging.

293-T cells were maintained in at 37ºC in a 5% CO_2 atmosphere. Growth media composition was:

- Dulbecco's modified Eagle's Media-high glucose (DMEM-hg) with 4500g/mL of glucose (Sigma-Aldrich, Missouri, USA)
- L-glutamine 2mM (Sigma-Aldrich)
- Penicillin-Streptomycin (P/S) 50 u/mL (Sigma-Aldrich)
- 10% of Fetal Bovine Serum (FBS)(Sigma-Aldrich)
- 4-(2-hydroxyethyl)-1-piperazineethanesulfonic acid (HEPES) (Sigma-Aldrich) 25mM

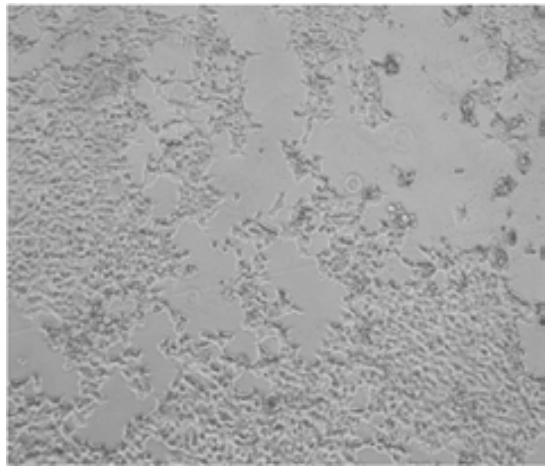

Fig. 24. Microphotography of a 293-T culture.

1.2. Human Adipose tissue-derived Mesenchymal Stem Cells (hAMSCs)

HAMSCs were isolated from adipose tissue derived from cosmetic subdermal liposuction of the lateral hip, with patient consent. After rinsing in Phosphate Buffered Saline (PBS), lipoaspirates were suspended in one volume of collagenase I (Invitrogen, Carlsbad, CA) solution and incubated 30 min at 37°C with gentle agitation. Digestion was terminated by inactivation of the collagenase I by addition of DMEM with 10% FBS. The resulting cell suspension was centrifuged at 450 g, and the pellet was washed in 50 mL Ringer's solution. The cell pellet was resuspended in 10 mL of erythrocyte lysis solution (0.16 M ammonium chloride) and incubated for 10 min at RT with gentle stirring. The suspension volume was completed to 50 mL with Ringer's lactate and centrifuged at 450 g. This step was repeated until no red color was detectable. The cell pellet was resuspended in 5 mL Ringer's lactate, filtered through a 70 m Nylon mesh, and centrifuged at 450 g. Cells resuspended in Ringer's lactate were counted using trypan blue to determine cell viability.

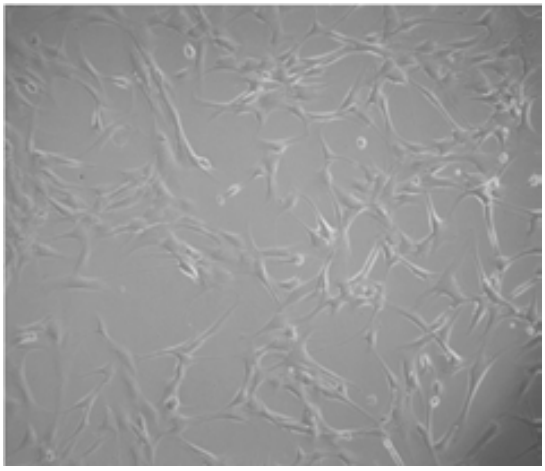

Fig. 25. Microphotography of a human adipose tissue-derived Mesenchymal Stem Cell (hAMSC) culture at passage 3.

HAMSCs were seeded at a density of 5,000 cells/cm^2, and incubated at 37ºC in at atmosphere with 5% of CO_2. The composition of the growth media used was:

- DMEM-hg
- L-Glutamine 2nM
- P/S 50 u/mL
- 10% of SBF

1.3. Cell freezing

Cell freezing media was composed of 90% of FBS and 10% of dimethyl sulfoxide (DMSO). Cell pellets were resuspended in cold (4^oC) freezing media at a concentration of 10^6 cells/ml and aliquoted into criotubes that were immersed in isopropanol and stored in a freezer at -80^oC to progressively cool them at a 1^o C/min rate.

For longer conservation times, cells were immersed in liquid nitrogen.

1.4. Human Adipose tissue-derived Mesenchymal Stem Cell characterization

1.4.1. Adipogenic differentiation

For adipogenic differentiation, hAMSCs were seeded at $8x10^4/cm^2$ the day previous to inducing the differentiation. Differentiation media was composed of:

- DMEM-hg
- 20% of FBS
- Isobutyl methylxanthine (IBMX) 0.5 mM of (Sigma-Aldrich)
- Indomethacin 60 µM (Sigma-Aldrich)
- Dexamethasone 10^{-6} M (Sigma-Aldrich)
- Risoglitazone 100 nM (Caiman Chemica, ann Arbor, USA)

Media was changed every 3 days during 3 weeks.

1.4.2. Osteogenic differentiation

HAMSCs were seeded at 1.5 x 10^4 cells/cm^2 and then induced to differentiate to the osteogenic lineage by the addition of the following differentiation media:

- DMEM
- 10% of FBS
- β-glicerolphosphate 2 mM (Sigma-Aldrich)
- L-ascorbic acid 50 µg/ml (Sigma-Aldrich)
- Dexamethasone 10^{-7} M
- Sodium dibasic phosphate 0.15 mM (Sigma-Aldrich)

Media was changed every 3 days during 3 weeks.

1.4.3. Condrogenic differentiation

HAMSCs were seeded at 1.5 x 10^4 cells/cm^2 and then induced to differentiate to the condrogenic lineage by the addition of the following differentiation media:

- 1:1 mixture of DMEM 4500 mg glucose and Ham's Nutrient Mixture F-12 (Sigma-Aldrich)
- 10% FBS
- L-Glutamine 2mM
- TGF-β1 10 ng/ml
- Dexamethasone 100 nM
- Insulin 6.24 g/ml
- Sodium pyruvate 110mg/l

Media was changed every 3 days during 3 weeks.

1.4.4. Analysis of cell surface marker expression

Flow cytometry analysis showed that HAMSCs were positive for the characteristic mesenchymal stromal cell surface markers, as shown in Table 4, and negative for surface markers expressed by other unrelated cell types such as endothelial cells or pluripotent stem cells.

Positive markers	Negative markers
CD9	CD11b
CD10	CD14
CD13	CD15
CD29	CD16
CD44	CD31
CD49a	CD34
CD51	CD45
CD54	CD49f
CD55	CD102
CD58	CD104
CD59	CD106
CD90	CD133
CD105	

Table 4. Surface markers expressed by hAMSCs

2. CELL LABELING

2.1. Lentiviral vectors constructs

Stable cell labeling of hAMSCs for expression of bioluminescence and fluorescent proteins was performed using viral vectors. As hAMSCs have a slow replication rate, lentiviral system, that is able to transduce non-replicating cells, was chosen.

2.1.1. Constitutive expressed vectors

Plox-G·PLuc construct.

This vector for expression of the fusion reporter PLuc-eGFP, referred to as "CMV:PLuc" was constructed as described previously (Bagó et al. 2012) by cloning the enhanced green fluorescent protein (eGFP) coding sequence from the pEGFP-N1 plasmid (Clontech Lab., Palo Alto, CA, USA) and the PLuc coding sequence from plasmid pGL4.10:PLuc (Promega Corporation, Madison, WI, USA) between the ClaI and BamHI sites of the lentiviral transfer vector Plox/Twgfp provided by Dr. D. Trono (École Polytechnique Fédérale de Lausanne) (*Fig. 26*).

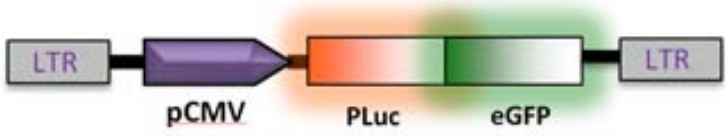

Fig. 26. Diagram of lentiviral vector Plox-G·PLuc . Sequences that integrate in the genome are those between LTRs.

CMV:hRLuc:mRFP:ttk construct.

This construct, abbreviated as CMV:RLuc, was kindly provided by Dr. S. Gambhir (Stanford University, USA). The construct contains a chimerical sequence comprising the coding sequences for the RLuc reporter gene and the

monomeric red fluorescent protein (mRFP1) gene under transcriptional control of the CMV promoter.

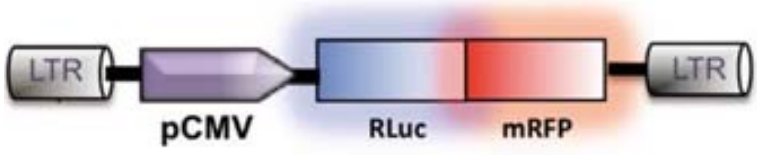

Fig. 27. Diagram showing the lentiviral vector CMV:hRLuc:mRFP:ttk construct. The genome integrating sequence is that comprised between the two LRTs.

2.1.2. Inducible promoter-regulated-expression vectors

The Plox-PLuc:eGFP lentiviral vector for expression of a fusion reporter comprising PLuc and eGFP, was obtained by polymerase chain reaction (PCR) amplification and standard cloning procedures as described (Bagó et al. 2012).

Plox:HRE-12p:PLuc:eGFP construct

The "Plox-HRE-12p:PLuc:eGFP" lentiviral vector for expression in hypoxic cells of the PLuc-eGFP chimerical reporter, comprises the PLuc and eGFP coding sequences under the control of 12 tandem repeats of the HRE binding sequence from the lactate deshydrogenase A (LDHA), phosphoglycerate kinase 1 (PGK1) and enolase 1 (ENO1) promoters. The vector was constructed as described (Bagó et al. 2012) by cloning the HRE-12p artificial promoter upstream of the chimerical Plox-PLuc:eGFP vector sequence (*Fig. 28*).

Plox:hPECAM-1p:PLuc:eGFP construct

The "Plox-hPECAM-1p:PLuc:eGFP" lentiviral vector for specific expression in endothelial cells of the PLuc-eGFP reporter, comprises the PLuc and eGFP coding sequences under the control of the Platelet/Endothelial Cell Adhesion Molecule-1 (PECAM-1) promoter. The vector was constructed as described

(Bagó et al. 2012) by cloning HPECAM-1p sequence (kindly provided by Dr.Bernabeu, Granada, Spain) upstream of the chimerical Plox-PLuc:eGFP sequence (*Fig. 28*).

Plox:hOCp:PLuc:eGFP construct

The "Plox-hOCp:PLuc:eGFP" lentiviral vector for specific expression in osteogenic lineage cells comprises the PLuc and eGFP coding sequences under the control of the human osteocalcin promoter (hOCp). The vector was constructed as described (Bagó et al. 2012) by cloning the hOCp fragment upstream of the chimerical Plox-PLuc:eGFP sequence (*Fig. 28*).

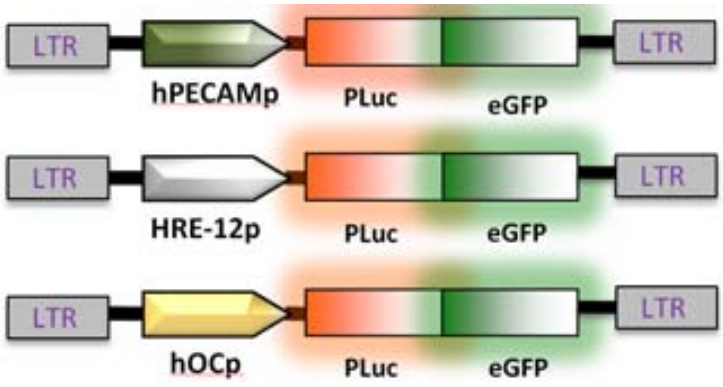

Fig. 28. Schematic representation of tissue specific/hypoxia controlled constructs.

2.2. Lentiviral particle production

Production of viral particles was performed using human embryonic kidney cells 293T (ATCC, CRL-11268™) grown in DMEM-hg, 10% heat-inactivated FBS, 2 mM L-glutamine, 50 U/ml P/S (Sigma), and HEPES 2 mM. The day previous to transfection, $4.5x10^6$ trypsinized cells were seeded on 10 cm^2 poly-D-lysine- (Sigma-Aldrich) treated plates. 6 µg of each lentiviral transfer vector was mixed with 2 µg of viral envelope plasmid (pMD-GVSV-G *env*) and 4 µg of packaging construct (pCMV ΔR 8.2) in 250 µl of 150mM NaCl. In a different tube, 48 µl of 1mg/ml Polyethylenimine (PEI) (Polyscience, Warrington, PA) were mixed with

202 µl of 150mM NaCl, and then added slowly to the vector solution. After 30 min of incubation at room temperature (RT) this DNA solution was added drop wise to the plate containing the 293-T cells plus medium, swirled gently and incubated for 16 h at 37^{o}C with 5% CO_2. The following day the transfection solution was removed, the cells were rinsed with PBS 1x and medium without FBS was added to the cells. Following a 48 h-incubation the supernatant was collected, centrifuged at 2000 r.p.m. to remove cell debris, and filtered through a 0.45 mm low protein-binding filter (Corning, Bath, UK).

2.2.1. Viral particles quantification

Virus titers were determined using flow cytometry to quantify cell transduction.

- On day 1, 3x10^5 293T cells/well were seeded in a 12-well plate.
- On day 2, one of the wells was used to count the number of cells. The rest of the wells were transduced with 500, 100, 50, 20 and 10 µl of crude supernatant. The volume was completed to 500 µl with fresh medium. Each transduction was performed in duplicate and one well was kept as nontransduced control.
- On day 5, percentage of cell transduction was evaluated by flow cytometry. Virus titer was calculated using the dilutions yielding 1% to 20% of transduction.

2.3. HAMSC transduction

HAMSCs were seeded at a density of 5,000 cells/cm^2 and grown in DMEM-hg, 10% heat-inactivated FBS, 2 mM L-glutamine, and 50 U/mL P/S. For transfection, Polybrene (hexadimethrine bromide)(Sigma-Aldrich) 8 µg/ml was added to the culture media. Concentrated virus were then added at a MOI=15 (2x10^6 TU/mL). After 24-48 h transfection media was changed for fresh media.

Efficiency of viral transduction was determined by detection of fluorescent proteins using a fluorescence microscopy or a flux cytometer.

2.3.1. Selection of transduced cells

Fluorescent-positive cells were selected by fluorescence-activated cell sorting (FACS). Approximately the highest 10% fluorescence expressing cells were selected.

In case of double labeling of cells with both a constitutively-expressed reporter gene and a specific-expressed gene, transduction was performed simultaneously with the same concentration for both vectors, so infection efficiency should be similar for both vectors, and then selecting for the constitutively-expressed gene by FACS.

3. BIOMATERIALS

3.1. Poly(lactic-acid)/calcium phosphate glass composite

This biomaterial was developed by Dr.J. Planell's laboratory (Institut de Bioenginyeria de Catalunya, IBEC, Barcelona, Spain).

3.1.1. Bioactive glass fabrication

Bioactive calcium phosphate (CaP) soluble glass was produced in the system $44.5P_2O_5$-$44.5CaO$-$6Na_2O$-$5TiO_2$ (molar %) as described (Navarro et al. 2004). Briefly, a homogeneous mixture of $NH_4H_2PO_4$, Na_2CO_3, $CaCO_3$ and TiO_2 was melted in a platinum crucible at 1350^{o} C for 3 hours, rapidly quenched and annealed at its transition temperature (533 ^{o}C). Glass particles were obtained after milling in an agate planetary mill.

3.1.2. Fabrication of the composites.

Biodegradable composites were elaborated as described (Navarro et al. 2004) by the solvent-casting method using NaCl as porogen agent. Briefly, PLA was dissolved in chloroform (5% solution w/v) in an orbital shaker at 200 rpm. NaCl particles in the range of 80-210 μm and glass particles of <40 μm size were then added and mixed to create an homogeneous paste that was casted in teflon moulds. Once the chloroform had evaporated at room temperature the scaffolds were unmoulded, immersed in distilled water for two days (3 water changes per day) to eliminate the NaCl and left to dry in air. The resulting structures presented a highly interconnected porosity (~95%), with a pore size diameter in the 80-210 μm range.

3.1.3. Seeding of scaffolds

Cylindrical samples of 5mm diameter and 3mm height were immersed in 70% ethanol and placed in a shaker overnight to improve water permeability, rinsed

several times with PBS, incubated in culture medium for 12-24 hours and then seeded with 100,000 cells distributed in 5 successive inoculations through the scaffold.

3.2. Engineered fibrin gels

Engineered fibrin gels were developed by Prof. J.A. Hubbell's Laboratory (École Polytechnique Fédérale de Lausanne, Lausanne, Switzerland).

3.2.1. Fibrin gel preparation

A "cross-linking" and a "fibrinogen plus growth factors" solutions were prepared separately and mixed in equal proportions just before implantation (Martino et al. 2011).

The "cross-linking" mix was obtained by mixing human thrombin 8U/mL, factor XIII 16U/mL and $CaCl_2$ 10 mM in HEPES buffer (HEPES 20 mM, NaCl 150 mM, pH 7.6).

The "fibrinogen+ growth factors" solution was obtained by mixing 24 mg/mL of human fibrinogen (plasminogen, vWF and fibronectin depleted, Milan Analytica AG, Switzerland), 68 μg/mL of aprotinin (Roche, Switzerland) and 10 μg/mL of the growth factors BMP-2 (PeproTech, USA) and TG-PDGF-BB (Laboratory for Regenerative Medicine and Pharmabiology, EPFL, Switzerland) in HEPES buffer (20 mM HEPES, 150 mM NaCl, pH 7.5).

Production and purification of α_2PI_{1-8}-PDGF-BB

Fibrin-binding PDGF-BB was engineered to contain, at the N-terminus, the factor XIIIa sensitive sequence derived from α2-plasmin inhibitor (α2PI1-8). Sequence encoding for α_2PI_{1-8}-PDGF-BB was synthetized by Genscript and subcloned into the mammalian expression vector pXLG (Protein Expression Core Facility, École Polytechnique Fédérale de Lausanne, Switzerland). A

sequence encoding for 6 His was added at the C-terminus for further purification of the recombinant protein. Suspension-adapted HEK-293E cells were routinely maintained in serum-free ExCell 293 medium (SAFC Biosciences, St. Louis, MO) with 4 mM glutamine as described (Muller et al. 2005). On the day before transfection, cells were inoculated into fresh medium at a density of 1 x 10^6 cells/ml. The next day, the cells were harvested by centrifugation at 1,200 rpm for 5 min and resuspended at a density of 100 x 10^6 cells in 5 mL of RPMI 1640 medium with 0.1% pluronic F68 (SAFC Biosciences) in a TubeSpin® bioreactor 50 tube (TPP, Trasadingen, Switzerland). Plasmid DNA of $\alpha_2PI_{1\text{-}8}$-PDGF-BB (125 µg) and linear 25 kDa PEI (250 µg; 1 mg/mL in H_2O; Polysciences, Eppenheim, Germany) were sequentially added and mixed. The culture was agitated by orbital shaking at 180 rpm in an ISF-4-W incubator (Kühner AG, Birsfelden, Switzerland) at 37°C in the presence of 5% CO_2. After 90 min, 95 mL of FreeStyle medium (Invitrogen) with 4 mM glutamine was added along with valproic acid (500 mM in H_2O) (SAFC Biosciences) to a final concentration of 3.75 mM (Backliwal et al. 2008). The culture was transferred to an incubator shaker at 37°C with 5% CO_2 with agitation at 110 rpm. At 7 days post-transfection, the cell culture medium containing $\alpha_2PI_{1\text{-}8}$-PDGF-BB was recovered by centrifugation at 1,500 rpm for 10 min and filtered through a 0.22 µm filter. Medium containing $\alpha_2PI_{1\text{-}8}$-PDGF-BB was loaded into a HisTrap HP 5 mL column (GE Healthcare), using an ÄKTA Explorer (GE Healthcare). After extensive washing of the column with binding buffer (10 mM imidazole, 20 mM NaH2PO4, 0.5 M NaCl, pH 7.4), $\alpha_2PI_{1\text{-}8}$-PDGF-BB was eluted with a gradient of 1 M imidazole (in 20 mM NaH2PO4, 0.5 M NaCl, pH 7.4) for 15 column volumes. Fractions of proteins were analyzed by SDS-PAGE and fractions containing $\alpha_2PI_{1\text{-}8}$-PDGF-BB were pulled together and further dialyzed against PBS overnight at 4 °C. The solution was then sterile-filtered through a 0.22 µm filter and concentrated with Amicon tube (10 kDa cutoff, Millipore), before storage at –80°C. The concentration of $\alpha_2PI_{1\text{-}8}$-PDGF-BB was determined using ELISA

(Human PDGF-BB DuoSet, R&D systems) and the protein was verified as >99% pure by SDS-PAGE and MALDI-TOF. The level of endotoxin was verified as under 0.01 EU/µg of protein (HEK-Blue LPS Detection Kit, InvivoGen).

Bioactivity of α_2PI_{1-8}-PDGF-BB

MSCs were starved overnight in MEM-α containing 2% serum. Starved MSCs were stimulated for 5 min with 20 ng/mL of wild-type PDGF-BB (Invitrogen), with 20 ng/mL of α_2PI_{1-8}-PDGF-BB, or with PBS. Then, cells were lysed with a lysis buffer (20 mM Tris, 137 mM NaCl, 1% NP-40, 10% glycerol, 2 mM EDTA, 1 mM activated sodium orthovanadate, pH 8.0) supplemented with protease inhibitor cocktail (Roche) and the lysates were stored at -80°C. The amount of phosphorylated PDGF-receptor β was quantified using phospho-ELISA kit (phospho-PDGF-R, R&D Systems). ELISA plates were coated with a capture antibody for PDGF-receptor β and further incubated with cell lysates. The phosphorylation states were detected with an anti-phospho-tyrosine antibody and normalized to a standard according to manufacturer instructions.

GF release from fibrin matrix

Fibrin matrices were made as previously described (Martino & Hubbell 2010) with human fibrinogen. Briefly, fibrin matrices were generated with 8 mg/mL fibrinogen (Fib 3, Enzymes Research Laboratories), 2 U/mL human thrombin (Sigma–Aldrich), 4 U/mL factor XIIIa (Fibrogammin, Behring), 5 mM $CaCl_2$, and 500 ng/mL of growth factor (PDGF-BB (Invitrogen), α2PI1-8-PDGF-BB, BMP-2 (R&D systems)). Fibrin gels were polymerized at 37°C for 1 h and transferred in Ultra Low Cluster 24-well plate (Corning Incorporated) containing 500 µL of buffer (20 mM Tris-HCl, 150 mM NaCl, 0.1% BSA, pH 7.4). A control well that served as 100% released control contained only the GF in 500 µl of buffer. Each 24 h, buffers were removed, kept at -20°C and replaced with fresh buffer. For the 100% release control well, 20 µL of buffer was taken out every day and

stored at -20°C. After 7 days, GF cumulative release was quantified using ELISA kits (human BMP-2 DuoSet, human PDGF-BB DuoSet, R&D Systems), using the 100% released control as reference.

3.2.2. Seeding of fibrin matrices

When used, cells were added to the "fibrinogen plus GFs" solution, after being washed twice with serum-free medium. Cells were resuspended in a volume that represents de 10% of the final gel volume.

Gel polymerization was performed *in situ*, by mixing both solutions just before injecting or depositing the solution

4. *IN VITRO* 3D SYSTEM

A transparent perfusion minibioreactor was developed to analyze cell distribution and behavior during and after seeding on a 3D scaffold.

The perfusion system was composed by the following components (*Fig. 29*):

- Medium reservoir placed in a heated bath at 36°C and provided with an agitation system.
- Peristaltic Pump.
- Perfusion chamber made of glass to allow light transmission placed inside a detection chamber of an ImagEM X2 System (Hamamatsu Photonics, Hamamatsu City, Japan) provided with a C9100-23B camera fitted with 512 x 512 pixel Charge Coupled Device (CCD) cooled at -80°C and an electron multiplier (EM).

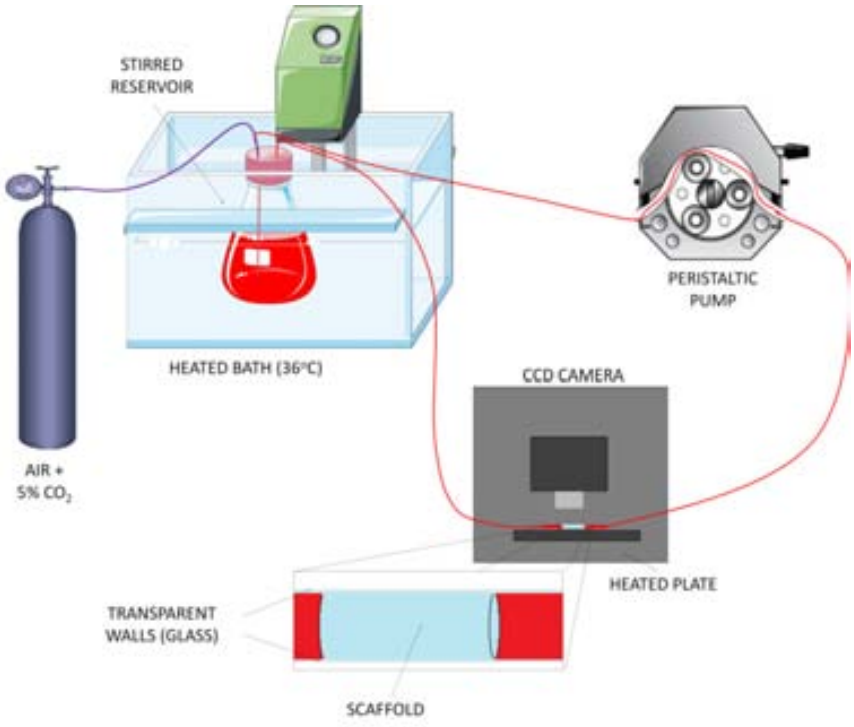

Fig. 29. Schematic representation of the perfusion system

Leibovitz L-15 medium (Sigma Aldrich), suitable for culturing hAMSCs in CO_2 free systems, was used to maintain physiological pH during the experimental time. In cases were a special medium had to be used, a CO_2 buffering atmosphere was generated by administration of a gas mixture containing 5% of CO_2, 20% of O_2 and 75% of N_2 to the medium reservoir.

4.1. Perfusion Scaffold seeding

For perfusion cell seeding, cylindrical scaffolds, 6 mm diameter and 12 mm height were immersed in 70% ethanol and placed in a shaker overnight to improve water permeability, rinsed several times with PBS, incubated in culture medium for 12 hours and then placed inside the perfusion chamber of the bioreactor system. The reservoir was filled with 100 mL of culture medium (L-15 medium, Sigma) pre-warmed (36^{o}C) and supplemented with 10% SBF, 1% of P/S and 1% of L-Glutamine) in which 2 million cells had been suspended. Following, the pump was switched on at the desired flow rate, and the solution circulated through the scaffold for at least 2 cycles.

4.2. Estimation of shear stress on cells

Shear stress resulting from fluid flow on cells adhered to the scaffold was estimated by modeling the scaffold geometry as a bundle of hollow cylinders arranged in parallel (Grayson et al. 2008). It was assumed that the pathways through the scaffold were straight tubes of uniform diameter between 80 and 210 μm according to the size of the pore generating agent (Koch et al. 2010). The fluid induced wall shear stress τ_w was calculated using the culture medium viscosity μ (770 cP) (Moreira et al. 1995; Grayson et al. 2008), the linear fluid flow velocity v, and the conduct diameter *d*. The equation used was derived for the Hagen-Poiseuille relation for laminar flow through a round conduit (τ_w= 8vμ/ds).

Actual flow velocities of 0.5, 2.2, 4 and 5.8 mm/s were adjusted to a sample porosity of 95 % (0.6, 2.3, 4.2 and 6.1 mm/s, respectively). Additionally for all velocities and diameters, the Reynolds number was calculated to ensure that the flow was laminar; a prerequisite for the use of the Hagen-Poiseuille relation. For fluid path diameters ranging from 80 to 210 µm, shear stresses of up to 0.47 Pa were estimated (*Table 5*).

Conduit diameter (µm)	Fluid flow velocity (mm/s)			
	0.57	**2.26**	**4.16**	**6.09**
80	0.04	0.17	0.32	0.47
210	0.02	0.07	0.12	0.18

Table 5. Wall Shear stress in tubular conduits was calculated to model shear stress in PLA and PLA with calcium phosphate glass (PLA/CaP) scaffolds of the indicated porosity.

4.3. Induction of endothelial differentiation

Endothelial differentiation of hAMSCs seeded in the scaffolds was induced by changing the culture media for an endothelial differentiation medium (EGM-2 BulletKit, Lonza, Switzerland), the utilization of a modified PLA scaffold containing CaP glass particles, which have been shown to increase the angiogenic capacity of PLA both *in vitro* and *in vivo* (Aguirre et al. 2010; Vila et al. 2012). For this experiment cells expressing both the CMV:RLuc and the PECAM:PLuc vectors were used. As a control, the same PECAM:PLuc-expressing cells where seeded in traditional PLA and cultured in L-15 medium at a lower flow rate.

5. ANIMAL MODELS

For the evaluation of the *in vivo* behavior of the different biomaterials, two murine models were developed, an ectopic model (sc or im) and a calvarial defect model.

All animal-related procedures of these studies were performed with the approval of the animal care committee of the Cardiovascular Research Center and the Government of Catalonia

5.1. Mice strains

5.1.1. Severe combined immunodeficiency disease (SCID) mice

SCID mice were purchased from Charles-River (Wilmington, MA) and maintained in a specific pathogen-free (SPF) environment throughout all the experimentation period.

SCIC mice lack of T and B lymphocytes, due to a recessive mutation on chromosome 16, responsible of the inefficient activity of the enzyme Prkdc (proteinkinase, catalytic polypeptide) involved on DNA reparation. Immune system of these mice does not maturate so there are unable to combat infections or reject transplants. This fact makes possible to use human cells in mice models.

5.1.2. Transgenic Green Fluorescent mice

Transgenic GFP mice were provided by Dr. Masaru Okabe (Osaka University) (Okabe et al. 1997). These mice are C57BL/6 mice genetically modified to express GFP in all their cells. In this work transgenic GFP mice are used to evaluate host cell invasion and vascularization of the implanted scaffolds.

5.2. Ectopic model

5.2.1. Analysis of cell survival and differentiation.

For studying the cell survival and expression of tissue-specific or hypoxia genes, scaffolds were ectopically implanted (SC or IM) in 6-week-old SCID mice.

Before scaffold implantation, the animals were anesthetized by an ip injection of 100 mg/kg ketamine (Merial, Duluth, GA) and 3.3 mg/kg xilacine (Henry Schein, Melville, NY) and immobilized. The surgical site was cleaned with povidone-iodine (Braun, Melsungen, Germany). A sagital incision was performed on the skin and a cell seeded scaffold was introduced using forceps and the incision closed using 7-0 absorbable suture (Ethicon, New Brunswick, EEUU). In the case of fibrin gels no incision was needed because they were directly injected as a liquid that polymerized once inside the animal. Mice were treated with buprenorphine (Schering-Plough, Kenilworth, NJ) during the 72 hours after intervention.

5.2.2. Material Biocompatibility

In order to study biocompatibility of the scaffolds, a transgenic GFP animal model was used. The protocol used was the same than in SCID mice but the scaffolds were not seeded with cells.

5.3. Calvarial defect model

To compare the bone reparation capacity of different materials a calvarial defect model was used. Mice were prepared for surgery by ip injection of 100 mg/kg ketamine (Merial) and 3.3 mg/kg xilacine (Henry Schein), and a sc analgesic injection of 0.05 mg/kg buprenorphine (Schering-Plough). The surgical site was cleaned with povidone-iodine (Braun). A sagital midline incision was performed on the skin and the periosteum was then cut, exposing the calvarial bone. Two defects, 3 mm diameter (critical size defect) were performed in the

calvarial bone of each mice using a sterile drill bit (Dremel, Racine, WI), avoiding perforation of the dura. The surgical area was cleaned with saline and each defect was filled with a 3 mm diameter x 1 mm thickness scaffold. In case of fibrin gel biomaterial, the polymerization was performed *in situ*, to perfectly adjust to the defect. The incision was closed using absorbable sutures.

6. IMAGING

6.1. Noninvasive bioluminescence imaging

6.1.1. *In vitro* BLI determination of PLuc activity

For *in vitro* proliferation assays, cell seeded scaffolds were placed in six-well plates with culture medium. For imaging, the following protocol was used:

- Medium was removed from the plates and scaffolds were rinsed with PBS 1x
- 100 ml of D-luciferin (Promega) was added to each scaffold
- After a minute incubation plates were placed in the detection chamber of an ORCA-2BT Imaging System (Hamamatsu Photonics, Hamamatsu City, Japan) provided with a C4742-98-LWG-MOD camera fitted with 512 x 512 pixel CCD detector cooled at -80^{o}C.
- Images were acquired during 1 min using 1 x1 pixel arrays (binning 1 x1).
- In order to register the position of the light signal, an additional black and white image was obtained using the illumination lamp in the detection chamber.
- Pseudo color images were generated using the same arbitrary color display settings for all images in the same experiment. Arbitrary color bars represent standard light intensity levels (blue= lowest; red = highest).

6.1.2. *In vivo* noninvasive BLI and image analysis

For the *in vivo* noninvasive BLI of mice bearing hAMSCs seeded scaffolds, the followed protocol was:

- Mice were anesthetized by injecting ip 100mg/kg of ketamine and 3.3 mg/kg xilacine.

- PLuc substrate, luciferin, was ip injected (150 mg/kg of D-luciferin) (Caliper Life Science, MA, USA). Alternatively, RLuc substrate, colenterazine (CTZ), was iv injected through tail vein (30 µl of benzyl colenterazine, 1 mg/ml in 50/50 propilenglycol/ethanol) (Prolume, Pinetop, AZ, USA) diluted in 125 ml of water.
- Mice were then placed in the detection chamber of an ORCA-2BT Imaging system provided with a C4742-98-LWG-MOD camera and a 512x512 pixel, CCD cooled at -80oC at a distance of 200mm from the camera objective (HFP-Schneider Xenon 0.95/25 mm).
- Imaging was performed routinely 5 min after substrate inoculation. Two images were generated from each mouse, one using a light source inside the chamber to register the animal position and a second one, in total darkness, during a 10 min period to acquire photons from the light emitting cells. To increase detection sensitivity the read out noise of the recorded signal was reduced by adding the light events recorded by arrays of 8 x8 adjacent pixels (binning 8x8) in the camera CCD.

In case of double labeled cells, images with each one of the substrates were taken in alternatively days.

6.1.3. BLI monitoring of cell seeding in a 3D *in vitro* system

For monitoring cell distribution in the scaffold during seeding benzyl-coelenterazine (PJK GmbH, Germany) (substrate of the RLuc) was added to the culture media at a concentration of 2 µg/L just before adding the RLuc-expressing cells and starting the seeding. The transparent perfusion chamber was placed in the in the detection chamber of an ImagEM X2 System. Images were acquired during 1, 10 or 30 second periods using 1x1 pixel arrays (binning 1 x1) and an EM gain value of 400. In order to register the position of the light

signal, an additional black and white image was obtained using the illumination lamp in the detection chamber at the beginning of the experiment.

Images were taken until light intensity started to decrease due to coelenterazine consumption. After seeding, spent medium was replaced with fresh one without coelenterazine.

6.1.4. BLI monitoring of PLuc and RLuc activities in a 3D *in vitro* system

Imaging of cells seeded inside a continuous perfusion system is not as trivial as in a traditional *in vitro* approach. The followed strategy consisted on injecting a fixed volume of substrate (20 µg of benzyl-coelenterazine or 1.6 µg of luciferin in 10 mL of fresh media) and letting it pass though the scaffold once, being then removed from the system. Bioluminescence images were obtained continuously using 1x1 pixel arrays (bunning 1x1) with EM gain off until signal completely stopped. The total number of photons emitted during the whole period was quantified. Imaging was always performed at the same flow rate.

6.1.5. Construction of a standard curve of light in the bioreactor *versus* cell number.

To calibrate imaging performance and assess the whether a linear correlation between the number of photons emitted by the system and the number of cells seeded in the scaffold existed, known number of cells were seeded and imaged as described in the previous section. To assure an optimum seeding yield, cells were directly deposited in the top of the scaffold and allowed to pass through, first by gravity and then with the aid of the pump generated fluid flow.

However, as hAMSCs are not always transduced at the same level and slight changes in luciferin expression may occur due to the increasing number of passages, the number of photons emitted inside the bioreactor was correlated with the number of photons emitted by the same cells *in vitro*, generating in this manner a standard curve independent of the level of cell transduction. The

number of photons emitted *in vitro* can also be related to cell number using a standard curve of "emitted photons" versus "number of cells" that is specific for each cell line.

6.1.6. Photon quantification and statistical analysis

Quantification of photon events from selected areas was performed using the HokawoTM Imaging Software (Hamamatsu Photonics). Results were expressed as photon counts (PHCs).

- Area of interest was selected using the Hokawo TM Software, obtaining the total PHC detected in this area. Background signal was obtaining by selecting an area of the image that do not present signal.
- The PHCs emitted by the cells in our area of interest was then calculated using the formula:

PHCs = (total number of PHCs in the area of interest) - [(number of pixels in the area of interest) x (background average PHCs/pixel)].

For analysis of *in vitro* cell proliferation in scaffolds, the average number of PHCs from cells at different times of growth was normalized relative to that at day 0.

For *in vivo* analysis cell proliferation in scaffolds, RLuc PHCs from each scaffold image were averaged and normalized relative to that at day 0.

In case of the 3D *in vitro* system, the peak values of photon emission during the pulse of substrate were used for analysis.

To evaluate cell distribution throughout the scaffold, a 'column average plot' was constructed using ImageJ software, where the X-axis represents the longitudinal axis of the cylindrical scaffold and the Y-axis the averaged pixel

intensity in the radial (perpendicular) direction. In order to normalize plots from different experiments, the averaged pixel intensity was expressed as the percent of the maximum value for each scaffold.

Changes in gene expression (PECAM, osteocalcin or hypoxia genes), reflected as changes of PLuc expression were calculated in relation to that of the RLuc reporter (ratio: PLuc/RLuc). Statistical analysis was performed using the two-way ANOVA test (GStat 2.0 software). $p < 0.01$ values were considered significant.

6.2. Micro-Computerized Tomography

6.2.1. Bone micro-Computerized Tomography

Micro-CT was used to evaluate the bone regeneration in the calvarial defects. With this technique we can compare the % of regenerated area and the bone density in defects filled with different combinations of biomaterial, growth factors and cells.

Images were obtained at the end of the experiments, 6 weeks after scaffold implantation. Mice were anesthetized by injecting ip 100mg/kg of ketamine and 3.3 mg/kg xilacine and sacrificed by cervical dislocation. Heads were separated from the body and immersed in a 10% formalin solution at 4^{o}C. After 24-48h heads were washed in PBS and transferred to 70% ethanol for conservation.

Micro-CT measurements were performed in a microCT 40 (Scanco Medical AG, Brüttisellen, Switzerland). The X-ray tubes was operated at 55 kVp and 145 µA. Over 180° 500 projections were acquired with 200 ms integration time, resulting in a voxel size of 30 µm. After application of a constrained Gaussian filter (sigma 1.2, support 1) to suppress the noise, bone was segmented with a global threshold of 22.4 % of maximal grey value. The defect regions were identified with a cylindrical mask. Bone volume fraction was calculated in this

volume of interest. Coverage was calculated from pseudo-radiograph created by a projection of the region in superior-inferior direction (Lutolf et al. 2003).

6.2.2. Vascular micro-Computerized Tomography

Vascular corrosion casts were produced for ex vivo analysis with ultra-high resolution µCT. The protocol was adapted from the one described by Beckmann et al (Beckmann et al. 2003). Briefly, mice were deeply anesthetized with Isoflurane (5%) and Pentobarbital. The thorax was opened to expose the heart and aortic arc. A small catheter (Fine Bore Polythene Tubing, 0.58/0.96 mm ID/OD, Smiths Medical, UK) was carefully introduced in the aorta and fixed there with surgical thread (Safil®, B-Braun, Germany). The animal was then perfused through the aorta, first with PBS containing 2% Heparin, then with 2% paraformaldehyde (PFA) in PBS and the polymer resin PU4ii (Polyurethane for Improved Imaging, VasQtec, Switzerland) (Krucker et al. 2006), all infused at 4 mL/min, 100 mm Hg and at body temperature (37°C). The resin is a mixture of PU, solvent (50% Ethylmethylketone – EMK) and a blue dye. After resin curing, the lower hind limbs were excised from the animals and the skin was removed. Soft tissue was macerated in 7.5% KOH for 24h at 50°C. Bone tissue was kept in the samples as a reference feature to allow future registration with the corresponding *in vivo* image datasets. Casts were then washed with water and stained for 24h with Osmium solution (2%) to obtain radiopacity. The samples were then immersed in home-made Pluronic gel (polyoxyethylene-polyoxypropylene triblock copolymer), a thermo-reversible gel that is solid at room temperature and liquid below.

The prepared samples were scanned with µCT (µCT 50, Scanco Medical AG, Brüttisellen, Switzerland). The scanner was operated at 55 kVp and 145 µA, with an integration time of 200 ms, and frame averaging of 3. All µCT scans were performed at room temperature. The CT scanner was calibrated weekly

for mineral equivalent value, and monthly for determining in plane spatial resolution. An imaging protocol consisting of two consecutive scans was carried out to allow the identification of the region of interest. The first scan was acquired at medium resolution to provide an overview for orientation within the sample; the second one at ultra-high resolution for detailed vascular analysis of the region of interest. In the medium-resolution scan, the following settings were applied: 2000 projections were captured per 180 degrees with a field of view of 10 mm in diameter and a total length of 3.70 mm, leading to a nominal isotropic resolution of 10 µm. The medium-resolution images were then downscaled to 17.5 µm to match the *in vivo* voxel size and the two image datasets (*in vivo* and ex vivo) were registered using rigid registration (Thévenaz et al. 1998). After identification of the matching region, an ultra-high resolution scan was carried out at that position with the following settings: 2000 projections were captured per 180 degrees with a field of view of 7 mm in diameter and a total length of 1.86 mm, leading to a nominal isotropic resolution of 1.4 µm. A Gaussian filter was applied to the ultra-high resolution images to reduce noise (sigma 1.2, support 1). Blood vessels were segmented by a fixed thresholding procedure (20% of the maximum grayscale value) and bone was excluded by manual contouring. A morphological closing procedure (3 dilation and 3 erosion steps) was applied to refill hollow structures that appeared in the vessels after thresholding. Global standard morphometric analysis was performed on the ultra-high resolution images using the software package IPL (Image Processing Language, Scanco Medical AG, Brüttisellen, Switzerland).

7. HISTOLOGICAL TECHNIQUES

7.1. *In vitro* differentiations

Tissue specific staining protocols were used to evaluate differentiation of hAMSCs to adipogenic, condrogenic and osteogenic lineages.

7.1.1. Oil Red O Staining for lipids

Oil Red O, dye generates a red coloration when dissolved in lipids and is used to detect triglycerides, fatty acids and lipoproteins (Fig. 30).

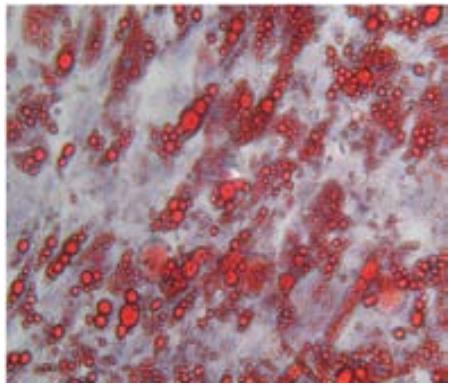

Fig. 30. Microphotography of a hAMSCs culture differentiated to adipose lineage and stained with Oil Red O.

- Cell were rinsed with PBS 1x and fixed with a 10% formalin solution (PFA) (Sigma-Aldrich).
- Fixed cells were rinsed with 60% isopropanol (Panreac, Barcelona, Spain) for 1 minute.
- Cells were then stained with Oil Red O Solution (60% of a saturated Oil Red O solution in isopropanol and 40% of distilled water) for 5 minutes.
- Cells were rinsed twice with 60% isopropanol for 1 minute and once with distilled water for 5 minutes.

- Nuclei were then stained with Mayer's Hematoxylin Solution (Sigma-Aldrich) for 2-3 minutes.
- Finally, cells were rinsed with tap water for 3 minutes and with distilled water for another 3 minutes.

7.1.2. Von Kossa staining for bone

Von Kossa Staining is used to visualize calcium deposits of salts. The staining reaction is based on the substitution of Ca^{+2} ions (phosphates or carbonates) by Ag^{+2} ions, forming silver phosphates or carbonates. These silver salts are reduced to black metallic silver upon exposure to light (Fig. 31).

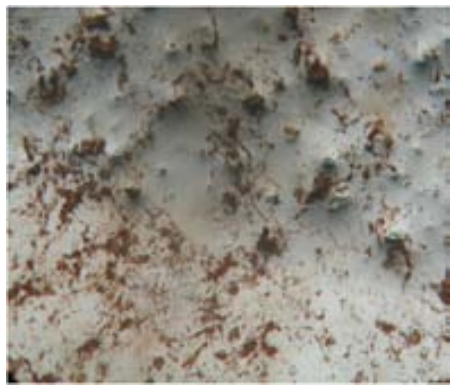

Fig. 31. Microphotography of a hAMSC culture differentiated to osteogenic lineage and stained for Von Kossa.

- Cell were rinsed with PBS 1x and fixed with a 10% formalin solution for one hour.
- Cells were rinsed with distilled water for 5 minutes 3 times.
- Cells were then dehydrated by incubation for 3 minutes in 70% ethanol, 3 minutes in 90% ethanol and 3 minutes in absolute ethanol.
- Cells were air-dried for 2-3 minutes and then rehydrated by incubation for 3 min in absolute ethanol, 3 min in 90% ethanol, 3 min in 70% ethanol and finally, 5 minutes in distilled water.

- Cells were then stained with 2% silver nitrate (Sigma) for 1 hour under a 70 W light source.
- Cells were rinsed 3 times with distilled water for 5 minutes.
- Silver nitrate reaction was stopped by the addition of 5% sodium thiosulfate (Panreac) for 5 minutes.
- Nuclei were stained with Mayer's Hematoxylin Solution for 2-3 minutes.
- Cells were rinsed with distilled water twice for 5 minutes.

7.1.3. Alcian Blue Staining for cartilage

Alcian Blue, comprising a center copper atom surrounded by four nitrogenated aromatic rings, is a basic molecule that binds to acidic groups in mucopolysaccharides, forming a blue salt at low pH.

- Cell were rinsed with PBS 1x and fixed with a 10% formalin solution for one hour.
- Cells were rinsed twice with distilled water for 5 minutes.
- Cells were rinsed with HCl 0,1M.
- Cells were then stained with 1% Alcian Blue (Fluka) (2g of Alcian Blue, 97 ml of distilled water and 100 ml of glacial acetic acid), pH 1, for 1.5 hours.
- Cells were rinsed with HCl 0,1M for 5 minutes.
- Cells were then counterstained with Nuclear Fast Solution (Sigma) for 5-10 minutes.
- Cells were finally rinsed with distilled water.

7.2. Tissue samples

7.2.1. Fluorescent Angiography

Anesthetized mice were iv injected with 200 µl of fluoresceine isothiocyanate (FITC) dextran, 2,000 kD MW, 10 mg/ml (Sigma). After 10 minutes, mice were sacrificed and scaffolds retrieved and fixed in formalin solution 10% (Sigma). Samples were sectioned and observed by confocal microscopy.

7.2.2. OCT inclusion and block preparation and sectioning

- Mice were anesthetize and sacrificed by cervical dislocation
- Scaffolds were retrieved from the animal and washed in PBS.
- Samples were then fixed in a formalin solution 10% at 4^{o}C
- After 4-12h (depending of the size of the sample) scaffolds were washed in PBS and transferred to 30% sucrose in PBS solution until the tissues sinks to the bottom of the tube at 4ºC.
- After a couple of hours half the volume of sucrose solution was removed and 30% OCT™ (Tissue-Tek, Sakura, Holland) solution was added, making a 1:1 30% sucrose/OCT solution, and kept at 4^{o}C.
- After 1 or 2 hours samples were embedded in OCT using plastic molds placed in dry ice. A layer of OCT was placed in the mold, the sample was placed in the middle of the mold, and then a layer of OCT was applied to cover the sample.
- When the OCT was frozen (white) molds were transferred to a -80^{o}C freezer until sectioning
- Sections of 5 µm were made using a cryostat (Jung CM3000, Leica).

7.2.3. Decalcification

Calvarial bone samples were decalcified using TBD-2 (Thermo) after fixation and before inclusion. The protocol used was:

- Samples were washed with PBS 1x and transferred to a glass or plastic beaker.
- A volume of TBD-2 equivalent to 20 times the volume of the sample was added and left for 24 hours at RT.
- Samples were washed with PBS before inclusion.

7.2.4. Basic histological stainings

Slides with OCT sections were heated for 1 hour at 40ºC before staining.

Hematoxylin- Eosin (HE)

This is a procedure widely-used to visualize cells. Hematoxylin, a natural basic dye very selective for nuclear chromatin stains cell nuclei blue; while eosin, an acidic dye that comprising 2 (eosin B) or 4 (eosin Y) bromide and diffuses easily through tissues binding to proteins stains cytoplasm and extracellular components pink. The protocol used for staining was:

- Slides of tissue sections were washed with distilled H2O for 5 minutes.
- Slides were stained with Mayer's Hematoxylin Solution (Panreac) for 5 minutes.
- Slides were then rinsed for 5 minutes with tap water and 5 minutes with distilled H2O.
- Slides were stained with Eosin (Sigma) for 20 seconds and rinsed with ethanol 96%.
- Slides were dehydrated with 95% ethanol for 2 minutes and absolute ethanol for 2 minutes.
- Slides were then rinsed twice with Histoclear (National Diagnostics, Atlanta, USA) for 3 minutes and then mounted with Histomount® (Natural Diagnostics).

7.2.5. Vascular staining

Isolectin B4 staining

Lectins are specific carbohydrate-binding proteins of nonimmune origin and have been used to characterize the glycosylation status specifically in a variety of tissues.

Griffonia simplicifolia (*Bandeiraea*) isolectin B_4 (GSL-IB_4) specifically binds terminal α-galactosyl residues expressed by various cells including, but not limited to, endothelial cells (Laitinen 1987) in normal mouse, rabbit, rat, and human tissues.

Samples were stained using a biotin conjugated GSL-IB_4 (Vector labs, Burlingame, CA) using the following protocol:

- Slides were rinsed in Tris-buffered saline (TBS) 3 times for 5 minutes and then rinsed with Triton X-100 0.5% in TBS 3 times for 5 minutes.
- Lectin incubation: Biotinylated GSL-IB_4 was diluted in TBS-Triton X-100 0.5%, 1% BSA (dilution 1:25). Sections were incubated overnight at 4ºC in a humid chamber.
- Sections were then tempered for 1 hour at room temperature.
- Slides were rinsed TBS-Triton X-100 0.5% for 5 minutes three times.
- Sections were then incubated in Streptavidin-Alexa Fluor 647 in TBS (dilution 1:500) for 1h at 37ºC in a humid chamber, protected from light.
- Sections were rinsed with TBS for 5 minutes 3 times.
- Nuclei were stained with Hoechst Stain (Sigma-Aldrich) for 10 minutes.
- Finally, sections were rinsed with TBS and mounted with Fluoromount™ (Sigma-Aldrich).

7.2.6. Scanning Electronic Microscopy

Extracted scaffolds were fixed with 2.5% glutaraldehyde during 4 hours and post-fixed with 1% osmium tetraoxyde for one hour. Following, samples were dehydrated, dried to critic point, coated with gold and observed using a Jeol JSM-6400 scanning electronic microscope (SEM).

VI. **RESULTS AND DISCUSSION**

1. CHAPTER I: ASSESSMENT OF THE ANGIOGENIC CAPACITY OF PLA SCAFFOLDS

The reconstruction of hard and soft tissues is a major challenge in regenerative medicine, aggravated by the increasing number of tissue defects in the aging population. The shortage of donor tissue and organs for transplants has promoted a large research and development effort aimed at generating alternative therapeutic solutions. TE applies principles of material engineering and life sciences toward the development of biological substitutes that can combine scaffolds and live cells to restore, maintain, or improve tissue function (Langer & Vacanti 1993).

Biomaterial scaffolds should mimic the three-dimensional environment of the ECM, provide short-term mechanical stability for the transplant, and increase surface area for migration, adhesion and differentiation of cells, supporting the growth of new tissue (Zippel et al. 2010). Additionally, scaffolds should promote colonization by specific cell types and finally degrade in response to matrix remodeling enzymes released by the colonizing cells as tissue repair progresses (Hubbell 1999). Use of an inorganic phase in biodegradable composite polymers to allow fine control of porosity, connectivity and surface properties, could be a promising approach to meet some of the above requirements.

One of the principal constraints on the size of *in vitro* engineered tissues lacking a blood supply is the short distance over which oxygen can diffuse before being consumed. Once implanted in the patient, cells in the engineered material will consume the available oxygen within a few hours, but it will take several days before new blood vessels colonizing the implant can deliver oxygen and nutrients (Griffith & Naughton 2002). Providing scaffolds with angiogenic inducing capacity will likely help colonization by cells from the host, for those materials implanted without them. Due to the different time constraints for

oxygen consumption and vascular colonization, it would be unrealistic to expect that providing angiogenic-induction capacity to biomaterials will effectively rescue cells deeply seeded in large scaffolds. However, such strategy may help survival of cells in, or near the surface of implants.

There are multiple cell types with potential use for tissue regeneration e.g.: embryonic stem cells, hematopoietic stem cells or mesenchymal stem cells(Polak & Hench 2005) . Among the latter, adult stem cells derived from bone marrow and adipose tissue appear as ideal candidates for autologous cell therapies, avoiding problems associated with immune rejection, pathogen transmission and ethical issues (Pittenger et al. 1999; Bianco et al. 2001; Chamberlain et al. 2007; Pansky et al. 2007; Zuk et al. 2002; De Ugarte et al. 2003; Kern et al. 2006). While mesenchymal stromal cells from the bone marrow, having a rich differentiation potential and anti-inflammatory capacity, would be ideal candidates for tissue repair, their use is hampered by their relative low abundance, availability in small volumes and pain associated with its extraction. More recently identified mesenchymal stromal cells from adipose tissue (AMSCs) offer an easily extractable and abundant alternative source of therapeutic cells with similar phenotype and equivalent differentiation potential to their homologues from the bone marrow, but in larger supply (Zuk et al. 2002; De Ugarte et al. 2003; Kern et al. 2006). Furthermore, these cells have shown undetectable predisposition to oncogenic transformation after *in vitro* cultivation and implantation in mice (Vilalta et al. 2008).

Although mechanisms underlying the vascular differentiation of hAMSC and their contribution to neovascularization are poorly understood, there is evidence supporting MSC participating in angiogenesis (Al-Khaldi et al. 2003; Chung et al. 2009; Whyte et al. 2011).

In the current work we evaluate the capacity of a new composite material comprising poly(lactic acid) and calcium phosphate (CaP) soluble glass to

promote angiogenesis. The incorporation of a CaP phase in the polymeric matrix, not only enhances the mechanical properties of the material and controls its degradation rate, but also modifies its surface properties and ionic environment, modulating cell behavior (Navarro et al. 2004; Charles-Harris et al. 2008). Aguirre et al. (Aguirre et al. 2010) have reported that extracellular calcium is physiological modulator of MSC angiogenic response, inducing up-regulation of important angiogenic cytokines and growth factors through the activation of a Calcium Sensing Receptor-like receptor. Here we focus on the *in vivo* angiogenic capacity of the new biomaterial in comparison with that of PLA only.

To monitor the behavior of cells in live animal implants we use a non-invasive bioluminescence imaging (BLI) platform. In this study we use two different inducible promoters to regulate expression of the *Photinus pyralis* luciferase (PLuc) as a reporter of endothelial cell differentiation and hypoxia state. In the former case we use the promoter for the platelet endothelial cell adhesion molecule-1 (PECAM-1) gene, a frequently used marker of endothelial cells, platelets and specific immune system cells (Newman & Albelda 1992), and in the latter case we use a composite promoter comprising multiple repeats of the hypoxia response element (HRE) binding sequence, responsible of regulating the activity of multiple hypoxia response genes (Semenza et al. 1996). The *Renilla reniformis* luciferase (RLuc) under the control of the CMV promoter is used to monitor changes in cell number.

In a complementary set of experiments without hAMSCs, we analyze the PLA/G5 scaffolds capacity of for inducing scaffold colonization and vascularization by the host own cells when compared with PLA.

1.1. Results

1.1.1. HAMSCs survive and proliferate in PLA/CaP scaffolds *in vitro*

HAMSCs were transduced with a lentiviral construct for expression of PLuc regulated by the constitutively active CMV promoter and then seeded in PLA/CaP scaffolds. Bioluminescence images were obtained weekly to monitor cell growth (*Fig. 32*).

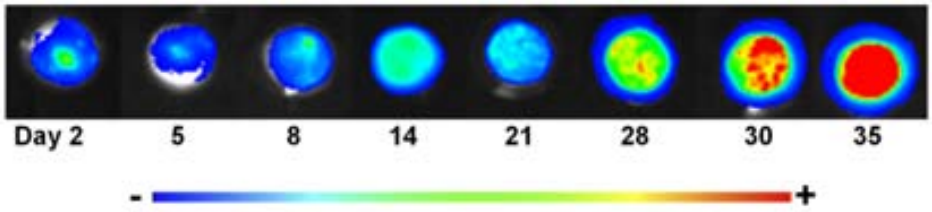

Fig. 32. Representative BLI images from hAMSCs-PLuc cells, at the indicated days post-seeding, overlaid on the corresponding white light images of scaffold. The color bar shows the arbitrary standard rainbow color scale used to depict relative light intensities (red= highest; blue= lowest).

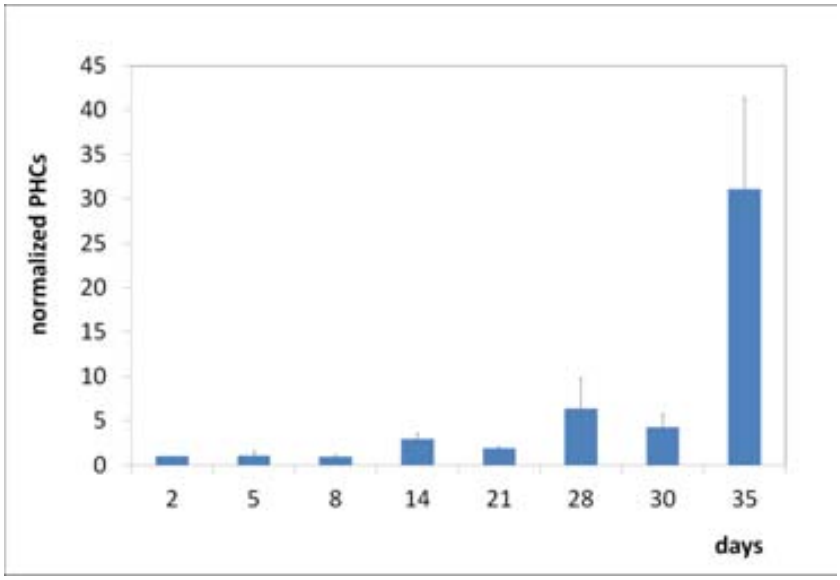

Fig. 33. Proliferation of hAMSCs seeded on PLA/CaP scaffolds. (a) Quantitative analysis of light produced by hAMSCs-PLuc cells expressed as total photon counts (PHCs) normalized relative to day 2. Bars represent the standard error of the mean.

Quantification of these images showed a slight drop in the number of cells during the first week, followed by a proliferation stage that continued up to the end of a seven week observation period, reaching a cell number 30 x higher that at day 2 *(*Fig. 33).

At the end of the monitoring period, the scaffold samples were harvested, fixed and prepared for scanning electronic microscopy. SEM images (Fig. 34) show cell growing both in the surface and inside the material.

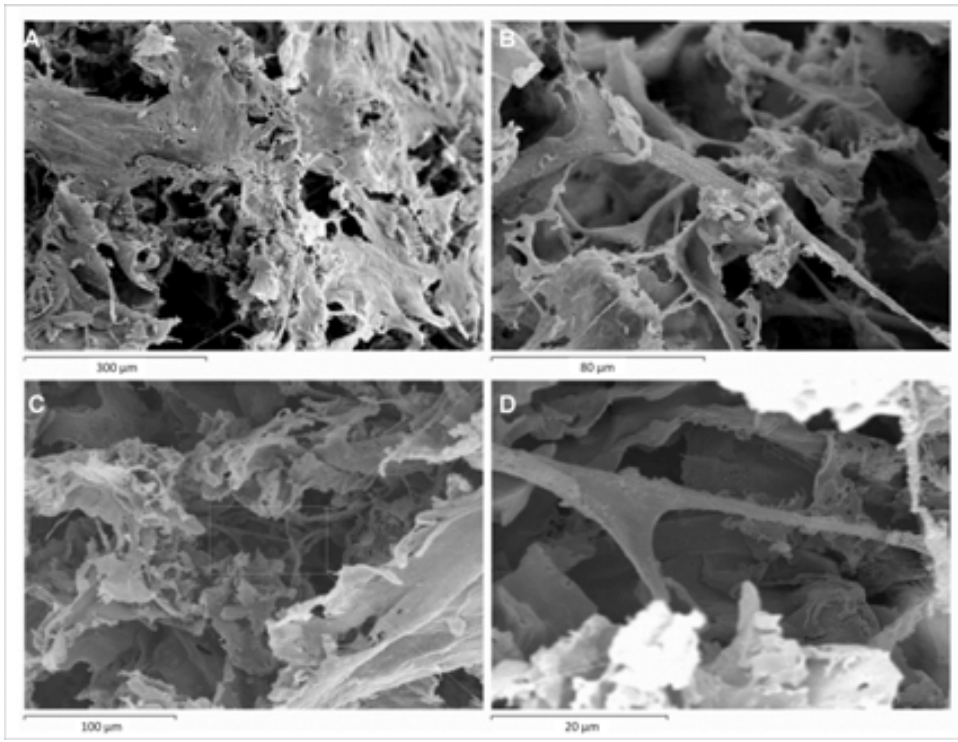

Fig. 34. Scanning electronic microscope (SEM) images of hAMSCs grown on PLA/CaP scaffolds during 35 days. (A) Image of biomaterial surface (160x). (B) enlarged detail showing a cell (700x). (C, D) Scaffold pores, showing surface lining cells (400x and 2300x respectively).

1.1.2. HAMSCs seeded on PLA/CaP scaffolds and implanted on SCID mice proliferate after overcoming an initial growth crisis

While the proliferation of cells in scaffolds *in vitro* may be an indicator of their affinity for the material surface, the physiological environment of within

implanted scaffolds is considerably more complex due to restriction in the availability of oxygen and nutrients and changing conditions as the wound repairs.

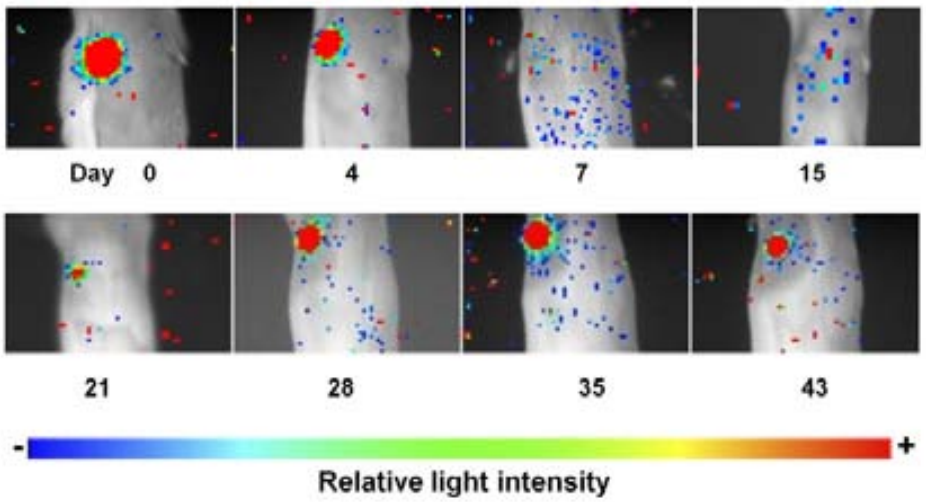

Fig. 35. Proliferation of hAMSCs seeded on PLA/CaP scaffolds and implanted sc on SCID mice. Representative BLI images from a hAMSCs-PLuc cell seeded PLA/CaP scaffold at a sc site at the indicated days post-implantation, overlaid on the corresponding b&w images of the mouse. The color bar shows the arbitrary standard rainbow color scale used to depict relative light intensities (red) highest; blue= lowest).

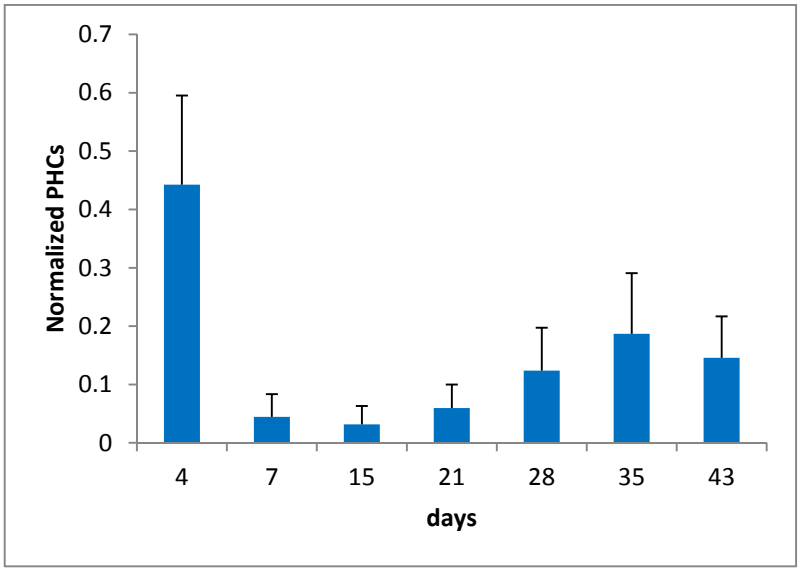

Fig. 36. Quantitative analysis of light produced by hAMSCs-PLuc cells expressed as PHCs normalized to day 0. Bars represent the standard error of the mean.

1.1.3. CaP glass promotes differentiation of hAMSCs to the endothelial lineage

The kinetics of cell growth on implanted scaffolds suggested that changes in gene expression triggered by restrictions in nutrients and oxygen may result in adaptations to the changing physiological environment.

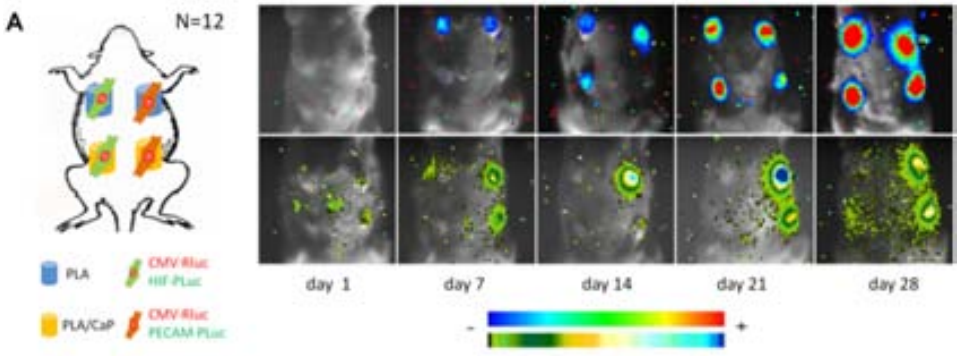

Fig. 37. Non-invasive BLI images of RLuc and PLuc-expressing hAMSCs cells seeded on PLA and PLA/CaP scaffolds sc implanted in SCID mice. (a) Representative BLI images showing RLuc (top row) and PLuc (bottom row) activity from dually labeled hAMSCs, on PLA and PLA/CaP scaffolds, superimposed on b&w dorsal images of the corresponding mouse. The diagram illustrates the implantation strategy and sites (top left). Color bars illustrate relative light intensities from RLuc (blue: low, red: high,) and PLuc (black: low, blue: high).

To analyze the differentiation state of hAMSCs seeded on both PLA and PLA/CaP scaffolds, cells initially labeled with the CMV:RLuc reporter were also labeled with a *PLuc* reporter regulated by an inducible promoter. A human PECAM-1 promoter or, alternatively, an HRE promoter, was used to image endothelial differentiation or hypoxia estate, respectively. An additional advantage of this double reporter strategy was that changes in the expression of the inducible PLuc could be directly related to the activity of constitutively expressed RLuc, as a reference reporter, avoiding potential cell proliferation and imaging artifacts. Labeled cells of both types were seeded on the biomaterial and implanted on 12 SCID mice as indicated in the diagram of Fig.4, and then subjected to BLI analysis during a 4 week period.

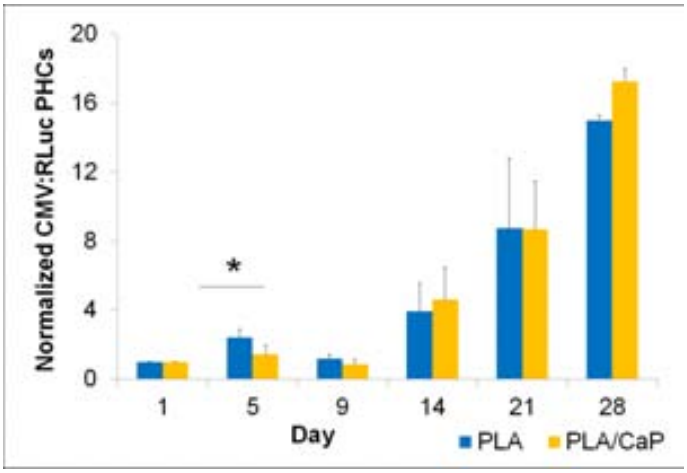

Fig. 38. Quantification of BLI images (b) Histogram summarizing cell proliferation data, RLuc PHCs are normalized to day 1. Bars represent the standard error of the mean. * p<0.05 according to Student T test

Quantification of photon events recorded from BLI captures (*Fig. 37*) shows that cell growth during this period was comparable in PLA and PLA/CaP scaffolds (*Fig. 38*). However, PECAM-1 promoter regulated light production was significantly higher for cells in the PLA/CaP material (two- way ANOVA test, p< 0.01) (*Fig. 39*A), indicating that PLA/CaP is a better inducer of vascular differentiation for hAMSCs.

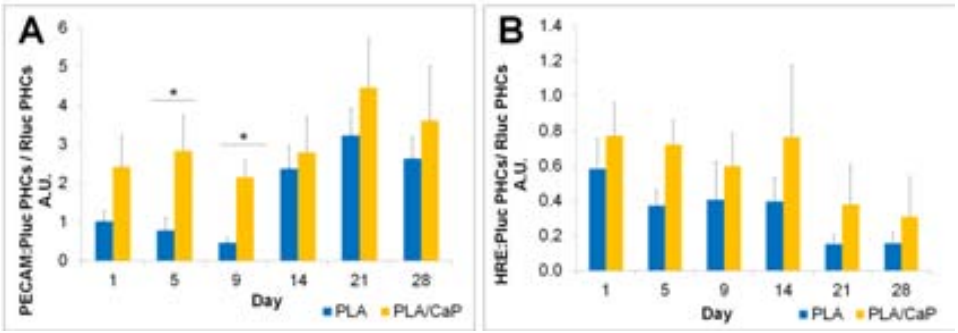

Fig. 39. (A) Histogram summarizing evolution of Platelet/Endothelium Cell Adhesion Molecule-2 (PECAM-2) expression, data is represented as the ratio PLuc/RLuc PHCs (p<0.01 according to the two-way ANOVA test); (B) Histogram summarizing the evolution of hypoxia, expressed as the ratio PLuc/RLuc (p=0.026 according to the two-way ANOVA test). Bars represent the standard error of the mean. * p<0.05 according to Student T test; AU = arbitrary units.

Interestingly, the observed increase in expression of the PECAM-promoter regulated reporter correlated with a decrease in the expression of the HER-promoter regulated reporter for both materials, indicating a decrease of the hypoxia level in the material as angiogenesis proceeds (*Fig. 39*B). However, cells in the PLA/CaP material appear to be under a slightly higher (p=0.026.) hypoxic stress than those in PLA.

1.1.4. PLA/CaP scaffolds promote angiogenesis

The pro-angiogenic capacity of the PLA/CaP scaffold detected by BLI was also validated by standard histological procedures. To facilitate visualization of colonizing cells within the scaffold, 12 transgenic GFP mice were implanted sc (6 mice) and in a calvarial defect model (6 mice) with PLA/CaP scaffolds.

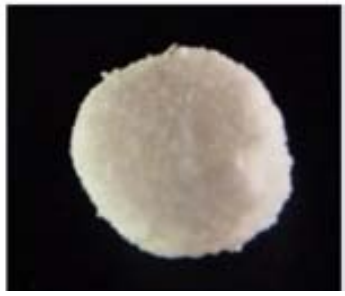

Fig. 40. Appearance of a PLA/CaP scaffold before implantation

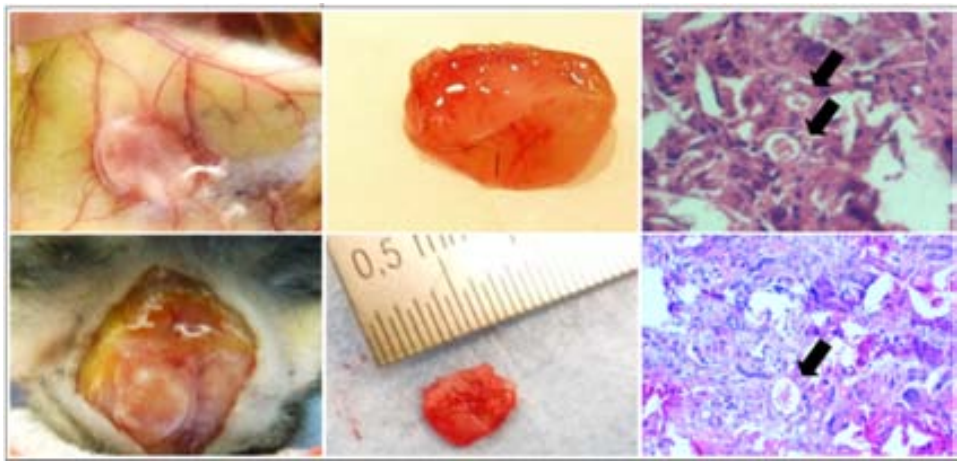

Fig. 41. Cell colonization and angiogenesis of PLA/CaP scaffolds implanted without cells in Green Fluorescent Protein (GFP) transgenic mice during one month. Images of sc (upper panels) and calvarial lesion (lower panels) implanted scaffolds showing visual appearance (left and middle) and invading capillaries arrows) in Hematoxylin-eosin stained scaffold sections (right).

Scaffolds harvested 4 weeks after implantation had changed their macroscopic appearance significantly and had attracted a network of host blood vessels (*Fig.*

40 and *Fig. 41*). HE stained sections from both sc and calvarial lesion implants also showed the presence of abundant host cells and micro vascular structures.

Laser confocal microscope and SEM images of scaffold sections confirmed the presence of GFP expressing host cells and cellular structures, respectively, within the PLA/CaP scaffold (*Fig. 42*).

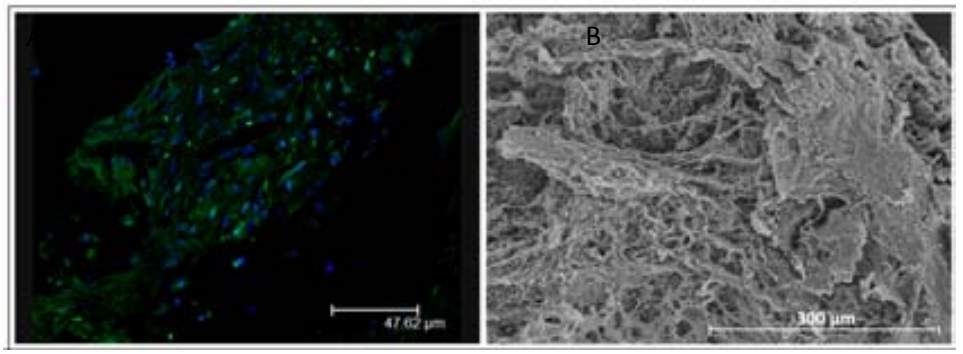

Fig. 42. Cell colonization and angiogenesis of PLA/CaP scaffolds implanted without cells in transgenic GFP mice during one month. (A) Laser confocal microscope image showing invading green fluorescent host cells (objective: 20x/0.4, eyepiece 10x/20) (left). (B) SEM image showing host cell colonization (200x) (right).

To ascertain that host blood vessels colonized the scaffolds, 3 SCID mice sc implanted with PLA/CaP scaffolds during a 2 month period were perfused through the tail vein with a high MW (2,000 kD) FITC conjugated dextran unable to penetrate the endothelial barrier. Fluorescence confocal microscope examination of PFA fixed scaffold sections showed the presence of colonizing green fluorescent micro vascular structures in the interior of the scaffolds that were well connected to the host

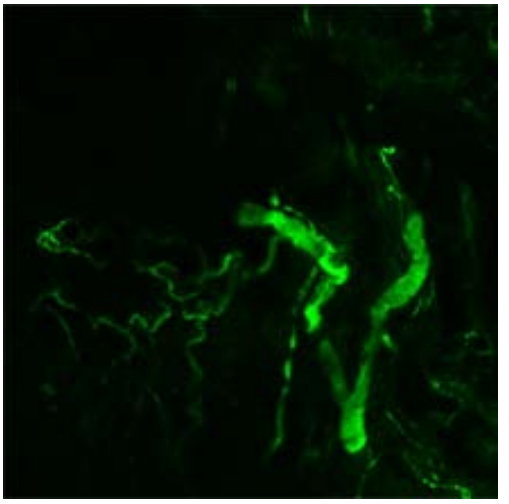

Fig. 43. Microvascular structures in PLA/CaP scaffolds implanted without cells. Laser confocal microscope image showing tail vein injected FITC-dextran filling tubular structures at different depths of a PLA scaffold implanted during two months in a SCID mouse (objective: 20x/0.4, eyepiece 10x/20).

vascular system (*Fig. 43*).

1.1.5. CaP glass improves the angiogenic capacity of PLA scaffolds

To further validate BLI results and compare the angiogenic capacity of PLA/CaP and standard PLA only material, 4 SCID mice were implanted sc with PLA/CaP and PLA scaffolds that were harvested after a 2 month period. Following fixation the scaffolds were sectioned and stained using biotin conjugated endothelial cell surface specific GSLI Isolectin B_4 (endothelial cell specific marker) and streptavidin-conjugated Alexa Fluor® 647 (*Fig. 44*).

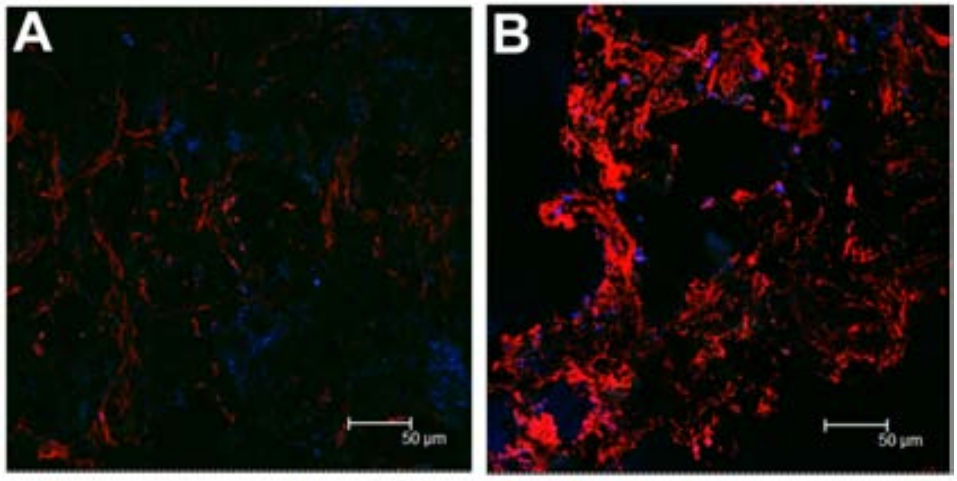

Fig. 44. Endothelial cell specific Isolectin B4 (red) and Hoechst (blue) staining of scaffold sections. Representative images obtained after a two-month implantation without cells in GFP transgenic mice using a laser confocal microscope (objective: 20x/0.4, eyepiece 40x/20). (A) PLA scaffold. (B) PLA/CaP scaffold.

	n	mean	T Student Test
PLA	290	6.1	0.029
PLA/CaP	194	12.7	

Table 6. Table showing the percentage of area stained with Isolectin B4, calculated using ImageJ software. Difference is significative with p<0.05. n: number of fields analyzed.

Quantitative analysis of fluorescence confocal microscope images showed that the amount of surface stained by Isolectin B4 was significantly higher ($p<0.05$) in the PLA/CaP than in the PLA only scaffolds (*Table 6*).

1.2. Discussion

The aim of the current work was to analyze the *in vivo* angiogenic inducing capacity of a new biomaterial composed by poly(lactic acid) and calcium phosphate glass (PLA/CaP), in combination with hAMSCs known to differentiate to the endothelial lineage under appropriate stimulus. Previous *in vitro* studies with MG-63 cells (Navarro et al. 2004; Charles-Harris et al. 2008) had shown that these cells are able to attach, colonize, proliferate and differentiate in this material *in vitro*.

We used a non-invasive BLI platform, based on the use of a high sensitivity video camera to detect visible light photons generated by luciferase reporters genetically introduced in cells and monitor their behavior. By using constitutively active promoters to regulate luciferase expression, we observed that PLuc expressing hAMSCs were compatible with PLA/CaP scaffolds and proliferate well in them during a seven week period when cultivated *in vitro*, a good indicator of the affinity of the cells for the scaffold material. However, when implanted in live SCID mice, cell behavior was very different, and viability dropped by nearly 20 fold, in the first week, to finally recover by the fifth week post-implantation. This drop and recovery in the proliferative behavior of hAMSCs on implanted scaffolds were indicative of an adaptive response, governed by changes in gene expression, to stressing physiological conditions within recently implanted scaffolds.

The use of tissue specific promoters, only active in certain cell lineages, to regulate luciferase reporter activity may allow *in vivo* monitoring of cell differentiation. However, BLI measurements contain information on spatial

distribution and photon fluxes, the latter of which may also reflect changes in cell number. Thus, changes in inducible reporters can best be quantified by relating them to internal cell number controls. To understand the adaptive changes of hAMSCs in scaffolds, we labeled hAMSC-RLuc cells with an additional PLuc-eGFP reporter regulated by either the PECAM or a hypoxia response element promoter. In this manner changes in the inducible luciferase activity could be related to those of the constitutively expressed one, and expressed as the ratio of their photon fluxes. With this approach, we were able to observe that both materials were generally equivalent at supporting cell growth, although at days 5 the number of cells in PLA/CaP is significantly lower than that in PLA. Also, during the whole experiment, the overall trend of hAMSC differentiation to the endothelial lineage was significantly (ANOVA) higher in PLA/CaP than in PLA. Comparison of PECAM regulated PLuc expression at specific times showed no significant differences except for days 5-9, where cells in PLA/CaP express significantly higher levels of light that those in PLA, in correspondence with slower proliferation, and in agreement with current believe that generally differentiating cells proliferate slower. HAMSCs differentiated to the endothelial lineage in correlation with a decrease in the hypoxia sensed by the cells within the scaffold. However, endothelial differentiation was faster and more robust in the PLA/CaP than in the PLA only material. Interestingly, cells in the PLA/CaP material appear to be under slightly higher hypoxic stress than those in PLA. At this point is difficult to offer a rationalization for this observation. However, a tempting but speculative explanation could be that the hypoxic state drives the observed enhanced endothelial differentiation in PLA/CaP. Alternatively, higher hypoxia could result from different metabolic requirements associated to cell differentiation.

Results from BLI were also supported by observations using more standard procedures. Visual inspection of PLA/CaP scaffolds implanted without cells in GFP transgenic mice showed that within a one month period there was an

evident recruitment of vascular system from the host. Histological analysis by conventional and laser confocal microscopy corroborated the invasion of the material by fluorescent host cells that also formed part of vascular structures. Further analysis by inoculation of a high molecular weight FITC-conjugated dextran in live mice revealed dextran filled fluorescent vascular structures within the PLA/Cap scaffolds, demonstrating their functional connectivity with the host vascular system. Moreover, the surface of GSLI B4 isolectin-stained endothelial cells lining PLA/CaP scaffolds was significantly larger than that in PLA only scaffolds, in support of BLI results showing the higher capacity of the former material to induce endothelial differentiation of hAMSCs. Thus, in agreement with previous reports (Aguirre et al. 2010), slow dissolution of CaP may be generating an ionic environment inducing migration and differentiation of angiogenic precursors within the PLA/CaP material.

2. CHAPTER II: ANALYSIS OF THE BONE REGENERATION CAPACITY OF AN GROWTH FACTOR-DELIVERING FIBRIN GEL

Research has shown the importance of growth factors (GFS) in tissue repair and regeneration and GF-based therapies are very promising (Kanitkar et al. 2011). For example, two GFs approved by the FDA that have received considerable attention for are platelet derived growth factor (PDGF) and bone morphogenetic proteins (BMPs) (Govender et al. 2002). PDGF was initially discovered as a fibroblast mitogen present in human serum and localized in the alpha granules of platelets. In adults, most of the proposed functions of PDGF relate to different responses to injury, for example, inflammation and wound healing (Levéen et al. 1994), blood vessels maturation and chemotactic activity towards MSC (Phipps et al. 2012). BMPs are members of the TGF- β 1 superfamily initially described by Urist about 40 years ago (Urist et al. 1973). More than 14 types of human BMPs have been described. BMPs mostly influence bone, but also hematopoietic cell differentiation (Chadwick et al. 2003). Several BMPs induce migration and differentiation of MSCs to the osteogenic phenotype (Lind et al. 1996; Reddi & Cunningham 1993) and this features have been used in therapeutic bone repair and regeneration (Kanakaris et al. 2009; Calori et al. 2008; Ronga et al. 2006; Grgurevic et al. 2011; Hollinger et al. 1998).

While GFs are very promising in regenerative medicine, there is some recent controversy relative to their safety for clinical use, in particular their association with cancer risk/mortality and other side effects (Carragee et al. 2011; Frieden 2008). Thus, there exists a strong motivation to engineer smart biomaterial systems that can deliver GFs doses precisely at low doses to potentially improve safety and cost-effectiveness (Martino & Hubbell 2010). In this work we combine the use of BMP-2, which due to its natural affinity for fibrinogen is retained in a fibrin matrix (Martino et al. 2013; Kaipel et al. 2012) and an engineered fibrin-binding PDGF-BB, to locally deliver controlled doses of

growth factors at sites of tissue repair. We also evaluate the role of human Mesenchymal Stem Cells derived from adipose tissue (hAMSCs), seeded in the described engineered fibrin matrix, in bone regeneration, using a mouse calvaria defect model.

To analyze the effect of GFs in cell behavior, luciferase expressing hAMSCs served as reporters. Cells were seeded in the fibrin scaffolds, implanted intramuscularly or in calvarial defects in SCID mice and monitored using a non-invasive bioluminescence imaging (BLI) platform. Moreover, by using inducible tissue specific gene promoters to regulate luciferase reporters, biologically significant changes in promoter activity were easily measured as photon fluxes, providing information on cell growth, distribution and time related changes in gene expression associated to cell differentiation (Iyer et al. 2001; Contag et al. 1997; Marta Vilalta et al. 2009). We used two different inducible promoters to regulate expression of the *Photinus pyralis* luciferase (PLuc). The promoter of bone gamma-carboxyglutamate protein or osteocalcin (BGLAP/OC), the major noncollagenous bone matrix protein expressed cells of the osteoblasts lineage (Briot & Roux 2005; Yeung et al. 2002) was used as a reporter of osteoblastic differentiation. The *Renilla reniformis* luciferase (RLuc) under the control of the CMV promoter is used to monitor changes in cell number.

While the promoter for the platelet endothelial cell adhesion molecule-1 (PECAM-1) gene, a frequently used marker of endothelial cells, platelets and specific immune system cells (Newman & Albelda 1992) was used to monitor endothelial differentiation.

Results from BLI were complemented with micro-Computed Tomography (μCT) of skulls to analyze bone regeneration under the different treatments and with high-resolution μCT of vascular casts of mice perfused with a polymeric resin, to visualize the vascularization of the defects.

2.1. Results

2.1.1. Design and production of fibrin-binding PDGF-BB

In order to be covalently incorporated into fibrin during the natural polymerization process of the hydrogel, PDGF-BB was designed to contain the factor XIIIa substrate at their N-terminus (α2PI1-8)(Schense & Hubbell 1999). To evaluate the bioactivity of α2PI1-8-PDGF-BB, MSCs, which highly express PDGF receptor-β (PDGFR-β), were stimulated with wild-type PDGF-BB or α2PI1-8-PDGF-BB. The addition of α2PI1-8 at the N-terminus of PDGF-BB did not alter the bioactivity of the GF, since α_2PI_{1-8}-PDGF-BB could promote the phosphorylation of PDGFR-β (pPDGFR-β) to the same level of wild-type PDGF-BB (*Fig. 45* A).

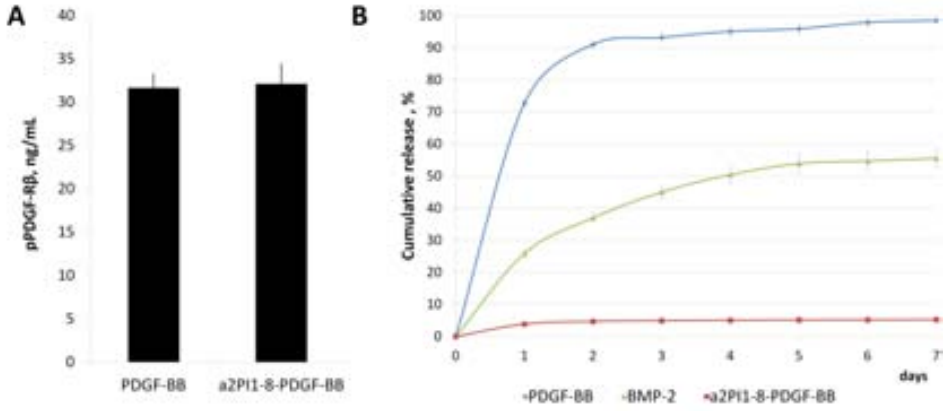

Fig. 45. Bioactivity and fibrin affinity analysis of the engineered Platelet Derived Growth Factor-BB (PDGF-BB). A) Phosphorylated Platelet Derived Growth Factor-BB (pPDGF-BB) quantification using ELISA. No significative difference between wild type PDGF-BB and α2PI1-8-PDGF-BB was found (n = 4); B) Growth Factor (GF) release from fibrin matrices. Graphs show the cumulative release of GFs over 7 days (n = 4). Bars represent the standard error of the mean.

2.1.2. Growth factors release from fibrin matrix

An *in vitro* release assay was performed to verify if BMP-2 and α_2PI_{1-8}-PDGF-BB could be sequestered into fibrin matrix. Fibrin matrices comprising wild-type PDGF-BB, α2PI1-8-PDGF-BB, or BMP-2 were incubated in excess of physiological

buffer during a week. The buffer was changed every day, and released GFs were quantified by ELISA (*Fig 1B*). As previously reported (Martino et al. 2013), BMP-2 was sequestered in fibrin matrix and slowly released. Wild-Type PDGF-BB was quickly released (more than 90% after 2 days), while only 5% of α_2PI_{1-8}-PDGF-BB was released after 7 days.

2.1.3. Delivering BMP-2 and α_2PI_{1-8}-PDGF-BB by fibrin enhances cell growth and OC expression, but not PECAM expression in intramuscularly implanted MSCs

MSCs expressing luciferase reporters could be sensitive sentinels reporting on the physiological environment within implants, as well as GF generators influencing/guiding tissue repair. Dually labeled hAMSCs (10^5 cells) expressing CMV-regulated RLuc and either OC-promoter regulated PLuc or PECAM-promoter regulated PLuc were polymerized with fibrin gels containing BMP-2 and α_2PI_{1-8}-PDGF-BB and im implanted in the left tight (OC-PLuc) or right tight (PECAM-PLuc) of 6-week old SCID mice. A group of mice implanted with the same number of MSCs in fibrin gels without GFs was used as control and monitored for RLuc and PLuc activity during 14 days. Quantification of bioluminescence images from constitutively expressed RLuc photons show that implanted cells proliferated up to day 7 post implantation, after which there was a decline in cell number. Moreover, cells grew better in fibrin plus GFs that on fibrin alone.

Fig. 46 (next page). Non-invasive BLI imaging of RLuc and PLuc-expressing hAMSCs seeded on fibrin scaffolds implanted IM in SCID mice. Right panels, representative BLI images showing Luciferase activity superimposed on b&w images of the corresponding implantation site (left fibrin plus GF; right, fibrin control) at the indicated days. Left panel histograms summarize bioluminescence data acquired from corresponding images. A: Histogram summarizing PLuc activity normalized to day 1; (p=0.025, two-way ANOVA test); B: Histogram summarizing evolution of osteocalcin expression; data represents the ratio OC-PLuc/RLuc (p=0.016, two-way ANOVA test); C: Histogram summarizing evolution of PECAM expression; data represents the

ratio PECAM-PLuc/RLuc, * p<0.05 Student T test; AU = arbitrary units. Color bars illustrate relative light intensities from RLuc (blue: low, red: high,) and PLuc (black: low, blue: high). N=6.

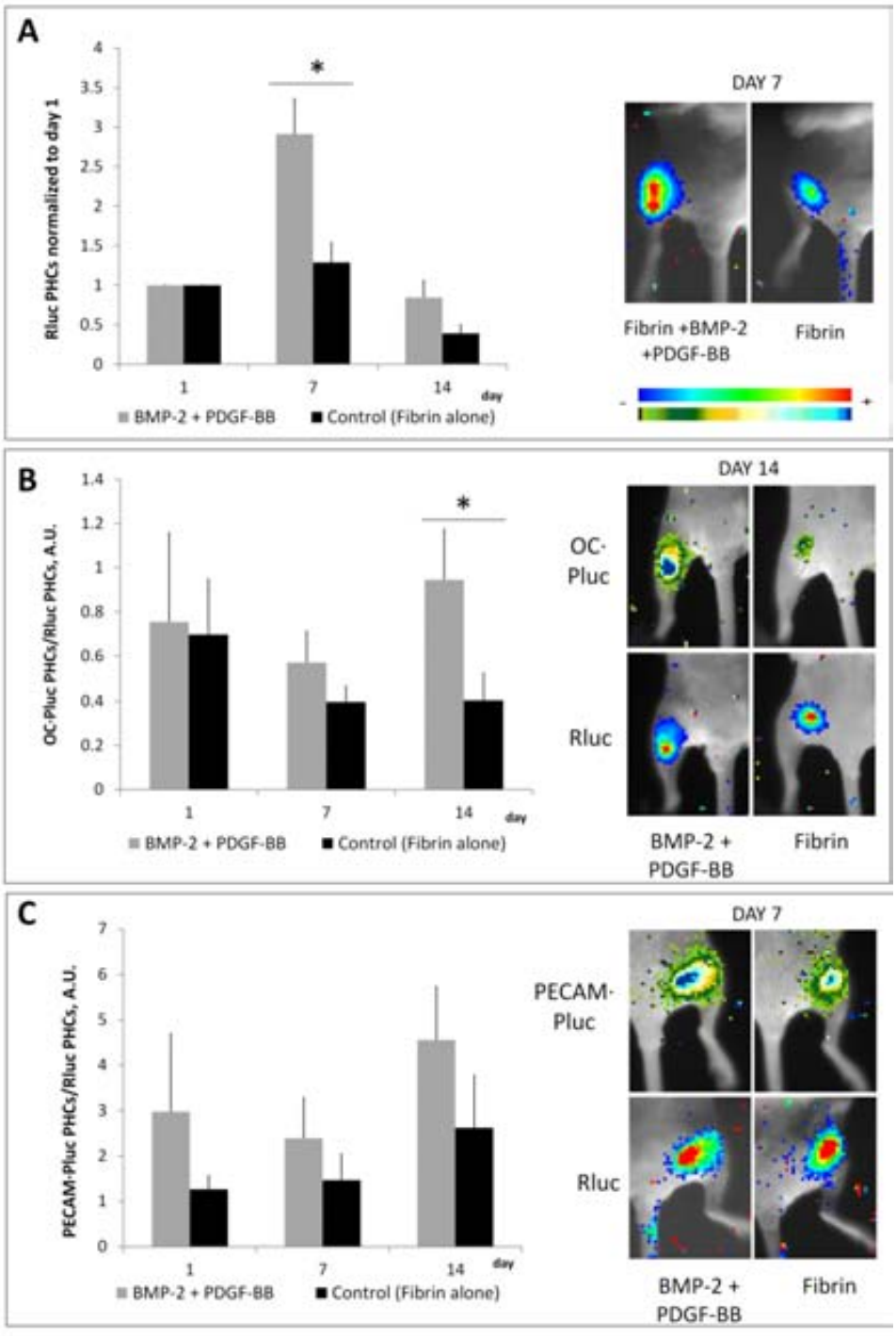

Evaluation of the Pluc/RLuc ratio, that measures changes in gene specific expression relative to cell number, showed that the inclusion of GFs in the fibrin scaffolds resulted in a trend of higher gene expression for both OC-PLuc and PECAM-PLuc, although such trend was only statistically significant in the former case (*Fig. 46*).

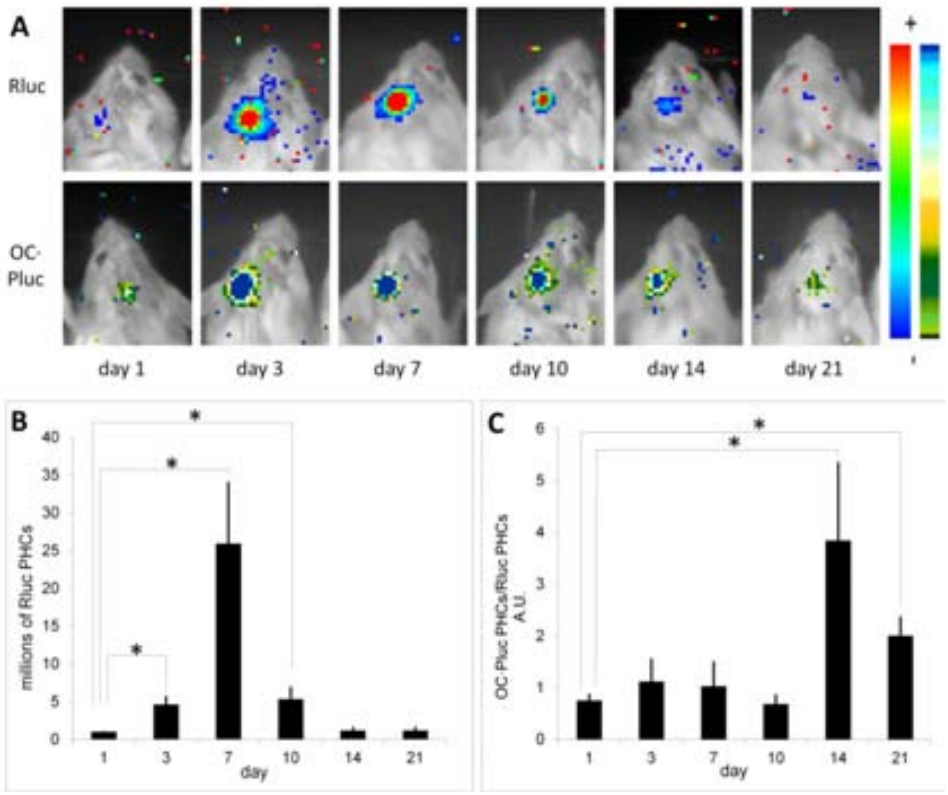

Fig. 47. Non-invasive bioluminescence imaging (BLI) of RLuc and OC•PLuc-expressing hAMSCs cells seeded on fibrin scaffolds implanted in a 3mm-calvarial defect in SCID mice. (a) Representative BLI images showing RLuc (top row) and PLuc (bottom row) activities from dually labeled hAMSCs, superimposed on b&w head images of the corresponding mouse head. Color bars illustrate relative light intensities from RLuc (blue: low, red: high,) and PLuc (black: low, blue: high); (b) Histogram summarizing cell proliferation data, RLuc PHCs are normalized to day 1; (c) Histogram summarizing evolution of osteocalcin expression, data is represented as the ratio PLuc/RLuc. Bars represent the standard error of the mean. * p<0.05 according to Student T test; AU = arbitrary units. N=9.

2.1.4. OC expression but not PECAM expression is activated in hAMSCs during bone regeneration

Genetically modified hAMSCs expressing CMV regulated RLuc and either OC regulated PLuc or PECAM regulated PLuc were implanted in combination with fibrin gels containing bone growth factors (BMP-2 and α2PI1-8-PDGF-BB) in a calvarial bone defect in SCID mice.

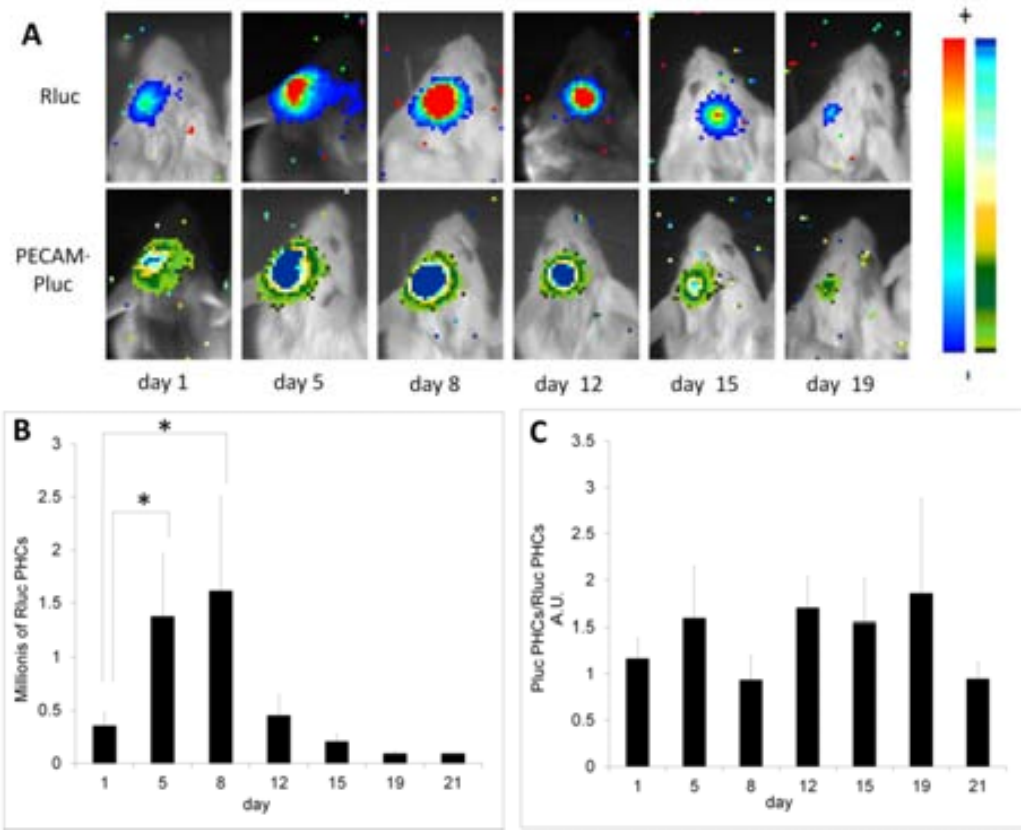

Fig. 48. Non-invasive imaging of RLuc and PECAM•PLuc-expressing hAMSCs cells seeded on fibrin scaffolds implanted in a 3mm-calvarial defect in SCID mice. (a) Representative BLI images showing RLuc (top row) and PECAM•PLuc (bottom row) activity from dually labeled hAMSCs, superimposed on b&w head images of the corresponding mouse head. Color bars illustrate relative light intensities from RLuc (blue: low, red: high,) and PLuc (black: low, blue: high); (b) Histogram summarizing cell proliferation data, RLuc PHCs are normalized to day 1; (c) Histogram summarizing evolution of PECAM expression, data is represented as the ratio PLuc/RLuc. Bars represent the standard error of the mean. * p<0.05 according to Student T test; AU = arbitrary units. N=9.

To monitor cell growth and changes in gene expression, RLuc and PLuc activities, were monitored in live animals during 3 weeks using BLI. Results show that the cell proliferation pattern, as measured by RLuc activity, was similar regardless of whether cells were additionally labeled with OC:PLuc or PECAM:PLuc. Cells proliferated up to days 7-8 following which cell number decreased progressively. However, there was a difference in gene expression behavior, with a significant increase in OC, but not in PECAM expression, as measured by the ratio of RLuc/PLuc activities (*Fig. 47* and *Fig. 48*).

2.1.5. Delivering BMP-2 and α_2PI_{1-8}-PDGF-BB by fibrin does not improve bone coverage but promotes the formation of thicker bone

Previous results suggest that inclusion of BMP-2 and α_2PI_{1-8}-PDGF-BB in fibrin matrix induces changes in gene expression indicative of osteogenic lineage differentiation in "sentinel" cells seeded in the fibrin material.

In order to determine if addition of BMP-2 and α_2PI_{1-8}-PDGF-BB to fibrin gels improves bone regenerative capacity, a 3 mm diameter calvaria bone defect was produced in 6 week old SCID mice and implanted with fibrin alone, fibrin plus BMP-2 and α_2PI_{1-8}-PDGF-BB or fibrin plus BMP-2 and α_2PI_{1-8}-PDGF-BB and hAMSCs, as indicated in the diagram in *Fig. 49D*. . In an additional control group the bone defect was left without implant. Following a 6 week growth period, mice were sacrificed and mice heads analyzed by microCT imaging to determine the change in defect size and bone volume regenerated.

Histograms representing the percent of defect surface covered with new bone during this period (*Fig. 49A*) indicate that while fibrin improved defect filling with bone, in comparison with no fibrin, inclusion of GFs or cells had no significant additional effect.

However, evaluation of changes in bone volume (*Fig. 49B*) and thickness (*Fig. 49C*) showed that the inclusion of GFs did result in a significant increase in bone

volume relative to no scaffold or fibrin alone. Inclusion of hAMSCs in the fibrin scaffold had no significant effect on regenerated bone volume over that of fibrin scaffold alone.

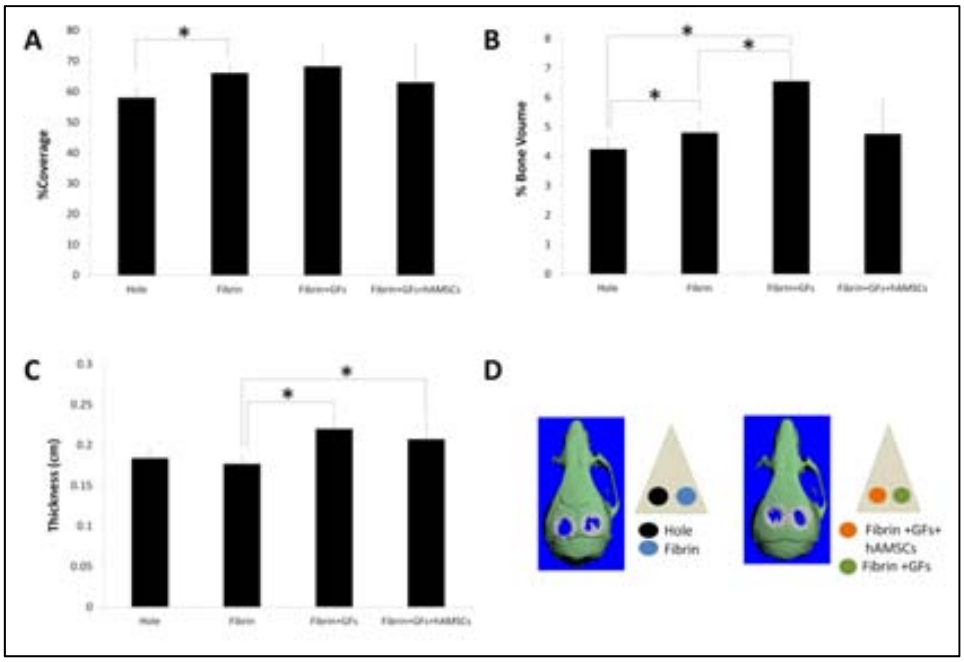

Fig. 49.Micro Computed Tomography (µCT) analysis of bone formation in a calvaria defect regeneration model in SCID mice (6 weeks post implantation). Defects were implanted with : nothing (empty), fibrin, fibrin + BMP-2 + PDGF-BB and fibrin + BMP-2 + PDGF-BB + hAMSCs. (a) Histogram summarizing surface coverage results for each test; (b) Histogram summarizing bone volume results for each group; (c) Histogram summarizing bone thickness results for each group; (d) representative µCT images of skulls and diagram showing disposition of implants. Bars represent the standard error of the mean. * p<0.05 according to Student T test. N=14.

2.1.6. Delivering BMP-2 and $\alpha_2PI_{1\text{-}8}$-PDGF-BB with fibrin improves vascularization of the new bone

In order to analyze the effect of the different treatment combinations in the vascularization of the new bone, half of the mice from the previous experiment were perfused with a polymeric resin to perform a vascular cast. Once corroded and stained with osmium, casts were analyzed by utra-high resolution micro-computerized tomography. Vascular cast images showed a denser vascular network in the defects treated with fibrin plus BMP-2 and $\alpha_2PI_{1\text{-}8}$-PDGF-BB

when compared to those non-treated or treated with fibrin only (*Fig. 50*). Quantitative analysis of cast images showed that relative vessel volume, vessel number and vessel thickness were significantly higher in the defects treated with fibrin plus BMP-2 and $\alpha_2PI_{1\text{-}8}$-PDGF-BB when compared with the non-treated defects or those treated with fibrin alone (*Fig. 51: A, B and C*). Vessel spacing, in the other hand, was significant lower, indicating higher compaction, in the defects treated with fibrin and GFs (*Fig. 51D*). Inclusion of hAMSCs in the fibrin plus GFs scaffolds had no significant effect in any of these parameters.

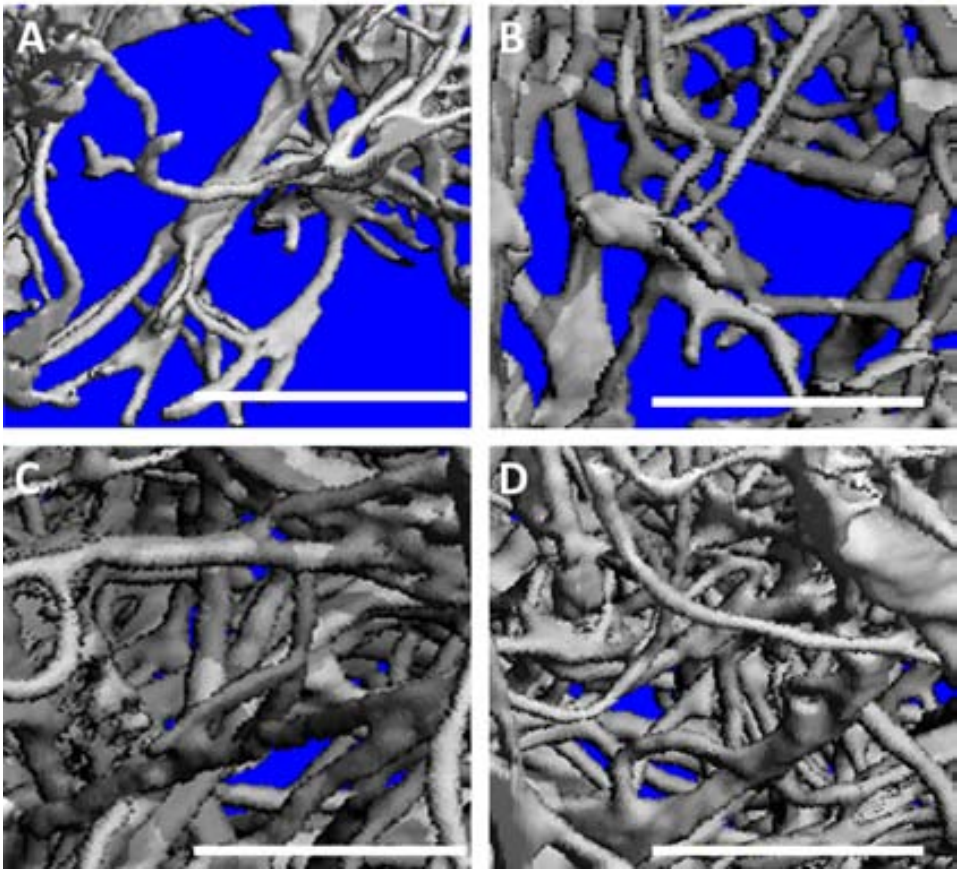

Fig. 50. High resolution µCT images of calvarial defect vascular casts. Defects were left empty (A), treated with fibrin alone (B), treated with fibrin with BMP-2 and α2PI1-8-PDGF-BB (C) and treated with fibrin BMP-2 and PDGF-BB and hAMSCs. Scale bar: 1 µm.

2.1.7. Addition of hAMSCs to fibrin plus BMP-2 and $\alpha_2PI_{1\text{-}8}$-PDGF-BB matrices improves connectivity of the vascular network of the newly formed bone.

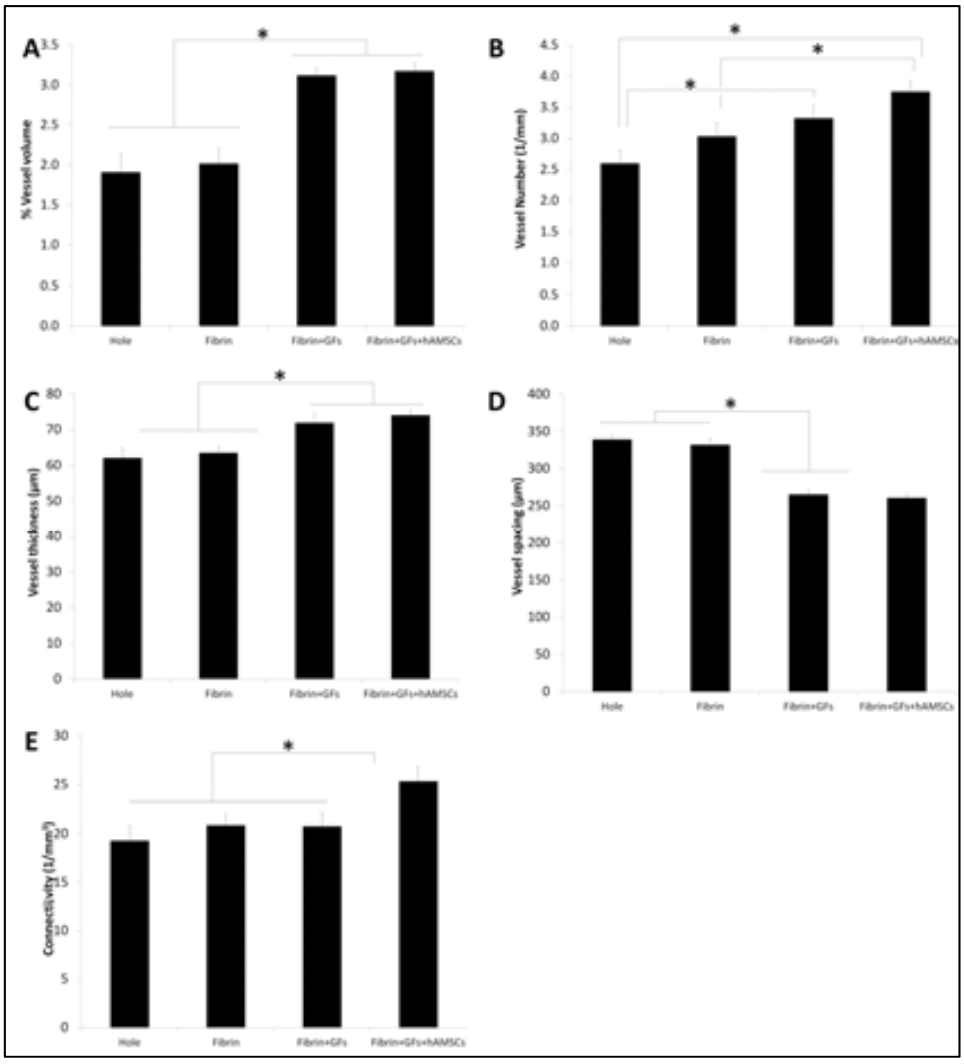

Fig. 51. µCT analysis of vascularization of a calvarial defect in SCID mice (6 weeks post implantation). Calvarial defects were treated with: nothing (empty defect), fibrin, fibrin plus GFs and fibrin plus GFs and hAMSCs. Histogram summarizing percentage of vessel volume (A), vessel number (B), vessel thickness (C),vessel spacing (D), and density of intervascular connections (E), for each group. Bars represent the standard error of the mean. * p<0.05 according to Student T test. N=6.

Analysis of data form vascular cast topographies showed that while vascular connectivity in the newly formed bone was similar in the defects treated with fibrin, with fibrin plus GFs, and with the controls, it was significant improved by the addition of hAMSCs (*Fig. 51E*).

2.2. Discussion

Designing biomaterials that aid in tissue regeneration requires agile *in vivo* evaluation procedures that facilitate an iterative strategy based on cycles of material design - *in vivo* testing - modification- *in vivo* testing. The aim of the current work was to develop a novel multimodal analysis platform to evaluate the capacity of BMP-2 and fibrin-binding PDGF-BB delivered through fibrin to treat bone defect. The two GFs were used at the same time, as we believe that the delivery of several GFs at low doses may present a rational clinical approach for tissue healing, since multiple GFs are involved during natural healing processes.

We combined an *in vivo* procedure for imaging luciferase expressing hAMSCs and an ex-vivo microCT imaging procedure to evaluate the extent of bone and vascular regeneration. With this approach, *in vivo* imaging of luciferase expressing hAMSCs that served as sentinel provided real-time information on physiological conditions inductive of cell growth and differentiation, while ex vivo microCT analysis served to evaluate the amount and quality of newly formed bone and vascular structures.

We used a non-invasive BLI procedure based on the use of a high sensitivity video camera, to detect visible light photons generated by luciferase reporters genetically introduced in hAMSCs. By including constitutively active promoters to regulate luciferase expression we can observe the evolution in the number of hAMSCs seeded in the fibrin scaffolds implanted in mice. Moreover, by introducing in hAMSCs additional luciferase reporters regulated by tissue

specific promoters, only active in specific cell lineages, it is also possible to monitor changes in gene expression leading to cell differentiation. Changes in the activity of inducible reporters can best be quantified by relating them to the activity of the constitutively active luciferase, and expressing them as the ratio of their respective photon fluxes, avoiding in this manner artifacts due to in-vivo fluctuations in cell number.

Due to the capacity of hAMSCs to differentiate to multiple lineages, e.g., chondrogenic, adipogenic and osteogenic lineages, in response to external clues, these cells can be used as living reporters of growth and differentiation conditions within scaffolds. Thus, we used hAMSCs dually modified to express RLuc, regulated by a constitutively active promoter (CMV-RLuc), and with an additional PLuc-eGFP chimerical reporter. The latter regulated by either the PECAM or the human osteocalcin (hOC) inducible promoters to analyze the capacity of the material to induce cell differentiation.

With this approach, we were able to observe that in im implanted fibrin matrices containing BMP-2 and $\alpha_2PI_{1\text{-}8}$-PDGF-BB and luciferase expressing hAMSCs there was an induction of the osteocalcin but not of the PECAM endothelial reporter activity. We also used a calvarial bone defect model to determine whether selective osteocalcin induction capacity was also observed when the material was implanted in a bone defect.

Using the BLI procedure we were able to corroborate that, since fibrin containing BMP-2 and $\alpha_2PI_{1\text{-}8}$-PDGF-BB induced an increase in osteocalcin but not PECAM expression during bone repair.

While *in vivo* imaging was a useful tool to monitor ongoing cellular processes *in vivo*, BLI results were complemented with microCT as a standard endpoint analysis of bone and vascular development. Our results indicate that inclusion of BMP-2 and $\alpha_2PI_{1\text{-}8}$-PDGF-BB (1 µg of each GF) in the fibrin scaffold did not

result in the generation of more bone surface, as compared to fibrin alone. Nevertheless, the addition of GFs did have a significant effect in the formation of thicker bone. Surprisingly, inclusion of the hAMSC reporters did not have a detectable effect on the amount of bone formed. A possible interpretation for this result could be that the number of cells used was too small to have a significant mass effect.

Since tissue repair is normally accompanied by angiogenesis, we also generated vascular casts of the treated mice by perfusion with a polymeric resin, followed by tissue corrosion. Analysis of 3D microCT images generated from the plastic casts revealed that the inclusion of BMP-2 and $\alpha_2PI_{1\text{-}8}$-PDGF-BB in the fibrin scaffold improved its angiogenic capacity, resulting in formation of more and thicker vessels as compared to controls treated with fibrin only. While the inclusion of hAMSCs did not appear to improve any of the above parameters, they did have a statistically significant role in producing more abundant inter-vascular connections. Thus, even if luciferase expressing hAMSCs did not appear to differentiate to endothelial lineage, they did play a more complex organizational role in vascularization. This result supports the hypothesis that hAMSCs included in scaffolds contribute more importantly to the paracrine regulation of the physiological environment than to the formation of new tissue, in accordance with recent results from their use in the repair of other tissues.

3. CHAPTER III: DEVELOPMENT OF A MINI-BIOREACTOR SYSTEM FOR THE ANALYSIS OF BIOMATERIAL-STEM CELLS INTERACTIONS

Bioreactors are generally defined as devices in which biological and/or biochemical processes develop under closely monitored and tightly controlled environmental and operating conditions (e.g. pH, temperature, pressure, nutrient supply and water removal) (Martin et al. 2004).

Bioreactor systems play an important role in Tissue Engineering (TE), as they allow safe and reproducible production of tissue constructs. For clinical applications, the use of bioreactors should be an advantageous method to produce materials with low contamination risk, ease of handling and scalability (Pörtner et al. 2005). Bioreactors may also provide reliable model systems to investigate tissue growth under reasonably realistic conditions, (e.g. fluid flow, shear stress, etc.) providing technical means to perform controlled studies aimed at understanding specific biological, chemical or physical aspects of tissue regeneration.

The most widely used bioreactors for TE are perfusion bioreactors, since they allow the modulation of mass transport for nutrients and oxygen and waste removal from the tissue culture environment. Furthermore, interstitial perfusion is considered to be an important stimulus in the mechanobiology of several three-dimensional tissues, and hydrodynamic shear stresses may positively affect cell viability, differentiation and protein production (Martin et al. 2004). Grayson et al (Grayson et al. 2008) showed that the rate of medium perfusion during cultivation has an important effect on the characteristics of engineered bone formed in a bioreactor. Lee and Niklason (Lee & Niklason 2010) demonstrated that fluid flow facilitates the formation of microvessels and stimulates the production of growth factors in a tridimensional endothelial and mesenchymal stem cell gel coculture.

Cell seeding of scaffolds is the first step in establishing a 3D culture, and might play a crucial role in determining the progression of tissue formation (Vunjak-Novakovic et al. 1998). Seeding cells into scaffolds at high densities has been associated with enhanced tissue formation in 3D constructs, including higher rates of cartilage matrix production, increased bone mineralization (Holy et al. 2000) and enhanced cardiac tissue structure. Thus, engineering autologous grafts for clinical applications using high initial cell densities requires the cells to be seeded with the highest possible efficiency. Furthermore, the initial distribution of cells within the scaffold after seeding has been related to the distribution of tissue subsequently formed within engineered constructs (Holy et al. 2000; Kim et al. 1998), suggesting that uniform cell-seeding could establish the basis for uniform tissue generation.

The main problem of the cell seeding in perfusion bioreactor systems is the selection of the right fluid flow velocity (Wendt et al. 2003). High velocities do not allow cell adherence to the material, whereas low velocities do not move the cells fast enough, resulting in their adhesion to the tubing of the perfusion system or sinking to the lower parts of the system due to gravity becoming unavailable. Wendt et al. (Wendt et al. 2003) found that the optimal seeding velocity depends highly on the scaffold microstructure. Thus, at this point, there are no general formulas to suggest optimal scaffold seeding rates, which are mainly determined by empirical approaches.

The goal of this work was to develop a non-destructive system to study cell growth and behavior in 3D scaffolds. Based on a non-invasive bioluminescence imaging (BLI) platform, we designed and validated a miniaturized, optically accessible bioreactor for interstitial perfusion and control of several working parameters that allows systematic analysis of optimal scaffold seeding and long-term maintenance conditions.

BLI provides a useful means for monitoring physiological processes in real-time, ranging from cell survival to gene expression. Due to the capacity of light photons to transverse tissues, BLI can be used to monitor the proliferation and distribution of cells expressing luciferase reporters in engineered tissues thinner than 2 cm (Massoud & Gambhir 2003a). Moreover, by using inducible tissue specific gene promoters to regulate the expression of luciferase reporters, biologically significant changes in promoter activity are reported as easily monitored photon fluxes. Thus, analysis of photon images provides information on cell growth, distribution and time related changes in gene expression associated to cell differentiation (Iyer et al. 2001; Contag et al. 1997; Bagó et al. 2012; Vila et al. 2012). In this work we use the inducible promoter of the platelet endothelial cell adhesion molecule-1 (PECAM-1) (Newman & Albelda 1992)to regulate the expression of the Photinus pyralis luciferase (PLuc) as a reporter of endothelial differentiation of cells seeded in our bioluminescent bioreactor prototype.

Human adipose-derived mesenchymal stromal cells (hAMSCs) are multipotent stem cells with a similar phenotype and equivalent differentiation potential to their homologues counterparts from bone marrow, although these cells are considerably easier to isolate in larger quantities. HAMSCs can differentiate into mesodermal lineages, including bone, cartilage, fat, tendon, ligament and muscle (Zuk et al. 2002; De Ugarte et al. 2003; Kern et al. 2006; Schäffler & Büchler 2007). Although mechanisms underlying the vascular differentiation of hAMSC and their contribution to neovascularization are poorly understood, there is evidence supporting MSC participating in angiogenesis (Al-Khaldi et al. 2003; Chung et al. 2009; Whyte et al. 2011).

Poly(lactic acid) scaffolds, previously shown to support cell adhesion and tissue growth (Charles-Harris et al. 2008; Vila et al. 2012), can be produced consistently with a regular architecture and are, therefore, a convenient model

to test the capacity of the system to continuously monitor cell seeding, proliferation and gene expression changes. A modified PLA scaffold containing calcium phosphate glass (PLA/CaP) with capacity to stimulate both endothelial and osteogenic differentiation (Vila et al. 2012; Aguirre et al. 2010) was also used for comparative purposes.

We show that the perfusion system developed in this work is useful for both determining optimal seeding conditions and monitoring a variety of culture parameters such as cell survival, distribution, differentiation or hypoxia state, showing potential as a useful tool for scaffold development and TE applications.

3.1. Results

3.1.1. BLI allows the visualization of scaffold seeding in a bioreactor

To evaluate the potential of BLI procedures to monitor the behavior of cells in a biomaterial, a transparent bioreactor model was constructed, comprising a cylindrical glass perfusion chamber that houses a scaffold material, connected to a medium reservoir situated inside a heating bath and provided with an agitation system (*Fig. 29*).

HAMSCs were transduced with a lentiviral vectors for the expression of RLuc regulated by a constitutively expressed CMV promoter, as a bioluminescent reporter and then injected in the agitated medium reservoir containing benzyl-coelenterazine. Time lapse images of the perfusion device and scaffold placed in the detection chamber of an ImagEM X2 Imaging System were acquired during 1 minute, at regular 2 minute intervals, as described in methods during the entire seeding process until the bioluminescence signal disappeared.

Time lapse bioluminescent images show (*Video 1*) the time dependent progressive loading of the scaffold and the generation of a cell occupancy gradient decreasing in the flow direction. Graphs representing the total number

of photons emitted by the whole scaffold versus time illustrate a saturation kinetics process taking place during the first 80 minutes (Fig. 52).

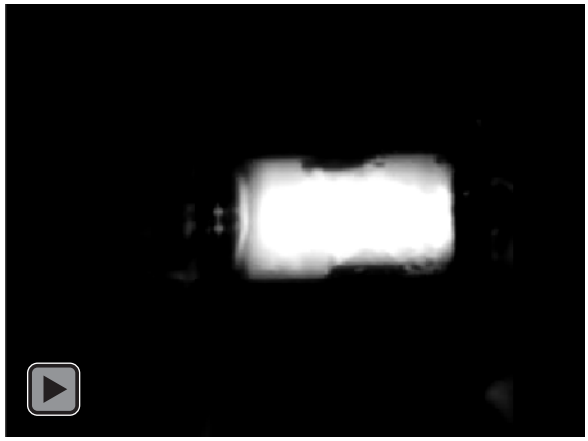

Video 1. Real-time bioluminescence imaging (BLI) of cell seeding of a PLA scaffold (see digital PDF version or video file in the attached CD-ROM)

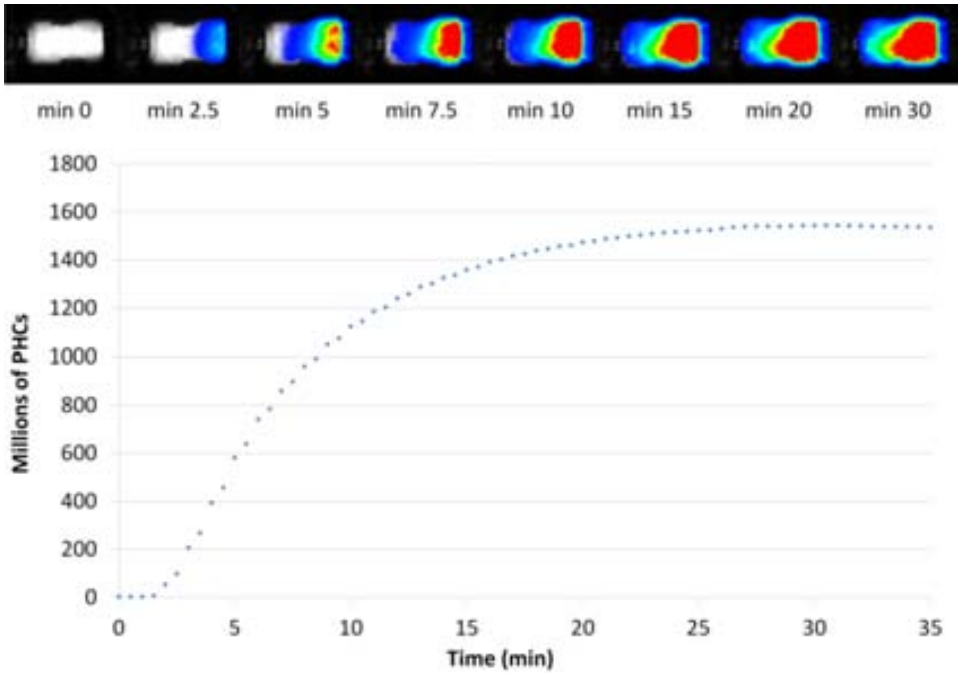

Fig. 52. Real-time BLI of scaffold seeding in the perfusion system. Representative images showing progressive loading of a scaffold. Fluid flow is from right to left. Arbitrary colors show light emission intensity (red=high; blue=low). The graph shows time related changes, every two minutes, in the number of light events recorded from the whole imaged area.

In order to verify that cells are seeded inside the scaffold and not in its surface, at the end of each experiment scaffolds were recovered, sliced perpendicular to the flow direction and imaged. Images show the presence of cells throughout the perpendicular section (*Fig. 53*).

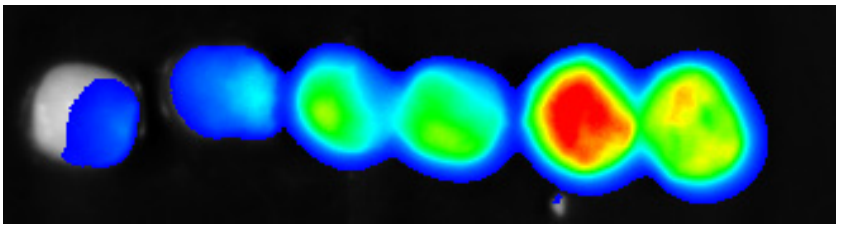

Fig. 53. Bioluminescent Images of PLA scaffold sections following seeding in the bioreactor system

3.1.2. BLI allows the quantification of cells inside the bioreactor

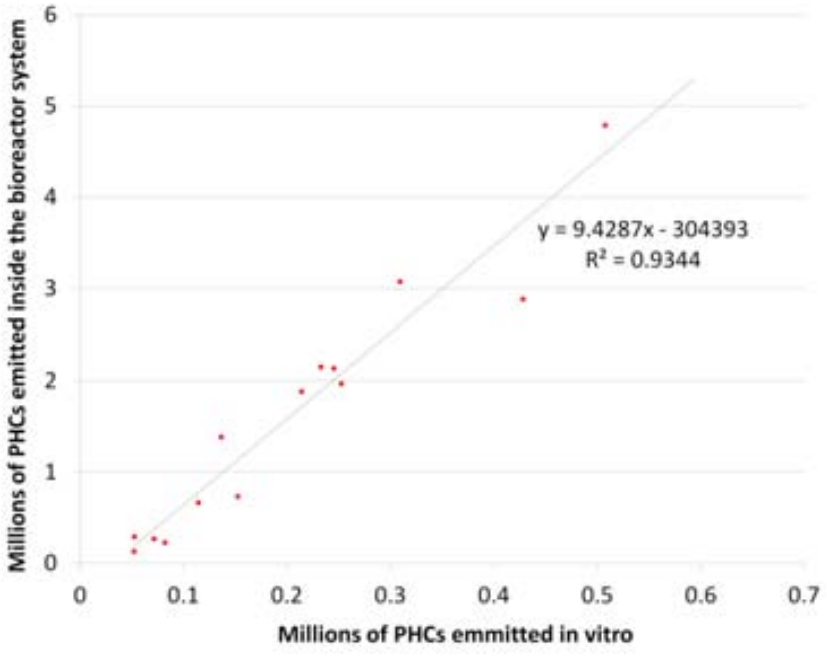

Fig. 54. Standard curve relating the total number of photons from the scaffold with the corresponding number of photons generated by the same cells in vitro

Once ascertained the possibility of using BLI to visualize the process of scaffold seeding within the bioreactor the possibility of obtaining quantitative data using this procedure was assessed. To do this, a scaffold seeded with cells was pulse by circulating substrate through the system, one cycle at a constant flow of 4mm/s, while the scaffold was continuously imaged every 10 seconds until the number of photons recorded began to decrease. Peak image values were used for the analysis.

For constructing a standard curve, $5x10^3$, $5x10^4$, $1x10^5$ and $2x10^5$ RLuc-expressing hAMSCs were seeded in PLA scaffolds, and imaged as previously described. At the same time, the same number of cells was seeded in 48-well plates to which 50 µL of benzyl-coelenterazine solution were added and imaged for one minute at binning 1x1. Results show that there is a linear correlation between the number of photons emitted by the cells in the bioreactor scaffold and *in vitro*, R^2 of 0.9344 (*Fig. 54*). The slope of the correlation curve describes the yield in photons generated by cells in the bioreactor compared with the same cells *in vitro* in the indicated conditions.

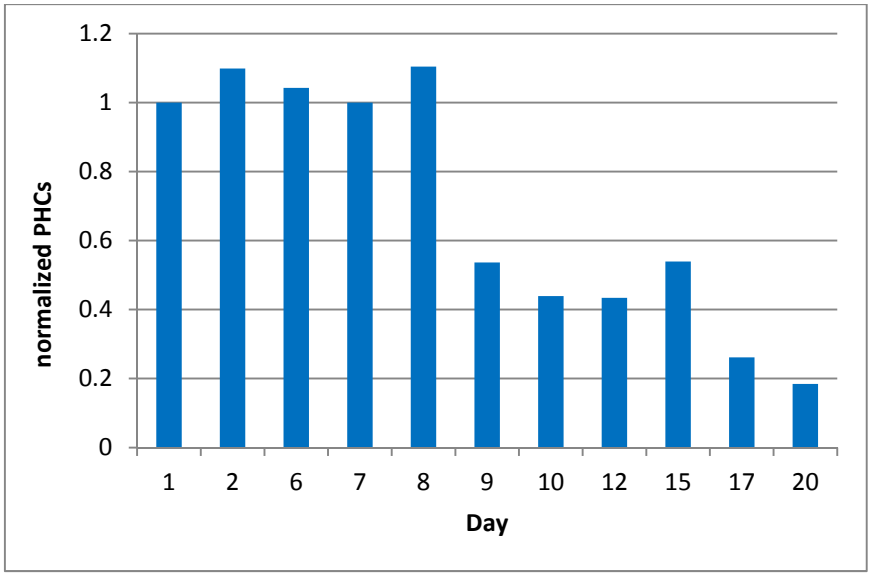

Fig. 55. Long-time survival of hAMSCs inside the bioreactor system.

3.1.3. Cells survive and can be observed during an extended time in the bioreactor system

PLA scaffolds were seeded with 2 million of RLuc-expressing hAMSCs and cultured in the bioreactor system for up to three weeks. Results of BLI monitoring show that cells survive, with little variation in the number of emitted photons during the whole period (*Fig. 55*). Longer culture periods with the PLA scaffolds were not possible due its biodegradability, but results suggest that cells could be maintained alive for longer periods providing an adequate scaffold.

3.1.4. Flow velocity influences cell seeding efficacy and distribution

Cell seeding was performed at four different flow velocities (0.5, 2.2, 4.0 and 5.8 mm/s). After seeding, RLuc activity was determined as explained in the methods section, and the number of seeded cells was calculated using the standard curve obtained in the previous section. Results show that cell seeding yields are optimum for a flow velocity of 4 mm/s (*Fig. 56*).

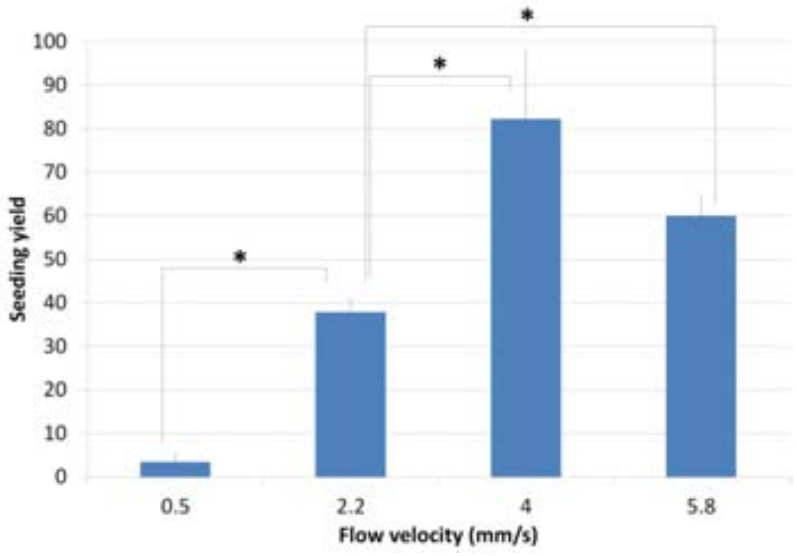

Fig. 56. Effect of flow on seeding performance. The histogram shows the seeding yield at different flow velocities. Bars represent the standard error of the mean. * p<0.05 according to Student T test. n=3.

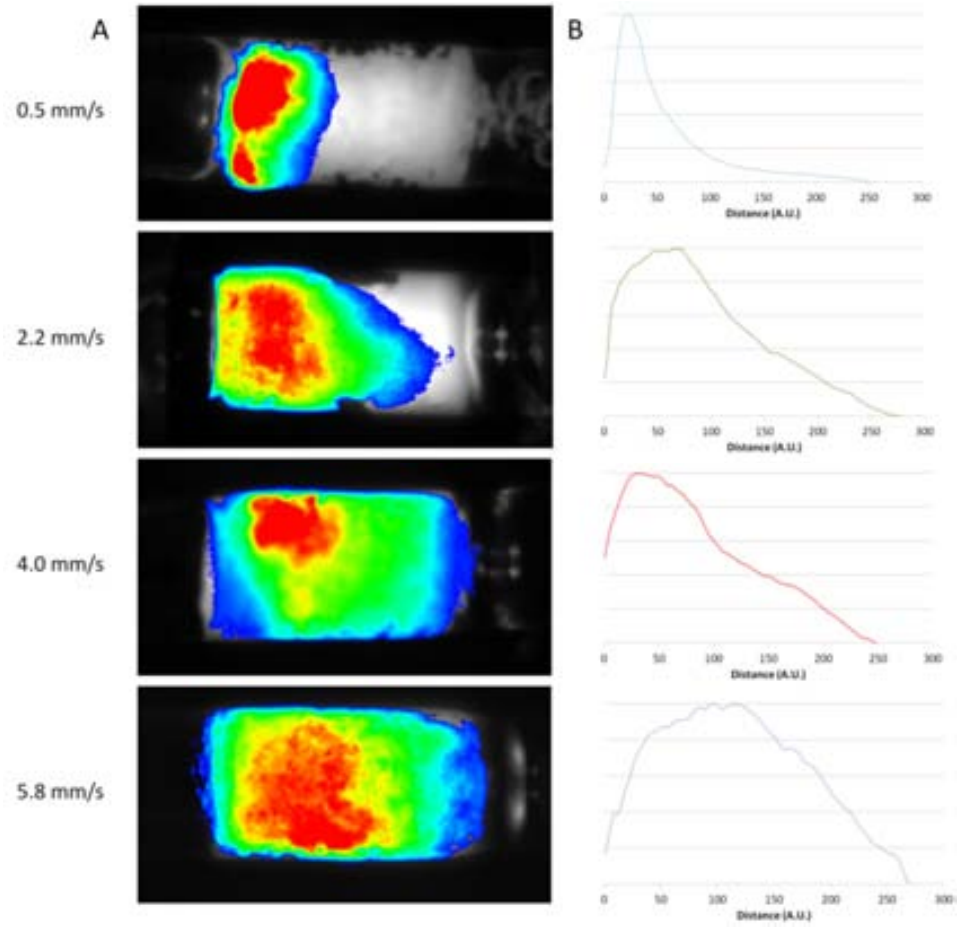

Fig. 57. A: Representative images of cell distribution 24h after seeding at different flow velocities. B: Profiles of cell distribution. A.U.= Arbitrary Units. Arbitrary colors show light emission intensity (red=high; blue=low).

3.1.5. Endothelial differentiation can be monitored inside the bioreactor

Dually labeled hAMSCs ($2x10^6$ cells) expressing CMV-regulated RLuc and PECAM-promoter regulated PLuc were seeded at 4.0 mm/s in a PLA scaffold containing calcium phosphate glass (PLA/CaP). The day after seeding, medium was changed for an endothelial differentiation medium and the culture conditions maintained for 14 days. As a control, the same cells were seeded in equal conditions in a normal PLA scaffold and cultured in L-15 medium.

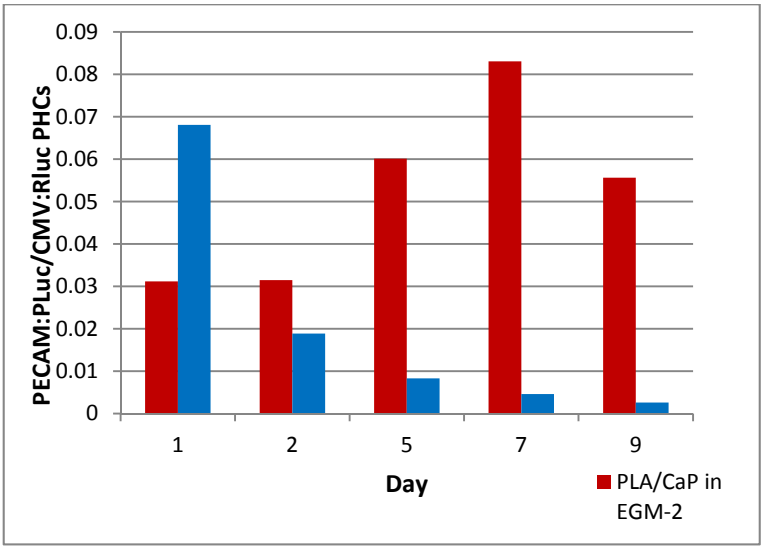

Fig. 58. Evolution of the ration PLuc/RLuc PHCs, indicative of the grade of PECAM expression, in hAMSCs seeded in either PLA or PLA/CaP and cultured in L-15 and EGM-2 medium respectively. Differences between two series were significative; p<0.05 according to the two-way ANOVA test).

Bioluminescent images from RLuc and PLuc activities were obtained as explained in the methods section, every 2-3 days during the whole period. Changes in PECAM expression were calculated as changes in the ratio PLuc/RLuc. Results showed that while the ratio PLuc/RLuc decreased with time in the control PLA scaffold, it increased progressively in the EGM-2 cultured PLA/CaP scaffold, indicating that endothelial differentiation was taking place (*Fig. 58*). Differences between two series were significative ($p<0.05$ according to the two-way ANOVA test).

3.2. Discussion

Bioreactor systems are gaining increasing importance in TE due to their capacity of producing tissue constructs in a safe and reproducible way. Furthermore, they can be used as an intermediate step between *in vitro* and *in vivo* studies for analyzing scaffold-cell interactions.

In this work we present a novel methodology to analyze bioreactor systems by non-invasive BLI. This technology allows real-time and non-destructive studies of cell-scaffold interactions, in contrast to traditional analysis methods that require sample destruction at the end of the test (e.g. histology, CT, microscopy).

We have developed a transparent mini-bioreactor system comprising a heated and stirred culture reservoir, a peristaltic pump and a transparent imaging chamber. This bioreactor sustains cell growth for long periods of time; at least up to three weeks tested, although current results suggest much longer survival would be possible.

There was a linear relationship between the photons emitted by the bioreactor and the number of RLuc-expressing hAMSCs seeded within it. Thus, our device can be used as a quantitative instrument to measure the number of living cells inside the scaffold at any time point, making it a useful instrument to study cell seeding and cell survival under different conditions.

The best flow rate for cell seeding in perfusion systems depends on the material architecture and it must be determined in each particular case. Our bioluminescent bioreactor has proved to be a useful tool for this type of analysis, allowing not only the quantification of the seeding efficiency but also the visualization of cell distribution throughout the scaffold.

We have also demonstrated the possibility of using inducible luciferase reporters to monitor changes in gene expression inside the bioreactor. Specifically, we have used hAMSCs that expressed CMV-regulated RLuc and PECAM-promoter regulated PLuc for real-time monitoring of endothelial differentiation.

This procedure could be applicable to a wide variety of materials, scaffold formats and cell types. The expression of a wide variety of genes of interest,

depending on promoter availability could also be monitored. Thus the current strategy shows potential for the analysis of cell behavior within scaffolds under different culture conditions.

VII. **GENERAL DISCUSSION**

Biomaterial development for TE is a very complex and prolific research field overlapping material engineering, chemistry, cell biology and medicine fields; every year promising new devises comprising materials, growth factors and cells are reported that require *in vitro* and *in vivo* studies previous to clinical evaluation. Unfortunately, *in vitro* conditions are very far removed from those in real life and many initially promising devices fail when tested in live animals.

One of the key factors than can determine the success or failure of a biomaterial is its capacity to induce angiogenesis. In implants that lack their own blood supply, oxygen can only diffuse for a few hundred of micrometers before being consumed (Griffith & Naughton 2002) causing cell death. Thus, engineering scaffolds to include factors that promote angiogenesis could be a solution.

The number of possible combinations between cell types, factors and biomaterials is so large that testing platforms that can rapidly screen and identify optimal formulas, e.g., that emphasize key characteristics such as angiogenic capacity or promotion of differentiation to specific lineages would facilitate devise development.

In this thesis we demonstrated the potential of noninvasive BLI to study and analyze cell-scaffold interactions in live animals. BLI technology allows the real-time monitoring of cell number and distribution within the scaffolds. Furthermore, by using tissue-specific inducible promoters, changes in expression of specific genes related to cell differentiation (PECAM, osteocalcin) or hypoxic state (HIF) can also be monitored.

This provides very useful information about the scaffold behavior *in vivo* and about what characteristics should be improved to obtain the desired results. By combining the real-time data from this bioluminescence platform with other

end point imaging technologies, it is possible to obtain a full vision of the biomaterial behavior.

In this work we used two very different biomaterials developed by collaborators to illustrate as “proof of principle” the application of *in vivo* BLI technology in the evaluation of bio-engineered scaffolds for tissue repair.

In the first case we proved the angiogenic capacity of a new composite biomaterial comprising PLA and calcium phosphate glass. Our BLI results, indicating that inclusion of calcium phosphate glass particles on PLA improved the angiogenic capacity of the material, were also validated using standard immunofluorescent staining and histological procedures for vessel quantification.

In the second proof of principle case, we evaluated a GF-delivering fibrin scaffold engineered for bone repair using a live bone regeneration model. Our BLI results indicated that the GF-delivering material had the capacity to induce osteoblastic, but not endothelial, differentiation in sentinel mesenchymal stem cells included in the scaffold. Again, our BLI results were corroborated by µCT analysis that showed not only that thicker bone, but also denser vascular structures of host origin were induced by the delivery of GF. Moreover, in this case we were able to partially seed light over an important issue in tissue repair; that is the role of stem cells included in scaffolds on the repair process. Again, the combination of BLI and µCT analysis indicated that sentinel cells while not differentiating to the endothelial lineage, did have a relevant paracrine role inducing abundant intervascular connections.

Understanding the response of cells within biomaterials to changing physical parameters (e.g.: response to shear stress, hypoxia etc.) is valuable information to guide the development of scaffolds for specific applications. Inspired by these considerations we initiated an ambitious approach to develop a

minibioreactor system useful for the analysis of cell-scaffold interactions without having to resort to live animals. This bioreactor system, based in the same bioluminescent platform, allows real-time analysis of cell survival and differentiation within the biomaterial under dynamic flow conditions and it could be considered as an intermediate step between *in vitro* and *in vivo* studies, facilitating the biomaterial design-test-redesign cycle. This type of device is important due to additional considerations. Bioreactors are becoming increasingly more important as they allow safe and reproducible production of scaffold-tissue composites for clinical applications. Thus, BLI monitored system could also be a useful tool for designing and optimizing cell seeding of scaffolds; allowing the quantification of cell survival, and the visualization of cell distribution along the scaffold under customizable culture conditions.

We have made progress in this area also, and a small bioreactor prototype comprising a model biomaterial was constructed and successfully used to illustrate cells distribution and survival under dynamic seeding conditions, as well as proliferation and differentiation in response to inducing agents.

While this is still work in progress, we believe it points in the right direction and more case studies should help support the use of this bioengineering strategy in the design of products for clinical applications.

VIII. **CONCLUSIONS**

1. CASE STUDY I: ASSESSMENT OF THE ANGIOGENIC CAPACITY OF PLA SCAFFOLDS

- Noninvasive BLI was useful to demonstrate that addition of calcium phosphate glass to PLA results in a composite material with better angiogenic capacity than PLA only.
- BLI allowed monitoring the proliferation of luciferase expressing hAMSCs in PLA/CaP scaffolds implanted in mice.
- BLI allowed monitoring the differentiation to the endothelial lineage of luciferase expressing hAMSCs seeded in PLA/CaP scaffolds implanted in mice.
- BLI allowed monitoring changes in the hypoxic state of luciferase expressing hAMSCs seeded in scaffolds implanted in mice, in correlation with differentiation of hAMSCs to the endothelial lineage.
- Standard histological analysis validated BLI results and showed that calcium phosphate glass particles in PLA scaffolds implanted in SCID mice induced the colonization of the material by host vascular structures functionally connected to the vascular system.

2. CASE STUDY II: ANALYSIS OF THE BONE REGENERATION CAPACITY OF AN ENGINEERED FIBRIN GEL

- *In vivo* BLI was useful to demonstrate that smart fibrins delivering BMP-2 and PDGF-BB induce the differentiation of hAMSCs to the osteogenic but not to the endothelial lineage.
- µCT analysis of bone showed that, BMP-2 and PDGF-BB comprising fibrins promote formation of new bone and vascular structures derived from the host.
- Luciferase expressing hAMSCs seeded in fibrin scaffolds had no effect on bone formation and did not influence he number or thickness of host derived vessels.

- Luciferase expressing hAMSCs had a paracrine-based organizational role, significantly promoting the formation of more interconnections between host derived vessels during bone regeneration

General conclusion from 1 and 2:

- Luciferase expressing hAMSCs were effective reporters of cell behavior *in vivo*, bone and endothelial differentiation.
- BLI is an effective tool for *in vivo* analysis of stem cell biomaterial interactions.
- The combination of BLI and µCT for imaging of gene expression and bone and vascular structures, respectively, is an effective multimodal approach for the analysis of scaffold performance.

3. CHAPTER III: DEVELOPMENT OF A MINI-BIOREACTOR SYSTEM FOR THE ANALYSIS OF BIOMATERIAL-STEM CELLS INTERACTIONS

- A transparent minibioreactor was developed that allowed real-time monitoring of cell-scaffold interactions.
- The developed device sustains prolonged survival of cells, up to the 3 weeks tested.
- There was a linear relationship between the number of photons emitted by the bioreactor and the number of cells seeded.
- The developed bioreactor allows real-time visualization of scaffold seeding, as well as cell seeding efficacy and cell distribution throughout the scaffold under a variety of flow conditions.
- The minireactor device allowed visualization and quantification of endothelial differentiation in a PLA/CaP scaffold.

IX. **ACKNOWLEDGEMENTS**

Mentiría si dijese que siempre he querido ser científica. Antes de eso quise ser escritora, después filósofa y en algún momento arquitecta; pero desde bastante joven, con la llegada de la genética mendeliana a mi vida, deseé ser de investigadora. Siempre me habían gustado las ciencias: las matemáticas, la física y la química me gustaban, pero la biomedicina me cautivó. No podía imaginar nada mejor que dedicar mis esfuerzos a aprender y descubrir nuevas cosas sobre ese apasionante campo!

En aquellos momentos el panorama para un científico en este país era mucho más prometedor. La situación de la ciencia había mejorado mucho en los años previos: se habían abierto centro de investigación nuevos, creado plazas, aumentado los presupuestos…Tenía como ejemplo la carrera científica de las generaciones anteriores, en las que a pesar de un inicio siempre precario, la deseada estabilidad laboral, aunque tarde, acababa llegando.

Las cosas son ahora muy distintas: doctorandos que acaban sus tesis tras bastantes meses sin cobrar, y dando gracias por tener, al menos, dinero para reactivos; jóvenes científicos que, tras regresar del extranjero con promesas (muchas veces en forma de beca) de un glorioso futuro en este país, se ven obligados a hacer las maletas otra vez y marcharse de nuevo, esta vez sin la ilusión de la primera vez; o científicos que, agotados por la eterna incertidumbre laboral, lo dejan todo para acabar dedicándose a cualquier otra cosa.

Está claro que el futuro que me espera con toda probabilidad no será el camino de rosas que imaginaba en mi adolescencia, y esa meta soñada de estabilidad laboral parece cada vez más lejana en lugar de acercarse. Y sin embargo, a pesar de todo ello, aunque el sueño científico de mis 18 años ya no exista, no podría imaginarme a mí misma haciendo otra cosa que no sea investigar. Investigadora no es algo que quiero ser, sino algo que ya soy, una forma de vida, una forma de ser. Así que con incertidumbre o sin ella, no queda más que

seguir adelante, esforzarse y seguir soñando. Como mi madre siempre dice: "tu hazlo siempre lo mejor que puedas y al final las cosas acabarán saliendo bien". Y la verdad es que no me puedo quejar, porque hasta ahora siempre me ha funcionado.

Y después de esta no-tan-breve introducción, agradecer a todos los que han ayudado de una manera u otra a que mi sueño científico se vaya haciendo poco a poco realidad. En primer lugar, como no podría ser de otra manera, agradecer a Jerónimo y Nuria la oportunidad de unirme a su grupo y realizar esta tesis doctoral. Todavía guardo en mi memoria el día de mi entrevista de trabajo en el ICCC; al salir de allí, rodeada de la belleza modernista de Sant Pau, con el sol acariciando mi piel, sabiendo que mi despedida de Barcelona quedaba atrasada al menos 4 años más y que además iban a ser dedicados a trabajar con ¡células madre!, fui feliz. El camino, sin embargo, ha sido más largo y arduo de lo esperado, pero Jerónimo y Nuria han sido siempre un gran apoyo. Su despacho tiene un "nosequé" mágico que hace que entres decepcionado con tus poco prometedores resultados y salgas mucho más seguro de ti mismo, y con ideas para dos o tres papers en mente. Además de unos grandes jefes, son unas grandes personas, siempre cercanas y comprensivas, con las que se puede hablar de cualquier tema, desde series de televisión, documentales y best sellers a política, independentismo y por supuesto, cualquier ámbito de la ciencia.

En segundo lugar, agradecer a todos los que han sido mis compañeros de laboratorio estos años: Marta V., Juli, Eli, María, Dídac: muchas gracias por compartir este camino conmigo en los que hemos vivido momentos buenos, no tan buenos, divertidos, surrealistas... Jordi, muchas gracias por todo tu apoyo y por estar siempre dispuesto a ayudar. Y por acogerme cuando volví *homeless* de California ¡Qué pena me dio que te fueses! Por suerte tu lugar lo ocupó otra gran persona: Marta, mi compañera de mudanzas. ¡Cuántas horas invertidas en

hacer cajas y cajas, con material que no dejaba de aparecer por los rincones más insospechados, qué desesperación! A pesar de lo duro que fue, ha sido genial compartir todo esto contigo: no podría imaginar una compañera mejor, siempre con una sonrisa en la cara y dispuesta a ayudar, muchas gracias por todo! Y también ha sido muy emocionante compartir contigo esa nueva aventura que has emprendido cuyo nombre es Quim :D. A Cris y Sara, nuestras dos nuevas incorporaciones andaluzas, sólo deciros que me alegro mucho de vuestra llegada, llevamos poquito tiempo juntas pero con las ganas que le ponéis parece mucho más.

Mencionar también a todos los miembros del CID que tan bien nos han acogido y nos han facilitado el difícil proceso de mudanza ayudando en todo lo que han podido. ¡Estamos abrumados de tanta amabilidad! Especialmente el grupo de los "Eritjas", nuestros compañeros de laboratorio y por tanto a los primeros que recurrimos cuando necesitamos ayuda.

Moltes gràcies també als meus enginyers, la majoria d'ells companys en aquesta aventura que es el doctorat, de tal forma que les reunions d'amics tendeixen a convertir-se amb facilitat en un "grup de suport a doctorands". Cris, Javi, Edu, Carles, conèixer-vos ha fet que mai m'hi hagués penedit d'aquesta aventura catalana que vaig emprendre fa ja set anys.

Ós meus enxeñeiros: Carliños, Yari e Dolo (ou para min, Hernández e Fernández). A cara mala de vir a Barcelona foi non comparti-los últimos anos da carreira con vos. Alédame saber que a pesar do tempo que ten pasado podemos seguir reuníndonos un par de veces oo ano e que sexa como se nada tivese cambiado. Moitas grazas por crer en min todo este tempo.

Moitas grazas tamén ás miñas dúas mellores amigas de toda a vida por seguir séndoo: Marta e Ana, cústanos moito coincidir no espazo-tempo, pero cando o conseguimos é unha gran ledicia. Espero que nalgún momento o universo nos

"arrexunte" de novo na mesma cidade, ou ao menos na mesma comunidade. Nus, moitas grazas pola túa axuda co deseño da portada e por ese rato tan bonitiño, estás feita unha artista! Espero que por Toledo saiban apreciarte como ti te mereces.

Por sorte neste "exilio catalán" os galegos abundamos, e non teñen sido poucos os amigos cos que comparti-la morriña: Ana, María, Leti e Rober, xuntos temos feito polbo, empanada, filloas, orellas, queimadas… non son o mesmo que as da casa pero axudan.

Por suposto, moitas grazas a toda a miña familia. Agradecerlles sobre todo ós meus pais por terme apoiado sempre en tódalas miñas decisións, aínda que algunhas lles gustasen menos que outras. Mami, aínda se me enchen os ollos de bágoas cando lembro o día que nos despedimos porque marchaba para Barcelona por primeira vez. Que peniña! Pero a pesar dos mil quilómetros que nos separas ti segues sendo sempre o meu principal apoio, e a factura do teléfono é testemuña delo. Moitas grazas a ti tamén papá, que dende aí lonxe me axudas cos meus experimentos, dándome boas ideas e consellos e mesmo ¡enviándome labware polo correo!

E para ir rematando, faltas ti, Tali, que es amigo, familia e moito máis, o mellor que me levo de esta cidade. Grazas por apoiarme tanto nesta aventura como na que virá. Grazas polos teus ánimos. Grazas polos domingos de mimos, os regalos do mes e as guerras de almofadas á unha da mañá. Grazas por ti.

Para terminar, una última mención a todos los pequeños roedores que, aunque de forma involuntaria, han hecho posible este trabajo. Gracias. Y gracias también por no morder demasiado.

X. **REFERENCES**

Achen, M.G. et al., 1998. Vascular endothelial growth factor D (VEGF-D) is a ligand for the tyrosine kinases VEGF receptor 2 (Flk1) and VEGF receptor 3 (Flt4). *Proceedings of the National Academy of Sciences of the United States of America*, 95(2), pp.548–553.

Aguirre, A. et al., 2010. Extracellular calcium modulates in vitro bone marrow-derived Flk-1+ CD34+ progenitor cell chemotaxis and differentiation through a calcium-sensing receptor. *Biochemical and Biophysical Research Communications*, 393(1), pp.156–161.

Alfred, R. et al., 2011. Large-scale production of murine embryonic stem cell-derived osteoblasts and chondrocytes on microcarriers in serum-free media. *Biomaterials*, 32(26), pp.6006–6016.

Alieva, M. et al., 2012. Glioblastoma Therapy with Cytotoxic Mesenchymal Stromal Cells Optimized by Bioluminescence Imaging of Tumor and Therapeutic Cell Response. *PLoS ONE*, 7(4), p.e35148.

De Almeida, P.E., van Rappard, J.R.M. & Wu, J.C., 2011. In vivo bioluminescence for tracking cell fate and function. *American Journal of Physiology. Heart and Circulatory Physiology*, 301(3), pp.H663–671.

Angele, P. et al., 2004. Cyclic, mechanical compression enhances chondrogenesis of mesenchymal progenitor cells in tissue engineering scaffolds. *Biorheology*, 41(3-4), pp.335–346.

Auletta, J.J. et al., 2011. Fibroblast Growth Factor-2 Enhances Expansion of Human Bone Marrow-Derived Mesenchymal Stromal Cells without Diminishing Their Immunosuppressive Potential. *Stem Cells International*, 2011, p.235176.

Backliwal, G. et al., 2008. Valproic acid: a viable alternative to sodium butyrate for enhancing protein expression in mammalian cell cultures. *Biotechnology and bioengineering*, 101(1), pp.182–189.

Badylak, S.F. et al., 1995. The use of xenogeneic small intestinal submucosa as a biomaterial for Achilles tendon repair in a dog model. *Journal of biomedical materials research*, 29(8), pp.977–985.

Badylak, S.F., 2004. Xenogeneic extracellular matrix as a scaffold for tissue reconstruction. *Transplant immunology*, 12(3-4), pp.367–377.

Bagó, J.R. et al., 2012. In vivo bioluminescence imaging of cell differentiation in biomaterials: a platform for scaffold development. *Tissue engineering. Part A*.

De Bartolo, L. et al., 2009. Human hepatocyte functions in a crossed hollow fiber membrane bioreactor. *Biomaterials*, 30(13), pp.2531–2543.

Beckmann, N. et al., 2003. Age-dependent cerebrovascular abnormalities and blood flow disturbances in APP23 mice modeling Alzheimer's disease. *The Journal of neuroscience: the official journal of the Society for Neuroscience*, 23(24), pp.8453–8459.

Bhaumik, S. & Gambhir, S.S., 2002. Optical imaging of Renilla luciferase reporter gene expression in living mice. *Proceedings of the National Academy of Sciences of the United States of America*, 99(1), pp.377–382.

Bianco, P. et al., 2001. Bone marrow stromal stem cells: nature, biology, and potential applications. *Stem Cells (Dayton, Ohio)*, 19(3), pp.180–192.

Bohner, M. et al., 2005. Synthesis and characterization of porous beta-tricalcium phosphate blocks. *Biomaterials*, 26(31), pp.6099–6105.

Bolland, B.J.R.F. et al., 2008. The application of human bone marrow stromal cells and poly(dl-lactic acid) as a biological bone graft extender in impaction bone grafting. *Biomaterials*, 29(22), pp.3221–3227.

Bonnet, D., 2003. Biology of human bone marrow stem cells. *Clinical and Experimental Medicine*, 3(3), pp.140–149.

Bos, C. et al., 2004. In vivo MR imaging of intravascularly injected magnetically labeled mesenchymal stem cells in rat kidney and liver. *Radiology*, 233(3), pp.781–789.

Böstman, O.M., 1991. Absorbable implants for the fixation of fractures. *The Journal of bone and joint surgery. American volume*, 73(1), pp.148–153.

Branchini, B.R. et al., 2006. Luciferase from the Italian firefly Luciola italica: molecular cloning and expression. *Comparative Biochemistry and Physiology. Part B, Biochemistry & Molecular Biology*, 145(2), pp.159–167.

Branchini, B.R. et al., 2010. Red-emitting luciferases for bioluminescence reporter and imaging applications. *Analytical Biochemistry*, 396(2), pp.290–297.

Branchini, B.R. et al., 2007. Thermostable red and green light-producing firefly luciferase mutants for bioluminescent reporter applications. *Analytical Biochemistry*, 361(2), pp.253–262.

Briot, K. & Roux, C., 2005. [Biochemical markers of bone remodeling]. *Gynécologie, Obstétrique & Fertilité*, 33(12), pp.1009–1013.

Buckley, C.T., Thorpe, S.D. & Kelly, D.J., 2009. Engineering of large cartilaginous tissues through the use of microchanneled hydrogels and rotational culture. *Tissue engineering. Part A*, 15(11), pp.3213–3220.

Calori, G.M. et al., 2008. Application of rhBMP-7 and platelet-rich plasma in the treatment of long bone non-unions: a prospective randomised clinical study on 120 patients. *Injury*, 39(12), pp.1391–1402.

Calori, G.M. et al., 2009. Bone morphogenetic proteins and tissue engineering: future directions. *Injury*, 40 Suppl 3, pp.S67–76.

Carragee, E.J., Hurwitz, E.L. & Weiner, B.K., 2011. A critical review of recombinant human bone morphogenetic protein-2 trials in spinal surgery: emerging safety concerns and lessons learned. *The spine journal: official journal of the North American Spine Society*, 11(6), pp.471–491.

Carrier, R.L. et al., 2002. Perfusion improves tissue architecture of engineered cardiac muscle. *Tissue engineering*, 8(2), pp.175–188.

Chadwick, K. et al., 2003. Cytokines and BMP-4 promote hematopoietic differentiation of human embryonic stem cells. *Blood*, 102(3), pp.906–915.

Chamberlain, G. et al., 2007. Concise review: mesenchymal stem cells: their phenotype, differentiation capacity, immunological features, and potential for homing. *Stem Cells (Dayton, Ohio)*, 25(11), pp.2739–2749.

Charles-Harris, M. et al., 2008. A PLA/calcium phosphate degradable composite material for bone tissue engineering: an in vitro study. *Journal of Materials Science. Materials in Medicine*, 19(4), pp.1503–1513.

Chen, C.S., Tan, J. & Tien, J., 2004. Mechanotransduction at cell-matrix and cell-cell contacts. *Annual review of biomedical engineering*, 6, pp.275–302.

Chen, X. et al., 2004. MicroPET imaging of breast cancer alphav-integrin expression with 64Cu-labeled dimeric RGD peptides. *Molecular imaging and biology: MIB: the official publication of the Academy of Molecular Imaging*, 6(5), pp.350–359.

Cheung, W.F., Cruz, T.F. & Turley, E.A., 1999. Receptor for hyaluronan-mediated motility (RHAMM), a hyaladherin that regulates cell responses to growth factors. *Biochemical Society transactions*, 27(2), pp.135–142.

Chung, N. et al., 2009. HOX gene analysis of endothelial cell differentiation in human bone marrow-derived mesenchymal stem cells. *Molecular Biology Reports*, 36(2), pp.227–235.

Cobb, M.A. et al., 1996. Histology after dural grafting with small intestinal submucosa. *Surgical neurology*, 46(4), pp.389–393; discussion 393–394.

Colter, D.C., Sekiya, I. & Prockop, D.J., 2001. Identification of a subpopulation of rapidly self-renewing and multipotential adult stem cells in colonies of human marrow stromal cells. *Proceedings of the National Academy of Sciences of the United States of America*, 98(14), pp.7841–7845.

Contag, C.H., 2007. In vivo pathology: seeing with molecular specificity and cellular resolution in the living body. *Annual Review of Pathology*, 2, pp.277–305.

Contag, C.H. et al., 2000. Use of reporter genes for optical measurements of neoplastic disease in vivo. *Neoplasia (New York, N.Y.)*, 2(1-2), pp.41–52.

Contag, C.H. et al., 1997. Visualizing gene expression in living mammals using a bioluminescent reporter. *Photochemistry and Photobiology*, 66(4), pp.523–531.

Contag, P.R. et al., 1998. Bioluminescent indicators in living mammals. *Nature Medicine*, 4(2), pp.245–247.

Cornelissen, C.G. et al., 2012. Fibrin gel as alternative scaffold for respiratory tissue engineering. *Annals of biomedical engineering*, 40(3), pp.679–687.

Cui, K. et al., 2008. A quantitative study of factors affecting in vivo bioluminescence imaging. *Luminescence: The Journal of Biological and Chemical Luminescence*, 23(5), pp.292–295.

Cushing, M.C. & Anseth, K.S., 2007. Materials science. Hydrogel cell cultures. *Science (New York, N.Y.)*, 316(5828), pp.1133–1134.

Dai, C. et al., 2011. Osteogenic evaluation of calcium/magnesium-doped mesoporous silica scaffold with incorporation of rhBMP-2 by synchrotron radiation-based μCT. *Biomaterials*, 32(33), pp.8506–8517.

David, V. et al., 2008. Ex Vivo bone formation in bovine trabecular bone cultured in a dynamic 3D bioreactor is enhanced by compressive mechanical strain. *Tissue engineering. Part A*, 14(1), pp.117–126.

Davisson, T., Sah, R.L. & Ratcliffe, A., 2002. Perfusion increases cell content and matrix synthesis in chondrocyte three-dimensional cultures. *Tissue engineering*, 8(5), pp.807–816.

De, A., Yaghoubi, S.S. & Gambhir, S.S., 2008. Applications of lentiviral vectors in noninvasive molecular imaging. *Methods in Molecular Biology (Clifton, N.J.)*, 433, pp.177–202.

Demirbag, B. et al., 2011. Advanced cell therapies with and without scaffolds. *Biotechnology journal*, 6(12), pp.1437–1453.

Deshpande, N., Needles, A. & Willmann, J.K., 2010. Molecular Ultrasound Imaging: Current Status and Future Directions. *Clinical radiology*, 65(7), pp.567–581.

Dickhut, A. et al., 2010. Chondrogenesis of human mesenchymal stem cells by local transforming growth factor-beta delivery in a biphasic resorbable carrier. *Tissue Engineering. Part A*, 16(2), pp.453–464.

Doyle, A.M., Nerem, R.M. & Ahsan, T., 2009. Human mesenchymal stem cells form multicellular structures in response to applied cyclic strain. *Annals of biomedical engineering*, 37(4), pp.783–793.

Draper, J.S., Moore, H.D., et al., 2004. Culture and characterization of human embryonic stem cells. *Stem Cells and Development*, 13(4), pp.325–336.

Draper, J.S., Smith, K., et al., 2004. Recurrent gain of chromosomes 17q and 12 in cultured human embryonic stem cells. *Nature Biotechnology*, 22(1), pp.53–54.

Van der Elst, M. et al., 1999. Bone tissue response to biodegradable polymers used for intra medullary fracture fixation: a long-term in vivo study in sheep femora. *Biomaterials*, 20(2), pp.121–128.

Entwistle, J., Hall, C.L. & Turley, E.A., 1996. HA receptors: regulators of signalling to the cytoskeleton. *Journal of cellular biochemistry*, 61(4), pp.569–577.

Evans, G.R.D. et al., 2002. Bioactive poly(L-lactic acid) conduits seeded with Schwann cells for peripheral nerve regeneration. *Biomaterials*, 23(3), pp.841–848.

Fitzpatrick, J.C., Clark, P.M. & Capaldi, F.M., 2010. Effect of decellularization protocol on the mechanical behavior of porcine descending aorta. *International journal of biomaterials*, 2010. Available at: http://www.ncbi.nlm.nih.gov/pubmed/20689621 [Accessed October 1, 2012].

Foster, F.S. et al., 2009. A new 15-50 MHz array-based micro-ultrasound scanner for preclinical imaging. *Ultrasound in medicine & biology*, 35(10), pp.1700–1708.

Fraser, J.R., Laurent, T.C. & Laurent, U.B., 1997. Hyaluronan: its nature, distribution, functions and turnover. *Journal of internal medicine*, 242(1), pp.27–33.

Frieden, I.J., 2008. Addendum: Commentary on Becaplermin Gel (Regranex) for Hemangiomas. *Pediatric Dermatology*, 25(6), pp.590–590.

Friedenstein, A.J., Chailakhjan, R.K. & Lalykina, K.S., 1970. The development of fibroblast colonies in monolayer cultures of guinea-pig bone marrow and spleen cells. *Cell and Tissue Kinetics*, 3(4), pp.393–403.

Frith, J.E., Thomson, B. & Genever, P.G., 2010. Dynamic three-dimensional culture methods enhance mesenchymal stem cell properties and increase therapeutic potential. *Tissue engineering. Part C, Methods*, 16(4), pp.735–749.

Gaspar, A. et al., 2011. Collagen-based scaffolds for skin tissue engineering. *Journal of medicine and life*, 4(2), pp.172–177.

Gauthier, O. et al., 2005. In vivo bone regeneration with injectable calcium phosphate biomaterial: a three-dimensional micro-computed tomographic, biomechanical and SEM study. *Biomaterials*, 26(27), pp.5444–5453.

Gomes, M.E. et al., 2003. Effect of flow perfusion on the osteogenic differentiation of bone marrow stromal cells cultured on starch-based three-dimensional scaffolds. *Journal of Biomedical Materials Research. Part A*, 67(1), pp.87–95.

Gospodarowicz, D., 1975. Purification of a fibroblast growth factor from bovine pituitary. *The Journal of biological chemistry*, 250(7), pp.2515–2520.

Govender, S. et al., 2002. Recombinant human bone morphogenetic protein-2 for treatment of open tibial fractures: a prospective, controlled,

randomized study of four hundred and fifty patients. *The Journal of Bone and Joint Surgery. American Volume*, 84-A(12), pp.2123–2134.

Grayson, W.L. et al., 2008. Effects of Initial Seeding Density and Fluid Perfusion Rate on Formation of Tissue-Engineered Bone. *Tissue engineering. Part A*, 14(11), pp.1809–1820.

Grgurevic, L. et al., 2011. Bone morphogenetic protein (BMP)1-3 enhances bone repair. *Biochemical and Biophysical Research Communications*, 408(1), pp.25–31.

Griffith, L.G. & Naughton, G., 2002. Tissue engineering--current challenges and expanding opportunities. *Science (New York, N.Y.)*, 295(5557), pp.1009–1014.

Haddad, D. et al., 2012. Imaging Characteristics, Tissue Distribution, and Spread of a Novel Oncolytic Vaccinia Virus Carrying the Human Sodium Iodide Symporter. *PLoS ONE*, 7(8), p.e41647.

Harding, K.G., Morris, H.L. & Patel, G.K., 2002. Science, medicine and the future: healing chronic wounds. *BMJ (Clinical research ed.)*, 324(7330), pp.160–163.

Hart, C.E. et al., 1990. Purification of PDGF-AB and PDGF-BB from human platelet extracts and identification of all three PDGF dimers in human platelets. *Biochemistry*, 29(1), pp.166–172.

Heldin, C.H. & Westermark, B., 1999. Mechanism of action and in vivo role of platelet-derived growth factor. *Physiological Reviews*, 79(4), pp.1283–1316.

Hollinger, J.O. et al., 1998. Recombinant human bone morphogenetic protein-2 and collagen for bone regeneration. *Journal of Biomedical Materials Research*, 43(4), pp.356–364.

Holy, C.E., Shoichet, M.S. & Davies, J.E., 2000. Engineering three-dimensional bone tissue in vitro using biodegradable scaffolds: investigating initial cell-seeding density and culture period. *Journal of Biomedical Materials Research*, 51(3), pp.376–382.

Hope-Roberts, M., Wainwright, M. & Horobin, R.W., 2011. Real-time imaging of bacteria in living mice using a fluorescent dye. *Biotechnic & histochemistry: official publication of the Biological Stain Commission*, 86(2), pp.104–107.

Hsu, S.-H. et al., 2011. Peripheral nerve regeneration using a microporous polylactic acid asymmetric conduit in a rabbit long-gap sciatic nerve transection model. *Biomaterials*, 32(15), pp.3764–3775.

Huang, N.F. et al., 2012. Bioluminescence imaging of stem cell-based therapeutics for vascular regeneration. *Theranostics*, 2(4), pp.346–354.

Hubbell, J.A., 1999. Bioactive biomaterials. *Current Opinion in Biotechnology*, 10(2), pp.123–129.

Hubbell, J.A., 1995. Biomaterials in tissue engineering. *Bio/Technology (Nature Publishing Company)*, 13(6), pp.565–576.

Hurtado, A. et al., 2011. Robust CNS regeneration after complete spinal cord transection using aligned poly-L-lactic acid microfibers. *Biomaterials*, 32(26), pp.6068–6079.

Hussein, S.M. et al., 2011. Copy number variation and selection during reprogramming to pluripotency. *Nature*, 471(7336), pp.58–62.

Hwang, W.S. et al., 2004. Evidence of a pluripotent human embryonic stem cell line derived from a cloned blastocyst. *Science (New York, N.Y.)*, 303(5664), pp.1669–1674.

Hwang, W.S. et al., 2005. Patient-specific embryonic stem cells derived from human SCNT blastocysts. *Science (New York, N.Y.)*, 308(5729), pp.1777–1783.

Iyer, M. et al., 2001. Two-step transcriptional amplification as a method for imaging reporter gene expression using weak promoters. *Proceedings of the National Academy of Sciences of the United States of America*, 98(25), pp.14595–14600.

Jacobs, R.E. & Cherry, S.R., 2001. Complementary emerging techniques: high-resolution PET and MRI. *Current Opinion in Neurobiology*, 11(5), pp.621–629.

Janssen, M.L. et al., 2002. Tumor targeting with radiolabeled alpha(v)beta(3) integrin binding peptides in a nude mouse model. *Cancer research*, 62(21), pp.6146–6151.

Johnson, P.J., Parker, S.R. & Sakiyama-Elbert, S.E., 2010. Fibrin-based tissue engineering scaffolds enhance neural fiber sprouting and delay the accumulation of reactive astrocytes at the lesion in a subacute model of

spinal cord injury. *Journal of biomedical materials research. Part A*, 92(1), pp.152–163.

Johnstone, B. et al., 1998. In vitro chondrogenesis of bone marrow-derived mesenchymal progenitor cells. *Experimental Cell Research*, 238(1), pp.265–272.

Joukov, V. et al., 1996. A novel vascular endothelial growth factor, VEGF-C, is a ligand for the Flt4 (VEGFR-3) and KDR (VEGFR-2) receptor tyrosine kinases. *The EMBO Journal*, 15(7), p.1751.

Kaipel, M. et al., 2012. BMP-2 but not VEGF or PDGF in fibrin matrix supports bone healing in a delayed-union rat model. *Journal of Orthopaedic Research*, 30(10), pp.1563–1569.

Kanakaris, N.K. et al., 2009. Application of bone morphogenetic proteins to femoral non-unions: a 4-year multicentre experience. *Injury*, 40 Suppl 3, pp.S54–61.

Kang, S.-W. & Bae, Y.H., 2009. Cryopreservable and tumorigenic three-dimensional tumor culture in porous poly(lactic-co-glycolic acid) microsphere. *Biomaterials*, 30(25), pp.4227–4232.

Kanitkar, M., Tailor, H.D. & Khan, W.S., 2011. The use of growth factors and mesenchymal stem cells in orthopaedics. *The Open Orthopaedics Journal*, 5 Suppl 2, pp.271–275.

Kellomäki, M. et al., 2000. Bioabsorbable scaffolds for guided bone regeneration and generation. *Biomaterials*, 21(24), pp.2495–2505.

Kern, S. et al., 2006. Comparative analysis of mesenchymal stem cells from bone marrow, umbilical cord blood, or adipose tissue. *Stem Cells (Dayton, Ohio)*, 24(5), pp.1294–1301.

Kersemans, V. et al., 2012. Subcutaneous tumor volume measurement in the awake, manually restrained mouse using MRI. *Journal of magnetic resonance imaging: JMRI*.

Al-Khaldi, A. et al., 2003. Postnatal bone marrow stromal cells elicit a potent VEGF-dependent neoangiogenic response in vivo. *Gene Therapy*, 10(8), pp.621–629.

Kim, B.S. et al., 1998. Optimizing seeding and culture methods to engineer smooth muscle tissue on biodegradable polymer matrices. *Biotechnology and Bioengineering*, 57(1), pp.46–54.

Kircher, M.F. et al., 2003. In vivo high resolution three-dimensional imaging of antigen-specific cytotoxic T-lymphocyte trafficking to tumors. *Cancer research*, 63(20), pp.6838–6846.

Kirker, K.R. et al., 2002. Glycosaminoglycan hydrogel films as bio-interactive dressings for wound healing. *Biomaterials*, 23(17), pp.3661–3671.

Kisucka, J. et al., 2006. Platelets and platelet adhesion support angiogenesis while preventing excessive hemorrhage. *Proceedings of the National Academy of Sciences of the United States of America*, 103(4), pp.855–860.

Koch, M.A. et al., 2010. Perfusion cell seeding on large porous PLA/calcium phosphate composite scaffolds in a perfusion bioreactor system under varying perfusion parameters. *Journal of Biomedical Materials Research. Part A*, 95(4), pp.1011–1018.

Kochupura, P.V. et al., 2005. Tissue-engineered myocardial patch derived from extracellular matrix provides regional mechanical function. *Circulation*, 112(9 Suppl), pp.I144–149.

Koo, V., Hamilton, P.W. & Williamson, K., 2006. Non-invasive in vivo imaging in small animal research. *Cellular oncology: the official journal of the International Society for Cellular Oncology*, 28(4), pp.127–139.

Krawetz, R. et al., 2010. Large-scale expansion of pluripotent human embryonic stem cells in stirred-suspension bioreactors. *Tissue engineering. Part C, Methods*, 16(4), pp.573–582.

Krishnan, S. et al., 2012. Fish scale collagen-a novel material for corneal tissue engineering. *Artificial organs*, 36(9), pp.829–835.

Krucker, T., Lang, A. & Meyer, E.P., 2006. New polyurethane-based material for vascular corrosion casting with improved physical and imaging characteristics. *Microscopy research and technique*, 69(2), pp.138–147.

Laflamme, M.A. & Murry, C.E., 2011. Heart regeneration. *Nature*, 473(7347), pp.326–335.

Laitinen, L., 1987. Griffonia simplicifolia lectins bind specifically to endothelial cells and some epithelial cells in mouse tissues. *The Histochemical Journal*, 19(4), pp.225–234.

Langer, R. & Vacanti, J.P., 1993. Tissue engineering. *Science (New York, N.Y.)*, 260(5110), pp.920–926.

Lee, E.J. & Niklason, L.E., 2010. A Novel Flow Bioreactor for In Vitro Microvascularization. *Tissue Engineering. Part C, Methods*, 16(5), pp.1191–1200.

Lee, J., Cuddihy, M.J. & Kotov, N.A., 2008. Three-dimensional cell culture matrices: state of the art. *Tissue engineering. Part B, Reviews*, 14(1), pp.61–86.

Van Lenthe, G.H. et al., 2007. Nondestructive micro-computed tomography for biological imaging and quantification of scaffold-bone interaction in vivo. *Biomaterials*, 28(15), pp.2479–2490.

Lerou, P.H. & Daley, G.Q., 2005. Therapeutic potential of embryonic stem cells. *Blood Reviews*, 19(6), pp.321–331.

Levéen, P. et al., 1994. Mice deficient for PDGF B show renal, cardiovascular, and hematological abnormalities. *Genes & Development*, 8(16), pp.1875–1887.

Li, Z. et al., 2010. Chondrogenesis of human bone marrow mesenchymal stem cells in fibrin-polyurethane composites is modulated by frequency and amplitude of dynamic compression and shear stress. *Tissue engineering. Part A*, 16(2), pp.575–584.

Lind, M., Eriksen, E.F. & Bünger, C., 1996. Bone morphogenetic protein-2 but not bone morphogenetic protein-4 and -6 stimulates chemotactic migration of human osteoblasts, human marrow osteoblasts, and U2-OS cells. *Bone*, 18(1), pp.53–57.

Lionetti, V., Cecchini, M. & Ventura, C., 2011. Nanomechanics to drive stem cells in injured tissues: insights from current research and future perspectives. *Stem cells and development*, 20(4), pp.561–568.

Liu, J. et al., 2012. Human umbilical cord stem cell encapsulation in novel macroporous and injectable fibrin for muscle tissue engineering. *Acta biomaterialia*.

Liu, X. & Ma, P.X., 2004. Polymeric scaffolds for bone tissue engineering. *Annals of Biomedical Engineering*, 32(3), pp.477–486.

Loening, A.M., Wu, A.M. & Gambhir, S.S., 2007. Red-shifted Renilla reniformis luciferase variants for imaging in living subjects. *Nature Methods*, 4(8), pp.641–643.

Lorenz, W.W. et al., 1991. Isolation and expression of a cDNA encoding Renilla reniformis luciferase. *Proceedings of the National Academy of Sciences of the United States of America*, 88(10), pp.4438–4442.

Ludwig, T.E. et al., 2006. Derivation of human embryonic stem cells in defined conditions. *Nature biotechnology*, 24(2), pp.185–187.

Lutolf, M.P. et al., 2003. Repair of bone defects using synthetic mimetics of collagenous extracellular matrices. *Nature biotechnology*, 21(5), pp.513–518.

Maeshima, Y. et al., 2001. Identification of the anti-angiogenic site within vascular basement membrane-derived tumstatin. *The Journal of biological chemistry*, 276(18), pp.15240–15248.

Maglione, D. et al., 1991. Isolation of a human placenta cDNA coding for a protein related to the vascular permeability factor. *Proceedings of the National Academy of Sciences of the United States of America*, 88(20), pp.9267–9271.

Marcano, D.C. et al., 2012. Design of Poly(ethylene glycol)-functionalized Hydrophilic Carbon Clusters for Targeted Therapy of Cerebrovascular Dysfunction in Mild Traumatic Brain Injury. *Journal of neurotrauma*.

Martin, I., Wendt, D. & Heberer, M., 2004. The role of bioreactors in tissue engineering. *Trends in Biotechnology*, 22(2), pp.80–86.

Martino, M.M. et al., 2011. Engineering the growth factor microenvironment with fibronectin domains to promote wound and bone tissue healing. *Science Translational Medicine*, 3(100), p.100ra89.

Martino, M.M. et al., 2013. Heparin-binding domain of fibrin(ogen) binds growth factors and promotes tissue repair when incorporated within a synthetic matrix. *Proceedings of the National Academy of Sciences*. Available at: http://www.pnas.org/content/early/2013/02/27/1221602110 [Accessed March 5, 2013].

Martino, M.M. & Hubbell, J.A., 2010. The 12th-14th type III repeats of fibronectin function as a highly promiscuous growth factor-binding domain. *The FASEB Journal: Official Publication of the Federation of American Societies for Experimental Biology*, 24(12), pp.4711–4721.

Massagué, J., 1990. The transforming growth factor-beta family. *Annual review of cell biology*, 6, pp.597–641.

Massoud, T.F. & Gambhir, S.S., 2003a. Molecular imaging in living subjects: seeing fundamental biological processes in a new light. *Genes & Development*, 17(5), pp.545–580.

Massoud, T.F. & Gambhir, S.S., 2003b. Molecular imaging in living subjects: seeing fundamental biological processes in a new light. *Genes & Development*, 17(5), pp.545–580.

McCoy, R.J., Jungreuthmayer, C. & O'Brien, F.J., 2012. Influence of flow rate and scaffold pore size on cell behavior during mechanical stimulation in a flow perfusion bioreactor. *Biotechnology and Bioengineering*.

Mi, S. et al., 2011. Photochemical cross-linking of plastically compressed collagen gel produces an optimal scaffold for corneal tissue engineering. *Journal of biomedical materials research. Part A*, 99(1), pp.1–8.

Micol, L.A. et al., 2012. In-vivo performance of high-density collagen gel tubes for urethral regeneration in a rabbit model. *Biomaterials*, 33(30), pp.7447–7455.

Middleton, J.C. & Tipton, A.J., 2000. Synthetic biodegradable polymers as orthopedic devices. *Biomaterials*, 21(23), pp.2335–2346.

Miletic, H. et al., 2007. Bystander killing of malignant glioma by bone marrow-derived tumor-infiltrating progenitor cells expressing a suicide gene. *Molecular therapy: the journal of the American Society of Gene Therapy*, 15(7), pp.1373–1381.

Moreira, J.L. et al., 1995. Effect of viscosity upon hydrodynamically controlled natural aggregates of animal cells grown in stirred vessels. *Biotechnology progress*, 11(5), pp.575–583.

Mouw, J.K. et al., 2007. Dynamic compression regulates the expression and synthesis of chondrocyte-specific matrix molecules in bone marrow stromal cells. *Stem cells (Dayton, Ohio)*, 25(3), pp.655–663.

Mueller, D. et al., 2011. In-depth physiological characterization of primary human hepatocytes in a 3D hollow-fiber bioreactor. *Journal of tissue engineering and regenerative medicine*, 5(8), pp.e207–218.

Muller, N. et al., 2005. Orbital shaker technology for the cultivation of mammalian cells in suspension. *Biotechnology and Bioengineering*, 89(4), pp.400–406.

Muschler, G.F. et al., 2010. The design and use of animal models for translational research in bone tissue engineering and regenerative medicine. *Tissue engineering. Part B, Reviews*, 16(1), pp.123–145.

Nakagami, H. et al., 2006. Adipose tissue-derived stromal cells as a novel option for regenerative cell therapy. *Journal of Atherosclerosis and Thrombosis*, 13(2), pp.77–81.

Nambu, M. et al., 2011. Stimulatory Effect of Autologous Adipose Tissue-Derived Stromal Cells in an Atelocollagen Matrix on Wound Healing in Diabetic db/db Mice. *Journal of tissue engineering*, 2011, p.158105.

Navarro, M. et al., 2004. Development and cell response of a new biodegradable composite scaffold for guided bone regeneration. *Journal of Materials Science. Materials in Medicine*, 15(4), pp.419–422.

Newman, P.J. & Albelda, S.M., 1992. Cellular and molecular aspects of PECAM-1. *Nouvelle Revue Française D'hématologie*, 34 Suppl, pp.S9–13.

Ng, Y.L. & Chase, H.A., 2008. Novel bioreactors for the culture and expansion of aggregative neural stem cells. *Bioprocess and biosystems engineering*, 31(5), pp.393–400.

Nishi, M. et al., 2012. Engineered bone tissue associated with vascularization utilizing a rotating wall vessel bioreactor. *Journal of biomedical materials research. Part A*.

Ntziachristos, V. et al., 2002. Fluorescence molecular tomography resolves protease activity in vivo. *Nature medicine*, 8(7), pp.757–760.

Ntziachristos, V. & Weissleder, R., 2002. Charge-coupled-device based scanner for tomography of fluorescent near-infrared probes in turbid media. *Medical physics*, 29(5), pp.803–809.

Odorico, J.S., Kaufman, D.S. & Thomson, J.A., 2001. Multilineage differentiation from human embryonic stem cell lines. *Stem cells (Dayton, Ohio)*, 19(3), pp.193–204.

Ogle, B.M. & Platt, J.L., 2002. Genetic therapies and xenotransplantation. *Expert opinion on biological therapy*, 2(3), pp.299–310.

Ohyabu, Y. et al., 2006. Cartilaginous tissue formation from bone marrow cells using rotating wall vessel (RWV) bioreactor. *Biotechnology and bioengineering*, 95(5), pp.1003–1008.

Okabe, M. et al., 1997. “Green mice” as a source of ubiquitous green cells. *FEBS Letters*, 407(3), pp.313–319.

Olofsson, B. et al., 1996. Vascular endothelial growth factor B, a novel growth factor for endothelial cells. *Proceedings of the National Academy of Sciences of the United States of America*, 93(6), pp.2576–2581.

Organizacion Nacional de Transplantes, 2013. *Datos Históricos de Donaciones*, Available at: https://reports.ont.es/datoshistoricos.aspx.

Organizacion Nacional de Transplantes, R.M., 2007. *Datos de actividad 2007*,

Orr, A.W. et al., 2006. Mechanisms of mechanotransduction. *Developmental cell*, 10(1), pp.11–20.

Owen, M. & Friedenstein, A.J., 1988. Stromal stem cells: marrow-derived osteogenic precursors. *Ciba Foundation Symposium*, 136, pp.42–60.

Pansky, A., Roitzheim, B. & Tobiasch, E., 2007. Differentiation potential of adult human mesenchymal stem cells. *Clinical Laboratory*, 53(1-2), pp.81–84.

Park, J.S. et al., 2010. Chondrogenic differentiation of mesenchymal stem cells embedded in a scaffold by long-term release of TGF-beta 3 complexed with chondroitin sulfate. *Journal of Biomedical Materials Research. Part A*, 92(2), pp.806–816.

Pazzano, D. et al., 2000. Comparison of chondrogensis in static and perfused bioreactor culture. *Biotechnology progress*, 16(5), pp.893–896.

Phair, R.D. & Misteli, T., 2001. Kinetic modelling approaches to in vivo imaging. *Nature Reviews. Molecular Cell Biology*, 2(12), pp.898–907.

Phipps, M.C., Xu, Y. & Bellis, S.L., 2012. Delivery of platelet-derived growth factor as a chemotactic factor for mesenchymal stem cells by bone-mimetic electrospun scaffolds. *PloS One*, 7(7), p.e40831.

Pickhardt, P.J. et al., 2005. Microcomputed tomography colonography for polyp detection in an in vivo mouse tumor model. *Proceedings of the National Academy of Sciences of the United States of America*, 102(9), pp.3419–3422.

Pittenger, M.F. et al., 1999. Multilineage potential of adult human mesenchymal stem cells. *Science (New York, N.Y.)*, 284(5411), pp.143–147.

Polak, J. & Hench, L., 2005. Gene therapy progress and prospects: in tissue engineering. *Gene Therapy*, 12(24), pp.1725–1733.

Pörtner, R. et al., 2005. Bioreactor design for tissue engineering. *Journal of bioscience and bioengineering*, 100(3), pp.235–245.

Prokhorova, T.A. et al., 2009. Teratoma formation by human embryonic stem cells is site dependent and enhanced by the presence of Matrigel. *Stem cells and development*, 18(1), pp.47–54.

Puelacher, W.C. et al., 1994. Design of nasoseptal cartilage replacements synthesized from biodegradable polymers and chondrocytes. *Biomaterials*, 15(10), pp.774–778.

Puetzer, J.L., Ballyns, J.J. & Bonassar, L.J., 2012. The effect of the duration of mechanical stimulation and post-stimulation culture on the structure and properties of dynamically compressed tissue-engineered menisci. *Tissue engineering. Part A*, 18(13-14), pp.1365–1375.

Ray, P., 2011. Multimodality molecular imaging of disease progression in living subjects. *Journal of biosciences*, 36(3), pp.499–504.

Reddi, A.H. & Cunningham, N.S., 1993. Initiation and promotion of bone differentiation by bone morphogenetic proteins. *Journal of Bone and Mineral Research: The Official Journal of the American Society for Bone and Mineral Research*, 8 Suppl 2, pp.S499–502.

Rice, B.W., Cable, M.D. & Nelson, M.B., 2001. In vivo imaging of light-emitting probes. *Journal of Biomedical Optics*, 6(4), pp.432–440.

Richardson, T.P. et al., 2001. Polymeric system for dual growth factor delivery. *Nature Biotechnology*, 19(11), pp.1029–1034.

Robinton, D.A. & Daley, G.Q., 2012. The promise of induced pluripotent stem cells in research and therapy. *Nature*, 481(7381), pp.295–305.

Rome, C., Couillaud, F. & Moonen, C.T.W., 2007. Gene expression and gene therapy imaging. *European radiology*, 17(2), pp.305–319.

Ronga, M. et al., 2006. Recombinant human bone morphogenetic protein-7 for treatment of long bone non-union: an observational, retrospective, non-randomized study of 105 patients. *Injury*, 37 Suppl 3, pp.S51–56.

Schäffler, A. & Büchler, C., 2007. Concise review: adipose tissue-derived stromal cells--basic and clinical implications for novel cell-based therapies. *Stem Cells (Dayton, Ohio)*, 25(4), pp.818–827.

Schense, J.C. & Hubbell, J.A., 1999. Cross-linking exogenous bifunctional peptides into fibrin gels with factor XIIIa. *Bioconjugate chemistry*, 10(1), pp.75–81.

Schmidt, M.B., Chen, E.H. & Lynch, S.E., 2006. A review of the effects of insulin-like growth factor and platelet derived growth factor on in vivo cartilage healing and repair. *Osteoarthritis and cartilage / OARS, Osteoarthritis Research Society*, 14(5), pp.403–412.

Scott, R., Marquardt, L. & Willits, R.K., 2010. Characterization of poly(ethylene glycol) gels with added collagen for neural tissue engineering. *Journal of biomedical materials research. Part A*, 93(3), pp.817–823.

Semenza, G.L. et al., 1996. Hypoxia response elements in the aldolase A, enolase 1, and lactate dehydrogenase A gene promoters contain essential binding sites for hypoxia-inducible factor 1. *The Journal of Biological Chemistry*, 271(51), pp.32529–32537.

Senger, D.R. et al., 1983. Tumor cells secrete a vascular permeability factor that promotes accumulation of ascites fluid. *Science (New York, N.Y.)*, 219(4587), pp.983–985.

Shaikh, F.M. et al., 2008. Fibrin: a natural biodegradable scaffold in vascular tissue engineering. *Cells, tissues, organs*, 188(4), pp.333–346.

Shapira, K. et al., 2008. Hydrogels for cardiac tissue regeneration. *Bio-medical materials and engineering*, 18(4-5), pp.309–314.

Sherwood, J.K. et al., 2002. A three-dimensional osteochondral composite scaffold for articular cartilage repair. *Biomaterials*, 23(24), pp.4739–4751.

Sikavitsas, V.I. et al., 2005. Flow perfusion enhances the calcified matrix deposition of marrow stromal cells in biodegradable nonwoven fiber mesh scaffolds. *Annals of biomedical engineering*, 33(1), pp.63–70.

Da Silva Meirelles, L., Chagastelles, P.C. & Nardi, N.B., 2006. Mesenchymal stem cells reside in virtually all post-natal organs and tissues. *Journal of Cell Science*, 119(Pt 11), pp.2204–2213.

Song, K. et al., 2008. Three-dimensional fabrication of engineered bone with human bio-derived bone scaffolds in a rotating wall vessel bioreactor. *Journal of biomedical materials research. Part A*, 86(2), pp.323–332.

Spibey, C.A., Jackson, P. & Herick, K., 2001. A unique charge-coupled device/xenon arc lamp based imaging system for the accurate detection and quantitation of multicolour fluorescence. *Electrophoresis*, 22(5), pp.829–836.

Still, J. et al., 2003. The use of a collagen sponge/living cell composite material to treat donor sites in burn patients. *Burns: journal of the International Society for Burn Injuries*, 29(8), pp.837–841.

Suetsugu, A. et al., 2012. Non-invasive fluorescent-protein imaging of orthotopic pancreatic-cancer-patient tumorgraft progression in nude mice. *Anticancer research*, 32(8), pp.3063–3067.

Takahashi, K. & Yamanaka, S., 2006. Induction of pluripotent stem cells from mouse embryonic and adult fibroblast cultures by defined factors. *Cell*, 126(4), pp.663–676.

Tannous, B.A. et al., 2005. Codon-optimized Gaussia luciferase cDNA for mammalian gene expression in culture and in vivo. *Molecular Therapy: The Journal of the American Society of Gene Therapy*, 11(3), pp.435–443.

Tasso, R. et al., 2012. The role of bFGF on the ability of MSC to activate endogenous regenerative mechanisms in an ectopic bone formation model. *Biomaterials*, 33(7), pp.2086–2096.

Temenoff, J.S. et al., 2002. Effect of poly(ethylene glycol) molecular weight on tensile and swelling properties of oligo(poly(ethylene glycol) fumarate) hydrogels for cartilage tissue engineering. *Journal of biomedical materials research*, 59(3), pp.429–437.

Therin, M. et al., 1992. In vivo degradation of massive poly(alpha-hydroxy acids): validation of in vitro findings. *Biomaterials*, 13(9), pp.594–600.

Thévenaz, P., Ruttimann, U.E. & Unser, M., 1998. A pyramid approach to subpixel registration based on intensity. *IEEE transactions on image processing: a publication of the IEEE Signal Processing Society*, 7(1), pp.27–41.

Tibbitt, M.W. & Anseth, K.S., 2009. Hydrogels as extracellular matrix mimics for 3D cell culture. *Biotechnology and bioengineering*, 103(4), pp.655–663.

Turner, N.J. et al., 2004. A novel hyaluronan-based biomaterial (Hyaff-11) as a scaffold for endothelial cells in tissue engineered vascular grafts. *Biomaterials*, 25(28), pp.5955–5964.

De Ugarte, D.A. et al., 2003. Comparison of multi-lineage cells from human adipose tissue and bone marrow. *Cells, Tissues, Organs*, 174(3), pp.101–109.

Urist, M.R. et al., 1973. Bone Morphogenesis in Implants of Insoluble Bone Gelatin. *Proceedings of the National Academy of Sciences of the United States of America*, 70(12 Pt 1-2), pp.3511–3515.

Vila, O.F. et al., 2012. Calcium phosphate glass improves angiogenesis capacity of poly(lactic acid) scaffolds and stimulates differentiation of adipose tissue-derived mesenchymal stromal cells to the endothelial lineage. *Journal of biomedical materials research. Part A*.

Vilalta, M. et al., 2008. Biodistribution, long-term survival, and safety of human adipose tissue-derived mesenchymal stem cells transplanted in nude mice by high sensitivity non-invasive bioluminescence imaging. *Stem Cells and Development*, 17(5), pp.993–1003.

Vilalta, Marta et al., 2009. Dual luciferase labelling for non-invasive bioluminescence imaging of mesenchymal stromal cell chondrogenic differentiation in demineralized bone matrix scaffolds. *Biomaterials*, 30(28), pp.4986–4995.

Vilalta, M et al., 2009. Human adipose tissue-derived mesenchymal stromal cells as vehicles for tumor bystander effect: a model based on bioluminescence imaging. *Gene therapy*, 16(4), pp.547–557.

Viviani, V.R. et al., 2004. Cloning and characterization of the cDNA for the Brazilian Cratomorphus distinctus larval firefly luciferase: similarities with European Lampyris noctiluca and Asiatic Pyrocoelia luciferases. *Comparative Biochemistry and Physiology. Part B, Biochemistry & Molecular Biology*, 139(2), pp.151–156.

Vunjak-Novakovic, G. et al., 1998. Dynamic cell seeding of polymer scaffolds for cartilage tissue engineering. *Biotechnology Progress*, 14(2), pp.193–202.

Weber, S.M. et al., 2004. Imaging of murine liver tumor using microCT with a hepatocyte-selective contrast agent: accuracy is dependent on adequate contrast enhancement. *The Journal of surgical research*, 119(1), pp.41–45.

Weissleder, R., 2001. A clearer vision for in vivo imaging. *Nature Biotechnology*, 19(4), pp.316–317.

Wendt, D. et al., 2003. Oscillating perfusion of cell suspensions through three-dimensional scaffolds enhances cell seeding efficiency and uniformity. *Biotechnology and Bioengineering*, 84(2), pp.205–214.

White, A.G. et al., 2010. Optical imaging of bacterial infection in living mice using deep-red fluorescent squaraine rotaxane probes. *Bioconjugate chemistry*, 21(7), pp.1297–1304.

Whyte, J.L. et al., 2011. Density of human bone marrow stromal cells regulates commitment to vascular lineages. *Stem Cell Research*, 6(3), pp.238–250.

Widder, E.A., 2010. Bioluminescence in the ocean: origins of biological, chemical, and ecological diversity. *Science (New York, N.Y.)*, 328(5979), pp.704–708.

Wilson, T. & Hastings, J.W., 1998. Bioluminescence. *Annual Review of Cell and Developmental Biology*, 14, pp.197–230.

World Health Organization, 2013. World Health Statiscs. *WHO*. Available at: http://www.who.int/diabetes/en/ [Accessed October 10, 2012].

Wu, J.C. et al., 2001. Noninvasive optical imaging of firefly luciferase reporter gene expression in skeletal muscles of living mice. *Molecular Therapy: The Journal of the American Society of Gene Therapy*, 4(4), pp.297–306.

Wurdinger, T. et al., 2008. A secreted luciferase for ex vivo monitoring of in vivo processes. *Nature Methods*, 5(2), pp.171–173.

Yamane, S. et al., 2005. Feasibility of chitosan-based hyaluronic acid hybrid biomaterial for a novel scaffold in cartilage tissue engineering. *Biomaterials*, 26(6), pp.611–619.

Yang, M. et al., 2005. Real-time whole-body imaging of an orthotopic metastatic prostate cancer model expressing red fluorescent protein. *The Prostate*, 62(4), pp.374–379.

Ye, Q. et al., 2000. Fibrin gel as a three dimensional matrix in cardiovascular tissue engineering. *European Journal of Cardio-Thoracic Surgery: Official Journal of the European Association for Cardio-Thoracic Surgery*, 17(5), pp.587–591.

Yeung, F. et al., 2002. Regulation of human osteocalcin promoter in hormone-independent human prostate cancer cells. *The Journal of Biological Chemistry*, 277(4), pp.2468–2476.

Yuan Ye, K., Sullivan, K.E. & Black, L.D., 2011. Encapsulation of cardiomyocytes in a fibrin hydrogel for cardiac tissue engineering. *Journal of visualized experiments: JoVE*, (55).

Yun, Y.-R. et al., 2012. Fibroblast growth factor 2-functionalized collagen matrices for skeletal muscle tissue engineering. *Biotechnology letters*, 34(4), pp.771–778.

Zhao, F., Chella, R. & Ma, T., 2007. Effects of shear stress on 3-D human mesenchymal stem cell construct development in a perfusion bioreactor system: Experiments and hydrodynamic modeling. *Biotechnology and bioengineering*, 96(3), pp.584–595.

Zhao, F. & Ma, T., 2005. Perfusion bioreactor system for human mesenchymal stem cell tissue engineering: dynamic cell seeding and construct development. *Biotechnology and Bioengineering*, 91(4), pp.482–493.

Zhao, H. et al., 2004. Characterization of coelenterazine analogs for measurements of Renilla luciferase activity in live cells and living animals. *Molecular Imaging*, 3(1), pp.43–54.

Zhao, H. et al., 2005. Emission spectra of bioluminescent reporters and interaction with mammalian tissue determine the sensitivity of detection in vivo. *Journal of Biomedical Optics*, 10(4), p.41210.

Zhao, T. et al., 2011. Immunogenicity of induced pluripotent stem cells. *Nature*, 474(7350), pp.212–215.

Zhu, J., 2010. Bioactive modification of poly(ethylene glycol) hydrogels for tissue engineering. *Biomaterials*, 31(17), pp.4639–4656.

Zippel, N., Schulze, M. & Tobiasch, E., 2010. Biomaterials and mesenchymal stem cells for regenerative medicine. *Recent Patents on Biotechnology*, 4(1), pp.1–22.

Zuk, P.A. et al., 2002. Human adipose tissue is a source of multipotent stem cells. *Molecular Biology of the Cell*, 13(12), pp.4279–4295.

XI. **ANEX: PUBLICATIONS**

1. FIRST PUBLICATION

Calcium Phosphate Glass Improves Angiogenesis Capacity of Poly(lactic acid) Scaffolds and Stimulates Differentiation of Adipose Tissue-Derived Mesenchymal Stromal Cells to the Endothelial Lineage

Olaia F. Vila[a,c], Juli R. Bagó[a,c], Melba Navarro[b,c], Maria Alieva[a,c], Elisabeth Aguilar[a,c], Elisabeth Engel[b,c], Josep Planell[b,c], Nuria Rubio[a,c], Jerónimo Blanco[a,c]

[a] *Cardiovascular Research Center (CSIC-ICCC-UAB),Barcelona, Spain.*

[b] *Institute for Bioengineering of Catalonia (IBEC),Barcelona, Spain*

[c] *Networking Research Center on Bioengineering, Biomaterials and Nanomedicine (CIBER-BBN), Spain.*

JOURNAL OF BIOMEDICAL MATERIAL RESEARCH PART A. Volume 101A, Issue 4, pages 932-41, April 2013. doi: 10.1002

Society For Biomaterials

Calcium phosphate glass improves angiogenesis capacity of poly(lactic acid) scaffolds and stimulates differentiation of adipose tissue-derived mesenchymal stromal cells to the endothelial lineage

Olaia F. Vila,[1,2] Juli R. Bagó,[1,2] Melba Navarro,[2,3] Maria Alieva,[1,2] Elisabeth Aguilar,[1,2] Elisabeth Engel,[2,3] Josep Planell,[2,3] Nuria Rubio,[1,2] Jerónimo Blanco[1,2]

[1]Cardiovascular Research Center (CSIC-ICCC-UAB), Barcelona, Spain
[2]Networking Research Center on Bioengineering, Biomaterials, and Nanomedicine (CIBER-BBN), Spain
[3]Institute for Bioengineering of Catalonia (IBEC), Barcelona, Spain

Received 11 January 2012; revised 13 July 2012; accepted 30 July 2012
Published online in Wiley Online Library (wileyonlinelibrary.com). DOI: 10.1002/jbm.a.34391

Abstract: The angiogenic capacity of a new biomaterial composite of poly(lactic acid) and calcium phosphate glass (PLA/CaP) was analyzed by noninvasive bioluminescence imaging (BLI) and histological procedures. Human adipose tissue-derived mesenchymal stromal cells expressing cytomegalovirus (CMV) promoter regulated *Photinus pyralis* luciferase (hAMSC-PLuc) grew up to 30 times the initial cell load, *in vitro*, when seeded in PLA/CaP scaffolds, but suffered an initial growth crisis followed by recovery when the scaffolds were subcutaneously implanted in SCID mice. To analyze changes in gene expression, hAMSC-PLuc cells were double labeled with a CMV promoter regulated *Renilla reniformis* luciferase and a *Photinus pyralis* luciferase reporter regulated by either the PECAM promoter or a hypoxia response element (HRE) artificial promoter and seeded in PLA/CaP and PLA scaffolds implanted in SCID mice. Analysis by BLI showed that hAMSCs in scaffolds were induced to differentiate to the endothelial lineage and did this faster in PLA/CaP than in PLA scaffolds. Endothelial differentiation correlated with a decrease in the activity of HRE regulated luciferase expression, indicative of a reduction of hypoxia. Histological analysis showed that PLA/CaP scaffolds were colonized by a functional host vascular system. Moreover, colonization by isolectin B_4 positive host cells was more effective in PLA/CaP than in PLA scaffolds, corroborating BLI results. © 2012 Wiley Periodicals, Inc. J Biomed Mater Res Part A: 00A:000–000, 2012.

Key Words: scaffold, bioluminescence imaging, cell differentiation, angiogenesis, mesenchymal stromal cells

How to cite this article: Vila OF, Bagó JR, Navarro M, Alieva M, Aguilar E, Engel E, Planell J, Rubio N, Blanco J. 2012. Calcium phosphate glass improves angiogenesis capacity of poly(lactic acid) scaffolds and stimulates differentiation of adipose tissue-derived mesenchymal stromal cells to the endothelial lineage. J Biomed Mater Res Part A 2012:00A:000–000.

INTRODUCTION

The reconstruction of hard and soft tissues is a major challenge in regenerative medicine, aggravated by the increasing number of tissue defects in the aging population. The shortage of donor tissue and organs for transplants has promoted a large research and development effort aimed at generating alternative therapeutic solutions. Tissue engineering applies principles of material engineering and life sciences toward the development of biological substitutes that can combine scaffolds and live cells to restore, maintain, or improve tissue function.[1]

Biomaterial scaffolds should mimic the three-dimensional environment of the extracellular matrix, provide short-term mechanical stability for the transplant, and increase surface area for migration, adhesion and differentiation of cells, supporting the growth of new tissue.[2] Additionally, scaffolds should promote colonization by specific cell types and finally degrade in response to matrix remodeling enzymes released by the colonizing cells as tissue repair progresses.[3] Use of an inorganic phase in biodegradable composite polymers to allow fine control of porosity, connectivity and surface properties, could be a promising approach to meet some of the above requirements.

One of the principal constraints on the size of *in vitro* engineered tissues lacking a blood supply is the short distance over which oxygen can diffuse before being consumed. Once implanted in the patient, cells in the engineered material will consume the available oxygen within a few hours, but

Additional Supporting Information may be found in the online version of this article.
Correspondence to: J. Blanco; e-mail: jblancof@csic-iccc.org
Contract grant sponsor: European Community's Seventh Framework Program Angioscaff (Angiogenesis-inducing Bioactive and Bioresponsive Scaffolds in Tissue Engineering); contract grant number: NMP-LA-2008-214402
Contract grant sponsor: Spanish Government; contract grant number: SAF2009-07102
Contract grant sponsors: The University and Research Commission for Innovation; University and Company Department (Government of Catalonia)

it will take several days before new blood vessels colonizing the implant can deliver oxygen and nutrients.[4] Providing scaffolds with angiogenic inducing capacity will likely help colonization by cells from the host, for those materials implanted without them. Because of the different time constraints for oxygen consumption and vascular colonization, it would be unrealistic to expect that providing angiogenic-induction capacity to biomaterials will effectively rescue cells deeply seeded in large scaffolds. However, such strategy may help survival of cells in, or near the surface of implants.

There are multiple cell types with potential use for tissue regeneration, for example: embryonic stem cells, hematopoietic stem cells, or mesenchymal stem cells.[5] Among the latter, adult stem cells derived from bone marrow and adipose tissue appear as ideal candidates for autologous cell therapies, avoiding problems associated with immune rejection, pathogen transmission and ethical issues.[6–12] While mesenchymal stromal cells from the bone marrow, having a rich differentiation potential and anti-inflammatory capacity, would be ideal candidates for tissue repair, their use is hampered by their relative low abundance, availability in small volumes, and pain associated with its extraction. More recently identified mesenchymal stromal cells from adipose tissue (AMSCs) offer an easily extractable and abundant alternative source of therapeutic cells with similar phenotype and equivalent differentiation potential to their homologues from the bone marrow, but in larger supply.[10–12] Furthermore, these cells have shown undetectable predisposition to oncogenic transformation after *in vitro* cultivation and implantation in mice.[13] Although mechanisms underlying the vascular differentiation of hAMSC and their contribution to neovascularization are poorly understood, there is evidence supporting MSC participating in angiogenesis.[14–16]

In the current work we evaluate the capacity of a new composite material comprising poly(lactic acid) and calcium phosphate (CaP) soluble glass to promote angiogenesis. The incorporation of a CaP phase in the polymeric matrix, not only enhances the mechanical properties of the material and controls its degradation rate, but also modifies its surface properties and ionic environment, modulating cell behavior.[17,18] Aguirre et al.[19] have reported that extracellular calcium is physiological modulator of MSC angiogenic response, inducing upregulation of important angiogenic cytokines and growth factors through the activation of a calcium sensing receptor-like receptor. Here we focus on the *in vivo* angiogenic capacity of the new biomaterial in comparison with that of PLA only.

To monitor the behavior of cells in live animal implants we use a noninvasive bioluminescence imaging (BLI) platform. Because of the capacity of light photons to transverse living tissues BLI can be used to monitor the proliferation, distribution and differentiation of cells expressing luciferase reporters in live animals. Moreover, by using inducible tissue specific gene promoters to regulate the luciferase reporters, biologically significant changes in promoter activity are reported as easily monitored photon fluxes. Thus, analysis of photon images provides information on cell growth, distribution and time related changes in gene expression associated to cell differentiation.[20–23] In this work, we use two different inducible promoters to regulate expression of the *Photinus pyralis* luciferase (PLuc) as a reporter of endothelial cell differentiation and hypoxia state. In the former case we use the promoter for the platelet endothelial cell adhesion molecule-1 (PECAM-1) gene, a frequently used marker of endothelial cells, platelets and specific immune system cells,[23] and in the latter case we use a composite promoter comprising multiple repeats of the hypoxia response element (HRE) binding sequence, responsible of regulating the activity of multiple hypoxia response genes.[24] In a different set of experiment without hAMSCs, PLA/CaP scaffolds also showed at improved capacity for inducing colonization and vascularization of the scaffold by the host own cells when compared with PLA. Results from BLI and histological procedures show that inclusion of CaP glass enhances the angiogenic capacity of PLA, a desirable advantage in many tissue repair applications.

MATERIALS AND METHODS

Lentiviral vectors constructs

Four different constructs were used during the study.

A Plox-PLuc:eGFP vector was constructed as described[25] by cloning the enhanced green fluorescent protein (eGFP) coding sequence under the control of the simian virus early enhancer promoter (SV40) and the PLuc coding sequence (Promega Corporation, Madison, WI) under the control of the cytomegalovirus (CMV) promoter between the ClaI and BamHI sites of the lentiviral transfer vector Plox/Twgfp provided by Dr. D. Trono (École Polytechnique Fédérale de Lausanne).

A CMV:hRLuc:mRFP:ttk lentiviral vector (abbreviated as CMV:RLuc) containing a trifunctional chimeric construct comprising the coding sequences for the *Renilla reniformis* luciferase (RLuc) reporter gene, the monomeric red fluorescent protein (mRFP1) gene and a truncated version of the herpes simplex virus thymidine kinase gene sr39tk (ttk) under transcriptional control of the CMV promoter, a kind donation from Dr. S.S Gambhir (Stanford, CA).[26]

A Plox-hPECAM-1p:PLuc:eGFP lentiviral vector for tissue specific expression in endothelial cells (abbreviated as PECAM:PLuc) containing a chimeric construct of PLuc and eGFP coding sequences under the control of the PECAM promoter was constructed in a Plox lentiviral vector. HPECAM-1p was kindly provided by Dr. Carmelo Bernabéu (Granada, Spain) and cloned into pLox:PLuc:eGFP using XbaI/SpeI and SpeI enzymes, respectively.

A Plox-HRE-12p:PLuc:eGFP lentiviral vector for expression in hypoxic cells (abbreviated as HRE:PLuc) containing a chimeric construct of PLuc and eGFP coding sequences under the control of 12 repeats from the HRE binding sequence of the lactate deshydrogenase A (LDHA), phosphoglycerate kinase 1 PGK1 and enolase 1 (ENO1) promoters, was constructed in a Plox lentiviral vector. The HRE-12p artificial promoter was constructed as described.[27]

Lentiviral particle production

Production of viral particles was performed using human embryonic kidney cells 293 T grown in Dulbecco's Modified Eagle Media-high glucose (DMEM-hg) (Sigma, Steinheim, Germany), 10% heat-inactivated fetal bovine serum (FBS)

(Sigma), 2 m*M* L-glutamine (Sigma), 50 U mL^{-1} penicillin/streptomycin (Sigma), and 2 m*M* 4-(2-hydroxyethyl)-1-piperazineethanesulfonic acid (HEPES). The day before transfection, 4.5×10^6 trypsinized cells were seeded on 10 cm^2 poly-D-lysine-(Sigma)-treated plates. Each lentiviral transfer vector (6 μg) were mixed with viral envelope plasmid (pMD-GVSV-G) (2 μg) and packaging construct (pCMV ΔR 8.2) (4 μg) and carried to 250 μL with NaCl 150 m*M*. Then 48 μL of PEI were mixed with 202 μL of NaCl, and added slowly to the vectors. After 30 min of incubation at room temperature (RT) this DNA solution was added drop wise to the plate containing the 293 T cells plus medium, swirled gently and incubated for 16 h at 37°C with 5% CO_2. The following day, the transfection solution was removed, the cells were rinsed with PBS 1× and medium without FBS was added to the cells. Following a 48-h incubation the supernatant was collected, centrifuged at 2000 rpm. to remove cell debris, and filtered through a 0.45 mm low protein-binding filter (Corning, Bath, UK). The filtered supernatant was then loaded in 100 Da Amicon Ultra Tubes (Millipore, MA) and centrifuged at 4400 rpm for 30 min at 4°C. The virus pellets were resuspended in PBS and kept at −80°C for storage. Virus titers were determined using the HIV-1 p24 antigen EiA (Beckman Coulter) 96 test kit.

AMSCs culture and transduction

Human AMSCs (hAMSCs) were isolated from adipose tissue derived from cosmetic subdermal liposuction of the lateral hip, with patient consent, as previously described.[10] Briefly, after rinsing in PBS 1×, lipoaspirates were suspended in one volume of 1× collagenase I (Invitrogen, Carlsbad, CA) solution and incubated 30 min at 37°C with gentle agitation. Digestion was terminated by inactivation of the collagenase I by addition of DMEM + 10% FBS. The resulting cell suspension was centrifuged at 450*g*, and the pellet was washed in 50 mL Ringer's solution. The cell pellet was resuspended in 10 mL of erythrocyte lysis solution (0.16*M* ammonium chloride) and incubated for 10 min at RT with gentle stirring. The suspension volume was completed to 50 mL with Ringer's lactate and centrifuged at 450*g*. This step was repeated until no red color was detectable. The cell pellet was resuspended in 5 mL Ringer's lactate, filtered through a 70 m Nylon mesh, and centrifuged at 450*g*. Cells resuspended in Ringer's lactate were counted using trypan blue to determine cell viability.

The selected cells tested positive for cell surface markers characteristic of mesenchymal stem cells (see Supporting Information data).

Cells were seeded at a density of 5000 cells cm^{-2} and grown in DMEM-hg, 10% heat-inactivated FBS (Hyclone, Logan, UT), 2 m*M* L-glutamine (Sigma), and 50 U mL^{-1} penicillin/streptomycin (Sigma), and cultivated for two additional passages before transduction with lentiviral vectors. Cells were then infected with concentrated vector stock (2×10^6 transduction U mL^{-1}, MOI = 20) and then incubated for 24–48 h.

For analysis of changes in gene expression, cells were first labeled with lentiviral construct CMV:RLuc and positively transduced cells were selected using a fluorescence activated cell sorter (FACS). Selected cells were then transduced a second time using either the PECAM:PLuc or the HRE-PLuc lentiviral vectors for inducible expression of luciferase.

Changes in the ratio: photons generated by PECAM:PLuc or HRE:PLuc/photons generated by CMV:Rluc is a measurement of the increase in gene expression induced in cells by experimental conditions as described.

Bioactive glass fabrication

Bioactive soluble CaP glass was produced in the system $44.5P_2O_5$-44.5CaO-$6Na_2O$-$5TiO_2$ (molar%) as described.[14] Briefly, an homogeneous mixture of $NH_4H_2PO_4$, Na_2CO_3, $CaCO_3$ and TiO_2 was melted in a platinum crucible at 1350°C for 3 h, rapidly quenched and annealed at its transition temperature (533°C). Glass particles were obtained after milling in an agate planetary mill.

Fabrication of the composites

Biodegradable composites were elaborated as described[14] by the solvent-casting method using NaCl as porogen agent. Briefly, PLA was dissolved in chloroform (5% solution w/v) in an orbital shaker at 200 rpm. NaCl particles in the range of 80–210 μm and glass particles of <40 μm size were then added and mixed to create an homogeneous paste that was casted in teflon moulds (6 mm diameter, 12 mm length). Once the chloroform had evaporated at room temperature the scaffolds were unmolded, immersed in distilled water for 2 days (3 water changes per day) to eliminate the NaCl and left to dry in air. The resulting structures presented a highly interconnected porosity (∼95%), with a pore size diameter in the 80–210 μm range.

Seeding of scaffolds

Cylindrical samples of 5-mm diameter and 3-mm height were immersed in 70% ethanol and placed in a shaker overnight to improve water permeability, rinsed several times with PBS, incubated in culture medium for 12–24 h and then seeded with 100,000 cells distributed in five successive inoculations through the scaffold.

As measured by bioluminescence imaging seeding efficiency was 80%.

Scaffold implantation in immunodeficient mice

Six-week-old mice with Severe Combined Immunodeficy (SCID mice) were purchased from Charles-River (Wilmington, MA) and maintained in a specific pathogen-free environment throughout the experiment. All animal-related procedures were performed with the approval of the animal care committee of the cardiovascular research center and the government of Catalonia. Before scaffold implantation, the animals were anesthetized by an intraperitoneal (i.p.) injection of 100 mg kg^{-1} ketamine (Merial, Duluth, GA) and 3.3 mg kg^{-1} xilacine (Henry Schein, Melville, NY) and immobilized. Implantation was performed subcutaneously (s.c.) in the back of the mice. The surgical site was cleaned with povidone-iodine (Braun, Melsungen, Germany). A sagittal

incision was performed on the skin and a cell seeded scaffold was introduced using forceps and the incision closed using 7-0 absorbable suture (Ethicon, New Brunswick, EEUU). Mice were treated with buprenorphine (Schering-Plough, Kenilworth, NJ) during the 72 h after intervention.

Calvarial defect and scaffold implantation in transgenic green fluorescent mice

Six-week-old transgenic GFP mice were provided by Dr. Masaru Okabe (Osaka University) and maintained in a specific pathogen-free environment throughout the experiment. This mice line is a transgenic C57BL/6 strain that has being genetically modified to constitutively express GFP in all the animal cells, with the exception of erythrocytes and hair.[28] The fluorescent nature of the cells from these mice makes them very useful for scaffold colonization studies. Surgery was performed as described.[29] Briefly, mice were prepared for surgery by i.p. injection of 100 mg kg^{-1} ketamine (Merial) and 3.3 mg kg^{-1} xilacine (Henry Schein), and a s.c. analgesic injection of 0.05 mg kg^{-1} buprenorphine (Schering-Plough). The surgical site was cleaned with povidone-iodine (Braun). A sagittal midline incision was performed on the skin and the periosteum was then cut, exposing the calvarial bone. A defect, 4-mm diameter (critical size defect) was performed in the calvarial bone of each mice using a sterile drill bit (Dremel, Racine, WI), avoiding perforation of the dura. The surgical area was cleaned with saline and the defect was filled with a 3.5 mm diameter $\times$ 1 mm thickness PLA/CaP scaffold. The incision was closed using absorbable sutures. Subcutaneous implantation was performed as explained for SCID mice. After 4, 8, or 12 weeks the animals were sacrificed by cervical dislocation and implants harvested for analysis.

In vitro BLI determination of PLuc activity

For *in vitro* proliferation assays, cell seeded scaffolds were removed from the six-well plates and placed in a new dish. For imaging, 100 mL of D-luciferin (Promega) was added to each scaffold and after a minute incubation plates were placed in the detection chamber of an ORCA-2BT Imaging System (Hamamatsu Photonics, Hamamatsu City, Japan) provided with a C4742-98-LWG-MOD camera fitted with 512 $\times$ 512 pixel charge couple device (CCD) cooled at $-80^{\circ}C$. Images were acquired during 1 min using 1 $\times$ 1 pixel arrays (binning 1 $\times$ 1). To register the position of the light signal, an additional black and white image was obtained using the illumination lamp in the detection chamber.

Scaffolds were then rinsed with PBS and placed back in the plates adding fresh media. Quantification of photon events from selected areas was performed using the Hokawo^{TM} Imaging Software (Hamamatsu Photonics) and expressed as photon counts (PHCs) after discounting background using the formula: PHCs = (total number of PHCs in the area of interest)$-$[(number of pixels in the area of interest) $\times$ (background average PHCs/pixel)].

Pseudo color images were generated using the same arbitrary color display settings for all images in the same experiment. Arbitrary color bars represent standard light intensity levels (blue= lowest; red = highest).

In vivo noninvasive BLI and image analysis

For the *in vivo* noninvasive BLI of mice bearing hAMSCs seeded scaffolds, mice anesthetized with ketamine/xilacine were i.p. injected with 150 mg kg^{-1} of D-luciferin (16.7 mg mL^{-1} in physiological serum) (Caliper Life Science, MA) or intravenous (i.v.) injected through tail vein with 25 mL of benzyl colenterazine (hCTZ), the RLuc substrate (1 mg mL^{-1} in 50/50 propilenglycol/ethanol) (Prolume, Pinetop, AZ) diluted in 125 mL of water. Mice were then placed in the detection chamber of an ORCA-2BT Imaging system (Hamamatsu Photonics, Hamamatsu City, Japan) provided with a C4742-98-LWG-MOD camera and a 512 $\times$ 512 pixel, charge couple device (CCD) cooled at $-80^{\circ}C$ at a distance of 200 mm from the camera objective (HFP-Schneider Xenon 0.95/25 mm). Imaging was performed routinely 5 min after substrate inoculation. Two images were generated from each mouse, one using a light source inside the chamber to register the animal position and a second one, in total darkness, during a 10-min period to acquire photons from the light emitting cells. To increase detection sensitivity the read out noise of the recorded signal was reduced by adding the light events recorded by arrays of 8 $\times$ 8 adjacent pixels (binning 8 $\times$ 8) in the camera CCD. Mice were monitored during a 6-week period. Quantification and analysis of photons recorded in the areas of interest from images was done using the Hokawo^{TM} Imaging Software (Hamamatsu Photonics).

Fluorescent angiography

To compare the angiogenic capacity of PLA/CaP with PLA scaffolds, samples of each material seeded with hAMSCs were implanted sc in the back of three SCID mice. After 2 months, fluorescent angiography was performed. In brief, anesthetized mice were injected i.v. with 200 μL of fluoresceine isothiocyanate (FITC) dextran, 2000 kD MW, 10 mg mL^{-1} (Sigma). After 10 min, mice were sacrificed and scaffolds retrieved and fixed in formalin solution 10% (Sigma). Samples were observed under confocal microscopy.

Histology

At the end of the monitoring period the scaffolds were retrieved from the animals, fixed in formalin solution 10% (Sigma) for 24 h and embedded in paraffin or OCT. Sections of 5 μm thickness were stained with hematoxylin (Merck, Darmstadt, Germany) and eosin (Sigma) for optical microscopy or with biotinylated *Griffonia simplicifolia* lectin I B_4 (GSLI B_4 isolectin) (Vector labs, Burlingame, CA), streptavidin-conjugated Alexa Fluor 647 (Molecular Probes)[30] and Hoechst Stain Solution (Sigma) for confocal microscopy.

Scanning electronic microscopy (SEM)

Extracted scaffolds were fixed with 2.5% glutaraldehyde during 4 h and postfixed with 1% osmium tetroxide for 1 h. Following, samples were dehydrated, dried to critic point, covered with gold and observed with a Jeol JSM-6400 scanning microscope.

Quantitative imaging and statistical analysis

For analysis of *in vitro* cell proliferation in scaffolds, the average number of PHCs from cells at different times of growth was normalized relative to that at day 0.

For *in vivo* analysis cell proliferation in scaffolds, RLuc PHCs from each scaffold image were averaged and normalized relative to that at day 0.

Changes in PECAM-1 and HRE regulated expression of PLuc were calculated in relation to that of the RLuc reporter (ratio: PLuc/RLuc). Statistical analysis was performed using the two-way ANOVA test (GStat 2.0 software) to compare the behavior through time of cells seeded in PLA and PLA/CaP scaffolds. $p < 0.01$ values were considered significant. For individual time-points, a Student t test was performed considering significant values of $p < 0.05$.

To compare the angiogenic capacity of different scaffolds *in vivo*, the average of GSLI B_4 isolectin stained area was calculated in 50 sections from each type of scaffold (200 PLA and 300 PLA/CaP fields approximately, at 400× magnification). Data was analyzed using the Student t test (differences were considered significant when $p < 0.05$).

RESULTS

HAMSCs survive and proliferate in PLA/CaP scaffolds *in vitro*

HAMSCs were transduced with a lentiviral construct for expression of PLuc regulated by the constitutively active CMV promoter and then seeded in PLA/CaP scaffolds. Bioluminescence images obtained weekly from the hAMSCs-seeded scaffolds showed a slight drop in the number of cells during the first week, followed by a proliferation stage that continued up to the end of a 7-week observation period, reaching a cell number 30× higher that at day 2 (Fig. 1).

At the end of the monitoring period, the scaffold samples were harvested, fixed and prepared for scanning electronic microscopy. SEM images (Fig. 2) show cell growing both in the surface and inside the material.

HAMSCs seeded on PLA/CaP scaffolds and implanted on SCID mice proliferate after overcoming an initial growth crisis

While the proliferation of cells in scaffolds *in vitro* may be an indicator of their affinity for the material surface, the physiological environment of within implanted scaffolds is considerably more complex due to restriction in the availability of oxygen and nutrients and changing conditions as the wound repairs. To explore this, we next seeded PLA/CaP scaffolds with hAMSC·PLuc cells and implanted them s.c. in three SCID mice. *In vivo* monitoring of PLuc activity showed (Fig. 3) that a large proportion of cells died within the first week post-scaffold implantation. Nevertheless, after the third week surviving cells began to proliferate again, reaching a level of 30% relative to day 0 by the 5th week postimplantation.

CaP glass promotes differentiation of hAMSCs to the endothelial lineage

The kinetics of cell growth on implanted scaffolds suggested that changes in gene expression triggered by restrictions in nutrients and oxygen may result in adaptations to the changing physiological environment.

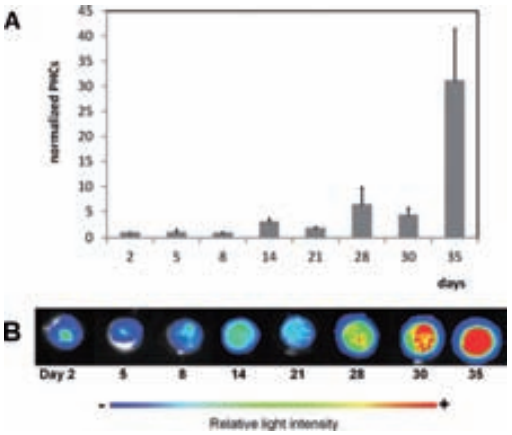

FIGURE 1. Proliferation of hAMSCs seeded on PLA/CaP scaffolds. (a) Quantitative analysis of light produced by hAMSCs-PLuc cells expressed as total photon counts normalized relative to day 2. Bars represent the standard error of the mean. (b) Representative composite images from hAMSCs-PLuc cells, at the indicated days postseeding, overlaid on the corresponding white light images of scaffold. The color bar shows the arbitrary standard rainbow color scale used to depict relative light intensities (red= highest; blue= lowest). [Color figure can be viewed in the online issue, which is available at wileyonlinelibrary.com.]

To analyze the differentiation state of hAMSCs seeded on both PLA and PLA/CaP scaffolds, cells initially labeled with the CMV:RLuc reporter were also labeled with a *PLuc* reporter regulated by an inducible promoter. A human PECAM-1 promoter or, alternatively, an HRE promoter, was used to image endothelial differentiation or hypoxia estate, respectively. An additional advantage of this double reporter strategy was that changes in the expression of the inducible PLuc could be directly related to the activity of constitutively expressed RLuc, as a reference reporter, avoiding potential cell proliferation and imaging artifacts. Labeled cells of both types were seeded on the biomaterial and implanted on 12 SCID mice as indicated in the diagram of Figure 4, and then subjected to BLI analysis during a 4-week period.

Quantification of photon events recorded from BLI captures [Fig. 4(A)] shows that cell growth during this period was comparable in PLA and PLA/CaP scaffolds [Fig. 4(B)]. However, PECAM-1 promoter regulated light production was significantly higher for cells in the PLA/CaP material (two-way ANOVA test, $p < 0.01$) [Fig. 4(C)], indicating that PLA/CaP is a better inducer of vascular differentiation for hAMSCs. Interestingly, the observed increase in expression of the PECAM-promoter regulated reporter correlated with a decrease in the expression of the HER-promoter regulated reporter for both materials, indicating a decrease of the hypoxia level in the material as angiogenesis proceeds. However, cells in the PLA/CaP material appear to be under a (slightly/higher) ($p = 0.026$.) hypoxic stress than those in PLA.

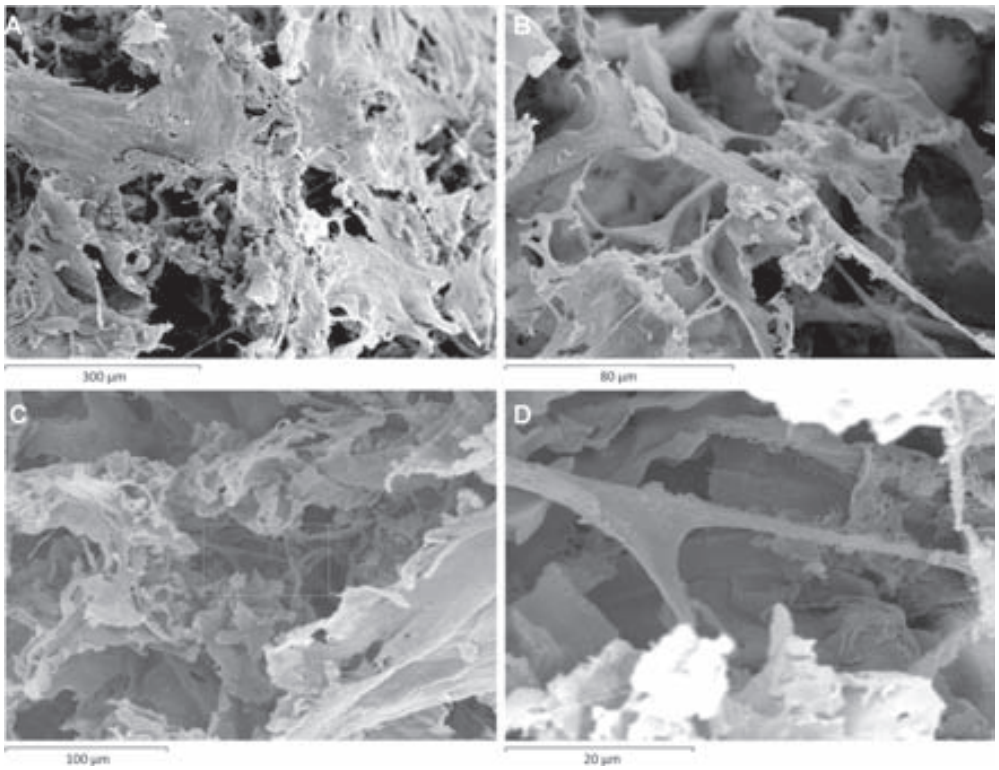

FIGURE 2. Scanning electronic microscope images of hAMSCs grown on PLA/CaP scaffolds during 35 days. (A) Image of biomaterial surface (×160). (B) enlarged detail showing a cell (×700). (C, D) Scaffold pores, showing surface lining cells (×400 and ×2300, respectively).

PLA/CaP scaffolds promote angiogenesis

In a different set of experiments, PLA/CaP scaffolds were implanted without cells to analyze the response of host cells. The proangiogenic capacity of the PLA/CaP scaffold detected by BLI was also validated by standard histological procedures. To facilitate visualization of colonizing cells within the scaffold, 12 transgenic GFP mice were implanted s.c. (6 mice) and in a calvarial defect model (6 mice) with

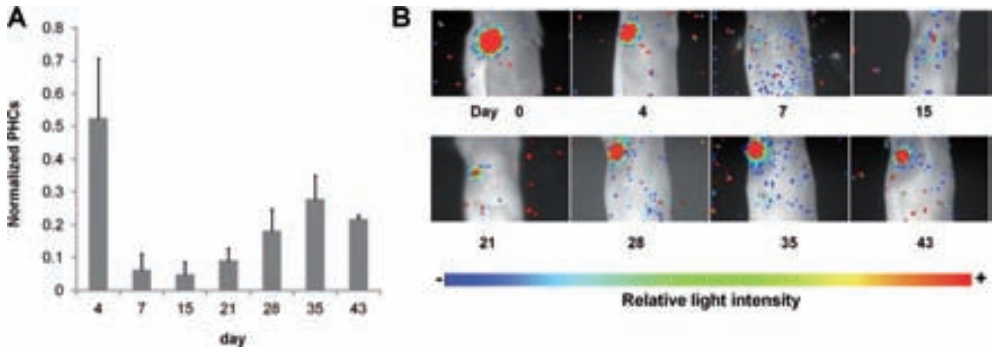

FIGURE 3. Proliferation of hAMSCs seeded on PLA/CaP scaffolds and implanted sc on SCID mice. (a) Quantitative analysis of light produced by hAMSCs-PLuc cells expressed as photon counts normalized to day 0. Bars represent the standard error of the mean. (b) Representative composite images from a hAMSCs-PLuc cell seeded PLA/CaP scaffold at a s.c. site at the indicated days postimplantation, overlaid on the corresponding black and white images of the mouse. The color bar shows the arbitrary standard rainbow color scale used to depict relative light intensities (red) highest; blue = lowest). [Color figure can be viewed in the online issue, which is available at wileyonlinelibrary.com.]

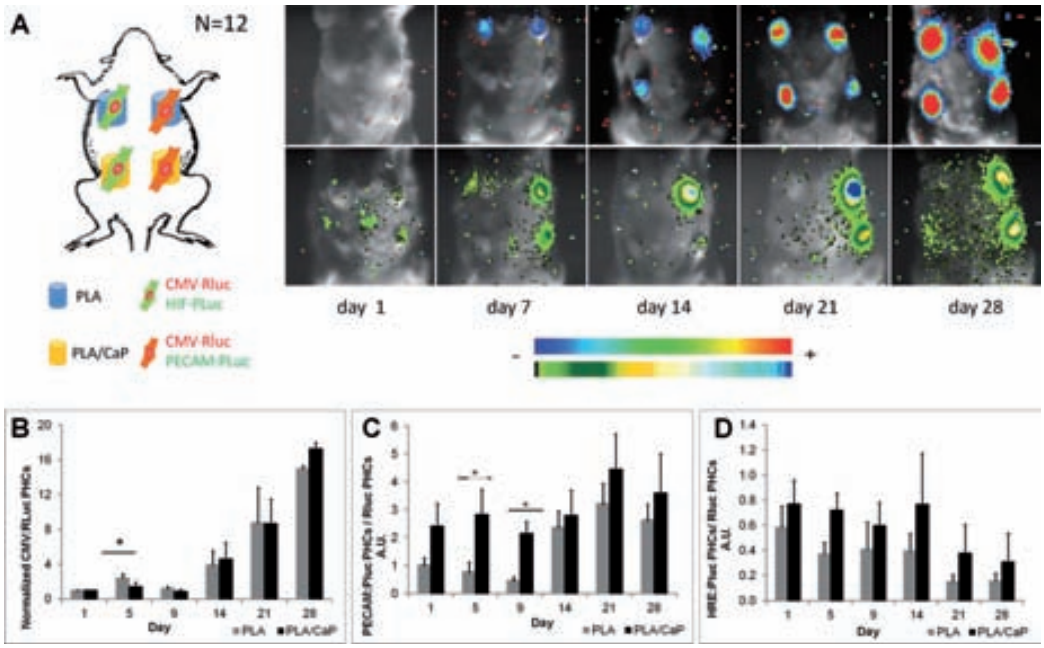

FIGURE 4. Noninvasive imaging of RLuc and PLuc-expressing hAMSCs cells seeded on PLA and PLA/CaP scaffolds s.c. implanted in SCID mice. (a) Representative BLI images showing RLuc (top row) and PLuc (bottom row) activity from dually labeled hAMSCs, on PLA and PLA/CaP scaffolds, superimposed on black and white dorsal images of the corresponding mouse. The diagram illustrates the implantation strategy and sites (top left). Color bars illustrate relative light intensities from RLuc (blue: low, red: high,) and PLuc (black: low, blue: high); (b) Histogram summarizing cell proliferation data, RLuc PHCs are normalized to day 1; (c) Histogram summarizing evolution of PECAM expression, data is represented as the ratio PLuc/RLuc PHCs ($p < 0.01$ according to the two-way ANOVA test) (d) Histogram summarizing the evolution of hypoxia, expressed as the ratio PLuc/RLuc ($p = 0.026$ according to the two-way ANOVA test) (A.U. =arbitrary units). Bars represent the standard error of the mean. *$p < 0.05$ according to Student t test; AU = arbitrary units. [Color figure can be viewed in the online issue, which is available at wileyonlinelibrary.com.]

PLA/CaP scaffolds. Scaffolds harvested 4 weeks after implantation had changed their macroscopic appearance significantly and had attracted a network of host blood vessels [Fig. 5(B)]. Hematoxylin–eosin-stained sections from both sc and calvarial lesion implants also showed the presence of abundant host cells and micro vascular structures. Laser confocal microscope and SEM images of scaffold sections confirmed the presence of GFP expressing host cells and cellular structures, respectively, within the PLA/CaP scaffold [Fig. 5(C)].

To ascertain that host blood vessels colonized the scaffolds, three SCID mice s.c. implanted with PLA/CaP scaffolds during a 2-month period were perfused through the tail vein with a high MW (2000 kD) FITC conjugated dextran unable to penetrate the endothelial barrier. Fluorescence confocal microscope examination of parafomaldehyde fixed scaffold sections showed the presence of colonizing green fluorescent micro vascular structures in the interior of the scaffolds that were well connected to the host vascular system (Fig. 6).

CaP glass improves the angiogenic capacity of PLA scaffolds

To further validate BLI results and compare the angiogenic capacity of PLA/CaP and standard PLA only material, four SCID mice were implanted sc with PLA/CaP and PLA scaffolds that were harvested after a 2-month period. Following fixation the scaffolds were sectioned and stained using biotin conjugated endothelial cell surface specific GSLI Isolectin B_4 (endothelial cell specific marker) and streptavidin-conjugated Alexa Fluor® 647. Quantitative analysis of fluorescence confocal microscope images showed that the amount of surface stained by Isolectin B4 was significantly higher ($p < 0.05$) in the PLA/CaP than in the PLA only scaffolds (Fig. 7).

DISCUSSION

The aim of the current work was to analyze the *in vivo* angiogenic inducing capacity of a new biomaterial composed by poly(lactic acid) and calcium phosphate glass (PLA/CaP), in combination with hAMSCs known to differentiate to the endothelial lineage under appropriate stimulus. Previous *in vitro* studies with MG-63 cells[17,18] had shown that these cells are able to attach, colonize, proliferate and differentiate in this material *in vitro*.

We used a noninvasive BLI platform, based on the use of a high sensitivity video camera to detect visible light photons generated by luciferase reporters genetically

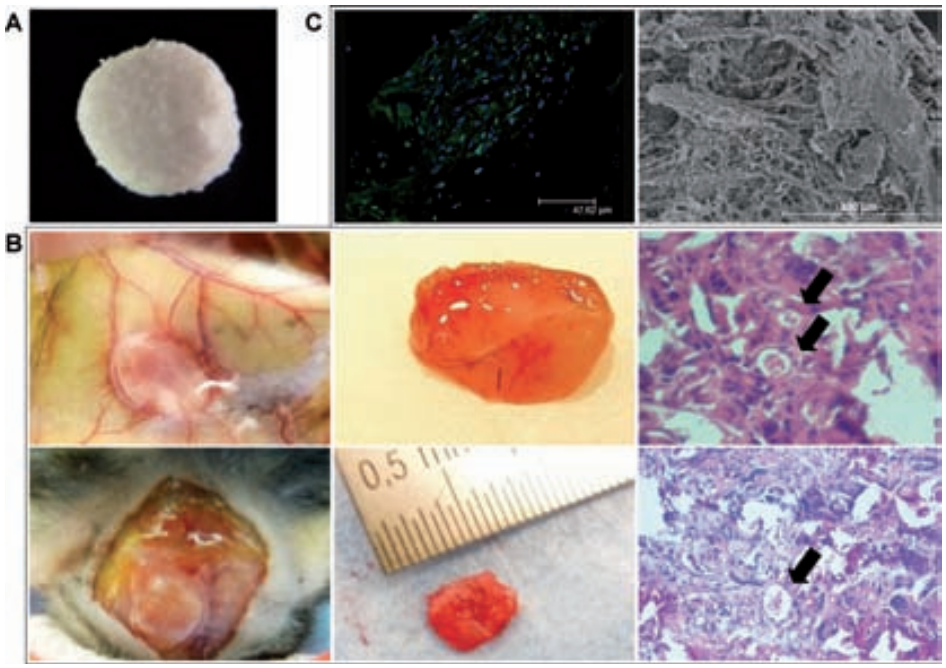

FIGURE 5. Cell colonization and angiogenesis of PLA/CaP scaffolds implanted without cells in transgenic GFP mice during 1 month. (A) Appearance of a PLA/CaP before implantation. (B) Images of sc (upper panels) and calvarial lesion (lower panels) implanted scaffolds showing visual appearance (left and middle) and invading capillaries arrows) in H-E stained scaffold sections (right). (C) Laser confocal microscope image showing invading green fluorescent host cells (objective: ×20/0.4, eyepiece ×10/20) (left) and SEM image showing host cell colonization (×200) (right). [Color figure can be viewed in the online issue, which is available at wileyonlinelibrary.com.]

introduced in cells and monitor their behavior. By using constitutively active promoters to regulate luciferase expression, we observed that PLuc expressing hAMSCs were compatible with PLA/CaP scaffolds and proliferate well in them during a 7-week period when cultivated *in vitro*, a good indicator of the affinity of the cells for the scaffold material. However, when implanted in live SCID mice, cell behavior was very different, and viability dropped by nearly 20 fold, in the first week, to finally recover by the fifth week postimplantation. This drop and recovery in the proliferative behavior of hAMSCs on implanted scaffolds were indicative of an adaptive response, governed by changes in gene expression, to stressing physiological conditions within recently implanted scaffolds.

The use of tissue specific promoters, only active in certain cell lineages, to regulate luciferase reporter activity may allow *in vivo* monitoring of cell differentiation. However, BLI measurements contain information on spatial distribution and photon fluxes, the latter of which may also reflect changes in cell number. Thus, changes in inducible reporters can best be quantified by relating them to internal cell number controls. To understand the adaptive changes of hAMSCs in scaffolds, we labeled hAMSC-RLuc cells with an additional PLuc-eGFP reporter regulated by either the PECAM

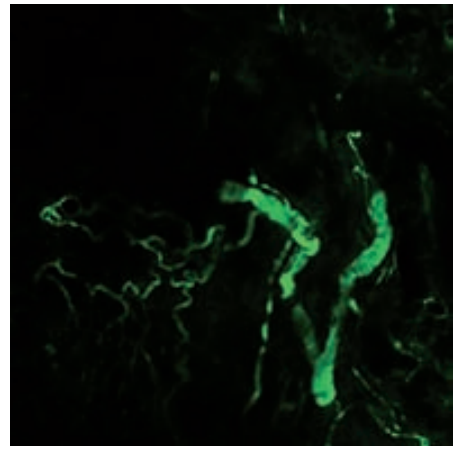

FIGURE 6. Microvascular structures in PLA/CaP scaffolds implanted without cells. Laser confocal microscope image showing tail vein injected FITC-dextran filling tubular structures at different depths of a PLA scaffold implanted during 2 months in a SCID mouse (objective: ×20/0.4, eyepiece ×10/20). [Color figure can be viewed in the online issue, which is available at wileyonlinelibrary.com.]

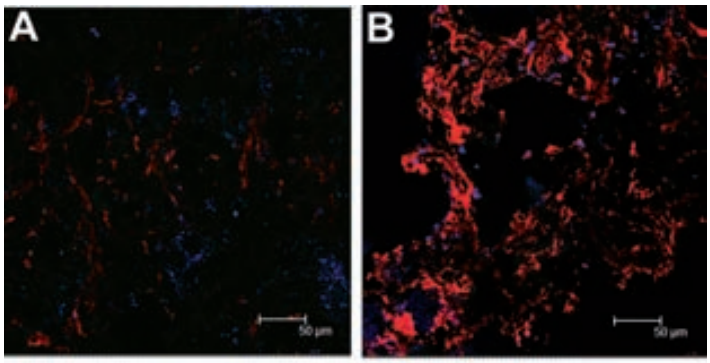

C

	n	mean	T Student Test
PLA	290	6.1	0.029
PLA/CaP	194	12.7	

FIGURE 7. Endothelial cell specific Isolectin B4 (red) and Hoechst (blue) staining of scaffold sections. Representative images obtained after a 2-month implantation without cells in Green Fluorescent Mice using a laser confocal microscope (objective: ×20/0.4, eyepiece ×40/20). (A) PLA scaffold. (B) PLA/CaP scaffold. (C) Table showing the percentage of area stained with Isolectin B_4, calculated using ImageJ software. Difference is significant with $p < 0.05$. *n*: number of fields analyzed. [Color figure can be viewed in the online issue, which is available at wileyonlinelibrary.com.]

or a hypoxia response element promoter. In this manner changes in the inducible luciferase activity could be related to those of the constitutively expressed one, and expressed as the ratio of their photon fluxes. With this approach, we were able to observe that both materials were generally equivalent at supporting cell growth, although at days 5 the number of cells in PLA/CaP is significantly lower than that in PLA. Also, during the whole experiment, the overall trend of hAMSC differentiation to the endothelial lineage was significantly (ANOVA) higher in PLA/CaP than in PLA. Comparison of PECAM regulated PLuc expression at specific times showed no significant differences except for days 5–9, where cells in PLA/CaP express significantly higher levels of light that those in PLA, in correspondence with slower proliferation, and in agreement with current believe that generally differentiating cells proliferate slower. HAMSCs differentiated to the endothelial lineage in correlation with a decrease in the hypoxia sensed by the cells within the scaffold. However, endothelial differentiation was faster and more robust in the PLA/CaP than in the PLA only material. Interestingly, cells in the PLA/CaP material appear to be under slightly higher hypoxic stress than those in PLA. At this point it is difficult to offer a rationalization for this observation. However, a tempting but speculative explanation could be that the hypoxic state drives the observed enhanced endothelial differentiation in PLA/CaP. Alternatively, higher hypoxia could result from different metabolic requirements associated to cell differentiation.

Results from BLI were also supported by observations using more standard procedures. Visual inspection of PLA/CaP scaffolds implanted without cells in GFP transgenic mice showed that within a 1-month period there was an evident recruitment of vascular system from the host. Histological analysis by conventional and laser confocal microscopy corroborated the invasion of the material by fluorescent host cells that also formed part of vascular structures. Further analysis by inoculation of a high molecular weight FITC-conjugated dextran in live mice revealed dextran-filled fluorescent vascular structures within the PLA/Cap scaffolds, demonstrating their functional connectivity with the host vascular system. Moreover, the surface of GSLI B4 isolectin-stained endothelial cells lining PLA/CaP scaffolds was significantly larger than that in PLA only scaffolds, in support of BLI results showing the higher capacity of the former material to induce endothelial differentiation of hAMSCs. Thus, in agreement with previous reports,[19] slow dissolution of CaP may be generating an ionic environment inducing migration and differentiation of angiogenic precursors within the PLA/CaP material.

CONCLUSIONS

In the current work we show that addition of calcium phosphate glass to PLA results in a composite material with higher angiogenic capacity than that of PLA only. Implanted in SCID mice, PLA/CaP scaffolds promote the colonization by host endothelial cells and functionally connected vascular structures that should promote its tissue repair capacity.

Using a BLI based strategy and standard histological procedures we analyzed cell proliferation, endothelial differentiation and response to hypoxia of hAMSCs expressing luciferase genes in PLA/CaP and PLA only materials. Our results indicating that PLA/CaP has superior proangiogenic capacity than PLA-only, supported those from more conventional histological procedures.

The agreement between standard histological and BLI analysis also validates the use of the latter as a flexible and effective tool for *in vivo* analysis of stem cell biomaterial interactions. This approach should facilitate preclinical development of scaffolds for specific tissue regeneration purposes.

REFERENCES

1. Langer R, Vacanti JP. Tissue engineering. Science 1993;260: 920–926.
2. Zippel N, Schulze M, Tobiasch E. Biomaterials and mesenchymal stem cells for regenerative medicine. Recent Pat Biotechnol 2010; 4:1–22.
3. Hubbell JA. Bioactive biomaterials. Curr Opin Biotechnol 1999;10: 123–129.
4. Griffith LG, Naughton G. Tissue engineering—Current challenges and expanding opportunities. Science 2002;295:1009–1014.
5. Polak J, Hench L. Gene therapy progress and prospects: In tissue engineering. Gene Ther 2005;12:1725–1733.
6. Pittenger MF, Mackay AM, Beck SC, Jaiswal RK, Douglas R, Mosca JD, Moorman A, Simonetti DW, Craig S, Marshak DR. Multilineage potential of adult human mesenchymal stem cells. Science 1999;284:143–147.
7. Bianco P, Riminucci M, Gronthos S, Robey PG. Bone marrow stromal stem cells: Nature, biology, and potential applications. Stem Cells 2001;19:180–192.
8. Chamberlain G, Fox J, Ashton B, Middleton J. Concise review: Mesenchymal stem cells: Their phenotype, differentiation capacity, immunological features, and potential for homing. Stem Cells 2007;25:2739–2749.
9. Pansky A, Roitzheim B, Tobiasch E. Differentiation potential of adult human mesenchymal stem cells. Clin Lab 2007;53:81–84.
10. Zuk PA, Zhu M, Ashjian P, De Ugarte DA, Huang JI, Mizuno H, Alfonso ZC, Fraser JK, Benhaim P, Hedrick MH. Human adipose tissue is a source of multipotent stem cells. Mol Biol Cell 2002;13: 4279–4295.
11. De Ugarte DA, Morizono K, Elbarbary A, Alfonso Z, Zuk PA, Zhu M, Dragoo JL, Ashjian P, Thomas B, Benhaim P, Chen I, Fraser J, Hedrick MH. Comparison of multi-lineage cells from human adipose tissue and bone marrow. Cells Tissues Organs (Print) 2003; 174:101–109.
12. Kern S, Eichler H, Stoeve J, Klüter H, Bieback K. Comparative analysis of mesenchymal stem cells from bone marrow, umbilical cord blood, or adipose tissue. Stem Cells 2006;24:1294–1301.
13. Vilalta M, Dégano IR, Bagó J, Gould D, Santos M, García-Arranz M, Ayats R, Fuster C, Chernajovsky Y, García-Olmo D, Rubio N, Blanco J. Biodistribution, long-term survival, and safety of human adipose tissue-derived mesenchymal stem cells transplanted in nude mice by high sensitivity non-invasive bioluminescence imaging. Stem Cells Dev 2008;17:993–1003.
14. Al-Khaldi A, Eliopoulos N, Martineau D, Lejeune L, Lachapelle K, Galipeau J. Postnatal bone marrow stromal cells elicit a potent VEGF-dependent neoangiogenic response in vivo. Gene Ther 2003;10:621–629.
15. Chung N, Jee BK, Chae SW, Jeon Y-W, Lee KH, Rha HK. HOX gene analysis of endothelial cell differentiation in human bone marrow-derived mesenchymal stem cells. Mol Biol Rep 2009;36: 227–235.
16. Whyte JL, Ball SG, Shuttleworth CA, Brennan K, Kielty CM. Density of human bone marrow stromal cells regulates commitment to vascular lineages. Stem Cell Res 2011;6:238–250.
17. Navarro M, Ginebra MP, Planell JA, Zeppetelli S, Ambrosio L. Development and cell response of a new biodegradable composite scaffold for guided bone regeneration. J Mater Sci Mater Med 2004;15:419–422.
18. Charles-Harris M, Koch MA, Navarro M, Lacroix D, Engel E, Planell JA. A PLA/calcium phosphate degradable composite material for bone tissue engineering: An in vitro study. J Mater Sci Mater Med 2008;19:1503–1513.
19. Aguirre A, González A, Planell JA, Engel E. Extracellular calcium modulates in vitro bone marrow-derived Flk-1+ CD34+ progenitor cell chemotaxis and differentiation through a calcium-sensing receptor. Biochem Biophys Res Commun 2010;393:156–161.
20. Iyer M, Wu L, Carey M, Wang Y, Smallwood A, Gambhir SS. Two-step transcriptional amplification as a method for imaging reporter gene expression using weak promoters. Proc Natl Acad Sci USA 2001;98:14595–14600.
21. Contag CH, Spilman SD, Contag PR, Oshiro M, Eames B, Dennery P, Stevenson DK, Benaron DA. Visualizing gene expression in living mammals using a bioluminescent reporter. Photochem Photobiol 1997;66:523–531.
22. Vilalta M, Jorgensen C, Dégano IR, Chernajovsky Y, Gould D, Noël D, Andrades JA, Becerra J, Rubio N, Blanco J. Dual luciferase labeling for noninvasive bioluminescence imaging of mesenchymal stromal cell chondrogenic differentiation in demineralized bone matrix scaffolds. Biomaterials. 2009;30:4986–4995.
23. Newman PJ, Albelda SM. Cellular and molecular aspects of PECAM-1. Nouv Rev Fr Hematol 1992;34:S9–S13.
24. Semenza GL, Jiang BH, Leung SW, Passantino R, Concordet JP, Maire P, Giallongo A. Hypoxia response elements in the aldolase A, enolase 1, and lactate dehydrogenase A gene promoters contain essential binding sites for hypoxia-inducible factor 1. J Biol Chem 1996;271:32529–32537.
25. Vilalta M, Dégano IR, Bagó J, Aguilar E, Gambhir SS, Rubio N, Blanco J. Human adipose tissue-derived mesenchymal stromal cells as vehicles for tumor bystander effect: A model based on bioluminescence imaging. Gene Ther 2009;16:547–557.
26. Ray P, De A, Min J-J, Tsien RY, Gambhir SS. Imaging tri-fusion multimodality reporter gene expression in living subjects. Cancer Res 2004;64:1323–1330.
27. Razorenova OV, Ivanov AV, Budanov AV, Chumakov PM. Virus-based reporter systems for monitoring transcriptional activity of hypoxia-inducible factor 1. Gene 2005;350:89–98.
28. Okabe M, Ikawa M, Kominami K, Nakanishi T, Nishimune Y. "Green mice" as a source of ubiquitous green cells. FEBS Lett 1997;407:313–319.
29. Dégano IR, Vilalta M, Bagó JR, Matthies AM, Hubbell JA, Dimitriou H, Bianco P, Rubio N, Blanco J. Bioluminescence imaging of calvarial bone repair using bone marrow and adipose tissue-derived mesenchymal stem cells. Biomaterials 2008;29:427–437.
30. Bayes-Genis A, Soler-Botija C, Farré J, Sepúlveda P, Raya A, Roura S, Prat-Vidal C, Gálvez-Montón C, Montero JA, Büscher D, Belmonte JCI. Human progenitor cells derived from cardiac adipose tissue ameliorate myocardial infarction in rodents. J Mol Cell Cardiol 2010;49:771–780.

2. SECOND PUBLICATION

Multimodal bioluminescent and Micro-Computed Tomography imaging of bone repair induced by fibrin-binding growth factors

Olaia F Vila[1,2], Mikäel Martino, Laura Nebuloni[3], Gisela Kuhn[3] , Ralph Müller[3], Jeffrey A Hubbell[4], Nuria Rubio[1,2], Jeronimo Blanco[1,2,*].

[1]*Catalonian Institute for Advanced Chemistry (IQAC-CSIC)*
[2]*Networking Research Center on Bioengineering, Biomaterials and Nanomedicine (CIBER-BBN), Spain.*
[3]*Institute for Biomechanics, ETH Zurich, Wolfgang-Pauli-Strasse 10, 8093 Zurich, Switzerland*
[4]*Institute of Bioengineering, Ecole Polytechnique Fédérale de Lausanne, Switzerland.*

BIOMATERIALS. In revision.

Multimodal bioluminescent and Micro-Computed Tomography imaging of bone repair induced by fibrin-binding growth factors

Olaia F Vila[1,2], Mikaël M Martino[3], Laura Nebuloni[4], Gisela Kuhn[4] , Ralph Müller[4], Jeffrey A Hubbell[3], Nuria Rubio[1,2], Jerónimo Blanco[1,2,*].

[1]*Catalonian Institute for Advanced Chemistry (IQAC-CSIC)*
[2]*CIBER-BBN*
[3]*Institute of Bioengineering, École Polytechnique Fédérale de Lausanne, Switzerland.*
[4]*Institute for Biomechanics, ETH Zurich, Wolfgang-Pauli-Strasse 10, 8093 Zurich, Switzerland*
**Corresponding author* Jeronimo.Blanco@iqac.csic.es

We evaluated the capacity of BMP-2 and fibrin-binding PDGF-BB to induce bone regeneration using multi-modal imaging technologies. Human mesenchymal stem cells from adipose tissue (hAMSCs) expressing two luciferase genes, one of them under the control of a tissue-specific promoter (osteocalcin or PECAM), were seeded in fibrin matrices containing BMP-2 and fibrin-binding PDGF-BB, and further implanted intramuscularly or in a mouse calvarial defects. Then, bone regeneration was monitored by bioluminescence imaging (BLI) to analyze the evolution of target gene expression, indicative of cell differentiation towards the osteoblastic and endothelial lineages. This non-invasive imaging was supplemented with micro-computed tomography (microCT) to evaluate bone regeneration and high-resolution microCT of plastic vascular casts. Results from BLI showed an increase of osteocalcin but not PECAM-1 expression three weeks after implantation. Results from microCT and histological procedures show that the delivery of BMP-2 and fibrin-binding PDGF-BB by fibrin induced the formation of thicker bone, and improves vascularization, resulting in more abundant and thicker vessels, in comparison with controls. Although inclusion of hAMSCs in the fibrin matrices made no significant difference in any of these parameters, there was an important increase in the number of intervascular connections between vessels in defects that were treated with hAMSCs.

Key words (4-6): Mesenchymal Stem Cells / fibrin/ bone regeneration/ bioluminescence imaging, BLI/ angiogenesis/ micro-CT

INTRODUCTION

The reconstruction of hard and soft tissues is a major challenge in regenerative medicine, a situation aggravated by the increasing number of tissue defects in the aging population. Research has widely shown the importance of growth factors (GFs), in tissue repair and regeneration and

GF-based therapies are very promising (1). For example, two GFs approved by the FDA that have received considerable attention are platelet derived growth factor-BB (PDGF-BB) and bone morphogenetic protein-2 (BMP-2) (2). In adults, most of the proposed functions of PDGF-BB relate to different responses to injury, for example, inflammation and wound healing (3), blood vessels maturation and chemotactic activity towards MSC (4). BMP-2 mostly influence bone, but also hematopoietic cell differentiation (5). BMP-2 induce migration and differentiation of MSCs to the osteogenic phenotype (6,7) and this features have been used in therapeutic bone repair and regeneration (8–12). While GFs are very promising in regenerative medicine, there is some recent controversy relative to their safety for clinical use, in particular their association with cancer risk/mortality and other side effects (13,14). Thus, there exists a strong motivation to engineer smart biomaterial systems that can deliver GFs precisely at low doses to potentially improve safety and cost-effectiveness (15).

On the other hand, there are multiple cell types having potential for tissue regeneration e.g.: embryonic stem cells, hematopoietic stem cells or mesenchymal stem cells (MSCs) (16). Among the latter, adult stem cells derived from bone marrow and adipose tissue appear as ideal candidates for autologous cell therapies, avoiding problems associated with immune rejection, pathogen transmission and ethical issues (17–23). While MSCs from the bone marrow, having a rich differentiation potential and anti-inflammatory capacity, would be ideal candidates for tissue repair, their use is hampered by their relative low abundance and pain associated with their extraction. More recently identified MSCs from adipose tissue (AMSCs) offer an easily extractable and abundant alternative source of therapeutic cells with similar phenotype and equivalent differentiation potential to their homologues from the bone marrow, but in larger supply (21–23). Furthermore, these cells have shown undetectable predisposition to oncogenic transformation after *in vitro* cultivation and implantation in mice (24).

In this current work, we intended developed a novel multimodal analysis platform to evaluate the regenerative capacity of BMP-2 and fibrin-binding PDGF-BB delivered by a fibrin-based scaffolds. In order to analyze the effect of GFs on cell behavior, luciferase expressing hAMSCs served as reporters. Using SCID mouse as an animal model, the cells were seeded in fibrin scaffolds, implanted intramuscularly or in calvarial defects and further monitored using a non-invasive bioluminescence imaging (BLI) platform. Moreover, by using inducible tissue specific gene promoters to regulate luciferase reporters, biologically significant changes in promoter activity were measured as photon fluxes, providing information on cell growth, distribution and time related changes in gene expression associated to cell differentiation (25–27). We used two different inducible promoters to regulate expression of the *Photinus pyralis* luciferase (PLuc). The promoter of bone gamma-carboxyglutamate protein or osteocalcin (BGLAP/OC), the major noncollagenous bone matrix protein expressed cells of the osteoblasts lineage (28,29) was used as a reporter of osteoblastic differentiation. While the promoter for the platelet endothelial cell

adhesion molecule-1 (PECAM-1) gene, a frequently used marker of endothelial cells, platelets and specific immune system cells (30) was used to monitor endothelial differentiation. Results from BLI were complemented with micro-Computed Tomography (microCT) of skulls to analyze bone regeneration under the different treatments and with high-resolution microCT of vascular casts of mice perfused with a polymeric resin, to visualize the vascularization of the defects.

MATERIALS AND METHODS

Lentiviral vectors constructs

Three different constructs were used during the study.

A CMV:hRLuc:mRFP:ttk lentiviral vector (abbreviated as CMV:RLuc) containing a trifunctional chimeric construct comprising the coding sequences for the *Renilla reniformis* luciferase (RLuc) reporter gene, the monomeric red fluorescent protein (mRFP1) gene and a truncated version of the herpes simplex virus thymidine kinase gene sr39tk (ttk) under transcriptional control of the CMV promoter, a kind donation from Dr. S.S Gambhir (Stanford, CA)(31).

A Plox-hOCp:PLuc:eGFP lentiviral vector for expression in cells of the osteoblast lineage (abbreviated as OC:PLuc) containing a chimeric construct of PLuc and eGFP coding sequences under the control of human osteocalcin promoter, constructed as described (32) in a Plox lentiviral vector.

A Plox-hPECAM-1p:PLuc:eGFP lentiviral vector for tissue specific expression in endothelial cells (abbreviated as PECAM:PLuc) containing a chimeric construct of PLuc and eGFP coding sequences under the control of the PECAM promoter was constructed as described (32) in a Plox lentiviral vector.

Lentiviral particle production

Production of viral particles was performed using human embryonic kidney cells 293T (ATCC, CRL-11268™) grown in Dulbecco's Modified Eagle Media-high glucose (DMEM-hg) (Sigma, Steinheim, Germany), 10% heat-inactivated fetal bovine serum (FBS) (Sigma), 2 mM L-glutamine (Sigma), 50 U/ml penicillin/streptomycin (Sigma), and 2 mM 4-(2-hydroxyethyl)-1-piperazineethanesulfonic acid (HEPES). The day previous to transfection, 4.5x106 trypsinized cells were seeded on 10 cm2 poly-D-lysine- (Sigma-Aldrich) treated plates. 6 µg of each lentiviral transfer vector was mixed with 2 µg of viral envelope plasmid (pMD-GVSV-G env) and 4 µg of packaging construct (pCMV ΔR 8.2) in 250 µl of 150mM NaCl. In a different tube, 48 µl of 1mg/ml polyethylenimine (PEI) (Polyscience, Warrington, PA) were mixed with 202 µl of 150mM NaCl, and then added slowly to the vector solution. After 30 min of incubation at room temperature this DNA solution was added drop wise to the plate containing the 293-T cells plus

medium, swirled gently and incubated for 16 h at 37°C with 5% CO_2. The following day the transfection solution was removed, the cells were rinsed with PBS 1x and medium without FBS was added to the cells. Following a 48 h-incubation the supernatant was collected, centrifuged at 2000 r.p.m. to remove cell debris, and filtered through a 0.45 mm low protein-binding filter (Corning, Bath, UK).

hAMSCs culture and transduction

Human AMSCs (hAMSCs) were isolated from adipose tissue derived from cosmetic subdermal liposuction of the lateral hip, with patient consent. Briefly, after rinsing in PBS 1X, lipoaspirates were suspended in one volume of 1X collagenase I (Invitrogen, Carlsbad, CA) solution and incubated 30 min at 37°C with gentle agitation. Digestion was terminated by inactivation of the collagenase I by addition of DMEM + 10% FBS. The resulting cell suspension was centrifuged at 450 g, and the pellet was washed in 50 mL Ringer's solution. The cell pellet was resuspended in 10 mL of erythrocyte lysis solution (0.16 M ammonium chloride) and incubated for 10 min at RT with gentle stirring. The suspension volume was completed to 50 mL with Ringer's lactate and centrifuged at 450 g. This step was repeated until no red color was detectable. The cell pellet was resuspended in 5 mL Ringer's lactate, filtered through a 70 m Nylon mesh, and centrifuged at 450 g. Cells resuspended in Ringer's lactate were counted using trypan blue to determine cell viability.

Cells were seeded at a density of 5000 cells/cm2 and grown in DMEM-hg, 10% heat-inactivated FBS (Hyclone, Logan, UT), 2 mM L-glutamine (Sigma), and 50 U/mL penicillin/streptomycin(Sigma), and cultivated for two additional passages before transduction with lentiviral vectors. Cells were then infected with concentrated vector stock ($2x10^6$ transduction units/mL, MOI=20) and then incubated for 24–48 h.

Production and purification of α_2PI_{1-8}-PDGF-BB

Fibrin-binding PDGF-BB was engineered to contain, at the N-terminus, the factor XIIIa sensitive sequence derived from α_2-plasmin inhibitor (α_2PI_{1-8}). Sequence encoding for α_2PI_{1-8}-PDGF-BB was synthetized by Genscript and subcloned into the mammalian expression vector pXLG (Protein Expression Core Facility, École Polytechnique Fédérale de Lausanne, Switzerland). A sequence encoding for 6 His was added at the C-terminus for further purification of the recombinant protein. Recombinant protein was prepared from growth medium of HEK-293E cells transfected with the engineered α_2PI_{1-8}-PDGF-BB sequences, as described (32) using a HisTrap HP 5 mL column (GE Healthcare), and ÄKTA Explorer (GE Healthcare) eluted with an imidazole gradient. The concentration of α_2PI_{1-8}-PDGF-BB in gradient fractions was determined using ELISA (Human PDGF-BB DuoSet, R&D systems) and the protein was verified as >99% pure by SDS-PAGE and MALDI-TOF. The level of endotoxin was verified as under 0.01 EU/µg of protein (HEK-Blue LPS Detection Kit, InvivoGen).

Bioactivity of α_2PI_{1-8}-PDGF-BB

MSCs were starved overnight in MEM-α containing 2% serum. Starved MSCs were stimulated for 5 min with 20 ng/mL of wild-type PDGF-BB (Invitrogen), with 20 ng/mL of α_2PI_{1-8}-PDGF-BB, or with PBS. Then, cells were lysed with a lysis buffer (20 mM Tris, 137 mM NaCl, 1% NP-40, 10% glycerol, 2 mM EDTA, 1 mM activated sodium orthovanadate, pH 8.0) supplemented with protease inhibitor cocktail (Roche) and the lysates were stored at -80°C. The amount of phosphorylated PDGF-receptor β was quantified using phospho-ELISA kit (phospho-PDGF-R, R&D Systems). ELISA plates were coated with a capture antibody for PDGF-receptor β and further incubated with cell lysates. The phosphorylation states were detected with an anti-phospho-tyrosine antibody and normalized to a standard according to manufacturer instructions.

GF release from fibrin matrix

Fibrin matrices were made as previously described (15) with human fibrinogen. Briefly, fibrin matrices were generated with 8 mg/mL fibrinogen (Fib 3, Enzymes Research Laboratories), 2 U/mL human thrombin (Sigma–Aldrich), 4 U/mL factor XIIIa (Fibrogammin, Behring), 5 mM $CaCl_2$, and 500 ng/mL of growth factor (PDGF-BB (Invitrogen), α_2PI_{1-8}-PDGF-BB, BMP-2 (R&D systems)). Fibrin gels were polymerized at 37°C for 1 h and transferred in Ultra Low Cluster 24-well plate (Corning Incorporated) containing 500 µL of buffer (20 mM Tris-HCl, 150 mM NaCl, 0.1% BSA, pH 7.4). A control well that served as 100% released control contained only the GF in 500 µL of buffer. Each 24 h, buffers were removed, kept at -20°C and replaced with fresh buffer. For the 100% release control well, 20 µL of buffer was taken out every day and stored at -20°C. After 7 days, GF cumulative release was quantified using ELISA kits (human BMP-2 DuoSet, human PDGF-BB DuoSet, R&D Systems), using the 100% released control as reference.

Fibrin matrix for *in vivo* application

Fibrin matrices were made as previously described (33). Fibrin matrices were generated with 12 mg/mL fibrinogen in HEPES buffer (20 mM HEPES, 150 mM NaCl, pH 7.5), 4 U/mL human thrombin, 8 U/mL factor XIIIa, 35 µg/mL aprotinin (Roche), 5 mM CaCl2, and 10 µg/mL of GFs.

Seeding of in fibrin matrices

When used, cells were added to the "fibrinogen plus GFs" solution, after being washed twice with serum-free medium and resuspended in 10% of the final gel volume of serum free medium. Gel polymerization was performed in situ, by mixing the fibrinogen solution and cell suspension just before implantation.

Animal procedures

Six-week old SCID mice were purchased from Charles-River (Wilmington, MA, USA) and maintained in a specific pathogen-free environment throughout the experiment. All animal-related procedures were performed with the approval of the animal care committee of the Government of Catalonia.

Subcutaneous implantation

Two subcutaneous (im) implantations were performed symmetrically in the back of each animal. Before scaffold implantation, the animals were anesthetized by an intraperitoneal injection with 100 mg/kg ketamine (Merial, Duluth, GA) and 3.3 mg/kg xilacine (Henry Schein, Melville, NY) and immobilized. To implant the material components were mixed with the cells, as previously described, and immediately 100 µl were injected in each site. Gelling of the mixture takes place within 5 minutes of implantation.

Intramuscular implantation

Two intramuscular (im) implantations were performed symmetrically in the thighs of each animal. Before scaffold implantation, the animals were anesthetized by an intraperitoneal injection with 100 mg/kg ketamine (Merial, Duluth, GA) and 3.3 mg/kg xilacine (Henry Schein, Melville, NY) and immobilized. To implant the material components were mixed with the cells, as previously described, and immediately 100 ml were injected in each site. The mixture gels inside the animal within 5 min.

Mice Calvarial defect model

Ten-week old SCID mice were purchased from Charles-River and maintained in a specific pathogen-free environment throughout the experiment. Surgery was performed as described (34). Briefly, mice were prepared for surgery by ip injection of 100 mg/kg ketamine (Merial) and 3.3 mg/kg xilacine (Henry Schein), and a sc analgesic injection of 0.05 mg/kg buprenorphine (Schering-Plough). The surgical site was cleaned with povidone-iodine (Braun). A sagital midline incision was performed on the skin and the periosteum was then cut, exposing the calvarial bone. Two defects, 3 mm diameter (critical size defect) were performed in the calvarial bone of each mice using a sterile drill bit (Dremel, Racine, WI), avoiding perforation of the dura. The surgical area was cleaned with saline and each defect was filled with a 6 ml scaffold, polymerized in situ, and containing, or not, hAMSCs. The incision was closed using absorbable sutures. After 6 weeks the animals were sacrificed by cervical dislocation skulls were harvested for analysis.

***In vivo* non-invasive BLI and image analysis**

For the *in vivo* non-invasive BLI of mice bearing hAMSCs seeded scaffolds, mice anesthetized with ketamine/xilacine were ip injected with 150 mg/kg of D-luciferin (16.7 mg/ml in physiological serum) (Caliper Life Science, MA, USA) or intravenous (iv) injected through tail vein with 25 ml of benzyl colenterazine (hCTZ), the RLuc substrate (1 mg/ml in 50/50 propilenglycol/ethanol) (Prolume, Pinetop, AZ, USA) diluted in 125 ml of water. Mice were then placed in the detection chamber of an ORCA-2BT Imaging system (Hamamatsu Photonics, Hamamatsu City, Japan) provided with a C4742-98-LWG-MOD camera and a 512x512 pixel, charge couple device (CCD) cooled at -80^{o}C at a distance of 200mm from the camera objective (HFP-Schneider Xenon 0.95/25 mm). Imaging was performed routinely 5 min after substrate inoculation. Two images were generated from each mouse, one using a light source inside the chamber to register the animal position and a second one, in total darkness, during a 10 min period to acquire photons from the light emitting cells. To increase detection sensitivity the read out noise of the recorded signal was reduced by adding the light events recorded by arrays of 8 x8 adjacent pixels (binning 8x8) in the camera CCD. Mice were monitored during a three week period. Quantification and analysis of photons recorded in the areas of interest from images was done using the Hokawo^{TM} Imaging Software (Hamamatsu Photonics).

Quantitative imaging and statistical analysis

For *in vivo* analysis cell proliferation in scaffolds, RLuc PHCs from each scaffold image were averaged and normalized relative to that at day 0. Changes in PECAM-1 and osteocalcin regulated expression of PLuc were calculated in relation to that of the RLuc reporter (ratio: PLuc/RLuc). Statistical analysis was performed using the t-Student test. $p < 0.05$ values were considered significant.

Bone micro computed tomography (µCT)

Six weeks after surgery the animals were euthanized by cervical dislocation. Heads were then fixed in a 10% formalin solution for 24 hours at 4ºC, and then transferred to 70% ethanol for conservation. Micro-CT measurements were performed in a microCT 40 (Scanco Medical AG, Brüttisellen, Switzerland). The X-ray tubes was operated at 55 kVp and 145 µA. Over 180° 500 projections were acquired with 200 ms integration time, resulting in a voxel size of 30 µm. After application of a constrained Gaussian filter (sigma 1.2, support 1) to suppress the noise, bone was segmented with a global threshold of 22.4 % of maximal grey value. The defect regions were identified with a cylindrical mask. Bone volume fraction and bone thickness was calculated in this volume of interest. Coverage was calculated from pseudo-radiograph created by a projection of the region in superior-inferior direction (35). Coverage, bone volume and bone thickness values of the

different groups were compared using an impaired Student's t-test. P-values smaller than 0.05 were considered significative.

Vascular corrosion casts

Vascular corrosion casts were produced for ex vivo analysis with ultra-high resolution micro-CT. The protocol was adapted from the one described by Beckmann et al (36). Briefly, mice were deeply anesthetized with Isoflurane (5%) and Pentobarbital. The thorax was opened to expose the heart and aortic arc. A small catheter (Fine Bore Polythene Tubing, 0.58/0.96 mm ID/OD, Smiths Medical, UK) was carefully introduced in the aorta and fixed there with surgical thread (Safil®, B-Braun, Germany). The animal was then perfused through the aorta, first with Phosphate Buffered Saline (PBS) containing 2% Heparin, then with 2% paraformaldehyde in PBS and the polymer resin PU4ii (Polyurethane for Improved Imaging, VasQtec, Switzerland) (37), all infused at 4 ml/min, 100 mm Hg and at body temperature (37°C). The resin is a mixture of PU, solvent (50% Ethylmethylketone – EMK) and a blue dye. After resin curing, the lower hind limbs were excised from the animals and the skin was removed. Soft tissue was macerated in 7.5% KOH for 24h at 50°C. Bone tissue was kept in the samples as a reference feature to allow future registration with the corresponding *in vivo* image datasets. Casts were then washed with water and stained for 24h with Osmium solution (2%) to obtain radiopacity. The samples were then immersed in home-made Pluronic gel (polyoxyethylene-polyoxypropylene triblock copolymer), a thermo-reversible gel that is solid at room temperature and liquid below.

Ultra-high resolution vascular µCT

The prepared samples were scanned with micro-CT (µCT 50, Scanco Medical AG, Brüttisellen, Switzerland). The scanner was operated at 55 kVp and 145 µA, with an integration time of 200 ms, and frame averaging of 3. All micro-CT scans were performed at room temperature. The CT scanner was calibrated weekly for mineral equivalent value, and monthly for determining in plane spatial resolution. An imaging protocol consisting of two consecutive scans was carried out to allow the identification of the defect region. The first scan was acquired at medium resolution to provide an overview for orientation within the sample; the second one at ultra-high resolution for detailed vascular analysis of the defect region. In the medium-resolution scan, the following settings were applied: 2000 projections were captured per 180 degrees with a field of view of 10 mm in diameter and a total length of 3.70 mm, leading to a nominal isotropic resolution of 10 µm. The medium-resolution images were then downscaled to 17.5 µm to match the *in vivo* voxel size and the two image datasets (*in vivo* and ex vivo) were registered using rigid registration (38). After identification of the matching region, an ultra-high resolution scan was carried out at that position with the following settings: 2000 projections were captured per 180 degrees with a field of view of 7 mm in diameter and a total length of 1.86 mm, leading to a nominal isotropic resolution of 1.4 µm. A Gaussian filter was applied to the ultra-high resolution images to reduce noise (sigma 1.2,

support 1). Blood vessels were segmented by a fixed thresholding procedure (20% of the maximum grayscale value) and bone was excluded by manual contouring. A morphological closing procedure (3 dilation and 3 erosion steps) was applied to refill hollow structures that appeared in the vessels after thresholding. Global standard morphometric analysis was performed on the ultra-high resolution images using the software package IPL (Image Processing Language, Scanco Medical AG, Brüttisellen, Switzerland). An unpaired Student's t-test was used to compare the vascular parameters for the different treatment groups. P-values smaller than 0.05 were considered significant.

RESULTS

Design and production of fibrin-binding PDGF-BB

In order to be covalently incorporated into fibrin during the natural polymerization process of the hydrogel, PDGF-BB was designed to contain the factor XIIIa substrate at their N-terminus (α_2PI_{1-8}) (REF Schense JC et al., 1999). To evaluate the bioactivity of α_2PI_{1-8}-PDGF-BB, MSCs, which highly express PDGF receptor-β (PDGFR-β), were stimulated with wild-type PDGF-BB or α_2PI_{1-8}-PDGF-BB. The addition of α_2PI_{1-8} at the N-terminus of PDGF-BB did not alter the bioactivity of the GF, since α_2PI_{1-8}-PDGF-BB could promote the phosphorylation of PDGFR-β (pPDGFR-β) to the same level of wild-type PDGF-BB (Fig. 1A).

Growth factors release from fibrin matrix

An *in vitro* release assay was performed to verify if BMP-2 and α_2PI_{1-8}-PDGF-BB could be sequestered into fibrin matrix. Fibrin matrices comprising wild-type PDGF-BB, α_2PI_{1-8}-PDGF-BB, or BMP-2 were incubated in excess of physiological buffer during a week. The buffer was changed every day, and released GFs were quantified by ELISA (Fig 1B). As previously reported (REF Martino et al., 2013, PNAS), BMP-2 was sequestered in fibrin matrix and slowly released. Wild-Type PDGF-BB was quickly released (more than 90% after 2 days), while only 5% of α_2PI_{1-8}-PDGF-BB was released after 7 days.

Delivering BMP-2 and α_2PI_{1-8}-PDGF-BB by fibrin enhances cell growth and OC expression, but not PECAM expression in intramuscularly implanted MSCs

MSCs expressing luciferase reporters could be sensitive sentinels reporting on the physiological environment within implants, as well as GF generators influencing/guiding tissue repair. Dually labeled hAMSCs (10^5 cells) expressing CMV-regulated RLuc and either OC-promoter regulated PLuc or PECAM-promoter regulated PLuc were polymerized with fibrin gels containing BMP-2 and α_2PI_{1-8}-PDGF-BB and im implanted in the left tight (OC-PLuc) or right tight (PECAM-PLuc) of 6-week old SCID mice. A group of mice implanted with the same number of MSCs in fibrin gels without GFs was used as control and monitored for RLuc and PLuc activity during 14 days.

Quantification of bioluminescence images from constitutively expressed RLuc photons show that implanted cells proliferated up to day 7 post implantation, after which there was a decline in cell number. Moreover, cells grew better in fibrin plus GFs that on fibrin alone. Evaluation of the Pluc/RLuc ratio, that measures changes in gene specific expression relative to cell number, showed that the inclusion of GFs in the fibrin scaffolds resulted in a trend of higher gene expression for both OC-PLuc and PECAM-PLuc, although such trend was only statistically significant in the former case (Fig 2).

OC expression but not PECAM expression is activated in hAMSCs during bone regeneration

Genetically modified hAMSCs expressing CMV regulated RLuc and either OC regulated PLuc or PECAM regulated PLuc were implanted in combination with fibrin gels containing bone growth factors (BMP-2 and $\alpha_2PI_{1\text{-}8}$-PDGF-BB) in a calvarial bone defect in SCID mice. To monitor cell growth and changes in gene expression, RLuc and PLuc activities, were monitored in live animals during 3 weeks using BLI. Results show that the cell proliferation pattern, as measured by RLuc activity, was similar regardless of whether cells were additionally labeled with OC:PLuc or PECAM:PLuc. Cells proliferated up to days 7-8 following which cell number decreased progressively. However, there was a difference in gene expression behavior, with a significant increase in OC, but not in PECAM expression, as measured by the ratio of RLuc/PLuc activities (Figs 3 and 4).

Delivering BMP-2 and $\alpha_2PI_{1\text{-}8}$-PDGF-BB by fibrin does not improve bone coverage but promotes the formation of thicker bone

Previous results suggest that inclusion of BMP-2 and $\alpha_2PI_{1\text{-}8}$-PDGF-BB in fibrin matrix induces changes in gene expression indicative of osteogenic lineage differentiation in "sentinel" cells seeded in the fibrin material.

In order to determine if addition of BMP-2 and $\alpha_2PI_{1\text{-}8}$-PDGF-BB to fibrin gels improves bone regenerative capacity, a 3 mm diameter calvaria bone defect was produced in 6 week old SCID mice and implanted with fibrin alone, fibrin plus BMP-2 and $\alpha_2PI_{1\text{-}8}$-PDGF-BB or fibrin plus BMP-2 and $\alpha_2PI_{1\text{-}8}$-PDGF-BB and hAMSCs, as indicated in the diagram in Fig 5D. In an additional control group the bone defect was left without implant. Following a 6 week growth period, mice were sacrificed and mice heads analyzed by microCT imaging to determine the change in defect size and bone volume regenerated.

Histograms representing the percent of defect surface covered with new bone during this period (Fig. 5A) indicate that while fibrin improved defect filling with bone, in comparison with no fibrin, inclusion of GFs or cells had no significant additional effect.

However, evaluation of changes in bone volume (Fig 5B) and thickness (Fig 5C) showed that the inclusion of GFs did result in a significant increase in bone volume relative to no scaffold or fibrin alone. Inclusion of hAMSCs in the fibrin scaffold had no significant effect on regenerated bone volume over that of fibrin scaffold alone.

Delivering BMP-2 and α_2PI_{1-8}-PDGF-BB with fibrin improves vascularization of the new bone

In order to analyze the effect of the different treatment combinations in the vascularization of the new bone, half of the mice from the previous experiment were perfused with a polymeric resin to perform a vascular cast. Once corroded and stained with osmium, casts were analyzed by utra-high resolution micro-computerized tomography. Vascular cast images showed a denser vascular network in the defects treated with fibrin plus BMP-2 and α_2PI_{1-8}-PDGF-BB when compared to those non-treated or treated with fibrin only (Fig. 6). Quantitative analysis of cast images showed that relative vessel volume, vessel number and vessel thickness were significantly higher in the defects treated with fibrin plus BMP-2 and PDGF-BB when compared with the non-treated defects or those treated with fibrin alone (Fig 7A, B, C). Vessel spacing, in the other hand, was significant lower, indicating higher compaction, in the defects treated with fibrin and GFs (Fig. 7D). Inclusion of hAMSCs in the fibrin plus GFs scaffolds had no significant effect in any of these parameters.

Addition of hAMSCs to fibrin plus BMP-2 and α_2PI_{1-8}-PDGF-BB matrices improves connectivity of the vascular network of the newly formed bone.

Analysis of data form vascular cast topographies showed that while vascular connectivity in the newly formed bone was similar in the defects treated with fibrin, with fibrin plus GFs, and with the controls, it was significant improved by the addition of hAMSCs (Fig. 6E).

DISCUSSION

Designing biomaterials that aid in tissue regeneration requires agile *in vivo* evaluation procedures that facilitate an iterative strategy based on cycles of material design - *in vivo* testing - modification- *in vivo* testing. The aim of the current work was to develop a novel multimodal analysis platform to evaluate the capacity of BMP-2 and fibrin-binding PDGF-BB delivered through fibrin to treat bone defect. The two GFs were used at the same time, as we believe that the delivery of several GFs at low doses may present a rational clinical approach for tissue healing, since multiple GFs are involved during natural healing processes.

We combined an *in vivo* procedure for imaging luciferase expressing hAMSCs and an ex-vivo microCT imaging procedure to evaluate the extent of bone and vascular regeneration. With this approach, *in vivo* imaging of luciferase expressing hAMSCs that served as sentinel provided real-time information on physiological conditions inductive of cell growth and differentiation, while ex

vivo microCT analysis served to evaluate the amount and quality of newly formed bone and vascular structures.

We used a non-invasive BLI procedure based on the use of a high sensitivity video camera, to detect visible light photons generated by luciferase reporters genetically introduced in hAMSCs. By including constitutively active promoters to regulate luciferase expression we can observe the evolution in the number of hAMSCs seeded in the fibrin scaffolds implanted in mice. Moreover, by introducing in hAMSCs additional luciferase reporters regulated by tissue specific promoters, only active in specific cell lineages, it is also possible to monitor changes in gene expression leading to cell differentiation. Changes in the activity of inducible reporters can best be quantified by relating them to the activity of the constitutively active luciferase, and expressing them as the ratio of their respective photon fluxes, avoiding in this manner artifacts due to in-vivo fluctuations in cell number.

Due to the capacity of hAMSCs to differentiate to multiple lineages, e.g., chondrogenic, adipogenic and osteogenic lineages, in response to external clues, these cells can be used as living reporters of growth and differentiation conditions within scaffolds. Thus, we used hAMSCs dually modified to express RLuc, regulated by a constitutively active promoter (CMV-RLuc), and with an additional PLuc-eGFP chimerical reporter. The latter regulated by either the PECAM or the human osteocalcin (hOC) inducible promoters to analyze the capacity of the material to induce cell differentiation.

With this approach, we were able to observe that in im. implanted fibrin matrices containing BMP-2 and α_2PI_{1-8}-PDGF-BB and luciferase expressing hAMSCs there was an induction of the osteocalcin but not of the PECAM endothelial reporter activity. We also used a calvarial bone defect model to determine whether selective osteocalcin induction capacity was also observed when the material was implanted in a bone defect.

Using the BLI procedure we were able to corroborate that, since fibrin containing BMP-2 and α_2PI_{1-8}-PDGF-BB induced an increase in osteocalcin but not PECAM expression during bone repair.

While *in vivo* imaging was a useful tool to monitor ongoing cellular processes *in vivo*, BLI results were complemented with microCT as a standard endpoint analysis of bone and vascular development. Our results indicate that inclusion of BMP-2 and α_2PI_{1-8}-PDGF-BB (1 μg of each GF) in the fibrin scaffold did not result in the generation of more bone surface, as compared to fibrin alone. Nevertheless, the addition of GFs did have a significant effect in the formation of thicker bone. Surprisingly, inclusion of the hAMSC reporters did not have a detectable effect on the amount of bone formed. A possible interpretation for this result could be that the number of cells used was too small to have a significant mass effect.

Since tissue repair is normally accompanied by angiogenesis, we also generated vascular casts of the treated mice by perfusion with a polymeric resin, followed by tissue corrosion. Analysis of 3D microCT images generated from the plastic casts revealed that the inclusion of BMP-2 and α_2PI_{1-8}-PDGF-BB in the fibrin scaffold improved its angiogenic capacity, resulting in formation of more and thicker vessels as compared to controls treated with fibrin only. While the inclusion of hAMSCs did not appear to improve any of the above parameters, they did have a statistically significant role in producing more abundant inter-vascular connections. Thus, even if luciferase expressing hAMSCs did not appear to differentiate to endothelial lineage, they did play a more complex organizational role in vascularization. This result supports the hypothesis that hAMSCs included in scaffolds contribute more importantly to the paracrine regulation of the physiological environment than to the formation of new tissue, in accordance with recent results from their use in the repair of other tissues.

CONCLUSIONS

As shown by *in vivo* BLI, BMP-2 and α_2PI_{1-8}-PDGF-BB delivered by fibrin induce the differentiation of implanted hAMSCs to the osteogenic but not to the endothelial lineage. Micro CT analysis of bone repair, revealed that BMP-2 and α_2PI_{1-8}-PDGF-BB comprising fibrin matrices promote formation of new bone and vascular structures derived from the host. Interestingly, luciferase expressing hAMSC included in scaffolds had no effect on bone formation and did not influence the number or thickness of host derived vessels. However, luciferase expressing hAMSCs had a paracrine-based organizational role, significantly promoting the formation of more interconnections between host-derived vessels during vascular regeneration in bone. In addition, luciferase expressing hAMSCs were effective reporters of bone differentiation-inducing conditions within fibrin scaffolds. The combination of BLI and microCT imaging to analyze changes in gene expression, bone and vascular structures during bone regeneration is an effective multimodal approach for the analysis of scaffold, cells and GFs performance.

Acknowledgements

Funding for this work was provided by the European Community's Seventh Framework Program Angioscaff NMP-LA-2008-214402 (Angiogenesis-inducing Bioactive and Bioresponsive Scaffolds in Tissue Engineering) and the Cell Therapy Network (TerCel). The University and Research Secretary from the Economy and Knowledge Department of the Government of Catalonia provided funding for the researcher O.F.Vila.

References

1. Kanitkar M, Tailor HD, Khan WS. The use of growth factors and mesenchymal stem cells in orthopaedics. Open Orthop J. 2011;5 Suppl 2:271–5.

2. Govender S, Csimma C, Genant HK, Valentin-Opran A, Amit Y, Arbel R, et al. Recombinant human bone morphogenetic protein-2 for treatment of open tibial fractures: a prospective, controlled, randomized study of four hundred and fifty patients. J Bone Joint Surg Am. 2002 Dec;84-A(12):2123–34.

3. Levéen P, Pekny M, Gebre-Medhin S, Swolin B, Larsson E, Betsholtz C. Mice deficient for PDGF B show renal, cardiovascular, and hematological abnormalities. Genes Dev. 1994 Aug 15;8(16):1875–87.

4. Phipps MC, Xu Y, Bellis SL. Delivery of platelet-derived growth factor as a chemotactic factor for mesenchymal stem cells by bone-mimetic electrospun scaffolds. PLoS ONE. 2012;7(7):e40831.

5. Chadwick K, Wang L, Li L, Menendez P, Murdoch B, Rouleau A, et al. Cytokines and BMP-4 promote hematopoietic differentiation of human embryonic stem cells. Blood. 2003 Aug 1;102(3):906–15.

6. Lind M, Eriksen EF, Bünger C. Bone morphogenetic protein-2 but not bone morphogenetic protein-4 and -6 stimulates chemotactic migration of human osteoblasts, human marrow osteoblasts, and U2-OS cells. Bone. 1996 Jan;18(1):53–7.

7. Reddi AH, Cunningham NS. Initiation and promotion of bone differentiation by bone morphogenetic proteins. J Bone Miner Res Off J Am Soc Bone Miner Res. 1993 Dec;8 Suppl 2:S499–502.

8. Kanakaris NK, Lasanianos N, Calori GM, Verdonk R, Blokhuis TJ, Cherubino P, et al. Application of bone morphogenetic proteins to femoral non-unions: a 4-year multicentre experience. Injury. 2009 Dec;40 Suppl 3:S54–61.

9. Calori GM, Tagliabue L, Gala L, d' Imporzano M, Peretti G, Albisetti W. Application of rhBMP-7 and platelet-rich plasma in the treatment of long bone non-unions: a prospective randomised clinical study on 120 patients. Injury. 2008 Dec;39(12):1391–402.

10. Ronga M, Baldo F, Zappalà G, Cherubino P. Recombinant human bone morphogenetic protein-7 for treatment of long bone non-union: an observational, retrospective, non-randomized study of 105 patients. Injury. 2006 Sep;37 Suppl 3:S51–56.

11. Grgurevic L, Macek B, Mercep M, Jelic M, Smoljanovic T, Erjavec I, et al. Bone morphogenetic protein (BMP)1-3 enhances bone repair. Biochem Biophys Res Commun. 2011 Apr 29;408(1):25–31.

12. Hollinger JO, Schmitt JM, Buck DC, Shannon R, Joh SP, Zegzula HD, et al. Recombinant human bone morphogenetic protein-2 and collagen for bone regeneration. J Biomed Mater Res. 1998;43(4):356–64.

13. Carragee EJ, Hurwitz EL, Weiner BK. A critical review of recombinant human bone morphogenetic protein-2 trials in spinal surgery: emerging safety concerns and lessons learned. Spine J Off J North Am Spine Soc. 2011 Jun;11(6):471–91.

14. Frieden IJ. Addendum: Commentary on Becaplermin Gel (Regranex) for Hemangiomas. Pediatr Dermatol. 2008;25(6):590–590.

15. Martino MM, Hubbell JA. The 12th-14th type III repeats of fibronectin function as a highly promiscuous growth factor-binding domain. FASEB J Off Publ Fed Am Soc Exp Biol. 2010 Dec;24(12):4711–21.

16. Polak J, Hench L. Gene therapy progress and prospects: in tissue engineering. Gene Ther. 2005 Dec;12(24):1725–33.

17. Pittenger MF, Mackay AM, Beck SC, Jaiswal RK, Douglas R, Mosca JD, et al. Multilineage potential of adult human mesenchymal stem cells. Science. 1999 Apr 2;284(5411):143–7.

18. Bianco P, Riminucci M, Gronthos S, Robey PG. Bone marrow stromal stem cells: nature, biology, and potential applications. Stem Cells Dayt Ohio. 2001;19(3):180–92.

19. Chamberlain G, Fox J, Ashton B, Middleton J. Concise review: mesenchymal stem cells: their phenotype, differentiation capacity, immunological features, and potential for homing. Stem Cells Dayt Ohio. 2007 Nov;25(11):2739–49.

20. Pansky A, Roitzheim B, Tobiasch E. Differentiation potential of adult human mesenchymal stem cells. Clin Lab. 2007;53(1-2):81–4.

21. Zuk PA, Zhu M, Ashjian P, De Ugarte DA, Huang JI, Mizuno H, et al. Human adipose tissue is a source of multipotent stem cells. Mol Biol Cell. 2002 Dec;13(12):4279–95.

22. De Ugarte DA, Morizono K, Elbarbary A, Alfonso Z, Zuk PA, Zhu M, et al. Comparison of multi-lineage cells from human adipose tissue and bone marrow. Cells Tissues Organs. 2003;174(3):101–9.

23. Kern S, Eichler H, Stoeve J, Klüter H, Bieback K. Comparative analysis of mesenchymal stem cells from bone marrow, umbilical cord blood, or adipose tissue. Stem Cells Dayt Ohio. 2006 May;24(5):1294–301.

24. Vilalta M, Dégano IR, Bagó J, Gould D, Santos M, García-Arranz M, et al. Biodistribution, long-term survival, and safety of human adipose tissue-derived mesenchymal stem cells transplanted in nude mice by high sensitivity non-invasive bioluminescence imaging. Stem Cells Dev. 2008 Oct;17(5):993–1003.

25. Iyer M, Wu L, Carey M, Wang Y, Smallwood A, Gambhir SS. Two-step transcriptional amplification as a method for imaging reporter gene expression using weak promoters. Proc Natl Acad Sci U S A. 2001 Dec 4;98(25):14595–600.

26. Contag CH, Spilman SD, Contag PR, Oshiro M, Eames B, Dennery P, et al. Visualizing gene expression in living mammals using a bioluminescent reporter. Photochem Photobiol. 1997 Oct;66(4):523–31.

27. Vilalta M, Jorgensen C, Dégano IR, Chernajovsky Y, Gould D, Noël D, et al. Dual luciferase labelling for non-invasive bioluminescence imaging of mesenchymal stromal cell chondrogenic differentiation in demineralized bone matrix scaffolds. Biomaterials. 2009 Oct;30(28):4986–95.

28. Briot K, Roux C. [Biochemical markers of bone remodeling]. Gynécologie Obstétrique Fertil. 2005 Dec;33(12):1009–13.

29. Yeung F, Law WK, Yeh C-H, Westendorf JJ, Zhang Y, Wang R, et al. Regulation of human osteocalcin promoter in hormone-independent human prostate cancer cells. J Biol Chem. 2002 Jan 25;277(4):2468–76.

30. Newman PJ, Albelda SM. Cellular and molecular aspects of PECAM-1. Nouv Rev Française Hématologie. 1992;34 Suppl:S9–13.

31. Ray P, De A, Min J-J, Tsien RY, Gambhir SS. Imaging Tri-Fusion Multimodality Reporter Gene Expression in Living Subjects. Cancer Res. 2004 Feb 15;64(4):1323 –1330.

32. Bagó JR, Aguilar E, Alieva M, Soler-Botija C, F Vila O, Claros S, et al. In vivo bioluminescence imaging of cell differentiation in biomaterials: a platform for scaffold development. Tissue Eng Part A. 2012 Sep 26;

33. Martino MM, Tortelli F, Mochizuki M, Traub S, Ben-David D, Kuhn GA, et al. Engineering the growth factor microenvironment with fibronectin domains to promote wound and bone tissue healing. Sci Transl Med. 2011 Sep 14;3(100):100ra89.

34. Dégano IR, Vilalta M, Bagó JR, Matthies AM, Hubbell JA, Dimitriou H, et al. Bioluminescence imaging of calvarial bone repair using bone marrow and adipose tissue-derived mesenchymal stem cells. Biomaterials. 2008 Feb;29(4):427–37.

35. Lutolf MP, Weber FE, Schmoekel HG, Schense JC, Kohler T, Müller R, et al. Repair of bone defects using synthetic mimetics of collagenous extracellular matrices. Nat Biotechnol. 2003 May;21(5):513–8.

36. Beckmann N, Schuler A, Mueggler T, Meyer EP, Wiederhold K-H, Staufenbiel M, et al. Age-dependent cerebrovascular abnormalities and blood flow disturbances in APP23 mice modeling Alzheimer's disease. J Neurosci Off J Soc Neurosci. 2003 Sep 17;23(24):8453–9.

37. Krucker T, Lang A, Meyer EP. New polyurethane-based material for vascular corrosion casting with improved physical and imaging characteristics. Microsc Res Tech. 2006 Feb;69(2):138–47.

38. Thévenaz P, Ruttimann UE, Unser M. A pyramid approach to subpixel registration based on intensity. IEEE Trans Image Process Publ IEEE Signal Process Soc. 1998;7(1):27–41.

FIGURE CAPTIONS

Fig. 59. **Bioactivity and fibrin affinity analysis of the engineered Platelet Derived Growth Factor-BB (PDGF-BB).** A) Phosphorylated PDGF-Rβ (pPDGF-Rβ) quantification using ELISA. No significative difference between wild type PDGF-BB and α2PI1-8-PDGF-BB was found (n = 4); B) GF release from fibrin matrices. Graphs show the cumulative release of GFs over 7 days (n = 4). Bars represent the standard error of the mean.

Fig.2. Non-invasive BLI imaging of RLuc and PLuc-expressing hAMSCs seeded on fibrin scaffolds implanted IM in SCID mice. Right panels, representative BLI images showing Luciferase activity superimposed on b&w images of the corresponding implantation site (left fibrin plus GF; right, fibrin control) at the indicated days. Left panel histograms summarize bioluminescence data acquired from corresponding images. A: Histogram summarizing PLuc activity normalized to day 1; (p=0.025, two-way ANOVA test); B: Histogram summarizing evolution of osteocalcin expression; data represents the ratio OC-PLuc/RLuc (p=0.016, two-way ANOVA test); C: Histogram summarizing evolution of PECAM expression; data represents the ratio PECAM-PLuc/RLuc, * $p<0.05$ Student T test; AU = arbitrary units. Color bars illustrate relative light intensities from RLuc (blue: low, red: high,) and PLuc (black: low, blue: high). N=6.

Fig.3. Non-invasive bioluminescence imaging (BLI) of RLuc and OC·PLuc-expressing hAMSCs cells seeded on fibrin scaffolds implanted in a 3mm-calvarial defect in SCID mice. (a) Representative BLI images showing RLuc (top row) and PLuc (bottom row) activities from dually labeled hAMSCs, superimposed on b&w head images of the corresponding mouse head. Color bars illustrate relative light intensities from RLuc (blue: low, red: high,) and PLuc (black: low, blue: high); (b) Histogram summarizing cell proliferation data, RLuc PHCs are normalized to day 1; (c) Histogram summarizing evolution of osteocalcin expression, data is represented as the ratio PLuc/RLuc. Bars represent the standard error of the mean. * $p<0.05$ according to Student T test; AU = arbitrary units. N=9.

Fig.4. Non-invasive imaging of RLuc and PECAM·PLuc-expressing hAMSCs cells seeded on fibrin scaffolds implanted in a 3mm-calvarial defect in SCID mice. (a) Representative BLI images showing RLuc

(top row) and PECAM·PLuc (bottom row) activity from dually labeled hAMSCs, superimposed on b&w head images of the corresponding mouse head. Color bars illustrate relative light intensities from RLuc (blue: low, red: high,) and PLuc (black: low, blue: high); (b) Histogram summarizing cell proliferation data, RLuc PHCs are normalized to day 1; (c) Histogram summarizing evolution of PECAM expression, data is represented as the ratio PLuc/RLuc. Bars represent the standard error of the mean. * $p<0.05$ according to Student T test; AU = arbitrary units. N=9.

Fig.5. µCT analysis of bone formation in a calvaria defect regeneration model in SCID mice (6 weeks post implantation). Defects were implanted with : nothing (empty), fibrin, fibrin + BMP-2 + PDGF-BB and fibrin + BMP-2 + PDGF-BB + hAMSCs. (a) Histogram summarizing surface coverage results for each test; (b) Histogram summarizing bone volume results for each group; (c) Histogram summarizing bone thickness results for each group; (d) representative µCT images of skulls and diagram showing disposition of implants. Bars represent the standard error of the mean. * $p<0.05$ according to Student T test. N=14.

Fig. 6. High resolution µCT images of calvarial defect vascular casts. Defects were left empty (A), treated with fibrin alone (B), treated with fibrin with BMP-2 and PDGF-BB (C) and treated with fibrin BMP-2 and PDGF-BB and hAMSCs. Scale bar:1 µm.

Fig. 7: **µCT analysis of vascularization calvaria defect regeneration in SCID mice (6 weeks post .implantation).** Calvarial defects were treated with: nothing (empty defect), fibrin, fibrin + BMP-2 + PDGF-BB and fibrin + BMP-2 + PDGF-BB + hAMSCs. Histogram summarizing percentage of vessel volume (A), vessel number (B), vessel thickness (C), , vessel spacing (D), and density of intervascular connections (E), for each group. Bars represent the standard error of the mean. * $p<0.05$ according to Student T test. N=6.

FIG 1:

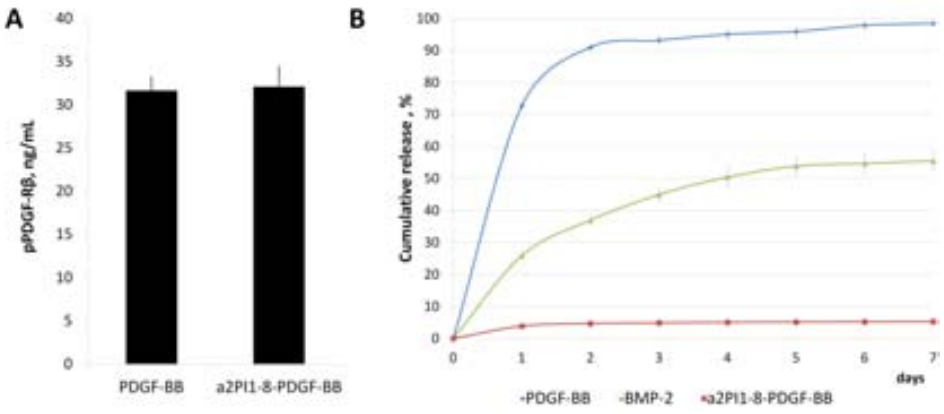
A
pPDGF-Rβ, ng/mL
40
35
30
25
20
15
10
5
0
PDGF-BB
a2PI1-8-PDGF-BB
B
Cumulative release , %
100
90
80
70
60
50
40
30
20
10
0
0
1
2
3
4
5
6
7
days
-PDGF-BB
-BMP-2
-a2PI1-8-PDGF-BB

FIG 2:

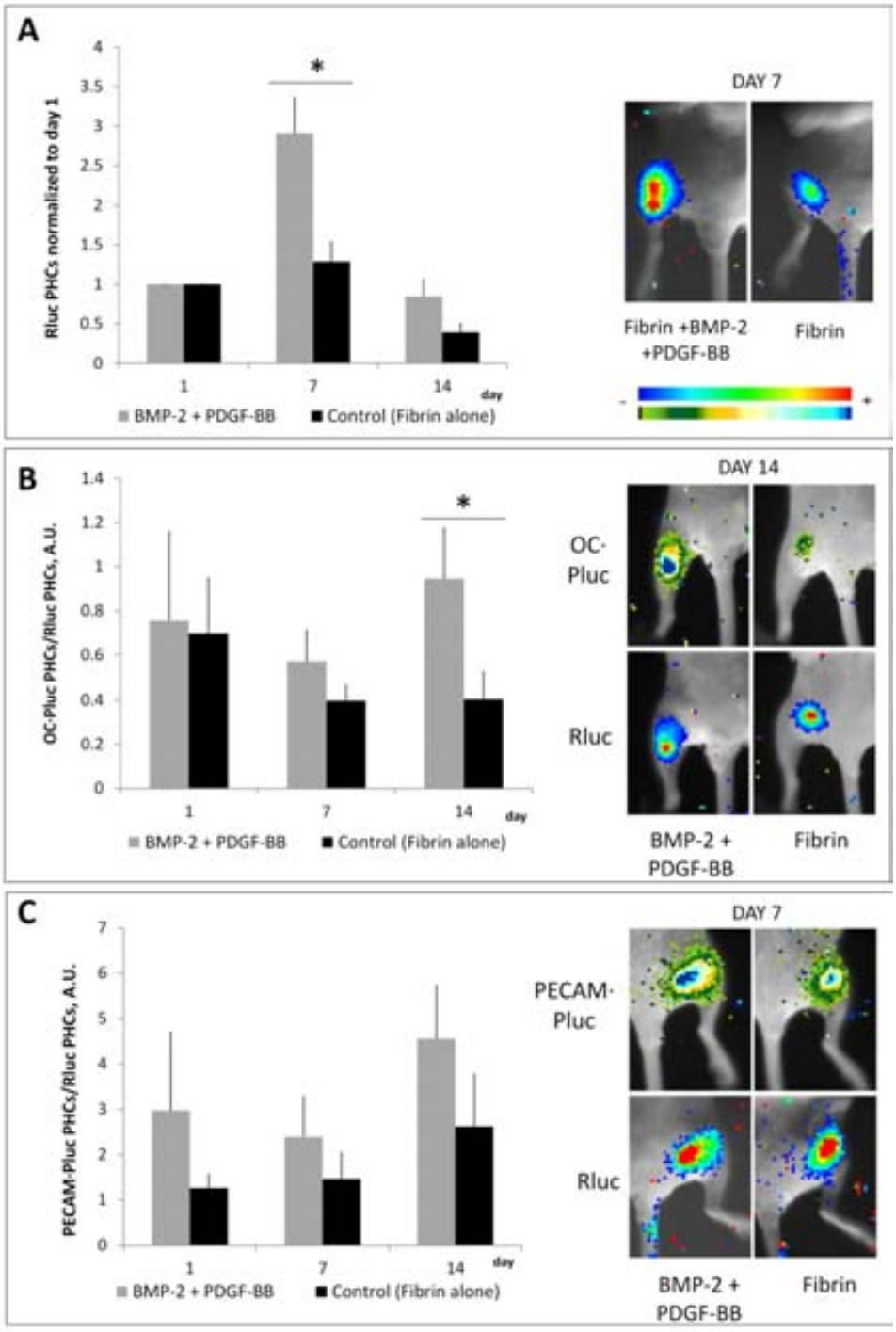
A
Rluc PHCs normalized to day 1
4
3.5
3
2.5
2
1.5
1
0.5
0
*
1
7
14
day
BMP-2 + PDGF-BB
Control (Fibrin alone)
DAY 7
Fibrin +BMP-2 +PDGF-BB
Fibrin
-
+
B
OC-Pluc PHCs/Rluc PHCs, A.U.
1.4
1.2
1
0.8
0.6
0.4
0.2
0
*
1
7
14
day
BMP-2 + PDGF-BB
Control (Fibrin alone)
DAY 14
OC-Pluc
Rluc
BMP-2 + PDGF-BB
Fibrin
C
PECAM-Pluc PHCs/Rluc PHCs, A.U.
7
6
5
4
3
2
1
0
1
7
14
day
BMP-2 + PDGF-BB
Control (Fibrin alone)
DAY 7
PECAM-Pluc
Rluc
BMP-2 + PDGF-BB
Fibrin

FIG 3:

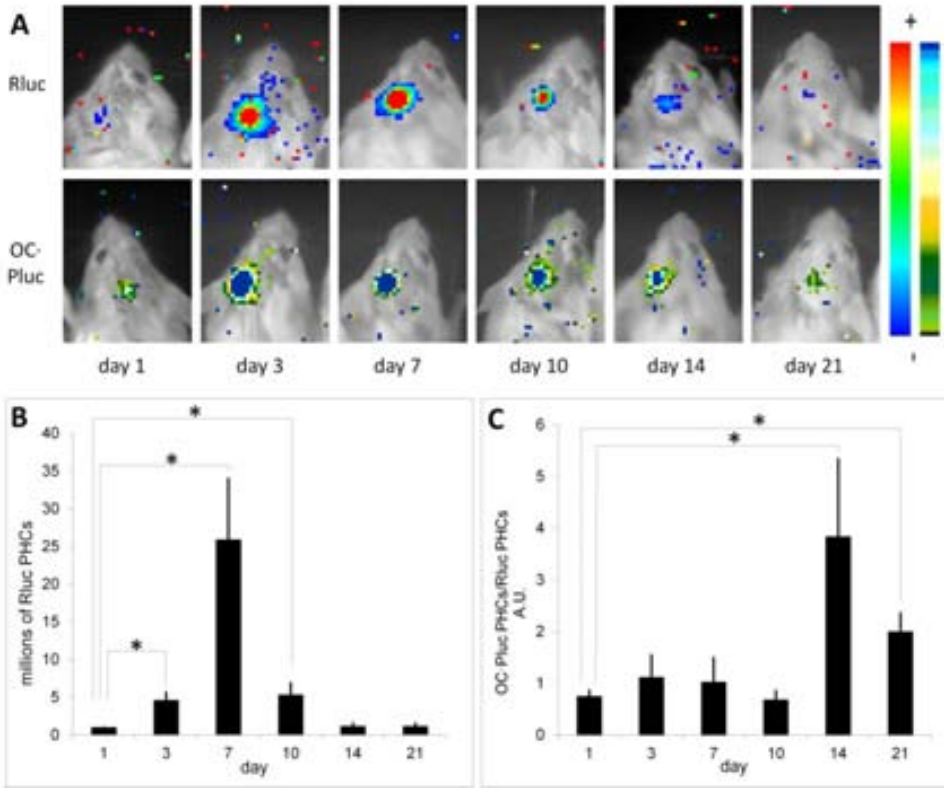
A
Rluc
OC-
Pluc
+
-
day 1
day 3
day 7
day 10
day 14
day 21
B
millions of Rluc PHCs
day
C
OC Pluc PHCs/Rluc PHCs
A.U.
day

FIG 4:

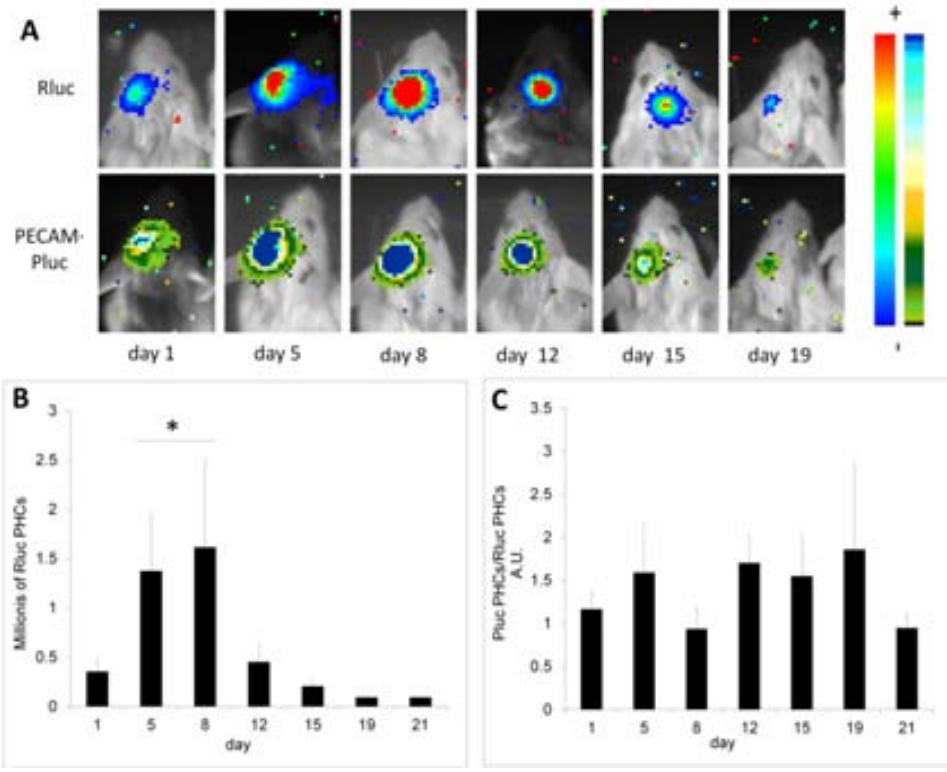
A
Rluc
PECAM-Pluc
day 1
day 5
day 8
day 12
day 15
day 19
+
-
B
Millionis of Rluc PHCs
day
C
Pluc PHCs/Rluc PHCs A.U.
day

FIG 5:

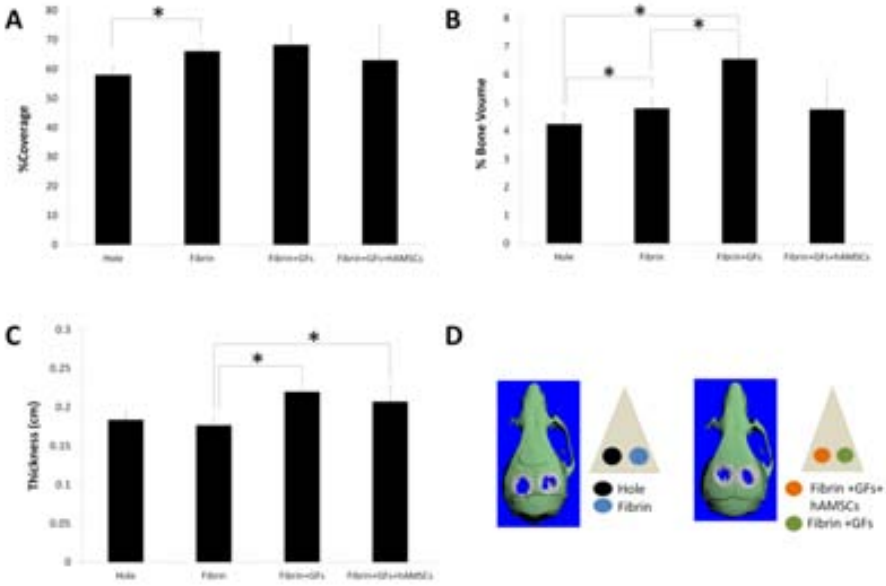
A
%Coverage
B
% Bone Vounie
C
Thickness (cm)
D
Hole
Fibrin
Fibrin +GFs+ hAMSCs
Fibrin +GFs

FIG 6:

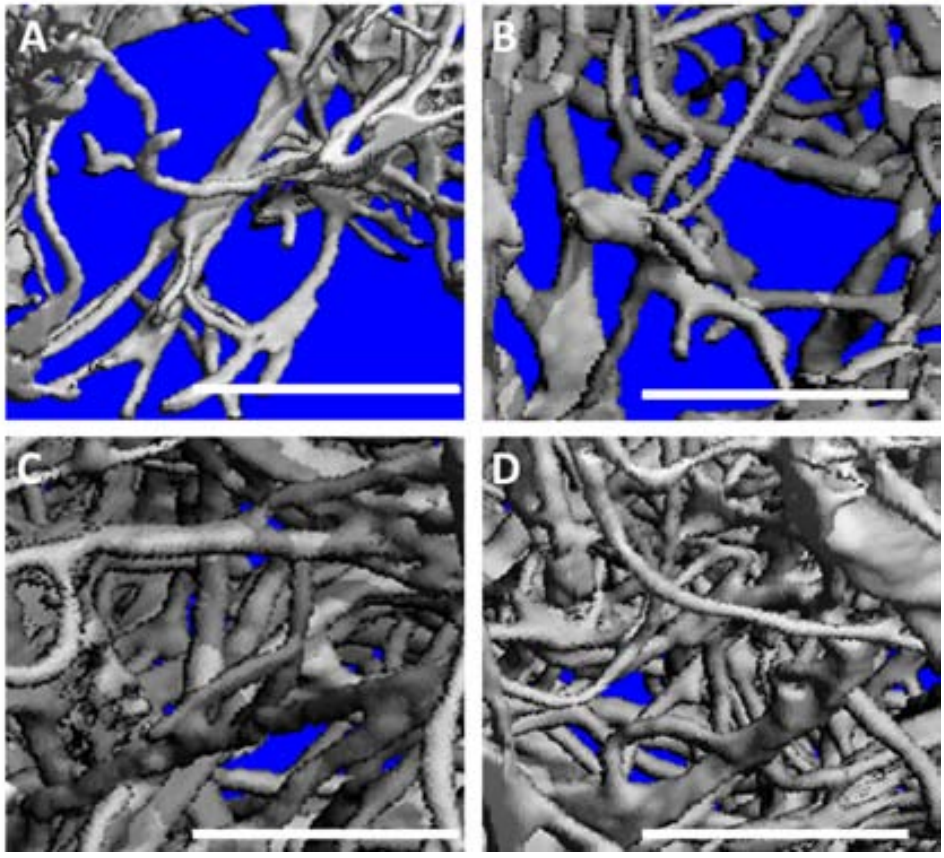

FIG 7:

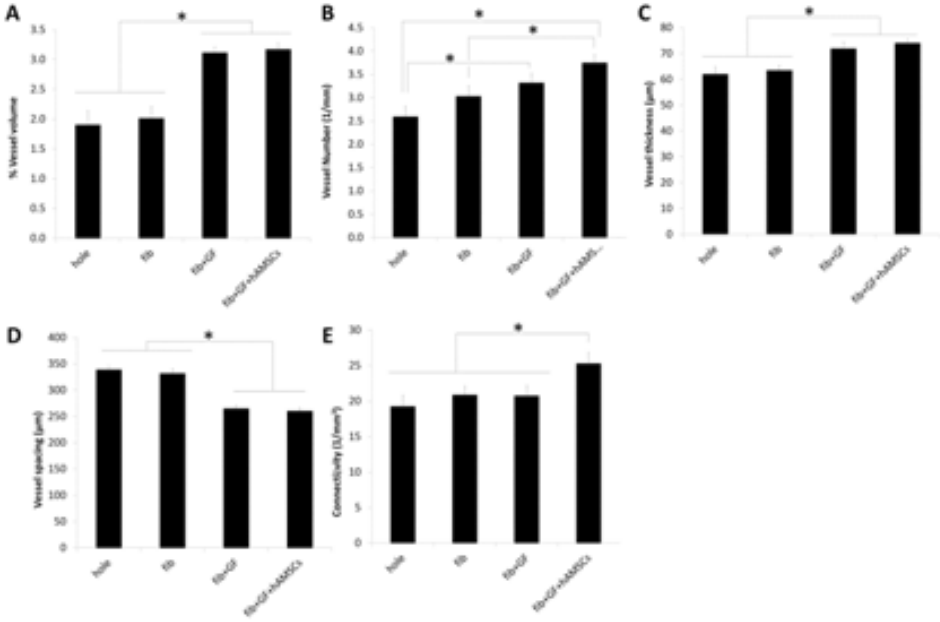
A
B
C
D
E
% Vessel volume
Vessel Number (1/mm)
Vessel thickness (μm)
Vessel spacing (μm)
Connectivity (1/mm³)
hole
fib
fib+GF
fib+GF+hMSCs